United Aircraft Research Laboratories

UNITED AIRCRAFT CORPORATION

EAST HARTFORD, CONNECTICUT

Report E-910262-6, Vol. II

Study of Low-Acceleration Space
Transportation Systems
Contract NAS8-11309

UNCLASSIFIED

Prepared for the
George C. Marshall Space Flight Center
National Aeronautics & Space Administration
Huntsville, Alabama

DATE June 1966

NO. OF PAGES _____

COPY NO. 8

FOREWORD

This document contains the Technical Report for the Study of Low-Acceleration Space Transportation Systems. The study effort was sponsored by the NASA G. C. Marshall Space Flight Center, Huntsville, Alabama, under Contract No. NAS8-11309. The results of the studies reported herein were obtained by the Systems Analysis Section of the United Aircraft Research Laboratories, with support from the Advanced Power Systems Organization of Pratt & Whitney Aircraft.

The complete results of the study are contained in the following volumes:

Volume I - Summary
Volume II - Technical Report

The initial period of performance began in July 1964 and ended in the latter part of June 1965. Additional tasks were added to the original statement of work and the supplemental period of performance covered July 1965 through June 1966.

Although the current document presents the results of the entire study insofar as the general study objectives are concerned, further detailed information showing the chronological development of data obtained in the first study phase may be found in United Aircraft Research Laboratories Report D-910262-3, Study of Low-Acceleration Space Transportation Systems (July 1965), Interim Report.

ACKNOWLEDGEMENTS

Significant contributions to this report were made by the following United Aircraft personnel:

R. V. Ragsac	Program Manager, and Mission and System Analyses
W. R. Fimple G. J. Thrasher C. P. Van Dine	Trajectory Analysis and Computation
B. Gitlow (P&WA) J. W. Schmitt (P&WA)	Power System Study
R. R. Titus R. Gogolewski	Spacecraft Conceptual Design and Planetary Operations Analysis
G. T. Peters	Life Support and Environmental Control System Analysis
Miss E. M. Mankauskas R. S. Gourd Mrs. L. E. Rufleth	Computer Programming

Report E-910262-6

Study of Low Acceleration Space Transportation Systems

TABLE OF CONTENTS

TABLE OF CONTENTS
(Contd.)

Report E-910262-6

Study of Low-Acceleration Space Transportation Systems

Contract NAS8-11309
Final Report

Technical Report

SECTION I
INTRODUCTION

This report documents the results of a two-year study on manned missions to Mars in the 1980 time period using combined high- and low-thrust space transportation systems. The analysis was performed for the National Aeronautics & Space Administration, G. C. Marshall Space Flight Center. The first year's study was executed under Contract NAS8-11309 which was subsequently enlarged to include another year's study of supplemental tasks. Report D-910262-3 (July 1965) details the results of the first year's study effort which is only briefly described in the present document. The majority of the information presented herein pertains to the results obtained during the second year of effort.

Objectives and Scope

The basic objective of the entire study was to determine whether a useful manned mission to Mars could be accomplished during the 1980 time period utilizing high- and low-thrust propulsion systems in combination. The principal specific objective was to investigate means for minimizing the vehicle mass placed on Earth parking orbit. During the initial period of performance it became evident that the conduct of the study relied almost entirely upon the low-thrust trajectory data needed to perform the mission studies. A promising approach was developed, and accordingly the initial tasks were supplemented by additional work. The prime objective of this additional effort was to further develop and check the simplified trajectory model for low-thrust systems, including calculation of near-optimum trajectories for combined high-low acceleration systems as applied to the manned Mars mission.

The underlying philosophy in the conduct of the study was oriented primarily towards integrating the requirements of the hybrid-thrust flight mode with the operating characteristics of the major vehicle subsystem, the

powerplant. It was believed that the basic study objectives would be fulfilled by an integrated analysis of the major characteristics of the flight profile, the mixed-thrust trajectories, and power system parameters which are peculiar to the combined high- and low-thrust interplanetary vehicles. The spacecraft and constituent subsystems (except the powerplant) were investigated only to the depth necessary to obtain the growth in mass as a function of the major mission and flight parameters. A brief analysis was performed, however, to uncover some of the more prominent problems associated with the vehicle system design. A conceptual vehicle design was established based on these preliminary results.

The study concentrated on manned trips to Mars occurring in the opposition of 1980. The prime mission of the hybrid-thrust interplanetary vehicle was thus to deliver the MEM onto a Martian parking orbit, loiter in the parking orbit for 30 days, rendezvous with the surface exploration team, and return the crew and scientific equipment and data to Earth. This basic flight profile was perturbed by varying the powerplant specific weight and output power, the high-low thrust mix, the total trip time, and the outbound and inbound leg durations. The major indicator of mission capability was considered to be the total vehicle mass required on Earth parking orbit as a function of the flight and powerplant parameters and in relation to the payload capability of the Saturn V.

The development of criteria and requirements for the low-acceleration propulsion system was limited first to two major considerations. The establishment of desired operating characteristics for the primary subsystem of interest, i.e., the powerplant. The second consideration was the determination of the optimum mix of high- and low-thrust propulsion which minimizes gross vehicle mass. The two considerations together, interpreted in terms of technology, constituted the comparison data employed to judge the usefulness of hybrid-thrust vehicle systems for manned exploration of Mars.

Basic Assumptions

For study purposes, certain basic assumptions were made regarding the low-thrust trajectory, the powerplant, and the vehicle system model. It is felt that these assumptions, while they may narrow the scope of the study, do not affect the conclusions made, which are based on relative comparisons, and the evaluation of the worth of hybrid-thrust systems for manned missions.

All low-thrust trajectories employed in the study were of the variable-thrust mode wherein the specific impulse of the electric propulsion system is assumed to vary in a manner such that propellant consumed is a minimum. The primary reason for this selection was that quantities of variable-thrust trajectory data, especially those containing hyperbolic excess speeds on the boundaries, required for routine missions studies were readily available. The constant-thrust mode, while being more attractive in terms of electric

thruster engineering design, requires rather definitive analyses in the corresponding numerical problem of rapidly and economically computing optimum trajectories. In view of the objectives of this study and the timeliness of the study results, the assumption of variable-thrust operation appeared justified.

Although the specific impulse was allowed to vary, the corresponding efficiency of the thruster was kept constant at an average value. In general, the output of the power system was permitted to vary with time in a probabilistic sense in order to assess the effects of discrete failures in components of the powerplant. The powerplant considered was an alkali-metal, nuclear Rankine cycle system utilizing a lithium-cooled fast reactor. The specific weight of this system was considered to vary between 5 and 20 kg/kw throughout the parametric phases of the study.

The vehicle system model employed in the mass calculations consists of a basic spacecraft (containing a solar flare shelter, life support system, etc.), the Mars excursion module, the Earth capture system, nuclear propulsion steps for Earth departure and planetary arrival or departure, and the electric propulsion system for the outbound and inbound heliocentric transfer. The nuclear propulsion system was considered to be of the NERVA/PHOEBUS type (I_{sp} = 800 sec). The computation of vehicle mass utilized weight scaling laws for the life support system, the Earth capture system, and the high-thrust nuclear propulsion systems.

Study Approach

In general the method of analysis was to bring together the trajectory requirements and powerplant operating characteristics through the vehicle system model. The low-thrust trajectory requirements reflect the influence of the mission duration and the corresponding distribution in leg times, the hyperbolic excess speeds at the terminals of the trajectory, and the powerplant decreasing power output. The powerplant operating characteristics directly affecting the vehicle system mass are specific weight and decreasing power profile. By computing the total vehicle mass as a function of the different parameters in the trajectory requirements and powerplant characteristics, it is possible to relate the effectiveness of changing the trip time, the powerplant specific weight, and the decreasing power profile.

The decreasing power profile is a key parameter in evaluating the effectiveness of technological approaches to enhancing powerplant performance. Accordingly, the majority of the study effort was spent in not only determining the optimum hybrid-thrust trajectory requirements but also in investigating methods of decreasing powerplant specific weight and of maintaining the power output at its original rating. This dichotomous approach merges when the various parameters are integrated by the mission effectiveness

studies. In these studies the trajectory characteristics and the power system technology areas are evaluated in terms of the corresponding vehicle mass requirements. This over-all method of analysis allows firm identification to be made of critical powerplant technology areas, their influence on the mission requirements, and the effectiveness of technological development to reducing such requirements.

SECTION II
ACCOMPLISHMENTS AND CONCLUSIONS

The major tasks which have been accomplished as a result of the study effort and the significant conclusions derived thereform are summarized in this section. The implications to technological research activities wherein further efforts are desirable are listed in Appendix J, Research and Technology Implications. Also listed in Appendix J are study areas recommended for the future analysis of manned interplanetary hybrid-thrust missions.

Major Study Accomplishments

The following list summarizes the major accomplishments of the study. The relevant section in which further detailed information may be obtained is indicated in parenthesis.

1. The finite-difference Newton-Raphson algorithm was successfully applied to solving the calculus of variations problem of variable low-thrust trajectory optimization. This approach resulted in a fundamental advance in the numerical solution of nonlinear two-point boundary value problems and has yielded optimum variable-thrust trajectories an order of magnitude faster than the most recent competitive methods. Typically, exact solutions are obtained on the average of 10 sec per trajectory (Section V and Appendix A).

2. The basic algorithm and associated computer program have been extended to include hyperbolic excess speeds of planetary departure and arrival (mixed high- and low-thrust systems), variable power in the exhaust jet (Section V), planetary flybys, and solar probes (Appendix B). Variable jet power includes variations in powerplant output due to sources such as radioisotope systems and solar cells, and component failures within the power system.

3. A numerical technique was developed for maximizing the payload of a vehicle operating under constant thrust and constant power with a single coast (Appendix B). A computer program was written which implements the optimization technique.

4. For variable-thrust operation, comparisons of optimum Earth to Mars trajectories were made for constant-power, radioisotope-power, and solar-power modes. In addition, using rendezvous boundary conditions (i.e., parabolic conditions with respect to the departure and arrival planets), contours of constant J were computed and organized for the Mars oppositions of 1978 and 1980 (Section V).

5. Because the trajectory optimization program made hybrid-thrust data readily available, a technique was developed which maximizes (under ideal

conditions) the payload-to-gross weight ratio of a combined high- and low-thrust vehicle system. This method and the implementing computer program is sufficiently flexible to include different propulsion parameters for the high-thrust and low-thrust systems, and also an atmospheric (rather than high-thrust) capture system (Section IV).

6. For hybrid-thrust systems employing rendezvous conditions at the boundaries of the low-thrust trajectories, the minimum mass trips were found to be those arriving at Mars after the opposition date. A simple graphical approach is used in determining the optimum distribution of outbound and inbound leg times for a given mission duration and for establishing the arrival date which minimizes vehicle mass (Section IV).

7. The relative importance of powerplant specific weight, component technology level, onboard maintenance, and reliability level on the hybrid-thrust vehicle system mass required on Earth parking orbit was determined for a range of total trip times. The influence of the different powerplant characteristics was evaluated for their effectiveness in reducing the mission requirements (vehicle mass), (Section III), and in establishing desired powerplant operating characteristics (Section VI).

8. The influence of the Mars parking orbit operational mode on the mass of the MEM and the parent spacecraft was established for highly elliptical (near parabolic) and circular (926-km) parking orbits. The trade-off of parking orbit mode between the MEM and the spacecraft was identified in terms of system mass and favored spacecraft departure and arrival propulsion systems (O_2/H_2 or solid-core nuclear) (Sections III and IV).

9. A simple hybrid-thrust spacecraft conceptual design was established. Variations of the basic design layout were determined for elliptical or circular orbit operations and nuclear or chemical spacecraft propulsion. Problem areas relevant to the over-all optimization of the space system and the design integration of such a system were tentatively identified (Section III).

10. Flight profile and system considerations which were determined to be important approaches for minimizing the vehicle mass required on Earth parking orbit were delineated (Section III).

11. Computer programs developed for use in the study include:

- Trajectory optimization for variable-thrust rendezvous, flyby, and solar probe trajectories under constant and variable power and with hyperbolic excess speeds (Section V and Appendices B and E).

- Trajectory optimization for constant-thrust single-coast rendezvous trajectories under constant power and with payload maximization (Appendix B and Section V).

- Hybrid-thrust system optimization for operations under high-, low-, high-thrust and high-thrust, low-thrust, atmospheric entry (Section IV).

- Mass computation for different propulsion system mixes (hybrid-thrust), powerplant characteristics, and various propulsion parameters (Appendix F).

12. Power system output as a function of operating time (power profiles) was established for different subsystem and component redundancies, probability levels, and component failure rate levels. The influence and importance of maintenance level and powerplant technology on the power frofile were determined for a two-reactor power system (Section VI).

13. Critical system design considerations and technology areas which strongly influence powerplant specific weight were identified (Section VI).

14. The time and cost for developing a 4-Mw maintained powerplant were evaluated (Section VI).

General Conclusions

1. A useful manned Mars mission employing a hybrid-thrust vehicle system can be performed in the 1980 time period. However, prompt initiation of the development of the nuclear electric powerplant and propulsion system is required due to the extended time required to develop this system. The "usefulness" of the mission is judged by the total vehicle mass required on Earth parking orbit (typically 600 to 800 metric tons) in relation to the payload delivered (MEM, 45 metric tons).

2. For extended trip times (about 500 to 600 days) the influence of powerplant specific weight on vehicle mass is reduced under hybrid-thrust operation so that high specific weights (15 to 20 kg/kw) are tolerable. This level of powerplant specific weight may be achieved by nuclear Rankine cycles with maximum cycle coolant temperatures in the range of 1800 to 2000 F and reactor fuel burnup in the range of 1 to 3 a/o uranium. Satisfactory powerplant reliability can be achieved if this type of system can achieve a state of development equivalent to that experienced by aircraft gas turbines and if an extensive inflight maintenance capability can be developed. It is estimated that the development program required for this type of powerplant will require about 13 to 17 years and 6 to 8 billion dollars. It is anticipated that any of the high temperature nuclear powerplant systems currently proposed will require development programs of a similar magnitude.

3. In order to significantly decrease vehicle mass requirements, the powerplant specific weight must be less than 5 kg/kwe. However, it is not possible to identify a power system design which would result in a specific

weight less than 12 kg/kw. There is little difference in required vehicle mass for specific weights between 12 and 20 kg/kw. Thus, there is little incentive for a developing powerplants to achieve above 2000 F reactor outlet temperatures or 3 a/o reactor fuel burnup (corresponding to a specific weight of 15.5 kg/kw).

4. Under hybrid-thrust operations, the power requirements for the manned Mars mission are about 4 mwe or less depending on the powerplant characteristics selected and the trip time. Reliability considerations indicate that the favored powerplant for this mission should employ two reactors. From preliminary conceptual design analysis, the vehicle system integration problems are alleviated considerably provided the favored powerplant can be contained in one power module.

5. The available power, and consequently those characteristics which affect power, strongly influences the mass of the entire vehicle system. Major power system characteristics which determine the power availability are maintenance level, component failure rates, and probability level.

6. The mass requirements for extended duration trips and high specific weights are essentially compatible with the Saturn V orbital payload capability. The actual number of Saturn V launches required to fulfill a given mission depends not only upon proper selection of the mass minimization techniques, but also on the level of sophistication in the design and packaging of the space transportation system for orbital assembly.

7. The hybrid-thrust system using a solid-core nuclear propulsion system in combination with electric propulsion is highly competitive with the vehicle systems employing highly advanced all high-thrust nuclear systems such as liquid-core and gaseous-core rockets. The major advantage of the advanced high-thrust nuclear system is the approximate 100 days less trip time required for the manned Mars mission.

8. Employing an Earth return rendezvous mode by using an Earth surface launched system to retrieve the crew at parabolic conditions results in a large mass penalty compared to an ablative atmospheric Earth capture system. The penalty in mass does not include the mass of the resulting Earth-based rendezvous system.

9. For optimum hybrid-thrust operation, the fractional hyperbolic excess speeds should be between 0.5 and 0.8 for Earth and Mars departure and 0.3 and 0.6 for Mars arrival, where the values represent the fraction of the impulsive (all high-thrust) transfer. For Earth arrival the values are about 1.0 depending upon the mass growth of the ablative entry system with atmospheric entry speed.

10. The over-all mission energy requirements are dependent on the orbital operations at the planet. The eccentricity of the parking orbit should be defined as a function of the retro ΔV accuracy, the number of monitoring passes

the spacecraft makes during surface exploration, and the required total stopover time. The energy requirements for the orbital operations are a strong function of the percent of the hyperbolic excess speed which is applied to the high-thrust system.

11. The spacecraft design is strongly influenced by the type of orbit established about Mars and the type of propulsion used for the retro-braking. Circular orbits tend to minimize the size of the MEM and maximize the Mars capture and departure propulsion requirements. As the eccentricity of the parking orbit is increased, the MEM weight increases while the capture and departure stage decrease in size. For highly elliptic parking orbits about Mars, the capture and departure energy requirements are so small that an O_2/H_2 chemical system can be used for planetary orbital operations and provide spacecraft weights which are lower than if solid-core nuclear propulsion were used. Also, the radiation problem is alleviated with a chemical system.

Mass Minimization Considerations

1. For a given total trip time, the best combination of outbound and inbound leg times should be analyzed along with the arrival date.

2. The benefits in reduced mass requirements derived from operating under combined high and low thrust indicate that the hybrid-thrust mode should be employed in the more difficult (higher-energy) missions.

3. Ablative entry via an "advanced" type Apollo entry system yields less required mass than arrival at Earth under parabolic conditions with retrieval by an Earth-based rendezvous vehicle.

4. Inflight maintenance strongly reduces the vehicle mass required, but it is an anticipated activity based on probability analyses.

5. Reduced probability levels tend to reduce mass requirements but also tend to reduce the probability of safe return of the crew.

6. The mission analysis should consider the operational mode at the planetary parking orbit for its effect on the mass of the MEM and parent spacecraft.

7. In some instances the velocity requirements for effecting the desired planetary parking orbit are of such magnitude that no one propulsion system (O_2/H_2 or solid-core nuclear) can be considered, a priori, to have a distinct mass advantage; both systems should be investigated.

SECTION III
MISSION ANALYSIS AND REQUIREMENTS

The basic purpose of the mission studies was to determine favored flight and propulsion modes, desired power system operating characteristics, and to identify the sensitivity of mission requirements to postulated changes in the trajectory and powerplant parameters. The approach entails integrating the different parameters in a mass computation procedure to determine the vehicle mass required on Earth parking orbit and its corresponding breakdown, and suitably varying these parameters over a range of expected values. The results are thus displayed in terms of mass on Earth orbit (MEO), the parameter indicating the mission requirements.

This section summarizes, in a mission-oriented sense, the salient results and accomplishments of the study and omits the supporting technical details which may be found in subsequent sections. Because all of the most significant results of the entire study have been obtained during the second phase of the contract only the major results of the previous phase are included in this section. The initial study phase generated preliminary information which is detailed in United Aircraft Report D-910262-3, "Study of Low Acceleration Space Transportation Systems," July 1965.

General Background

The primary mission of the manned Mars flight was assumed to be a surface exploration in 1980 for a period of 30 days, with a capability of returning 454 kg of scientific samples and information. A crew of 8 astronauts was fixed throughout the study with the number of men descending to the surface taken as not more than four. The Mars excursion module (MEM) weights 45 metric tons and the Mars parking orbit is 926 km.

The flight profile utilized to execute the above mission is depicted in Fig. III-1. The profile can be considered a "standard" one in which a large single parent vehicle is employed to deliver a payload, the MEM, onto a parking orbit about Mars. The MEM contains a module which transports the surface exploration team back onto the parking orbit and rendezvous with the parent vehicle for the return trip.

Three separate high-thrust nuclear systems are employed to depart from Earth parking orbit and to capture and depart from Mars. Solid-core nuclear rockets of the PHOEBUS type are the high-thrust systems used in all cases. An advanced Apollo type ablative entry system is used to capture the crew and scientific samples at Earth where the entry speeds are limited to about 20 km/sec. The scaling laws for the high-thrust nuclear propulsion system, the entry system, the life support and environmental control system, and the basic spacecraft are

all discussed in Section IV, Flight Profile Studies.

In all cases the heliocentric transfer portions of both the outbound and inbound legs are executed by a single electric propulsion system. Although some mass savings are available if a separate electric system were used for each leg (i.e., dual electric-electric propulsion) where the outbound electric system is staged at Mars, the problems of reliability concerning exposure and startup after months of storage appeared to favor the single-electric mode.

The proportioning of the high-thrust and low-thrust requirements was determined for minimum vehicle mass in all of the trips analyzed during the second phase of the study. That is, the outbound leg high-thrust departure from Earth, low-thrust heliocentric transfer, and capture at Mars were optimized between the high- and low-thrust systems to provide maximum payload-to-gross weight ratio; similarly for the return leg.

During the latter phases of the study a brief investigation was conducted on the interaction of parking orbit altitude and propulsion requirements on the general arrangement and mass of the interplanetary hybrid-thrust spacecraft and Mars excursion module. Problem areas peculiar to the variations in the orbital operational modes were identified and related to a possible vehicle conceptual design. Sufficient study was undertaken to uncover problems of and suggest approaches for the over-all vehicle design integration as influenced by the major spacecraft subsystems such as propulsion systems, manned modules, powerplant, MEM, Earth entry module, etc.

Powerplant-Trajectory Integration

The primary parameters of interest were considered to be the powerplant specific weight and power profile, the mission duration, the arrival date at Mars, and the high- and low-thrust propulsion mix. From the preliminary work, the arrival date at Mars and the distribution of outbound and inbound leg times which tended to minimize vehicle mass for a fixed mission duration were found. These trips, in a given total trip time, were then analyzed for the optimum combination of high- and low-thrust mix which minimized the gross vehicle mass on Earth parking orbit. Consequently the final results show only the effects of mission duration, specific weight, and power profile.

The power profile has been found to be the key element in relating postulated technological improvements in power system performance to the mission requirements. The level of output delivered by the power system depends on the assumed component failure rates and the probability level desired. In order to provide a link with presently known technology, the initial failure rates were assumed to be those experienced by commercial aircraft gas turbines. Improvements in component technology were postulated based on the NASA

objectives for the Apollo fuel cell program; these objectives correspond to failure rates about a factor of ten lower than those of aircraft gas turbines.

In addition to the failure rates, subsystem redundancies were analyzed to determine the effect on power output. Figure III-2 compares the power output between a single-reactor system and a two-reactor system. The reference failure rates or technology level assumed are indicated by λ for the aircraft gas turbine level. The curve shows, at any given time during the mission, that the probability of maintaining at least the power level shown is at least the stated probability, P. It can be seen that the two-reactor system is favored over the single-reactor case in terms of the power available at any time and at a given probability. From similar comparisons it was concluded that there are no significant improvements in power output to be obtained by employing redundancies in subsystems other than the reactor.

Employing failure rates lower, by a factor of ten, than those for gas turbines (improved component technology) results in a significant improvement in the power profile as indicated in Fig. III-3 for the two-reactor (reference) system. However, providing a maintenance capability on board the system yields an even better improvement, even at the lower failure rate level. The maintenance level is indicated by the number of spares available for certain subsystems except the reactors, which are not maintained.

In general, any component or subsystem within the power system which affects the power output can be evaluated in terms of the power profile. The major problem is to relate the power decay to the trajectory requirements which in turn affect the vehicle mass. The importance of this is shown by the payload-to-gross weight ratio μ_L:

$$\mu_L = \left(1-\sqrt{\frac{\alpha_w J}{2\eta}}\right)^2$$

where α_w is the powerplant specific weight, η is the average thruster efficiency, and J is the low-thrust trajectory requirement. The quantity J, analogous to incremental velocity in high-thrust systems, is defined as

$$J \equiv \int_0^T \frac{a^2}{\epsilon(t)}\, dt$$

where a is the thrust acceleration over the powered time T and $\epsilon(t)$ is the fraction of initial power rating that is available as a function of time, that is, the power profile.

The trajectory optimization program developed in this study determines the thrust acceleration time-history which minimizes J subject to the power decay, the departure and arrival conditions, and the hyperbolic excess speeds at these conditions. Minimum J under these constraints assures minimum propellant expenditure. The development of the trajectory optimization program was a significant step in the analysis of hybrid-thrust systems, for not only can trajectory data be economically and accurately computed, but they may also be obtained under decaying power output and hyperbolic excess speeds at the same time.

The rapidity of the trajectory computation and the fact that power profiles may be included as an intimate part of the computation provides the mission analyst with a powerful tool. As mentioned previously, any component or subsystem which affects the power putput can now be related to the mission requirements, regardless of whether the cause is probabilistic, as in component failures, or deterministic, such as a radioisotope or solar cell power source.

Results of Mission Analysis

Favored Trajectory Characteristics

Trip times of 430, 530, and 630 days duration were chosen for the trajectory analysis. In order to determine the best possible combination of dates and corresponding leg durations, the total J (outbound and inbound) resulting from planetocentric rendezvous was calculated for several arrival dates and for various combinations of outbound and inbound legs that made up the total trip time under consideration. Figure III-4 shows the results for the 1980 opposition. Each total J plotted therein is optimum with respect to the allocation of inbound and outbound leg durations for a given arrival date at Mars. Thus Fig. III-4 presents the best trips in terms of minimum total J and arrival date for planetocentric rendezvous trajectories (parabolic conditions at the planets).

Of the two likely candidate arrival dates in each trip time, the one desired in terms of minimum mass is that arriving after the opposition (Julian date 2444294.8). This result is illustrated in Fig. III-5 wherein the vehicle mass for both the single- and dual-electric propulsion modes were calculated at each arrival date. As can be seen, arrival at about 4450 yields lower mass than arrival at 4150 for both the single- and dual-electric modes.

Of further interest is the fact that in this particular case the single-electric propulsion mode requires less mass than the dual system. That is, less mass is required if a single electric propulsion system is utilized for the entire trip. However the choice of either type of operating mode is not quite so clear. As discussed in further detail later, for some powerplant configurations

and probability level, the dual-electric system is lighter than the single. It is felt that the use of hybrid-thrust operation at both Earth and Mars will cause the mass differences to become slight so that the selection of a favored operating mode will rely on other considerations. Along these lines it should be noted that the dual-electric system requires a high powerplant and propulsion system reliability considering the exposure time to the space environment that the return electric stage must undergo. Although not investigated in detail, it appears that the design problems encountered in packaging two electric propulsion systems on a rotating spacecraft are much more difficult than the integration of only one electric system. These considerations coupled with the fact that the mass differences between the two modes are not major, led to selection of the single-electric operating mode for the subsequent hybrid-thrust optimization and power system integration.

From Fig. III-1, the radius of closest approach to the sun is about 0.45 AU, almost to Mercury's orbit, and occurs during the inbound leg. Such a passage distance will greatly impair the power system heat rejection effectiveness and strongly influence the design of the environmental control and protection systems for both the crew and the spacecraft subsystems. Attempts to increase the minimum solar passage distance by redistributing the leg times resulted in very high trajectory requirements but in practically no effect on the radius (Fig. III-6). Consequently the minimum solar radii in all of the trips considered were accepted as computed. Further consideration of the solar approach should be given in the design of the vehicle.

Optimum Hybrid-Thrust Mix

In the majority of trans-Mars or trans-Earth trips analyzed the use of hybrid thrust yields higher payload ratios than the all high-thrust mode, regardless of the type of high-thrust propulsion employed (chemical or nuclear). In some instances the differences have been minor, but in general the results are usually as depicted in Figs. III-7 and III-8. For the particular case indicated in Fig. III-7 the hybrid system always yields higher payload ratios than the all high-thrust chemical system no matter what the relative step inert fractions are.

For the nuclear case shown in Fig. III-8 the advantages are not quite so clear-cut. In most of the cases analyzed where the step inert fractions for the two applications (all high-thrust or hybrid) were calculated the hybrid system required less mass.

The influence of powerplant specific weight on the over-all payload ratio for the nuclear hybrid-thrust system was investigated, and the results are shown in Fig. III-9. The plot is based on the assumption that the corresponding high-thrust step inert fraction remains the same even though the inert weight of the powerplant changes. This is a reasonable assumption since, under the

optimization procedure employed, the portion of the transfer requirements provided by the high-thrust system changes slowly even though powerplant specific weight may change considerably. Two sets of assumed values for inert weight fractions (in parenthesis) are shown for the Earth-departure and Mars-capture steps.

Based on the assumption that the step inert weight fractions change slowly from an initial set of values, decreases in specific weight do not yield significant increases in payload fraction until the specific weight is reduced to below 10 kg/kw. Hence, reducing the specific weight from 25 to 10 kg/kw is apparently not worth the return in payload (or gross mass decrease) if such a reduction requires a major advance in power system technology. Although only a one-way trip is indicated here for an assumed set of inert weight fractions, essentially the same conclusions apply to round-trip manned missions at extended mission durations. This conclusion is discussed later.

It is also interesting to note from Fig. III-9 that lower inert fractions are advantageous. A change in the departure and arrival fractions from (0.20, 0.40) to (0.10, 0.30) results in about a 20% increase in payload ratio. The 0.10 inert fraction, however, is beyond current nuclear propulsion technology and is included here only to show that even under optimum hybrid-thrust operation, low inert fractions are desirable.

For cases where capture at the planet is effected by atmospheric entry via an ablative system or a high-drag device, hybrid-thrust operation can still be optimized for maximum payload ratio. This mode of operation has been performed for Earth-return trajectories, and sample results are illustrated in Fig. III-10. In the hybrid mode indicated, high-thrust propulsion (chemical or nuclear) is used for departure from Mars parking orbit, low-thrust propulsion for heliocentric transfer, and atmospheric entry for surface landing of the crew and scientific materials.

For an advanced Apollo-type ablative entry system whose mass varies with atmospheric entry velocity, the maximum payload ratios were found as a function of departure step inert fraction and powerplant specific weight. The results show, for example, that if the chemical system inert fraction is typically 0.10, the nuclear system inert fraction must be not more than 0.45 to be competitive, assuming the same specific weight in each case.

The powerplant specific weight is seen to affect the payload ratio significantly only near lower values of specific weight, essentially the same result obtained for the previously discussed hybrid-thrust mode. Whether the specific weight is 10 or 15 kg/kw, the payload ratio is essentially the same, whereas at 5 kg/kw the improvement in payload is about 10% over that at 10 kg/kw. The difficulty in attaining the necessary decrease in specific weight determines, in part, the attractiveness of the corresponding increase in payload.

The outbound leg of the Mars mission involves a high-thrust departure from Earth parking orbit, a heliocentric transfer by low-thrust electric propulsion, and a high-thrust capture onto a parking orbit at Mars. Extensive analysis of this trip to maximize payload ratio discloses that the optimum fraction of the impulsive hyperbolic excess speed provided by the high-thrust systems ranges from 0.5 to 0.8 for Earth departure and from 0.3 to 0.6 for Mars capture. To use this information for quick preliminary studies, the impulsive hyperbolic excess speed must be multiplied by the appropriate optimum fraction to obtain the speeds to be used in the trajectory optimization program. The value of J can thus be found based on the estimated hyperbolic speeds for Earth departure and Mars arrival. The impulsive hyperbolic excess speeds, for the dates under consideration, are found from either NASA SP-35, Planetary Flight Handbook, or by use of a ballistic trajectory computer program.

Mission Requirements

The mass required for different mission durations and powerplant specific weights and for optimum nuclear-plus-electric operation is given in Fig. III-11. These values of mass represent the most optimistic cases considered, since the output of the powerplant was assumed to be constant at 100% of the initial power rating.

The dotted curve indicates the mission requirements under a rendezvous Earth-return mode. That is, rather than return to Earth with a direct entry using an ablative system, the spacecraft is braked by the electric propulsion system during the heliocentric phase until Earth's heliocentric orbital velocity is matched. In this case a rendezvous vehicle must be launched from Earth to retrieve the crew and scientific materials which are at parabolic conditions with respect to Earth.

As can be seen, the mass required for the rendezvous mode is significantly higher than the system employing an ablative entry system. Viewed in an overall sense, the rendezvous mode is even more unattractive because an additional launch of at least a Saturn V is required whose payload delivered on Earth parking orbit should be charged against the mass requirements shown by the dotted curve of Fig. III-11. In subsequent studies the ablative entry mode at Earth was utilized for the foregoing reasons.

As hinted in the hybrid-thrust optimization discussion given previously, the powerplant specific weight has essentially no effect on the mass required, provided the mission duration is greater than 500 days and ablative Earth capture is employed. The insensitivity of mass to specific weight is important because of the currently contemplated specific weight values for the nuclear Rankine cycle power system.

A general comparison of different propulsion system capabilities is shown in Fig. III-12. The all-high-thrust vehicle mass requirements for three

different nuclear rocket technologies are compared against the hybrid-thrust requirements. Compared strictly on the basis of mass, it is seen that the hybrid-thrust propulsion system (solid-core nuclear plus electric) is essentially equivalent to advanced nuclear propulsion systems. This means that combining an electric propulsion system with a solid-core nuclear rocket yields the same benefits as the highly advanced nuclear rockets. For the Mars trip at least, and under the attendant assumptions, it is conceivable that, in terms of the technological advances required, the hybrid-thrust system could be developed earlier and would yield about the same advantages.

A closer comparison of the hybrid solid-core nuclear and electric mode against all high-thrust operation is shown in Fig. III-13 for trip times of 370 and 485 days. The hybrid-thrust system requires less mass compared to the nonmixed solid-core nuclear system for both trip times. In fact the hybrid mode is almost competitive with a later generation of nuclear rockets, i.e., powerplants having a specific impulse on the order of 2000 sec. In the case of the 485-day mission, the hybrid system using a 5 kg/kw specific-weight powerplant requires about the same mass as the liquid-core nuclear system.

Introduction of the power profiles for different maintenance and reliability levels allows a comparison of the tradeoff effects between these two levels. The results are presented in Figs. III-14, 15, and 16, respectively, for the 430-, 530-, and 630-day missions. It is seen that a "desirable" system consisting of infinite repair capability (except for reactors) and a probability level of 0.999 requires almost the same mass as a technologically "early" system mode of a nonmaintained powerplant operating at a probability of 0.99, assuming specific weight is the same. Also note that the percent decrease in mass resulting from lowering the probability level is approximately the same for both the zero-maintenance and infinite-maintenance uses. The effect of powerplant weight on vehicle mass is seen to be less for the maintained powerplant compared to the nonmaintained plant. This effect would indicate that lessening the trajectory requirement (i.e., maintaining the powerplant and operating at lower probability levels) aids in mitigating the influence of specific weight. This aspect becomes important when consideration is given to the effective distribution of development effort toward achieving desired power system operating characteristics.

The desirability of an onboard maintenance activity was investigated further by selecting different maintenance levels and including the accompanying effect on powerplant specific weight in the mass computations. The results are shown in Fig. III-17. As would be expected, increasing the maintenance activity raises the power profile at the expense of specific weight. Some point in the maintenance level should be reached where the advantages of the higher profile are more than offset by the increase in specific weight. For the specific trip shown in Fig. III-17, the minimum mass is reached at about a maintenance level of 126 spares where the corresponding specific weight is just above 16 kg/kw.

The location of the minimum-mass point depends on the relationship between the number of spares and specific weight. If specific weight increased slowly or was essentially constant, the obvious maintenance level to employ would be that giving practically 100% power throughout the mission time. The effect of optimum hybrid-thrust operation on the required powerplant rating (initial power) is illustrated in Figs. III-18 and 19 for the 530- and 630-day missions, respectively. Power required to perform the mission decreases with trip time but does not increase as the specific weight becomes higher, because as specific weight does increase the optimization process utilizes more of the high-thrust systems (especially Earth-departure) rather than the low-thrust system. Hence the required powerplant mass does not increase as fast as the specific weight, thereby resulting in lower initial powerplant ratings. As described before, the operating points for a power system applied to the missions studied herein can be found by superimposing the candidate power system's specific weight versus power curve over plots of the mission power requirements.

As mentioned briefly above, as specific weight increases the Earth departure step carries more of the trajectory load. This effect is depicted in Figs. III-20 and 21 for the 530- and 630-day missions, respectively. The trends of the Earth-departure nuclear propulsion system propellant mass (liquid hydrogen) are essentially the same as those displayed by the vehicle mass on orbit, primarily because the departure step mass is a significant fraction of the total mass.

The preceding discussion observes the results of the study mainly in terms of the mission requirements; however, as noted, the power system operating characteristics strongly influence the vehicle mass which in turn identifies favored technological levels and operating modes. The implications of the mission studies to the power system analysis are discussed in detail in Section VI.

Spacecraft Concepts

The basic vehicle configuration applicable to the assumed systems model depends in part on the number of powerplant modules required by the flight profile. Judging from the results of the mission studies discussed previously, there are trips which can be performed with a single power module under certain assumptions of maintenance and reliability levels. For mission durations greater than 500 days, the initial powerplant ratings are less than 4 Mw for hybrid-thrust vehicle operation (see Figs. III-18 and 19). The basic power module analyzed in Section VI is rated at 4 Mw (single reactor); hence it appears that a vehicle design concept may be developed employing one, rather than two, power module as previously required in some instances.

The basic spacecraft concept is formulated for a 530-day, manned Mars landing mission. This conceptual design illustrates the placement of the various transportation system components and indicates general problem areas associated with using a nuclear-electric powerplant in conjunction with high-thrust systems. It is assumed that artificial gravity is required for the crew. Two types of high-thrust propulsion are analyzed, as are two types of orbits about Mars.

In the previous analysis of the Mars mission, the MEM mass was kept constant at 45 metric tons for the purpose of identifying promising over-all flight profiles. For the analysis of spacecraft concepts in which the effect of orbital operations are included, the MEM is strongly affected by such operations, and hence its mass was computed accounting for the different velocity requirements.

Effects of Mars Orbit on Spacecraft Design

An important study parameter affecting the design of the spacecraft is the type of orbit established about Mars. For this study, two extremes are considered. One is a 926-km circular orbit with a period of about 2 hours. The other orbit is highly elliptic with an eccentricity of about 0.98 and a 30-day period. The periapsis distance is 926 km above the Martian surface.

It is assumed that the electric propulsion system brakes the spacecraft to nearly parabolic speed upon approaching Mars. An additional ΔV is supplied by a high-thrust system to establish the desired orbit about Mars. If a circular orbit is desired, the spacecraft must retro-brake from some fraction of the V_∞ remaining from the low-thrust braking to circular velocity. The MEM then must de-orbit from this circular orbit, descend to the surface, ascend to the circular orbit, and rendezvous with the spacecraft. For this sequence of maneuvers, the propulsion required for the spacecraft to establish orbit is relatively large, while the MEM propulsion is minimized. Conversely, if a highly elliptical orbit is required, the propulsive braking required for the spacecraft is very small, since the orbit is nearly parabolic and the initial conditions are just above parabolic. The corresponding MEM propulsion is large since the de-orbit from the ellipse to the surface requires a large ΔV.

These operational modes have a profound effect on the size and weight of the MEM vehicle. Figure III-22 compares two MEM vehicles. Each vehicle consists of a basic 3.2-metric-ton command module which includes arresting gear and landing structure. The propellant is O_2/H_2 with a specific impulse of 430 sec.

Major Spacecraft Propulsion

The spacecraft design considered for this study does not include the Earth escape stage. The major high-thrust propulsion stages are for Mars capture and Mars escape. These primary stages use graphite-core nuclear engines with LH_2. Figure III-23 illustrates the general layout for the Earth-escape payload. The electric propulsion system used during the heliocentric transfer occupies one end of the spacecraft. The high-thrust systems are located at the opposite end. The Mars capture tanks and engine are jettisoned after the propellant is expended. The Mars escape tanks, engine, and structure are retained.

Spacecraft Definition

The spacecraft is essentially of modular construction. The electric powerplant, thrusters, solar shelter, ERM, and the manned modules comprise a basic section of the spacecraft which is independent of the type of high-thrust propulsion. As shown in Fig. III-23, the Mars capture and escape stages can be varied according to the requirements for orbital capture.

The mass of the spacecraft is centered around the axis of rotation. However, only the electric powerplant, solar shelter, and manned modules rotate. The compartment housing the ERM and the MEM and the high-thrust propulsion systems are nonrotating. The electric powerplant occupies one extremity of the spacecraft. Radiation shielding is installed at the reactor to provide a 30-deg half-angle shadow for the spacecraft. This shielding is in the plane of the manned modules. Conceivably, only the manned modules need rotation. However, the shadowing shielding would be required for the entire 360-deg sweep of the rotating modules. The corresponding weight of the radiation shielding would be very large. Therefore, for this spacecraft concept, only small "ears" are required for the shadow shielding, since the shielding rotates with the manned modules.

The thrusters are located in four panels which are erected radially from their stowed position in the outer vehicle skin surrounding the solar shelter. The size of the thruster array will vary considerably, depending on the type of thrusters used. It is assumed that 4 megawatts (electric) are supplied to the thrusters. If cesium contact thruster modules are used, the total required area of the thruster array is about 60 square meters. The use of mercury electron-bombardment modules would increase the total thruster panel area requirement to about 650 square meters. These areas assume that 26% to 28% of the thrusters are spares. Figures III-23 and III-24 illustrate, schematically, the thruster panels and cesium tanks.

The solar shelter is located between the electric powerplant and the manned module assembly. This module is used primarily for protection against solar radiation, predominantly solar flare protons. During these solar flares,

the rotation of the spacecraft is stopped. All crew members enter the shelter through the central hub of the rotating structure. The shelter contains basic control and communication instrumentation, and life support facilities for continuous periods up to 3 or 4 days duration. This module is also occupied during thrusting of the high-thrust nuclear propulsion systems.

The next section of the spacecraft is the manned modules with the accompanying extendable arms. These arms telescope inward during major high-thrust maneuvers to minimize structural bending. The two manned modules are extended to a radius of 25 meters during the phases of the mission in which artificial gravity is required. This spin radius is somewhat arbitrary, but was chosen as a compromise. The vehicle rotates at a rate of 0.4 rad/sec to provide a force of 0.4 g's at the floor of each module. It is assumed that one g is not necessary to permit proper functioning of the body organs. This combination of spin radius and spin rate lies within the currently accepted "comfort zone", which is partly based on data from centrifuge tests and the "slow-rotating room" tests where head movements and rotational rates are correlated relative to their effects on inner ear "canal sickness". One module is the primary command and control center for the spacecraft and is normally occupied by four men. The other module is a scientific module which serves as the crew's living and recreation area and contains the primary life support equipment. Also included in this module is the scientific equipment required for the mission.

The Earth-entry module is located at the centerline of the spacecraft adjacent to the manned-module unit. This vehicle is stowed in an interior location and is protected from the flight environment. It is capable of returning eight men to Earth with atmospheric braking, at speeds up to 20 km/sec. This entry vehicle also delivers scientific data, equipment, and materials to Earth.

The remainder of the spacecraft consists of the MEM vehicle and the Mars capture and escape stages.

Spacecraft Weights

The weights of the various spacecraft components are summarized in Table III-1 for two types of high-thrust propulsion systems and two types of orbits about Mars. The first eight items are the same for each system. A contingency of 4.5 metric tons is included for radiation shielding with high-thrust nuclear systems. The weight of the MEM is dependent on the orbital operations and is summarized in Table III-2 for the circular and elliptical orbital modes. Table III-3 summarizes the weights of the propellant and tanks for the Mars capture and escape maneuvers.

The minimum Earth escape payloads occur when the elliptic Mars orbit is utilized, with the chemical Mars stages resulting in slightly less over-all mass required. The circular orbit mission increases the mass requirements of

the Earth escape payload by about 27% for solid-core nuclear propulsion and about 47% for chemical.

Approaches to Minimizing Mass Requirements

Because of the importance placed on minimizing the mission mass requirements, and in order to effectively utilize the Saturn V booster, the results of the entire study were reviewed to delineate those considerations which tend to reduce the vehicle system mass. These items, given below, are relevant to the data and results generated during the performance of the study and the listing of these items is not meant to be conclusive or complete.

1. Trajectory Profile. For a given mission duration and planetary stay time, the distribution of outbound and inbound leg durations should be analyzed to determine the set which minimizes mass. This approach holds whether the propulsion systems employed are all high-thrust or mixed with electric systems. In terms of the total trip time, variations in this time should produce the optimum duration for all high-thrust systems. For hybrid operation the mass requirements decrease monotonically with mission duration; hence extended durations are desirable.

2. Hybrid-thrust Operation. The use of optimum combined high- and low-thrust systems requires less mass than the corresponding all high-thrust mode in the majority of trips analyzed to date. Hybrid-thrust operation, furthermore, is technologically appealing for, as was shown previously, it is equivalent in performance to highly advanced nuclear propulsion systems. The results of other related planetary mission studies (e.g., NAS2-2928) also indicate that hybridization is at least comparable in mass to all high-thrust modes applied to the easiest unmanned probe trips. The high-thrust system to be mixed with low-thrust should be a solid-core nuclear rocket.

3. Ablative Earth Entry. At the outset of the study it was believed that, by eliminating the Earth-entry mode and using a pickup vehicle to rendezvous with the returning spacecraft, some mass savings would result. Under hybrid-thrust operation this belief was not borne out. Significant reductions in mass are available if an advanced ablative (Apollo-type) Earth-entry system is utilized rather than an Earth rendezvous and pickup (at parabolic conditions).

4. Power System Maintenance. An onboard maintenance program should be provided to allow astronaut-initiated repair of any failed component or subsystem. This aspect is sufficiently strong to override considerations of reducing system specific weight. The optimum maintenance level can be established by analyzing the mass required for each maintenance level and its corresponding specific weight. An auxiliary advantage of maintenance is the reduced requirements on component failure rate and corresponding technology.

5. Probability Level. As would be expected, the lower power system operating probability reduces the vehicle mass. This results in exchanging an intangible requirement (system reliability) with a tangible benefit (mass reduction). However, regardless of the influence on mass, the high reliability level will prevail for the manned missions.

It should be noted that items 4 and 5 are probabilistic in nature, and the corresponding vehicle mass required reflects the expectation of failure within the power system.

6. Powerplant Specific Weight. Reductions in vehicle mass become significant for the longer mission durations if specific weight can be reduced by an order of magnitude from the values currently contemplated.

7. Planetary Parking Orbit Operations. The type of parking orbit (and the period) utilized with respect to the stay time is an important parameter in the over-all mission and flight-profile optimization study. The two extreme cases briefly studied herein (low circular and highly elliptic, near-parabolic orbits) indicate that a tradeoff exists between the mass of the MEM and the main spacecraft for various choices of parking orbit conditions and operational modes among the two foregoing extremes.

8. Spacecraft Propulsion. In accounting for different Mars parking orbits and operational modes, the velocity requirements on the parent spacecraft change sufficiently such that both nuclear and chemical propulsion systems should be analyzed to determine which yields less mass.

For a proper evaluation of the hybrid-thrust mix, the considerations in both items 7 and 8 should be made an integral part of the over-all hybrid-thrust optimization procedure.

TABLE III-1

SPACECRAFT WEIGHT SUMMARY
(metric tons)

	Circular Orbit		Elliptic Orbit	
	Nuclear	Chemical	Nuclear	Chemical
Powerplant (4 mwe, nom.)	45.36	45.36	45.36	45.36
Cesium	72.26	72.26	72.26	72.26
Earth Re-Entry Module	7.93	7.93	7.93	7.93
Thrusters & Structure	2.27	2.27	2.27	2.27
Command Module	14.20	14.20	14.20	14.20
Service & Scientific Module	14.20	14.20	14.20	14.20
Solar Shelter	11.35	11.35	11.35	11.35
Structure	4.53	4.53	4.53	4.53
Radiation Shielding	4.53	---	4.53	---
Mars Excursion Module	36.70	36.70	88.50	88.50
Mars Escape Step	72.40	85.40	17.40	14.70
Mars Capture Step	103.00	139.53	25.06	18.16
Miscellaneous	1.36	1.36	1.36	1.36
TOTALS	390.08	435.08	308.94	294.81

TABLE III-2

MEM WEIGHT SUMMARY
(kilograms)

	O_2/H_2 Chemical	
	Circular Orbit	Elliptic Orbit
Basic 4-Man Module	3170	3170
Rendezvous Step	158	1950
Mars Ascent Step	7590	11650
Mars Landing Step	24740	38100
De-Orbit Step	1042	33630
TOTAL MEM WEIGHT	36700	88500

TABLE III-3

MARS ESCAPE STAGE
(metric tons)

	Circular Orbit		Elliptic Orbit	
	Nuclear	Chemical	Nuclear	Chemical
Mars Escape Payload	145.00	140.50	145.00	140.50
Engine	10.00	0.77	6.80	0.68
Tank Structure	5.90	4.86	1.04	0.77
Boil-Off & Insulation	4.70	2.40	1.26	0.64
Meteroid Protection	6.50	0.14	1.50	0.36
Propellant	45.50	77.23	6.80	12.25
TOTALS	217.40	225.90	162.40	155.20

MARS CAPTURE STAGE
(metric tons)

	Circular Orbit		Elliptic Orbit	
	Nuclear	Chemical	Nuclear	Chemical
Mars Capture Payload	250.90	259.40	247.73	240.53
Engine	12.25	1.00	11.35	0.91
Tank Structure	8.62	6.63	1.36	1.04
Boil-Off & Insulation	6.17	3.37	1.54	0.82
Meteoroid Protection	7.90	1.64	1.73	0.41
Propellant	68.00	126.90	9.08	14.98
TOTALS	353.84	398.94	272.79	258.69
Outbound Cesium	36.24	36.24	36.24	36.24
Earth Escape Payload (Approx.)	390	435	310	295

TYPICAL HYBRID – THRUST FLIGHT PROFILE

630 – DAY MARS MISSION

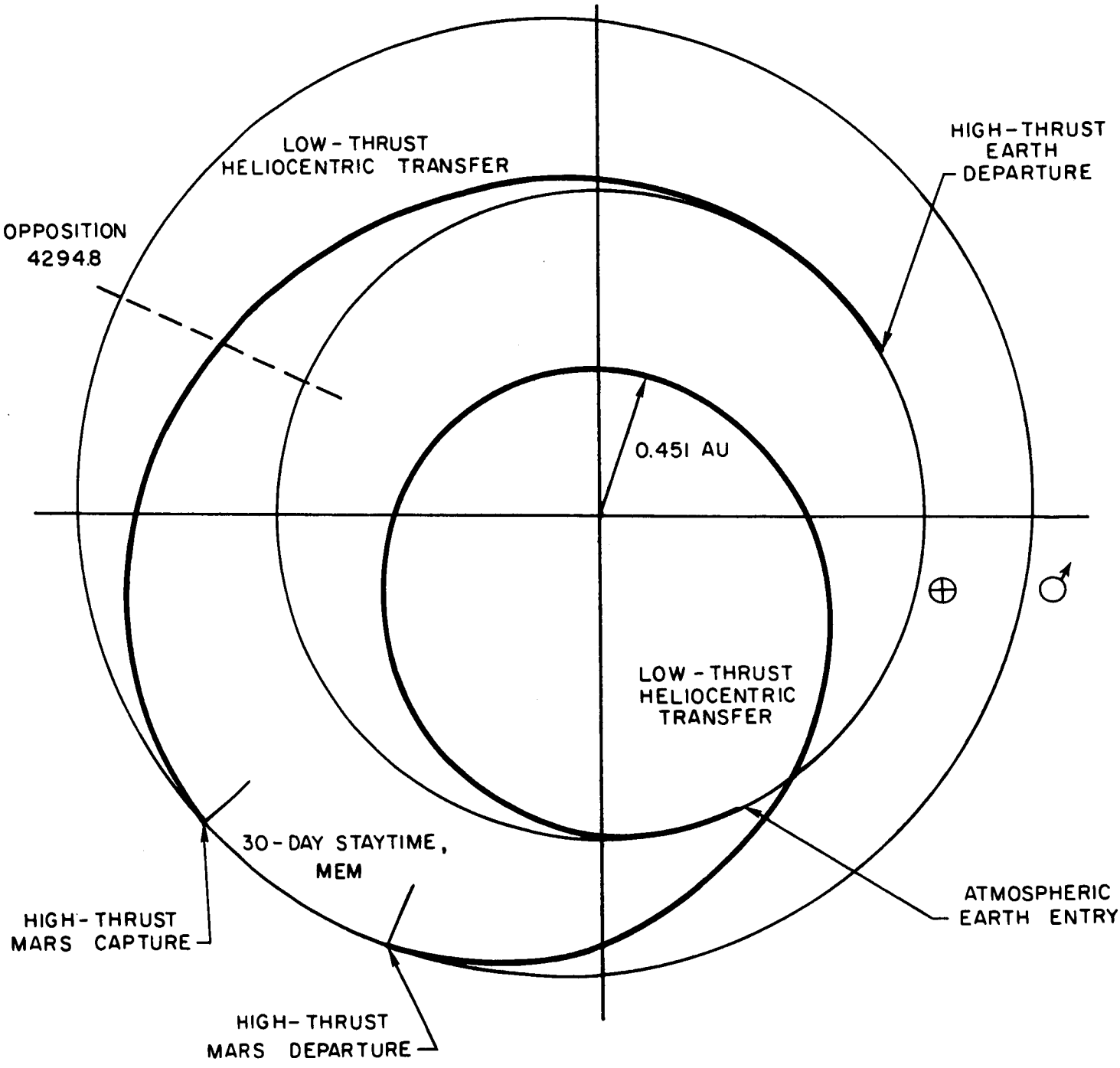

FIG. III-2

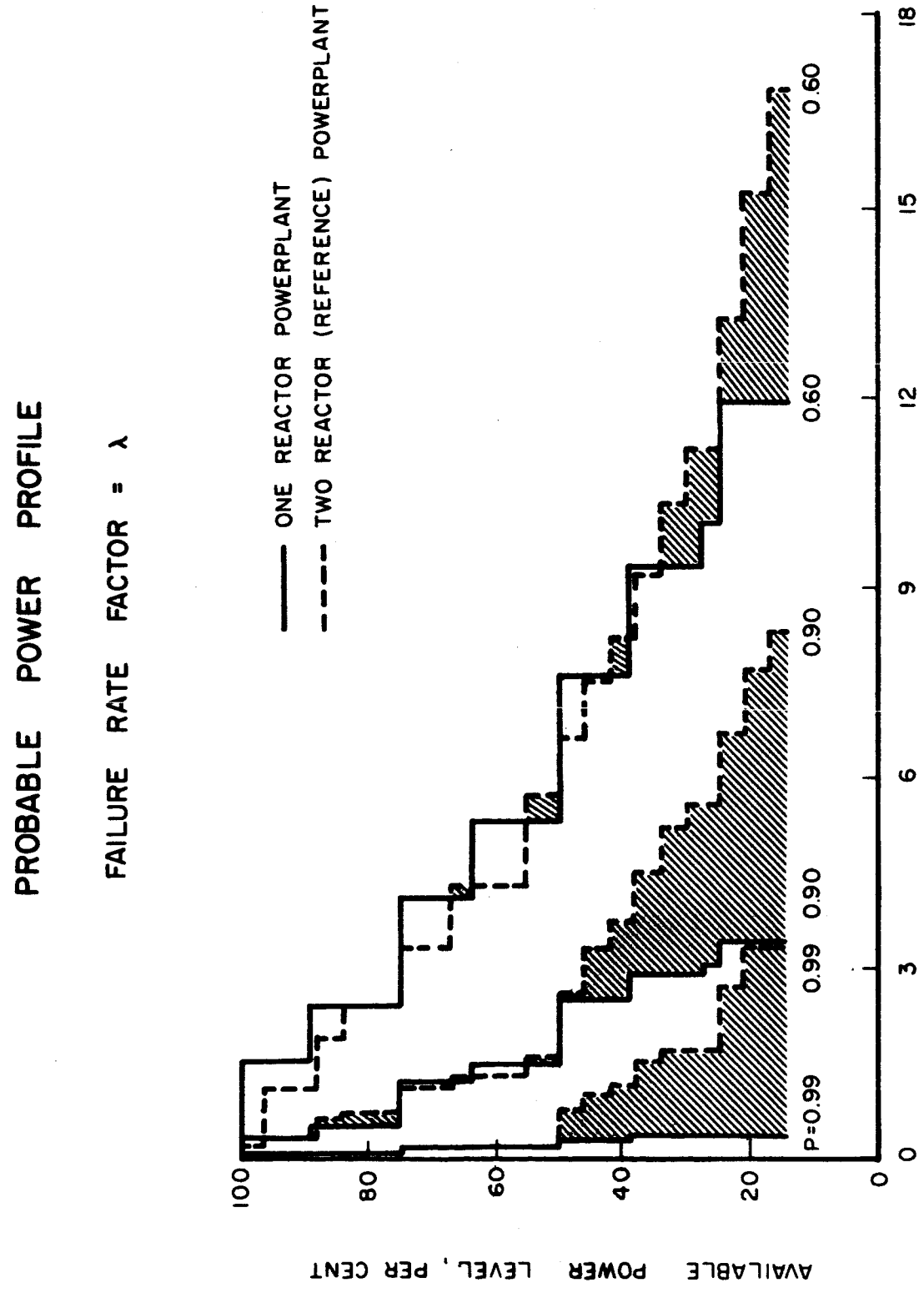
PROBABLE POWER PROFILE
FAILURE RATE FACTOR = λ
ONE REACTOR POWERPLANT
TWO REACTOR (REFERENCE) POWERPLANT
AVAILABLE POWER LEVEL, PER CENT
MISSION TIME, 1000 HR
P=0.99
0.99
0.90
0.90
0.60
0.60
0
20
40
60
80
100
0
3
6
9
12
15
18

FIG. III-3

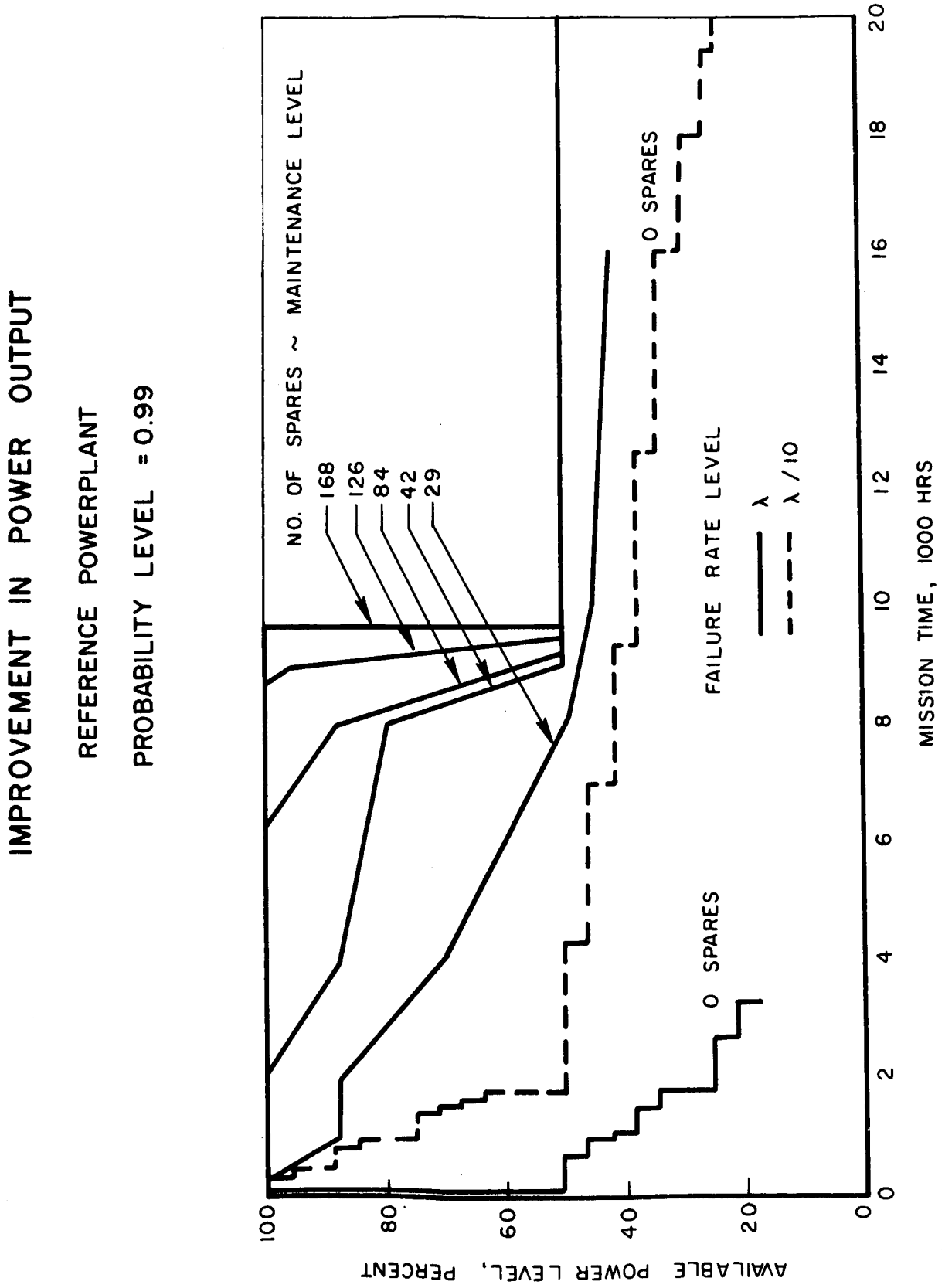
IMPROVEMENT IN POWER OUTPUT
REFERENCE POWERPLANT
PROBABILITY LEVEL = 0.99
NO. OF SPARES ~ MAINTENANCE LEVEL
168
126
84
42
29
0 SPARES
0 SPARES
FAILURE RATE LEVEL
λ
λ / 10
AVAILABLE POWER LEVEL, PERCENT
MISSION TIME, 1000 HRS
100
80
60
40
20
0
0
2
4
6
8
10
12
14
16
18
20

OPTIMUM LOW THRUST RENDEZVOUS TRAJECTORY REQUIREMENTS

30-DAY STAYTIME
1980 MARS ROUNDTRIPS

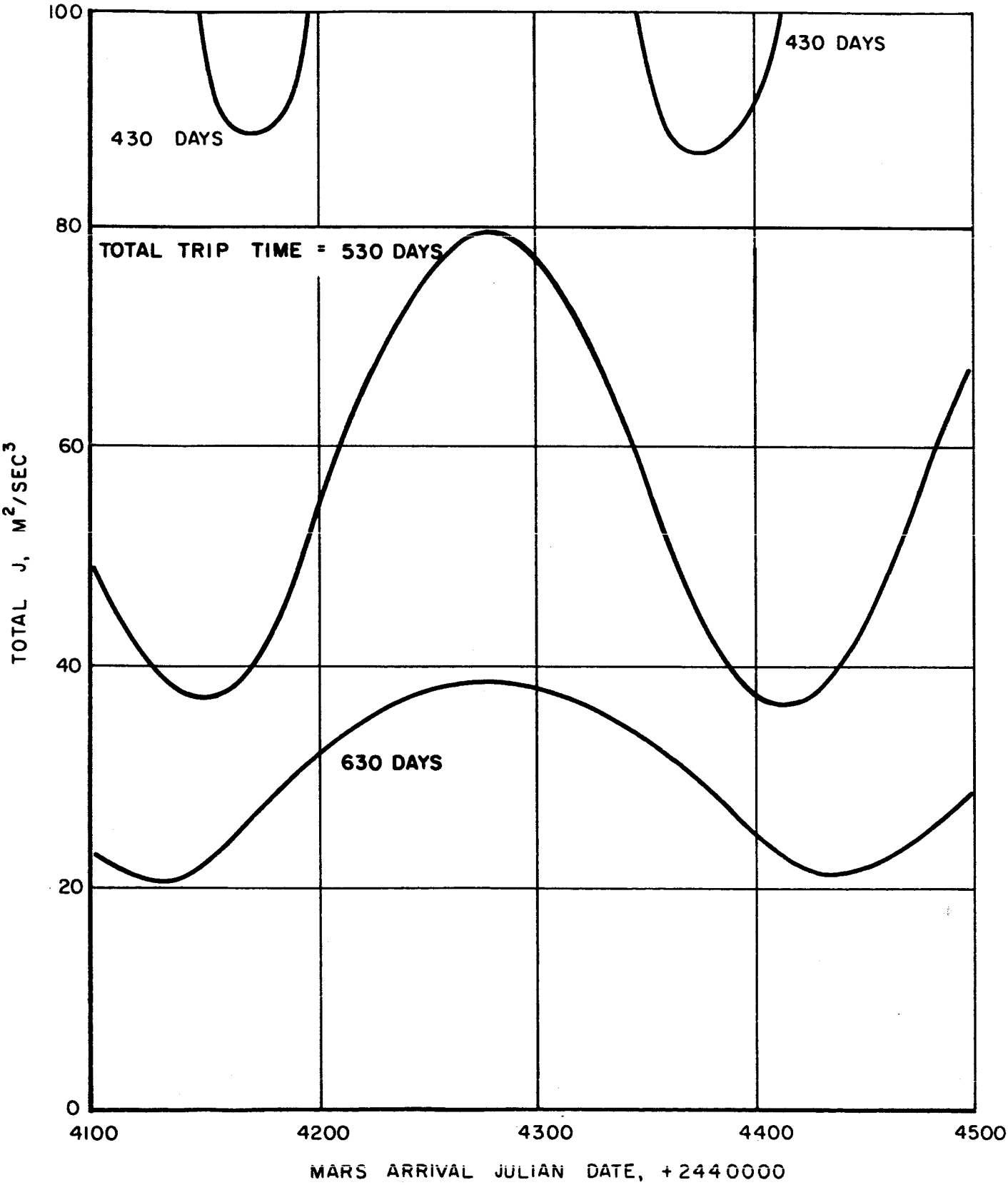

FIG. III-5

COMPARISON OF SINGLE AND DUAL ELECTRIC SYSTEMS

ONE-REACTOR POWERPLANT
IMPROVED TECHNOLOGY
POWER SYSTEM
PROBABILITY= 0.75

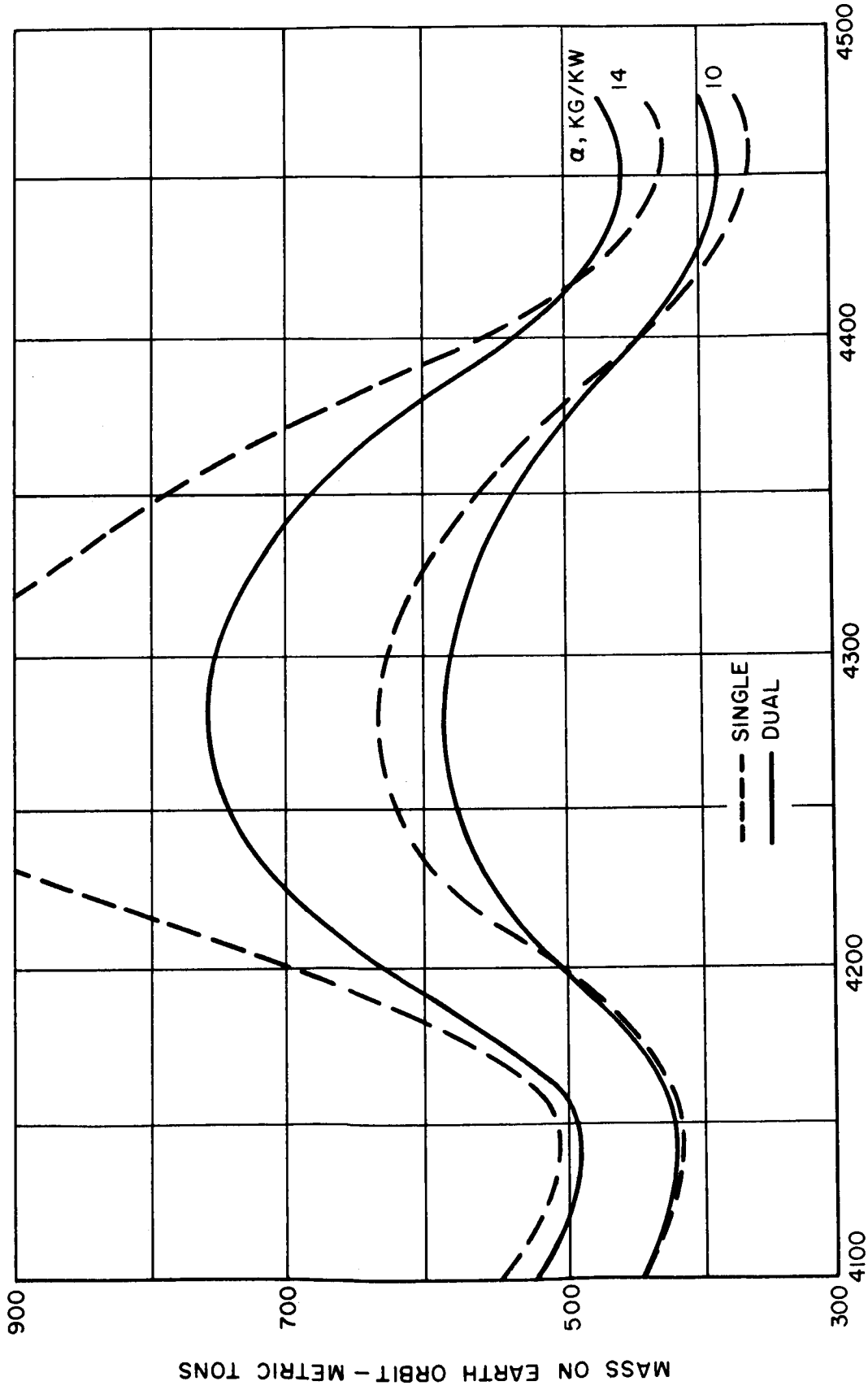

EFFECT OF DISTRIBUTION OF LEG TIME

TOTAL TRIP TIME = 630 DAYS
ARRIVE MARS 4450

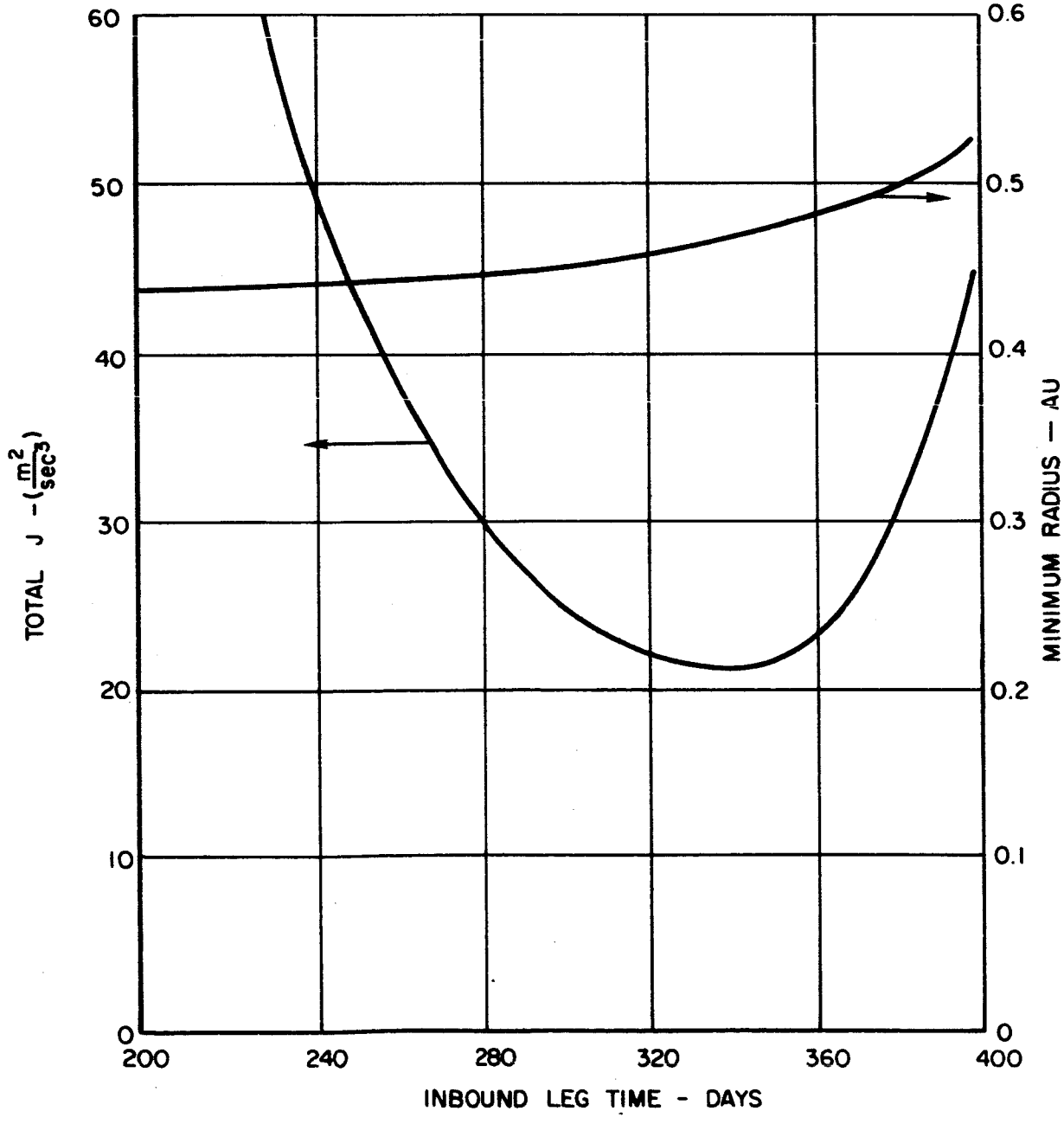

FIG. III-7

MAXIMUM PAYLOAD RATIOS

α_w = 10 KG/KW

LV ⊕ 4170 AR ♂ 4450

——— CHEMICAL + ELECTRIC + CHEMICAL

– – – CHEMICAL + CHEMICAL

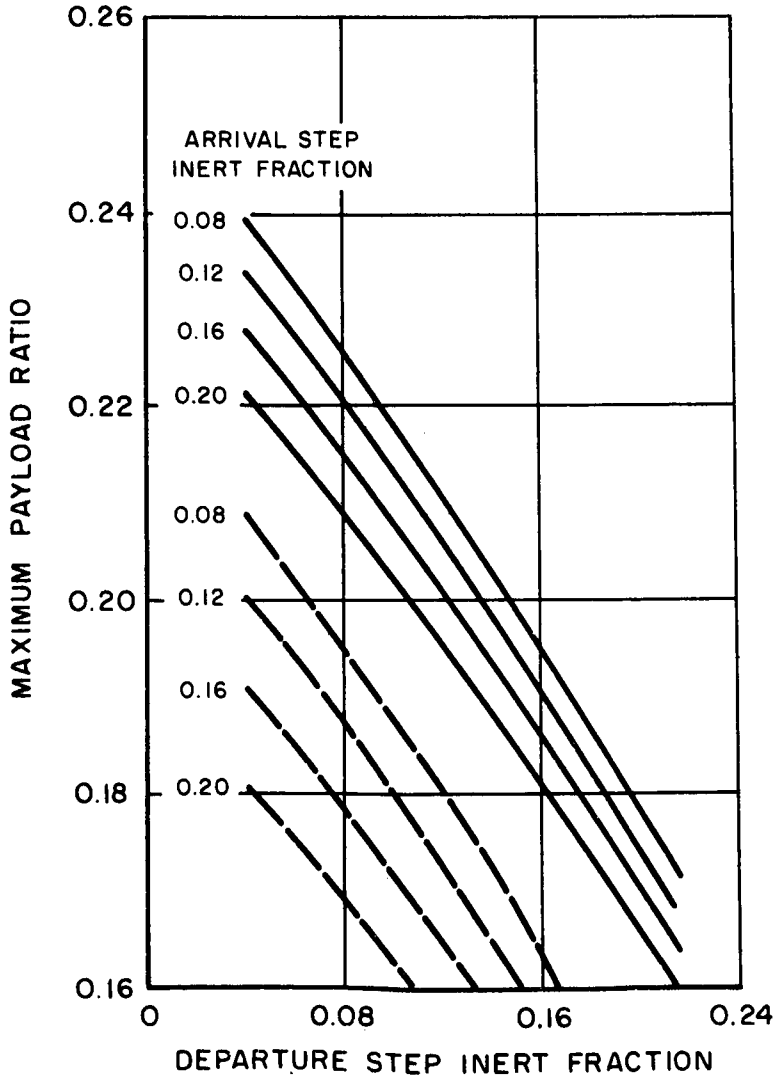

MAXIMUM PAYLOAD RATIOS

α_w = 10 KG/KW

LV ⊕ 4170 AR ♂ 4450

——— NUCLEAR + ELECTRIC + NUCLEAR

— — — NUCLEAR + NUCLEAR

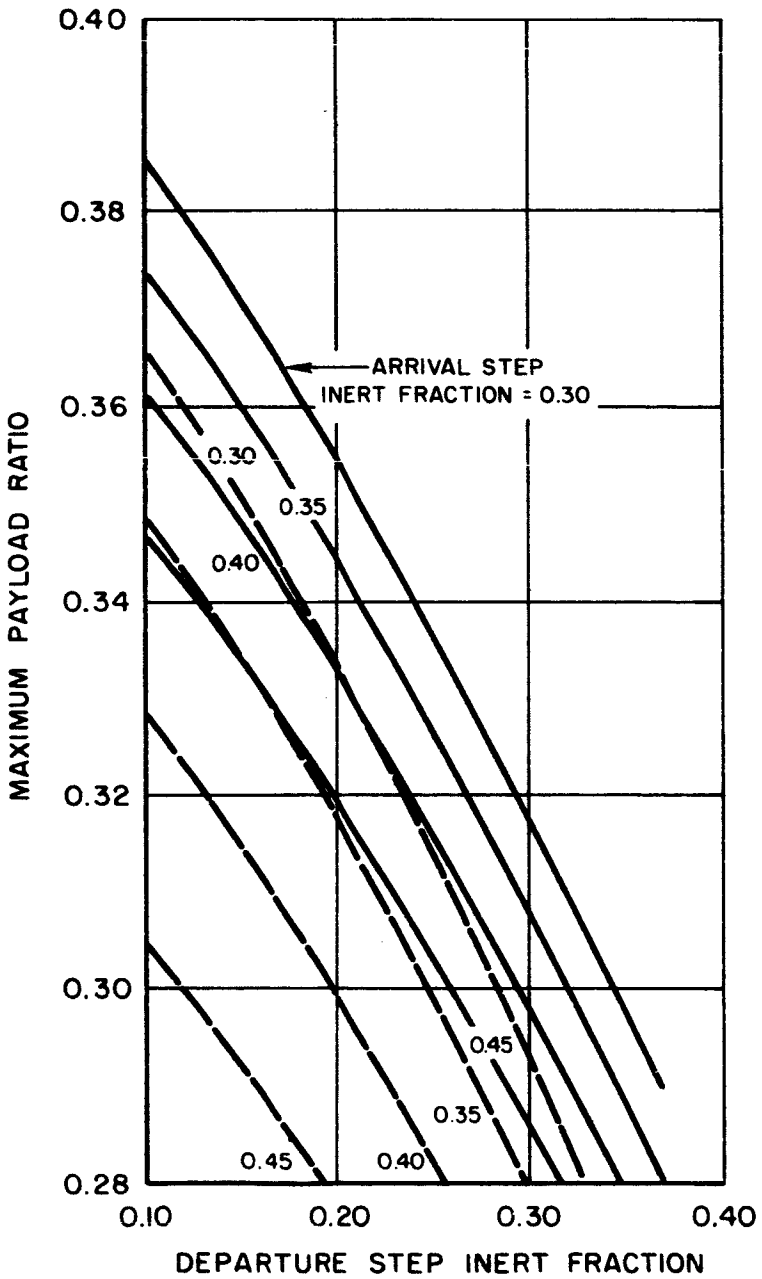

INFLUENCE OF POWERPLANT SPECIFIC WEIGHT

NUCLEAR + ELECTRIC + NUCLEAR

LV ⊕ 4170 AR ♂ 4450

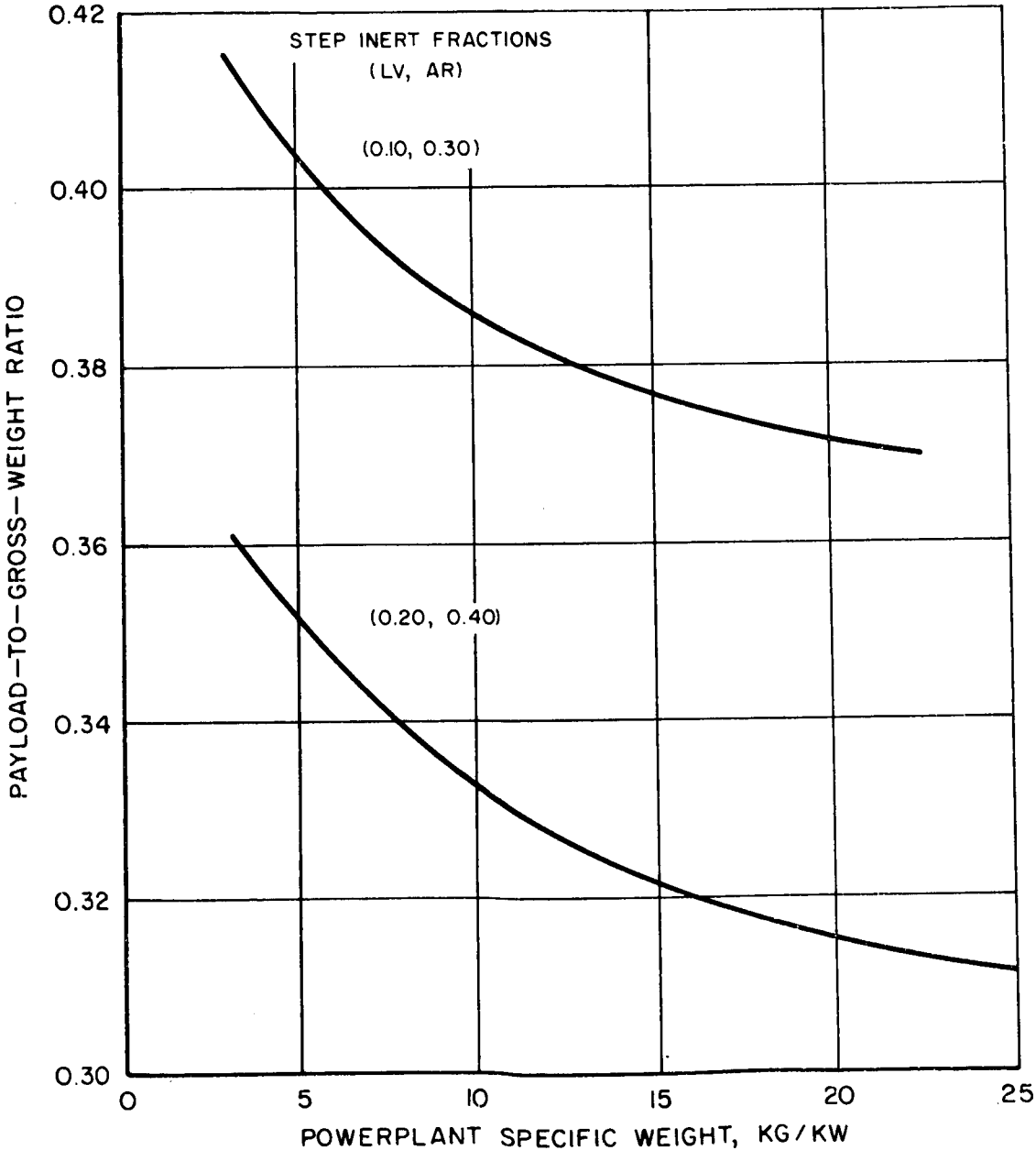

MAXIMUM PAYLOAD RATIOS

HIGH—THRUST + ELECTRIC + ATMOSPHERIC ENTRY

LV ⊕ 4405 AR ♂ 4645

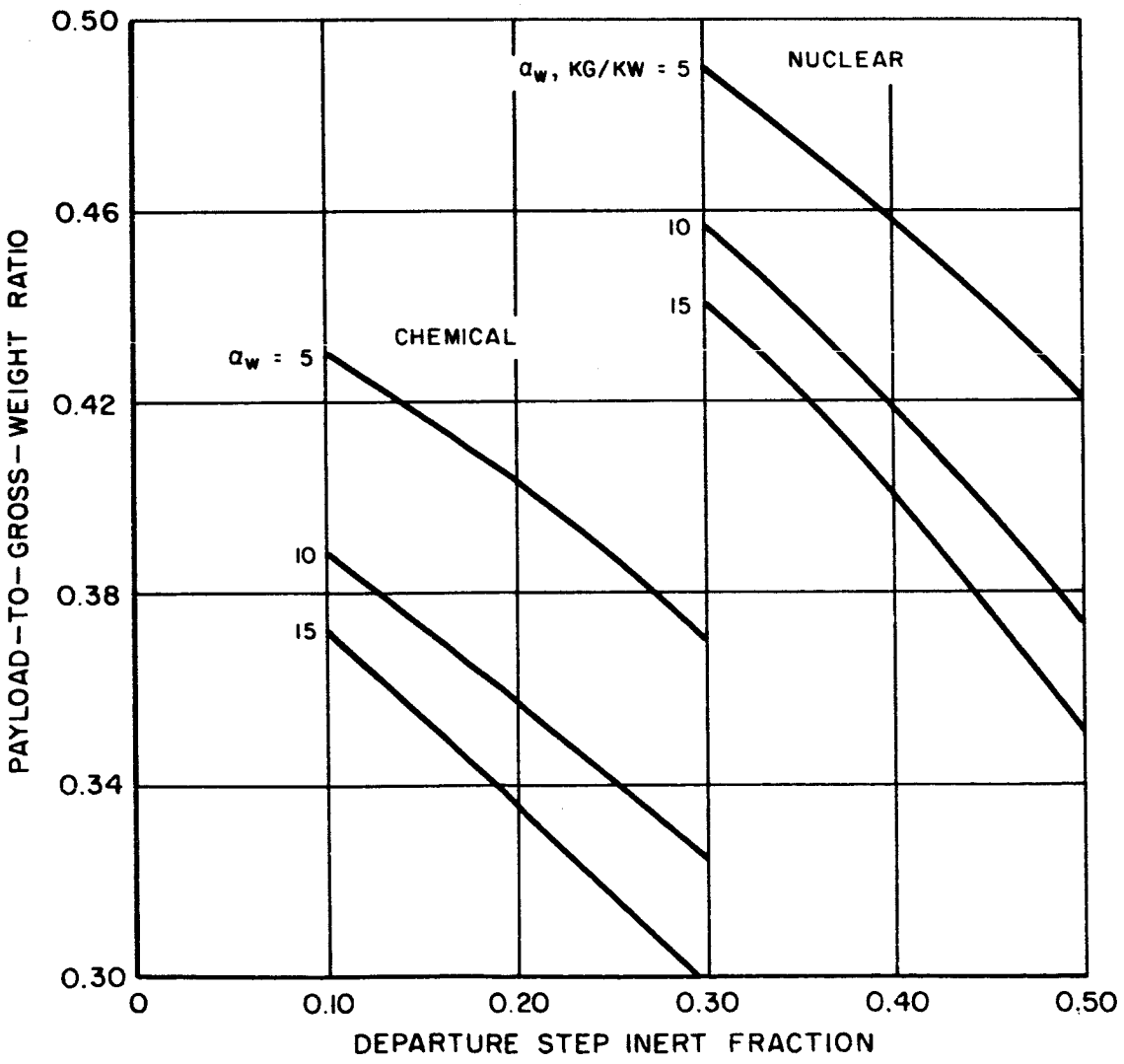

EFFECT OF SPECIFIC WEIGHT ON VEHICLE MASS

MARS ROUNDTRIP MISSION

OPTIMUM HYBRID - THRUST OPERATION

VARIABLE LOW - THRUST

NO POWER LOSS

30 - DAY STAYTIME

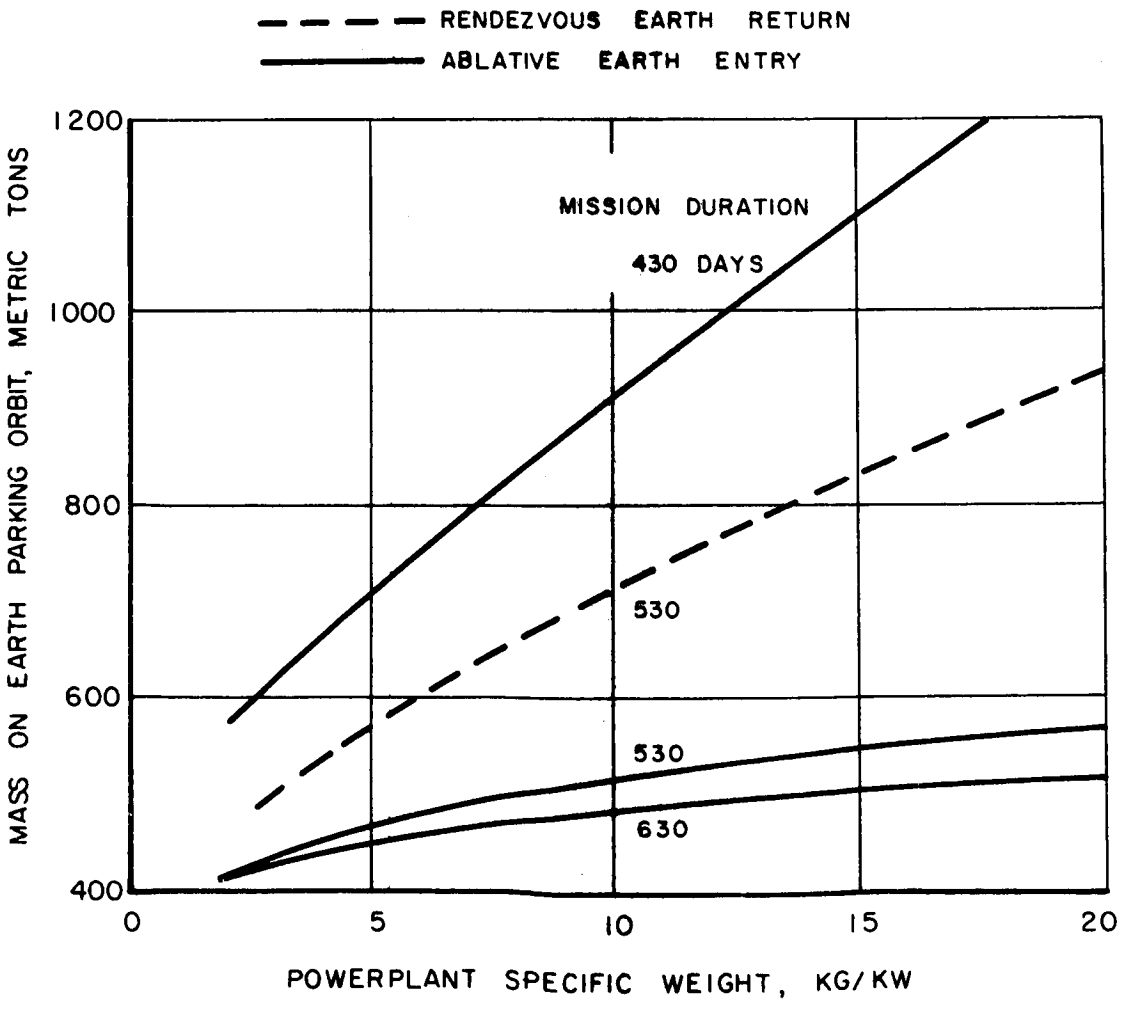

COMPARISON OF MISSION REQUIREMENTS FOR VARIOUS PROPULSION SYSTEMS

1980 MARS MISSION
30-DAY STAYTIME

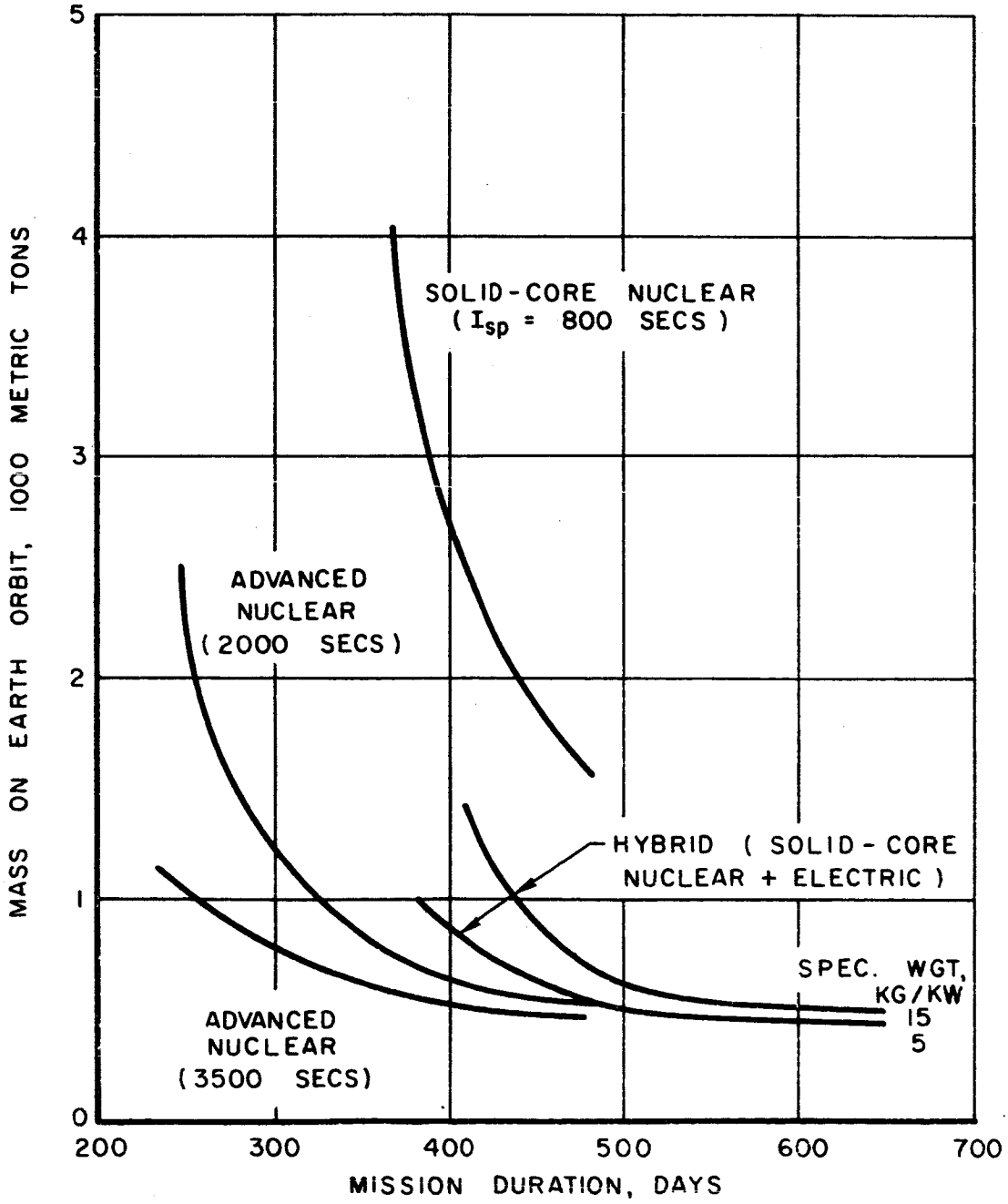

COMPARISION OF HIGH-LOW MIXED-THRUST AND NONMIXED-THRUST SYSTEMS

30-DAY STAYTIME
1980 MARS ROUNDTRIP

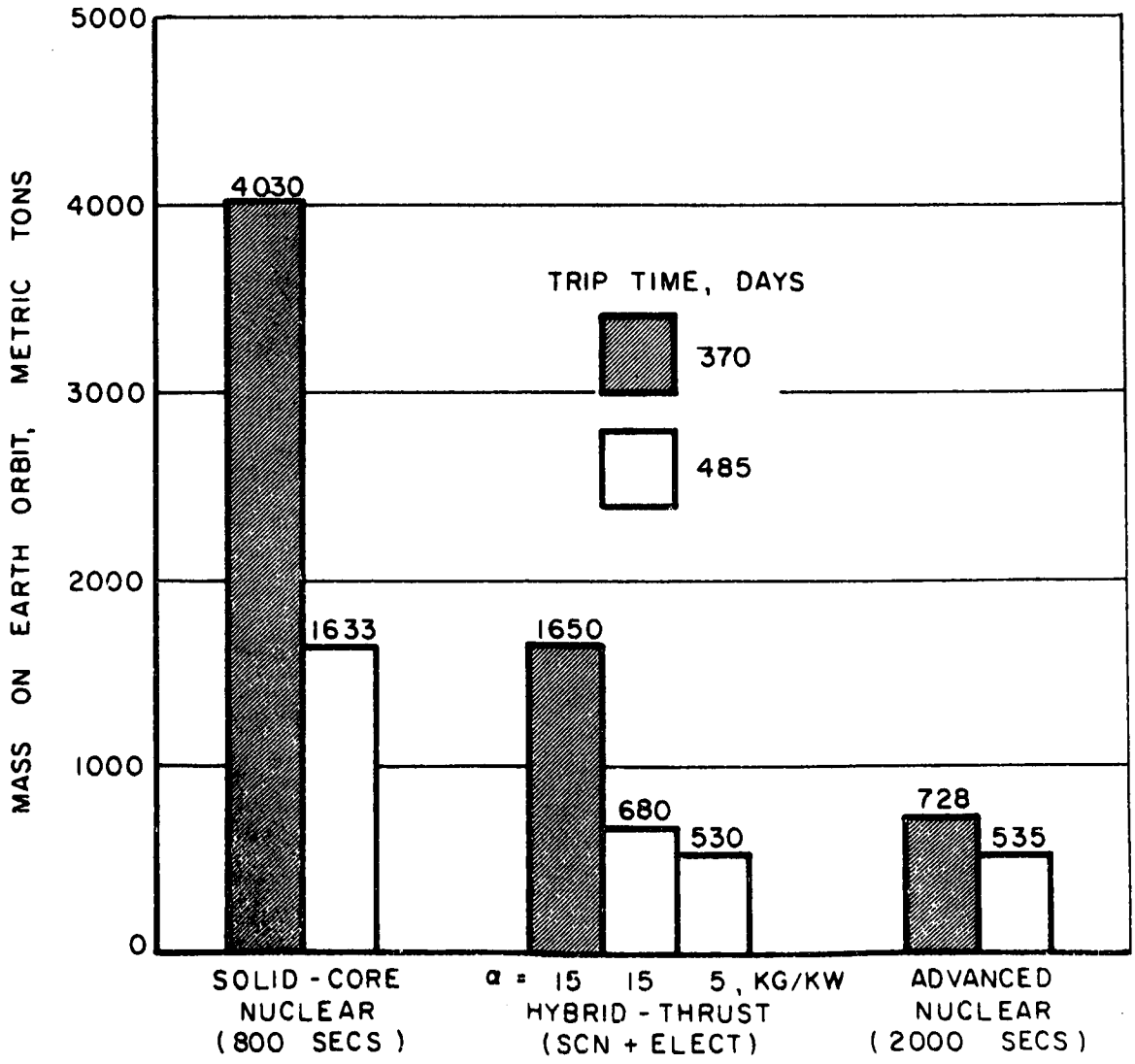

EFFECT OF POWERPLANT ON VEHICLE MASS

430 DAY MISSION

OPTIMUM NUC + ELECT OPERATION

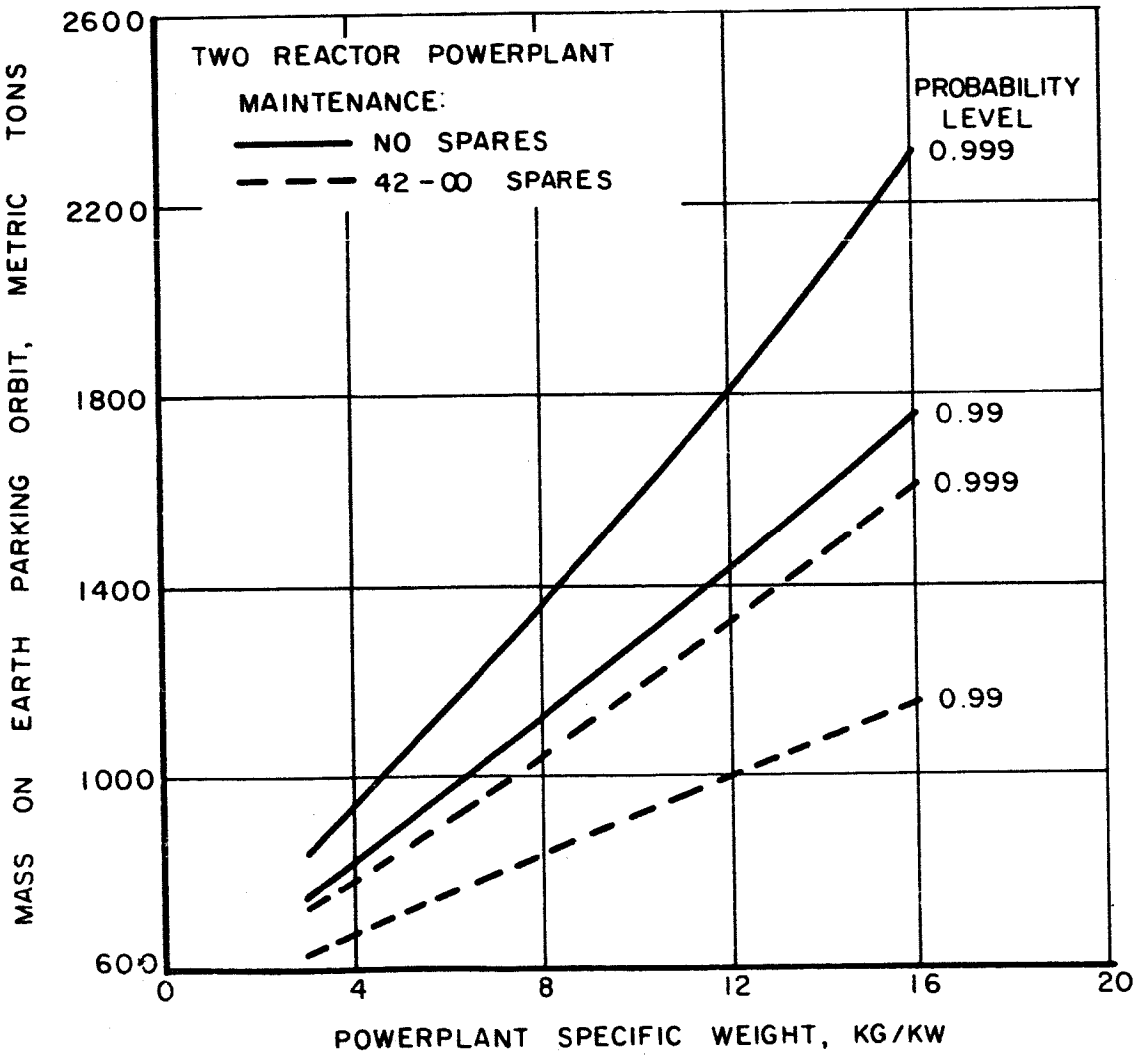

EFFECT OF POWERPLANT ON VEHICLE MASS

530 DAY MISSION

OPTIMUM NUC + ELECT OPERATION

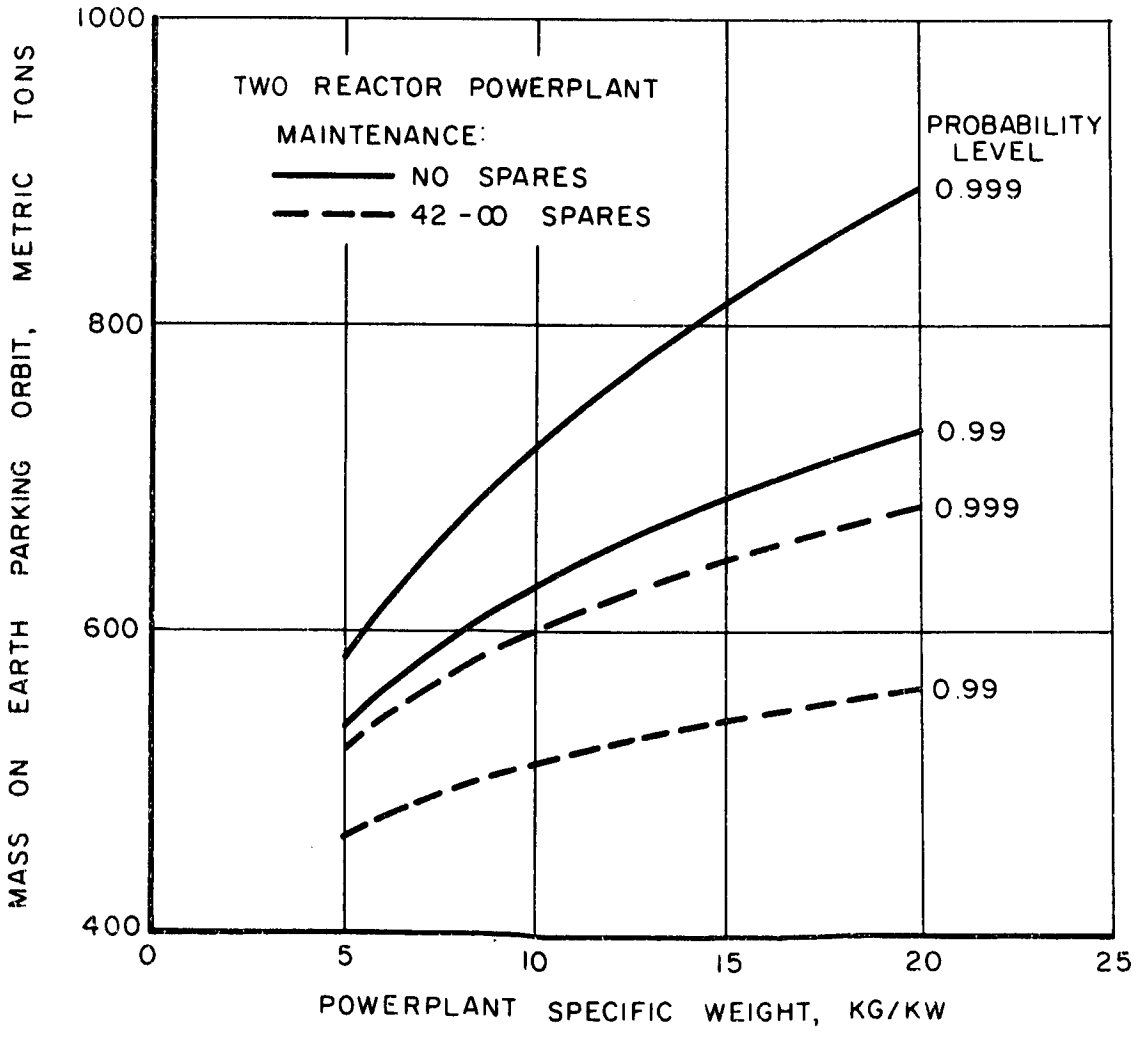

EFFECT OF POWERPLANT ON VEHICLE MASS

630 DAY MISSION

OPTIMUM NUC + ELECT OPERATION

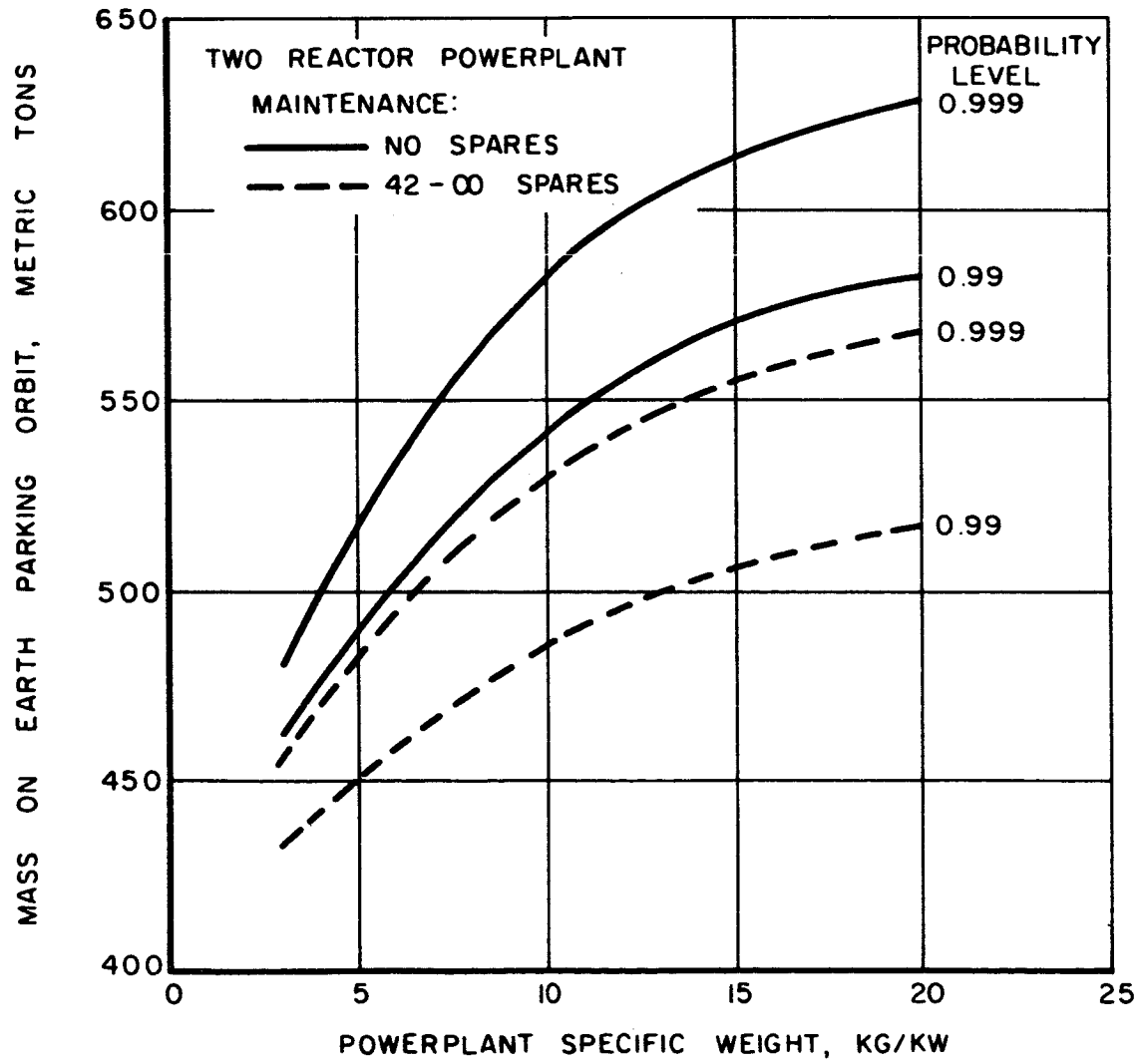

EFFECT OF POWERPLANT MAINTENANCE LEVEL ON VEHICLE MASS

530 - DAY MARS ROUNDTRIP

MAINTENANCE LEVEL = NO. OF SPARES

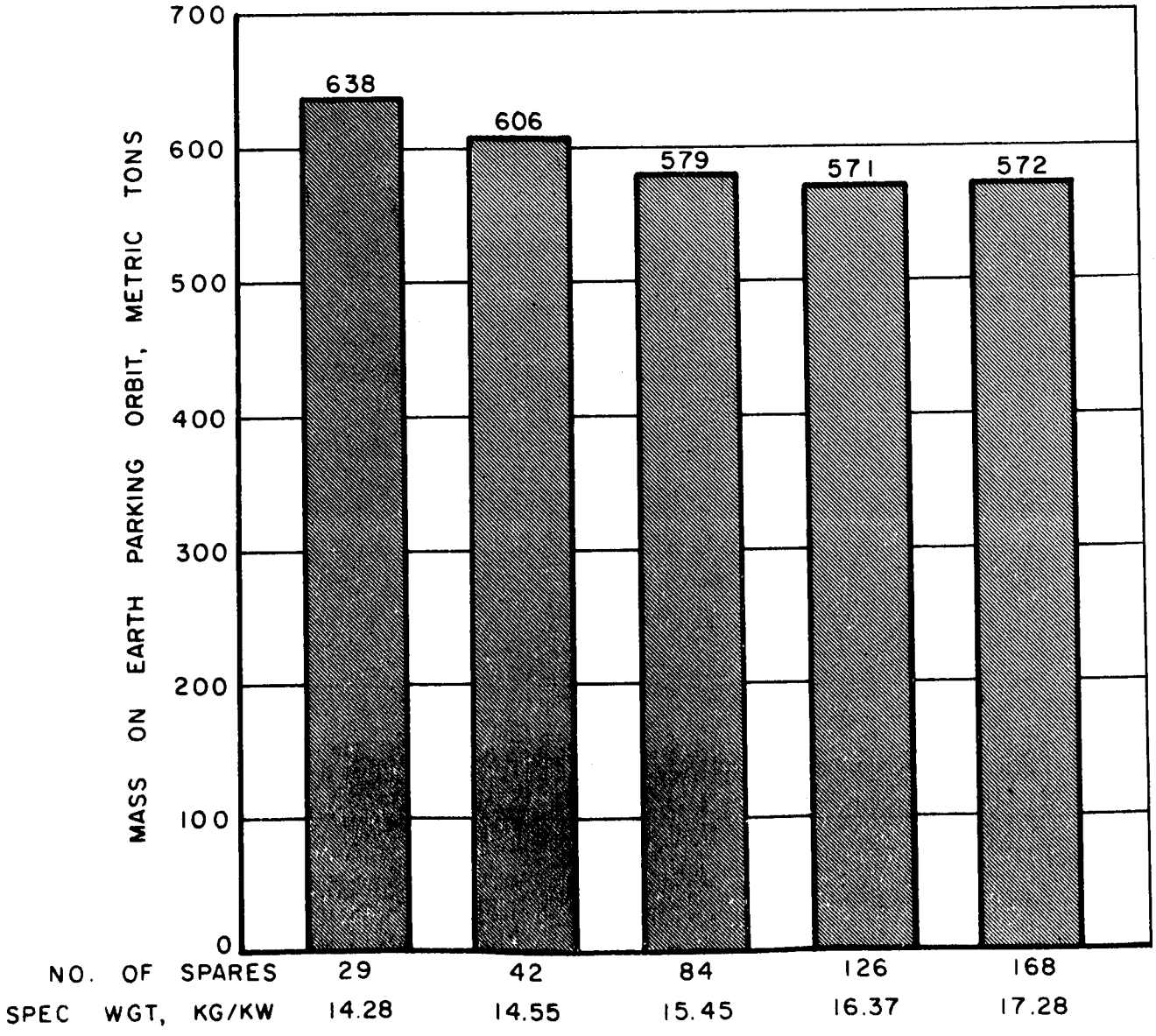

POWERPLANT REQUIREMENTS FOR 530-DAY MARS MISSION

OPTIMUM NUCLEAR + ELECTRIC OPERATION

TWO REACTOR POWERPLANT

MAINTENANCE :

—— NO SPARES

– – – 42-∞ SPARES

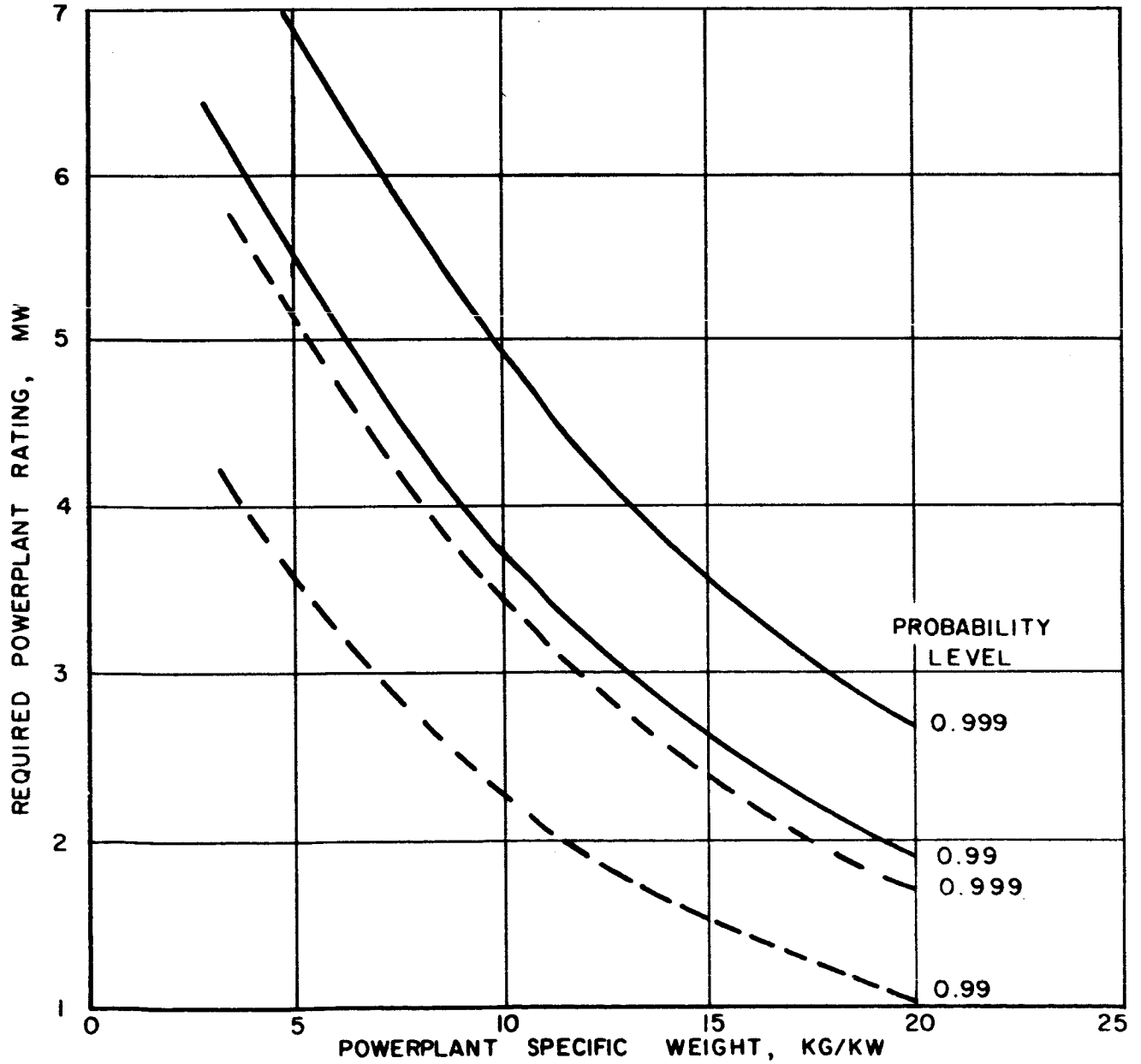

POWERPLANT REQUIREMENTS FOR 630 DAY MARS MISSION

OPTIMUM NUC + ELECT OPERATION

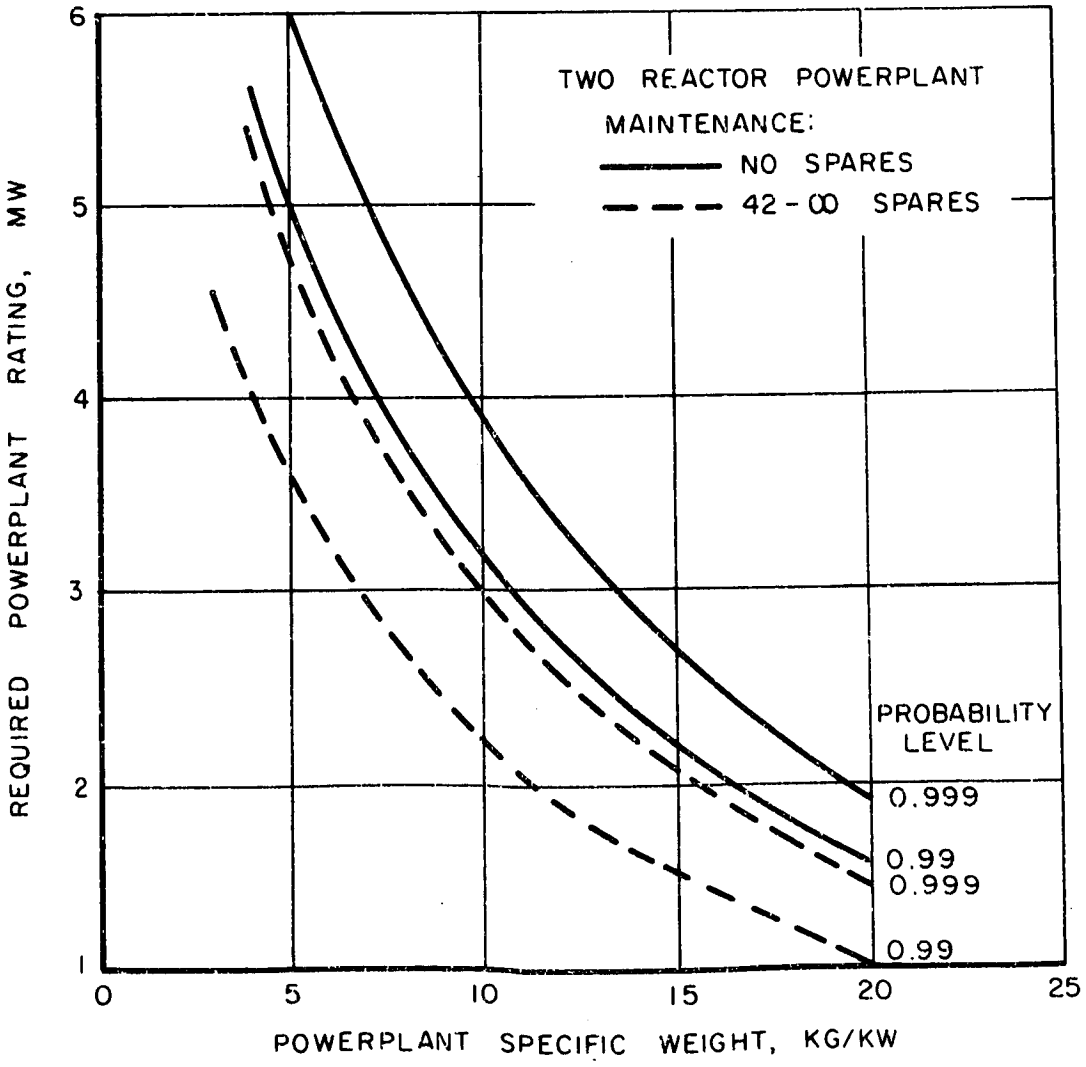

EFFECT OF POWERPLANT ON EARTH DEPARTURE NUCLEAR SYSTEM

530 DAY MISSION

OPTIMUM NUC + ELECT OPERATION

LV⊕ 4170 LV♂ 4480
AR♂ 4450 AR⊕ 4700

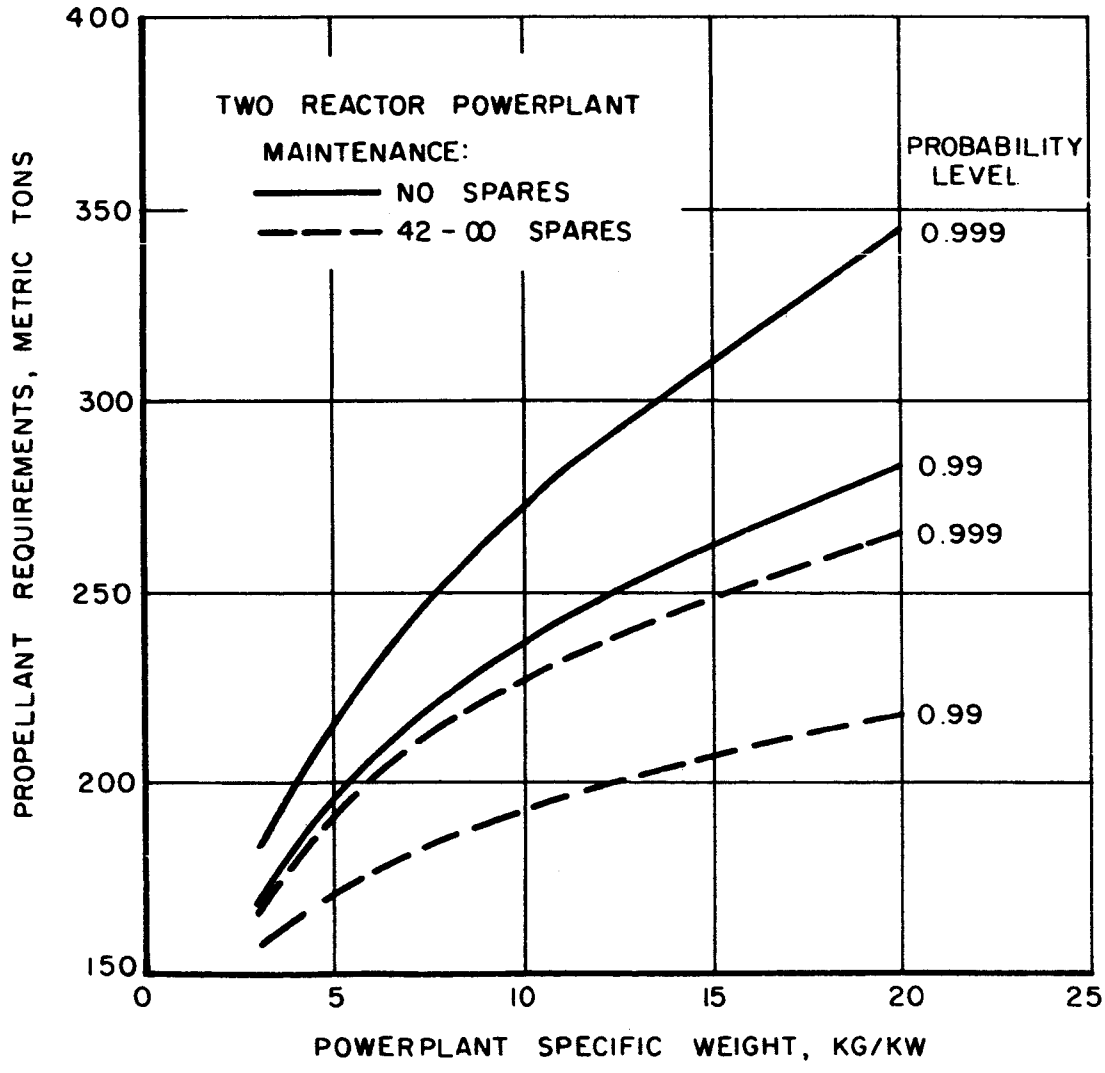

EFFECT OF POWERPLANT ON EARTH DEPARTURE NUCLEAR SYSTEM

630 DAY MISSION

OPTIMUM NUC + ELECT OPERATION

LV⊕ 4190 LV♂ 4490
AR♂ 4460 AR⊕ 4820

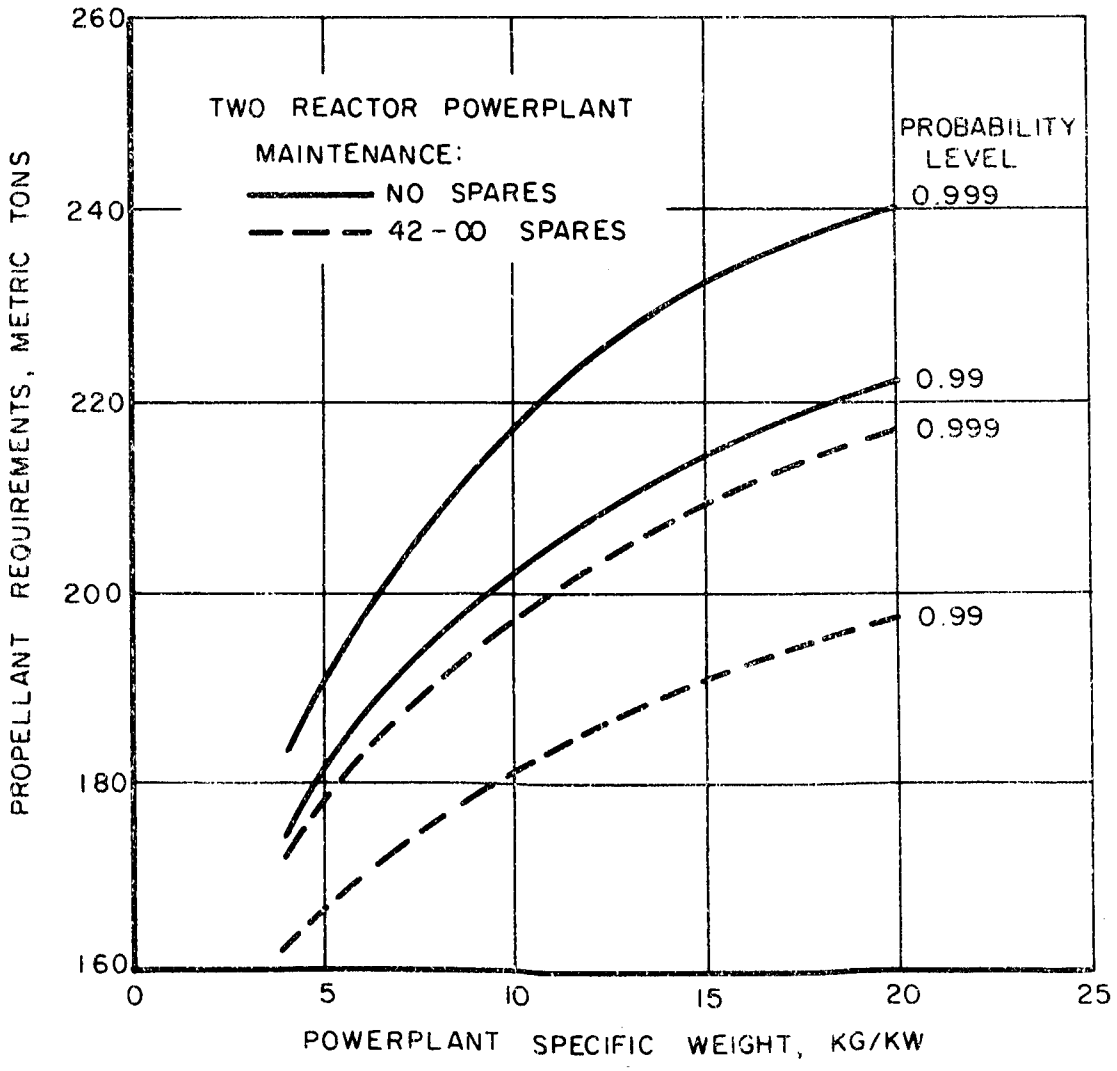

EFFECT OF PARKING ORBIT ALTITUDE ON MEM

O_2/H_2 PROPULSION (430 SECS)

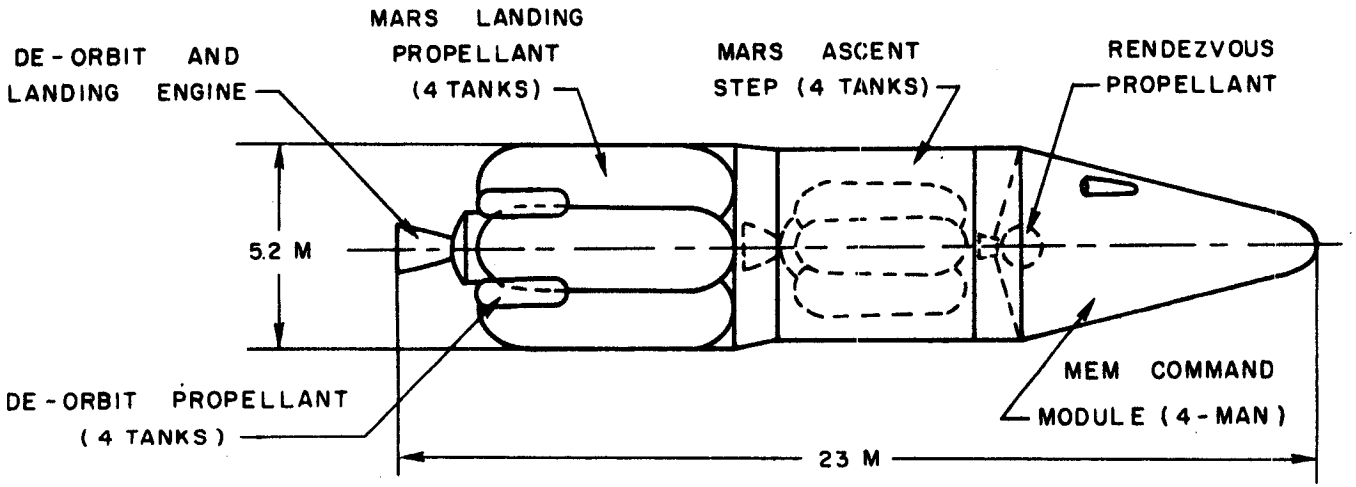

CIRCULAR ORBIT

(926 KM)

MASS = 36.8 METRIC TONS

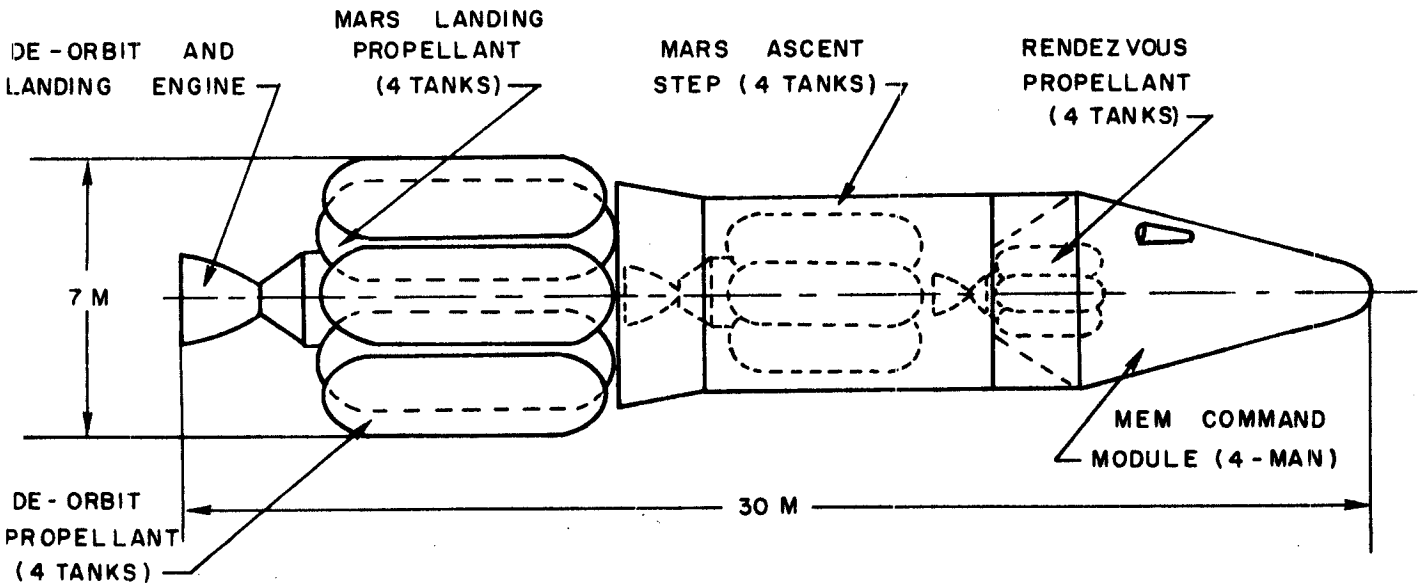

ELLIPTIC ORBIT

(330 KM PERIAPSIS)

MASS = 88.5 METRIC TONS

MARS HYBRID-THRUST SPACECRAFT

NUCLEAR + ELECTRIC PROPULSION

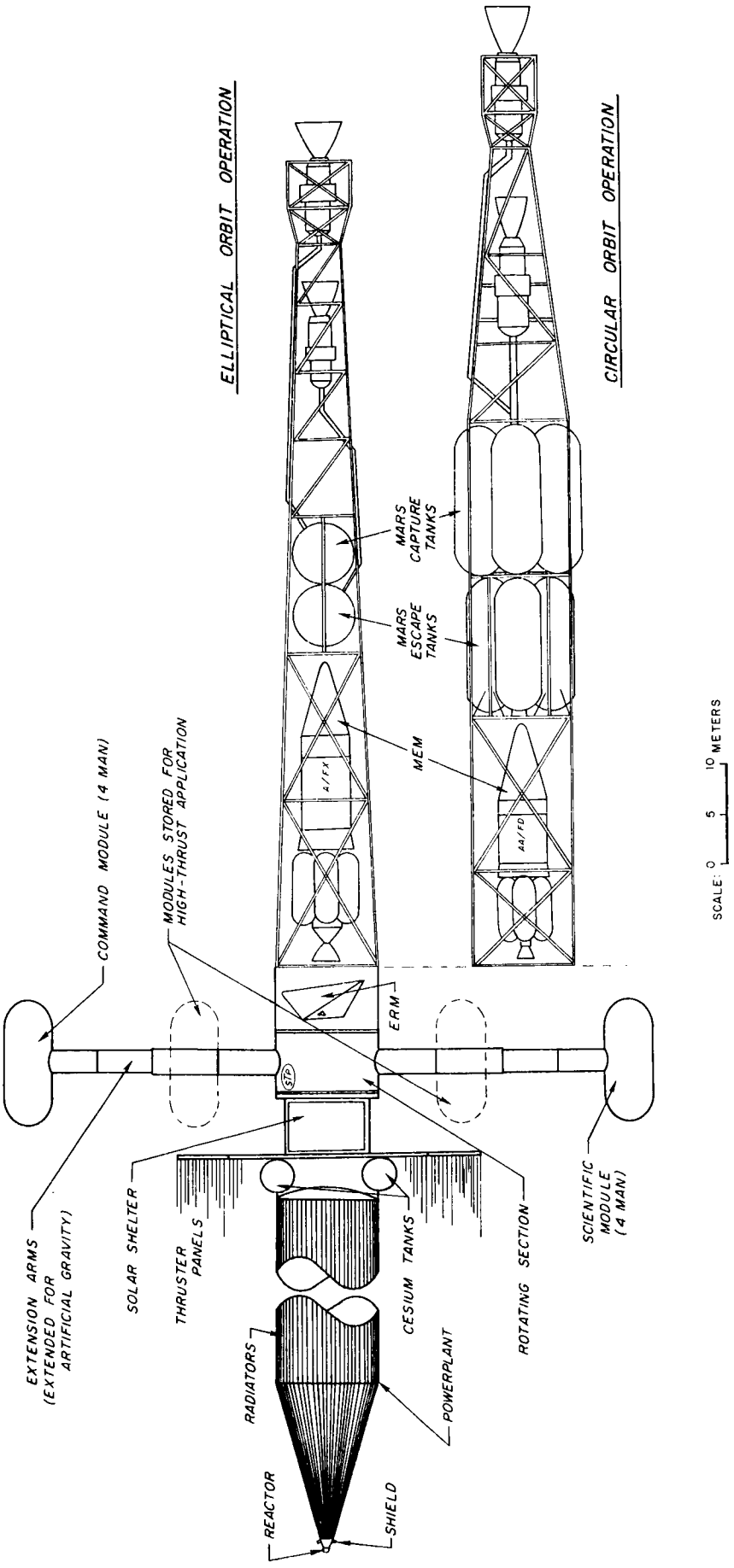

MARS HYBRID—THRUST SPACECRAFT

CHEMICAL + ELECTRIC PROPULSION

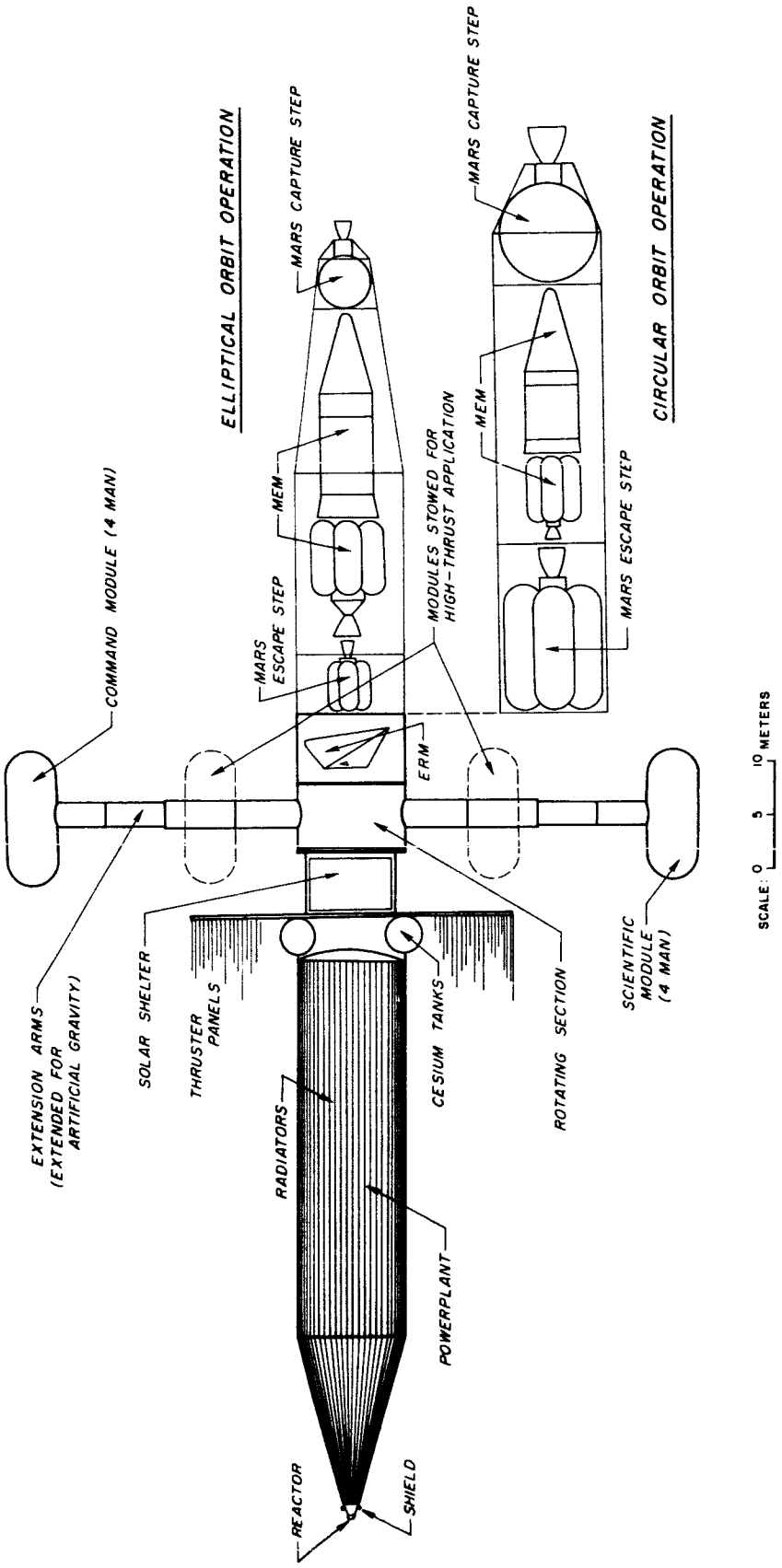

SECTION IV
FLIGHT PROFILE STUDIES

The purpose of the flight profile studies was to analyze the combinations of mission duration, leg-time distribution, low-thrust propulsion staging, and high-low thrust mixes which tended to minimize the vehicle mass required on Earth parking orbit. This approach was deemed necessary to determine the best combination of the various flight parameters which could be used for the in-depth hybrid-thrust optimization and studies of the power system characteristics. The most important parameters which were initially analyzed were mission duration, distribution of leg times and single- or dual-electric propulsion modes. The results of this analysis were used in the hybrid-thrust optimization studies and subsequent mass calculations which included the power system specific weight and power profiles.

This section presents the techniques of analysis and major accomplishments of the studies performed in support of the mission analysis. The salient subjects covered include the basic vehicle system model employed, the vehicle concepts applicable to the model, the comparisons between single- and dual-electric system operation, the optimum distribution of leg times, and the optimization of the combined high- and low-thrust vehicle system.

Vehicle Systems Model

In general, the system model selected conforms to propulsion performance capabilities and subsystem weights anticipated to be operational in the 1980 time period. As with all models of this type, the mass values derived therefrom are strictly estimates and are primarily used to compare different vehicle concepts and flight profiles. They should not be construed as definitive requirements for a particular mission. Mass values for the major subsystems such as the mission module and hardware contained therein, crew solar flare shelter, Mars excursion module, life support system, and Earth entry system were for the most part based on previous industry studies. No particular design analysis was performed on these systems.

Because of the desire to automate the mass computation, weight scaling laws were derived for the nuclear propulsion systems, the life support system, and the Earth entry module. Variations accounted for include impulse propellant weight (but not thrust-to-weight ratio), crew size, mission duration, hyperbolic excess speed, and attendant gravity losses. This continuous scaling technique, while advantageous from a computational viewpoint, assumes that the estimates will be reasonably close to a "point" design. Again, the justification for these assumptions is in the fact that comparisons are to be made as some parameter is varied, although it is believed that the resulting vehicle mass values give reasonable indications of the mission requirements within the scope of the

assumptions used.

It was assumed that the basic Mars mission objective is to deliver a 45-metric-ton excursion module onto a 926-km parking orbit. The actual deorbiting, surface touchdown, exploration, and subsequent rendezvous with the parent vehicle occurs within a 30-day time period and is accomplished entirely by the subsystems contained in the MEM. As discussed previously, the savings in total vehicle mass favored the used of an advanced ablative-type entry system capable of entry speeds to 20 km/sec (65,000 ft/sec)

In general, all that is required to compute a vehicle mass is the mission duration, the hyperbolic excess speed of planetary departure and arrival, the power system specific weight, α, and the low-thrust trajectory characteristic power, J. In addition, system selections, such as the crew size, mass of the excursion module and solar shelter, and Earth entry mode, are available. Further details concerning the mass computation are given in Appendix F.

The quantity of prime interest to the mass computation is the trajectory characteristic power as represented by the integral

$$J = \int_0^T \frac{a^2}{\epsilon\eta}\, dt$$

where T is the operating time, a the thrust acceleration, η the thruster efficiency, and ϵ the fraction of rated power available. As discussed in the trajectory work, the integral is simplified by assuming that the thruster efficiency is constant. The form of a given decreasing power profile as provided by the studies in Section VI, Power System Study, was approximated by an exponential curve fit. The resulting expression was then utilized in the trajectory optimization program. In this way, the influence of the expected output power profile for a given powerplant configuration may be assessed in terms of the vehicle mass requirements.

Scaling Laws

The spacecraft subsystems which vary with mission parameters (e.g., crew size, entry speed, duration) were grouped into four major computational elements for convenience; these are Earth entry system, life support and environmental control, mission module, and nuclear propulsion. For the most part the corresponding scaling laws were obtained from previous industry reports or were derived from basic information.

The mass of the ablative Earth-entry system, m_e, for atmospheric entry velocities less than 20 km/sec is given by

$$m_e = 2360 + 167\ n + [239 + 91\ (V_e - 11)]n^{2/3},\ kg$$

where n = crew size

V_e = entry speed, km/sec $\leq$ 20 km/sec

If the entry velocity is greater than 20 km/sec (65,000 ft/sec) the mass of the ablator (m_a) is given by the above expression evaluated at 20 km/sec. The incremental velocity (ΔV) above 20 km/sec is provided by a retro-rocket whose exhaust velocity is c. The mass of the total entry system under these conditions is then given by

$$m'_e = \frac{m_a}{1 - \frac{1}{3}\frac{e^{\Delta V/c} - 1}{e^{\Delta V/c}}}$$

A storable propellant retro-rocket was assumed (I_{sp} = 330 sec), and the propellant weight fraction was fixed at 0.75.

The mass (m_{LS}) of the life support and environmental control system (discussed in Section VII) is a function of the total trip duration (T, days) and the number of crewmen (n) and can be expressed as

$$m_{LS} = [1.48(n-4) + 7.1](T-200) + 500(n-4) + 2370,\ kg$$

The mission module mass is primarily a function of the volume necessary to enclose the crew and the life support and environmental control systems. For present purposes the mass (m_m) is given by

$$m_m = 4536\ n^{1/2} + CTGY,\ kg$$

where CTGY = contingency and miscellaneous inert masses

The variable CTGY was used to correct or change the basic spacecraft weight if necessary and to include miscellaneous items such as tie-in structure, auxiliary power, etc. If separate command modules and service modules are needed they may be introduced into the basic spacecraft through CTGY.

The nuclear high-thrust propulsion step (I_{sp} = 800 sec) is sized using an empirical equation for the inert weight fraction (β) as a function of the impulse propellant (kg).

$$\beta = 0.296 \left(\frac{m_p}{42200}\right)^{-0.264}$$

The propellant required by the mission is given by

$$m_p = \frac{(1-\beta)}{1-\mu\beta} (\mu-1)m_L$$

where μ = stage mass ratio
m_L = mass accelerated by the step

The two equations above are solved iteratively in the mass computation program. An updated and sophisticated high-thrust step inert mass computation routine which would have been useful to the vehicle mass program was not available at the time the mission studies were performed. The above inert fraction scaling law was readily available and proved to be expedient.

The computation of the electric propulsion systems utilized the optimum powerplant fraction equations for variable thrust operation. The optimum powerplant fraction μ_w is given by.

$$\mu_w = \sqrt{\frac{\alpha J}{2\eta}} \left(1-\sqrt{\frac{\alpha J}{2\eta}}\right)$$

where α_w = powerplant specific weight, kg/kw

$J = \int a^2 dt$, trajectory characteristic power, w/kg (m^2/sec^3)

and η = average thruster efficiency

The corresponding maximum payload to gross weight ratio (μ_L) is obtained from

$$\mu_L = \left(1-\sqrt{\frac{\alpha J}{2\eta}}\right)^2$$

and the propellant required is

$$\mu_p = \sqrt{\frac{\alpha J}{2\eta}}$$

A shelter is provided for protection against solar flare protons. Although this proton flux varies with distance from the sun and the exposure time, the integrated effect over the varying trip durations enables one to fix a given shelter

mass without introducing prohibitive error. A review of the expected flux for 1980 trips was performed, and a corresponding solar shelter mass was computed and fixed for that year. The shelter mass utilized was 12.6 metric tons.

Appendix F discusses the vehicle mass computation program which utilizes the foregoing scaling laws and subsystems mass estimates. It should be noted that the mass computations, while justified in their present form for mission analysis purposes, are essentially summations and evaluations of scaling laws with appropriate input and do not imply that a hybrid-thrust vehicle under a given set of mission assumptions can actually be designed to the computed mass.

Planetary Operations

The maneuvers employed at Mars are of primary importance in defining the over-all mission energy requirements and also affect vehicle design and the operational procedures employed for the surface exploration of the planet.

This study assumes that the electric propulsion system decelerates the spacecraft on the approach hyperbola until the trajectory is nearly parabolic at Mars' sphere of influence. The periapsis distance of the resulting trajectory is 1.28 Mars radii.

Near periapsis, the spacecraft retros into an orbit about Mars and then deploys the MEM for surface exploration. The total stay time is 30 days. If the eccentricity of the Mars parking orbit is varied, certain operational maneuvers are suggested. If it is assumed that a circular orbit is established at 1.28 Mars radii, the capture and departure ΔV's are high, while the energy requirements for de-orbiting the MEM are minimal. Conversely, as the eccentricity of the parking orbit increases, the capture and departure ΔV's decrease while the MEM de-orbit ΔV's increase. Thus, the mass of the total spacecraft (including MEM) may be strongly effected by the choice of parking orbit because of the tradeoff in ΔV between the spacecraft and its subsystem (MEM).

The period of the circular orbit is about 140 min. As the eccentricity is increased, the period increases monotonically. If one assumes that the orbital period of the parking orbit is equal to the stay time (30 days), the eccentricity is about 0.98, while the semimajor axis approaches 60 Mars radii. This type of orbit can be achieved with ΔV's in the order of 0.1 km/sec. However, there are disadvantages. First, the apoapsis of the parking orbit is near or beyond Mars' activity sphere, which requires that the planetary operations analysis become a three-body problem and no longer planetocentric. Secondly, the orbital period is extremely sensitive to the retro ΔV. For a 30-day period, an error of 0.001 km/sec will induce an error of 2 days in the period. Reducing the period to 10 days, such that the spacecraft makes three revolutions during the stopover, reduces the sensitivity to ΔV errors by an

order of magnitude. However, the capture and departure ΔV's double. Operationally, it would be better to accept the increased ΔV requirements to reduce the error sensitivity to ΔV. Likewise, it would be more advantageous to make several passes through periapsis to monitor the surface operations being performed. The accuracy of the retro maneuver should be used to define the maximum allowable period for the parking orbit. The operational period should be selected below this limiting value such that a number of complete passes can be performed during the required stay time. As an example, if a limiting period of 23 days is stipulated, and the required stay time is 30 days, the operational period should be 15 days, with the vehicle making two passes. If it is operationally necessary to define a minimum allowable number of passes, the operational period should be redefined.

Figure IV-1 presents the relationship between the orbital period and the capture ΔV requirement for Mars orbits having a periapsis of 1.28 Mars radii. The values of ν_B correspond to fractions of the total hyperbolic excess velocity, as described in the hybrid-thrust optimization analysis below. The circled point represents the design point for this study.

Single- and Dual-Electric Vehicle Systems

Viewed in terms of the over-all flight profile, it appears that the manned Mars mission may be performed using one of two heliocentric electric propulsion operating modes. The first approach would be to use a separate and completely independent electric propulsion system for each heliocentric leg. That is, one system is used for the trans-Mars leg and is staged upon completion of the outbound trip, while a second system is used for the return leg. Of course, the second system must be carried along and is inactive during the initial (outbound) phase of the mission. This dual-electric mode is an implementation of a logical distribution of staging presented by the major mission milestone: the planetary operations.

The second mode which suggests itself is the use of just one electric propulsion system for the entire mission, from the start of the heliocentric trans-Mars phase to just before Earth atmospheric entry. The major difference between this single-electric operation and the dual-electric mode is the unusually long time that the powerplant-thruster system must operate in the single-electric mode. Consequently, the power profile must play an important part in the comparison of the two modes. The single-electric mode inherently relies on the probable power profile for the single powerplant, whereas the dual mode employs two power profiles, one for each system. Consequently at the time of startup for the departure from Mars, the single-mode power output is probably less than half its original rating, while theoretically the dual system power output at startup is 100% since a "new" propulsion system (i.e., powerplant) is utilized.

The implications of the above considerations to total vehicle system mass were investigated in the study reported herein. The object was to determine which operating mode, under the influence of power profile and powerplant configuration, was favored in terms of vehicle mass required on Earth parking orbit. Additionally the purpose was to determine the distribution of leg times which result in minimum vehicle system mass for a given mission duration. The results of this study, derived during the early phase of the contract, formed the basis for the investigation of the optimum hybrid-thrust system and the powerplant's influence on the mission requirements.

From the early results of the powerplant studies presented in Section VI, it was determined that the major change in powerplant configuration that strongly influences power profile was reactor redundancy. Accordingly, the study included the influence of one- and two-reactor powerplant configurations as well as the component failure rate level. The one- and two-reactor powerplant configurations (configs. 2 and 8 respectively) were selected from a group of nine different powerplant configurations, each of which contained varying degrees and types of subsystem redundancies.

The major assumptions applicable to this brief substudy were: (1) the high-thrust system provided only parabolic conditions for Earth departure, (2) the electric propulsion system brought the spacecraft to parabolic conditions at Mars arrival, (3) the electric system at Mars departure started at parabolic conditions, and (4) no high-thrust systems were employed nor mixed with low thrust at Mars. In this instance, therefore, the MEM starts from parabolic conditions heading towards the planet's surface and subsequently rendezvous with the parent spacecraft which is still at parabolic conditions. For baseline comparison purposes, the vehicle mass was also computed for no power loss, i.e., 100% power at all times.

Single-Electric Vehicle System

Figures IV-2, IV-3 and IV-4 summarize the results obtained for the single-electric vehicle system. The probable profiles characteristic of each configuration are given in Section VI. The stated probability level corresponds to the probability level in the power profile which was used in the computation for J.

Configuration 8 is a dual-reactor unit and was applied to the single-electric system in the belief that this type of operation was suitable for long-lifetime demands. For the unimproved state of configuration 8, the highest probability level attainable was 0.60 before the corresponding power profile decreased to about 15%. This problem is characteristic of the single-electric system which requires unusually long operating times (1440 hr). Figure IV-2 clearly indicates that not only is the probability level unacceptably low from a man-rating standpoint, but also that the mass requirements are quite high for even the lowest expected specific weight, 10 kg/kw (22 lb/kw). For

comparison, the highly idealistic case of no power loss is also shown.

Note that the curves in general follow the same trends displayed by the curves of J as a function of Mars arrival date, as shown in Fig. III-4. However, at the middle arrival dates, the J's are quite high and, in fact, when applied to the mass computation, exceed the design limitation (zero payload). Hence, for the 0.60 probability curves, the curves do not connect at the middle arrival dates.

The rather significant effect of improving power system component failure rates is shown in Fig. IV-3. It now becomes possible to utilize high probability levels which previously displayed essentially zero available power and hence inordinately high J's. Whereas previously the mass for the idealistic case of no power loss and specific weight of 18 kg/kw (40 lb/kw) is about 600 metric tons, that same mass is achievable in the present case at a realistic probability level of 0.90. For the 0.99 cases, the mass requirements do not exist in the middle arrival dates because of the very high J's.

Improved powerplant configuration 2, a single-reactor system, was investigated for vehicle mass effects as brought about by probability level and specific weight. Considering either of the two minima in Fig. IV-4, it can be seen that changing the probability level from 0.75 to 0.90 does not cause as much increase in mass as changing the specific weight from 10 to 14 kg/kw, assuming 0.75 probability. Note that the 0.90 probability system using an α of 10 kg/kw is essentially equivalent to the unrealistic no-power-loss case with an α of 14 kg/kw.

Improved powerplant configuration 8 may be compared to the improved configuration 2 for a probability level of 0.90 by noting that configuration 2 at an estimated specific weight of 14 kg/kw yields about 100 metric tons less mass than configuration 8 at an estimated specific weight of 18 kg/kw. They would be almost identical in mass requirements if configuration 8 had a specific weight of 16 kg/kw.

Dual-Electric Vehicle System

Figures IV-5 through IV-8 present the results of applying both the unimproved and improved versions of powerplant configurations 2 and 8 to the dual-electric propulsion system. It was expected that the shorter operating times imposed on the powerplant would allow higher probability levels to be employed without resorting to the improved versions of the powerplants. However, it is characteristic of the unimproved power systems to display unacceptable power levels before the end of the operating period is reached. The following discussion, coupled with the foregoing results for single-electric systems, points out the desirability of obtaining improved power system component failure rates.

The curves depicted in Fig. IV-5 were computed for two probability levels of configuration 2, the 0.75 case being the highest achievable before the corresponding power profile drops to essentially zero. Note that the 0.60 and 0.75 curves are essentially equivalent at specific weights of 14 and 10 kg/kw, respectively. The curves also show that passing from a probability of 0.60 to 0.75 at a specific weight of 10 kg/kw yields almost the same mass increase as maintaining the lower probability but increasing the specific weight to 14 kg/kw.

Employing an improved component failure rate again results in higher probability levels being accessible and, further, causes lower mass requirements under the same specific weight as the previous unimproved case. Thus, in Fig. IV-6, for 0.95 probability the mass is about 600 metric tons, whereas in the previous case (Fig. IV-5), the requirement is about 750 metric tons at 0.75, both evaluated for 14 kg/kw specific weight. It appears, as in previous cases including the single-electric system, that the higher the probability level, the more sensitive is the vehicle mass to changes in specific weight. This sensitivity apparently stems from the fact that the trajectory requirements (with corrections for decreasing power) are already quite high at the increased probability levels, and any change in vehicle subsystem mass, such as powerplant specific weight, aggravates the ensuing mass requirements even further.

The use of the two-reactor power system appears attractive for the dual-electric vehicle, since the reactors operate at reduced level for shorter periods compared to the single-electric vehicle system. Figure IV-7 shows the result of this approach. The primary effect is that a probability level of 0.90 is now achievable at the cost of large mass, whereas in the single-electric case, using the same powerplant and specific weight, the 0.90 level is not attainable since the power profile rapidly approaches zero. For a probability of 0.90 the required mass is about 1250 metric tons, which occurs at the favored minimum where the trips arrive after opposition.

Improving powerplant configuration 8 drastically reduces the mass requirements as can be seen by comparing Fig. IV-8 with Fig. IV-7. Whereas previously the mass required was about 1250 metric tons, it here decreases to about 550 metric tons, a reduction of more than half. This reduction is obtained even if the specific weight is assumed to increase to 18 kg/kw instead of remaining at 16 kg/kw. The improvement may also be viewed in terms of the probability level. In the unimproved configuration, the highest probability level achievable was 0.90 at a cost of 1250 metric tons. A level of 0.99, which is commensurate with manned flight, is now realizable for 950 metric tons, even at a higher specific weight.

System Comparisons

The choice between the single- and dual-electric operating modes is not quite so clear-cut as suggested by Fig. IV-9 in comparison to Fig. III-5 of Section III. In most cases, the dual-electric system requires less mass than the single system. A striking example of this can be obtained by referring back to the previous figures for the improved configuration 8, 0.99 probability level, and corresponding estimated specific weight of 18 kg/kw; the single-electric system minimum requirement in this case is approximately 2000 metric tons while the dual system is 950. Furthermore, note that the dual system is almost insensitive to arrival date.

Because of the complexity in ascertaining the favored operating mode under all conditions of power profiles, probability levels, and powerplant configurations, it was decided to consider other criteria besides the vehicle system mass. From an operational standpoint, the single-electric system offers less spacecraft design integration problems than the dual system. No staging of the outbound system is required, and assembly of the entire spacecraft does not require handling the extra propulsion system, especially in view of the additional packaging necessary for the three high-thrust propulsion systems in hybrid-thrust operation. In addition it is imperative for safe return that, upon initiating Mars departure, the homebound propulsion in the dual system starts up reliably and deliver 100% power. This is a stringent requirement on a system exposed for some time to the space hazards and environment of the outbound leg.

The problem of comparing the single- and dual-electric modes in depth requires further study beyond the scope of the present effort. Besides comparisons of vehicle mass, the design integration problems of the spacecraft and the reliability aspects of operation should be considered. It may possibly be determined from a design investigation that, although the results of the current study indicate the dual system has a slight edge in mass, the packaging and tie-in necessary for transporting two propulsion systems (and associated power systems) negates the mass advantage.

Favored Trip

From Fig. III-4, the sum of the outbound and inbound J's displays two minima which appear to be attractive. As stated before, the resulting mass curves display the same general configuration of the trajectory curves; however, in reviewing Figs. IV-2 to IV-9, the favored minimum is associated with the trips arriving after opposition, on a date of about 244 4450. This appears to be true regardless of the system variations. Consequently, for this opposition (244 4295, 25 February 1980) at least, the minimum-mass trips are identified.

The effect of distributing the outbound and inbound leg durations (and hence J's) was analyzed for each arrival date and the given total trip time of 630 days (30-day stopover). It would appear from a mass point of view that a lower J is desirable on the outbound leg of a round-trip mission, during which time a very large mass is to be transported compared to that of the inbound leg. That this is so is illustrated in Figs. IV-10 and IV-11. For the given total trip time the corrected J's are plotted against the outbound leg duration, Fig. IV-10. As can be seen, the trips arriving at 244 4125 all display high J's for the outbound leg and low J's for the inbound. This situation is reversed, however, for trips arriving at 244 4450. These lower J's for the outbound leg are quite advantageous, since they have a major effect on the mass of the outbound propulsion system at which time it is accelerating a very large mass. This point is amplified in Fig. IV-11.

This figure was obtained by using the trajectory requirements, given in part by Fig. IV-10, for the dual-electric system employing the unimproved powerplant configuration 2. The various combinations of outbound and inbound legs that may be used to make up the given total trip time were analyzed at the two arrival dates identified by minimum total J. For all cases shown in Fig. IV-11, the later arrival date is favored. The importance of the distribution of the outbound and inbound leg durations (i.e., the J's) is evident from the significant difference in mass requirements. In these two arrival dates at least, the total minimum J is not always a true indicator of the favored trip. Note further that the higher probability causes the differences in mass between the two minima to become larger.

Hybrid-Thrust Optimization

In the mass computations discussed above, the boundary conditions for the optimum low-thrust trajectory are the arrival and departure planet's heliocentric position and velocity. In a general sense, the optimization of vehicle mass should include velocities other than the implied parabolic one; i.e., nonzero hyperbolic excess velocities should be utilized on the boundaries. From the operational viewpoint, these hyperbolic excess velocities require high-thrust devices for planetary departure and capture; or, for Earth return, a high-speed entry system may be necessary. The optimization of mixed-thrust operation, whether for maximum payload ratio or minimum gross vehicle mass, relies basically on determining the proper hyperbolic excess speeds of departure and arrival for each leg of the round trip.

The following discussion outlines two approaches utilized in optimizing the hybrid-thrust system. The first approach essentially uses a sequential computation of gross vehicle mass with respect to permutations in the hyperbolic excess speeds until minimum mass is determined. The second method employs an analytic formulation of over-all payload-to-gross weight ratio which includes

the hyperbolic excess speeds. In terms of ease of usage and relative computational speed, the second method has been found to be more desirable than the first.

Sequential Mass Computation

The over-all approach taken was to permute the various sets of hyperbolic excess speeds such that all possible combinations of the four speeds are included in the mass computations. The return leg mass requirements were analyzed first since, for a given set of dates, the optimum pair of hyperbolic speeds for this leg is independent of the outbound trip. The minimum vehicle mass conditions were determined by plotting the mass against the hyperbolic excess speed.

The optimization is illustrated by a sample 430-day Mars mission arriving at 244 4375, staying 30 days and employing a leg time distribution of 160 days outbound and 240 inbound. It should be remembered that this specific trip arrives after opposition and is optimum with respect to the all-low-thrust system but not necessarily for the mixed-thrust case.

The vehicle concept employed was the dual-electric system using the improved powerplant configuration 8 at a probability level of 0.90 and a specific weight of 18 kg/kw. Earth operations entail departure by a nuclear propulsion stage and capture by an ablative entry system (maximum hyperbolic excess speed at entry of 0.55 EMOS). The Mars capture phase utilizes a nuclear system to decelerate the parent spacecraft (including the excursion module) into a highly elliptic parking orbit (near-parabolic conditions). Departure from the planet is accomplished by a high-thrust nuclear stage which starts from the Martian parking orbit and delivers the return spacecraft (less the excursion module, outbound electric propulsion, and high-thrust capture systems) to the desired hyperbolic speed.

As the initial results were examined, it was noted that the return leg speed combination that minimized mass for any outbound speed combination was 0.10 and 0.5 EMOS for Mars departure and Earth arrival, respectively. All subsequent calculations kept these return leg speeds, and attention was focused on obtaining the optimum outbound set.

Figures IV-12 and IV-13 summarize the results of this brief analysis. For a given Earth departure speed, the influence of the Mars arrival speed is readily seen in Fig. IV-12. It is interesting to note that minimum mass seems to occur within a range of Mars arrival speeds from 0.22 to 0.23 EMOS, regardless of the Earth departure speed. A plot of the minimum mass values as a function of the departure speed results in the over-all curve of Fig. IV-13. Hence a dual-electric system, under the given assumptions, requires approximately 834 metric tons on Earth parking orbit. The proper combination of hyperbolic

speeds which yields this minimum mass is 0.148 EMOS for Earth departure, 0.238 EMOS for Mars arrival, 0.10 EMOS for Mars departure, and 0.50 EMOS for Earth arrival. As a comparison, the impulsive (ballistic) Earth-to-Mars transfer requires 0.163 EMOS for departure and 0.260 EMOS for arrival. The corresponding Mars-to-Earth leg requires 0.239 and 0.504 EMOS, respectively, for departure and arrival. The mass savings which result from employing mixed-thrust systems are tremendous, since the all-low thrust (i.e., dual-electric) system requires about 6160 metric tons for the given trip.

Judging from the pair of outbound speeds which was found to yield minimum mass, the optimum trip tends to utilize very little of the electric propulsion system. That is, the trans-Mars leg appears to be all high thrust. To further substantiate this observation with mass values, a vehicle system was analyzed using the Earth-to-Mars impulsive-transfer hyperbolic excess speeds and 0.10 and 0.50 EMOS for the inbound pair of speeds. This system employs an all-nuclear outbound propulsion system with a mixed-thrust inbound leg. The resulting vehicle mass required on Earth parking orbit was found to be 838 metric tons, slightly more than the previously identified mixed-thrust minimum of 834 tons. The difference of 4 metric tons is the net increase in the Mars high-thrust braking stage and Earth departure stage, with no intervening electric propulsion system.

Analytic Optimization

In general this method relies on deriving an expression for the over-all payload-to-gross weight ratio as a function of the propulsion and trajectory parameters for both the high-thrust and low-thrust systems. For a given set of propulsion parameters the equations are solved numerically for the optimum hyperbolic excess speeds which maximize the payload-to-gross weight ratio. To derive the expressions for the payload ratio it was necessary to eliminate the velocity-loss aspect from the high-thrust mass ratio equations. In addition the dependence of the high-thrust step inert weight fraction on incremental velocity and on the accelerated mass was neglected; the inert fractions were treated as parameters. These assumptions lead to considerable simplification of the optimizing procedure.

The computed hyperbolic excess speeds are used in a mass computation program to actually determine the vehicle system mass and the distribution of propulsion systems. The mass computation program employs scaling laws for the inert weight fractions and corrections for velocity loss. Because of the assumptions on the optimization of hyperbolic speeds, it is tacitly assumed that the minimum vehicle mass so computed corresponds closely to that obtained by the sequential mass computation procedure discussed above. No further iterations are made. It is believed however that these results are more than reasonable for the purposes of this study and, further, that the technique of analysis derived herein is sufficiently flexible to allow inclusion of variations in inert fraction and losses in incremental velocity.

The following discussion briefly outlines the formulation and analysis of the high-low thrust system optimization. The basic variable-thrust computer program which determines optimum hybrid-thrust trajectories is discussed elsewhere in this report.

High + Low + High-Thrust Operation

The flight profile usually associated with a planet-bound transfer (manned or unmanned orbiters) involves a high-thrust (chemical or nuclear) Earth-departure system, a low-(variable)-thrust heliocentric transfer, and a high-thrust capture into a parking orbit about the planet. The over-all payload-to-gross weight ratio for this mode is

$$\mu_L = \left[\frac{1-\mu_1\beta_1}{(1-\beta_1)\mu_1}\right](1-\gamma_m\Gamma)^2\left[\frac{1-\mu_2\beta_2}{(1-\beta_2)\mu_2}\right]$$

where

$$\mu_{1;2} = \exp\left[\sqrt{\nu_{A,B}^2\left(\frac{V_{\infty A,B}}{c_{1,2}}\right)^2 + \left(\frac{V_{e\,1,2}}{c_{1,2}}\right)^2} - \left(\frac{V}{c}\right)_{1,2}\right]$$

$$\gamma_m^2 \equiv \frac{\alpha_w J_m}{2}, \qquad \Gamma^2 \equiv \frac{J}{J_m}$$

The term $(1 - \gamma_m\Gamma)^2$ represents the low-thrust system payload-to-gross weight ratio which has been maximized with respect to the powerplant mass. The other two terms are the payload ratios of the departure and capture stages. The expression μ represents the ideal mass ratio for the high-thrust system at departure from (subscript 1) or arrival onto (subscript 2) a circular parking orbit.

The quantities ν_A, ν_B, and Γ, respectively, represent the hyperbolic excess speeds on the initial and final boundaries and the intervening low-thrust J as a result of these speeds. They are normalized with respect to the all-high-thrust hyperbolic excess speeds ($V_{\infty A}$, $V_{\infty B}$) and the all-low thrust J ($\equiv J_m$). The powerplant specific weight is α_w, and the high-thrust rocket exhaust velocity is c. The high-thrust step inert weight fraction, β, is defined as the ratio of the step inert weight to the weight of the propellant plus inerts. The escape velocity V_e is evaluated at the parking orbit radius where the circular velocity is V.

The dependence of Γ^2 on ν_A and ν_B may be easily computed for a given set of departure and arrival dates. Hence for given values of γ_m, V_∞, V_e, c, and V, the problem is to maximize

$$\mu_L = \mu_L (\nu_A, \nu_B, \Gamma)$$

subject to

$$\Gamma = \Gamma (\nu_A, \nu_B)$$

High + Low-Thrust + Atmospheric Entry

Employing an atmospheric entry system is considered to be a mode suitable for Earth return legs wherein the crew and scientific materials are recovered, but the return spacecraft is not. In this case the payload ratio is given by

$$\mu_L = \frac{\left[\frac{1-\mu_1\beta_1}{(1-\beta_1)\mu_1}\right](1-\gamma_m\Gamma)^2}{1 + \left(\frac{m_E'}{m_S}\right)\rho_E(\nu_B)}$$

where $\rho_E(\nu_B)$ represents the growth of a reference ablative entry system, m_E', with the (normalized) entry hyperbolic speed, ν_B. In the present analysis $\rho_E(\nu_B)$ may be represented by a linear or exponential growth. The quantity m_S is strictly the mass of the return spacecraft exclusive of the entry system and the low-thrust propulsion system. As before, the dependence of Γ on (ν_A, ν_B) may be computed for a given set of departure and arrival dates.

High Thrust + Constant Thrust + High Thrust

In this flight mode, the intervening low-thrust system operates under constant rather than variable thrust. The high-thrust systems on the boundaries function as before. The over-all payload ratio is thus

$$\mu_L = \left[\frac{1-\mu_1\beta_1}{(1-\beta_1)\mu_1}\right] \mu_{PL} \left[\frac{1-\mu_2\beta_2}{(1-\beta_2)\mu_2}\right]$$

where the notation used before applies and, in addition,

$$\mu_{PL} = \frac{1}{1 + \frac{(\gamma_m\Gamma)^2}{\mu_W\eta}} - \mu_W$$

which is the constant-thrust payload ratio to be maximized by determining the appropriate value of the powerplant fraction μ_W (Ref. IV-1). Note that, in

contrast to the payload ratio $(1 - \gamma_m \Gamma)^2$ for the variable-thrust system, the maximum ratio must be found for each set (ν_A, ν_B) and, hence, for the resulting Γ. The optimum powerplant fraction which maximizes μ_{PL} is given by

$$\mu_{w_o} = \frac{\mu_b (1-\mu_b)}{1 - \frac{2\mu_b}{1+\mu_b}\left(\frac{\eta' c}{\eta}\right)}$$

where

$$\frac{1}{\mu_b} = 1 + \frac{(\gamma_m \Gamma)^2}{\mu_w \eta}$$

$$\bar{a}\alpha_w c = 2\mu_w \eta + (\gamma_m \Gamma)^2$$

$$\gamma_m^2 = \frac{\alpha_w J_m}{2}$$

The thruster efficiency as a function of thruster exhaust velocity c could assume the form

$$\eta = \frac{1}{1 + \left(\frac{d}{c}\right)^2} \qquad d = 20 \text{ km/sec (hypothetical, Ref. IV-1)}$$

or

$$\eta = \frac{1}{1 + \left(\frac{5000}{I_{sp} + 5000}\right)^2} - 0.03 \qquad \text{electron bombardment,}$$

or

$$\eta = \frac{1}{1 + \left(\frac{2000}{I_{sp} + 2000}\right)^2} - 0.06 \qquad \text{heavy molecule}$$

The derivation of the equation for optimum μ_w is based on the assumptions that the average thrust acceleration, $\bar{a}$, for a trajectory with given Γ is invariant with μ_w and that the minimum value of Γ is also invariant with μ_w. Thus for different values of Γ (i.e., ν_A and ν_B), the average thrust acceleration must be determined, and this value is fixed during the solution of the foregoing series of equations.

Numerical Optimization Procedure

The major problem of the entire analysis is in deriving a functional form of $\Gamma(\nu_A, \nu_B)$. The trajectory optimization program has not been modified to include the system optimization as part of the over-all optimization primarily because of the various modes of operation desired and the numerous propulsion parameters required as input. It was felt expedient for present purposes to keep the hybrid-thrust system optimization separate and use a parametric approach to the computation of optimum ν_A and ν_B for a given set of dates. In this way, at fixed dates, the resulting Γ "surface" may be used many times for flight profile variations and different propulsion parameters rather than recompute the optimum trajectories as would be necessary if it were part of an over-all optimization procedure.

At first it appeared feasible to fit some functional form representing a geometric surface in three dimensions to the high-low thrust mix data. In a particular case for an Earth-to-Mars trajectory this fit yielded surprisingly accurate results if the surface was assumed to be approximated by an elliptic paraboloid of the form

$$\Gamma = \frac{[-d_2(\nu_A - 1) + d_1(\nu_B - 1)]^2}{a^2} + \frac{[d_1(\nu_A - 1) + d_2(\nu_B - 1)]^2}{b^2}$$

with vertex at $\nu_A = 1$, $\nu_B = 1$, and where a, b, d_1, d_2 are constants determined in the process of fitting the surface. An example of the Γ surface is shown in Fig. IV-14. This figure is the normalized version of that shown in Fig. V-6 of Section V.

As the analysis proceeded, it was noted that considerable time may be saved if, instead of attempting to fit an analytic expression to the different Γ surfaces, a table of Γ for various (ν_A, ν_B) was used. In this way, the table may be generated quickly by properly sequencing the series of computations in the trajectory optimization program for the different sets of hyperbolic excess speeds. Furthermore, it is not reasonable to expect, without further theoretical study, that the Γ surface can always be approximated by an elliptic paraboloid or any other simple geometric surface.

For interpolating within the table, a nonlinear fit is applied to the four adjacent points. The accuracy of the interpolation naturally depends on the number of rows (columns) used for ν in the range 0 to 1.0. From simple sensitivity studies performed using various table sizes, it was concluded that a 5 x 5 or 6 x 6 table is sufficient for the current mission analysis purposes. Some results of the sensitivity studies which used a tabular form of Fig. IV-14 are shown in Table IV-1. Note that the quantity of final interest, μ_L, is slightly affected even if the corresponding hyperbolic excess

speeds differ significantly among the various Γ sources, i.e., the function, or 9 x 9 or 5 x 5 table. The differences noted are referenced to the values obtained using the function, i.e., elliptic paraboloid.

Once the dependence of Γ on (ν_A, ν_B) is determined, the corresponding payload ratio equations are optimized using a numerical procedure termed direct search (Ref. IV-2). This procedure involves straightforward search strategies which do not necessarily require the usual classical techniques. In brief, a starting solution, i.e., first guesses for (ν_A, ν_B), is introduced into the appropriate equations and the solution evaluated. Small perturbations (or explorations) are made in one independent variable while keeping the others fixed, and a "direction" is determined which increases the value of the payoff. After each variable has acquired a direction, a "move" is then made which involves changing all variables by the determined amounts. After a move is made, the value of the payoff function is evaluated and compared to previous results to ensure that the directions used are successful. This procedure is repeated until a failure results, at which time exploratory moves are again instituted until a new set of directions is determined. If no improvements are made, the step size (or exploration) is decreased, and the procedure is started with the latest estimates for (ν_A, ν_B). A solution is obtained when the step size becomes less than some input tolerance. A more detailed discussion of this search technique and the associated computer program is given in Appendix G.

This simple numerical procedure has been quite successful in attacking the problems so far analyzed. Figure IV-15 typifies the numerical results obtained from a sample optimization. Note that the structural factor of a given high-thrust step is assumed constant during the optimization. Since the over-all approach is to obtain an estimate of the hyperbolic excess speeds to use in the actual mass computation, it is necessary to estimate what the structural factors would be after such computations have been performed. Fortunately the maximum payload ratio is not significantly affected (about 10%) by drastic changes in the structural factors. Thus a reasonable guess for these factors based on high-thrust steps previously computed should provide results close to the optimum. This approximate approach to the structural factors has been found to be expedient rather than attempting to correlate step inert weight growth with payload or propellant weight in order to include it in the optimization procedure itself.

REFERENCES

IV-1. Melbourne, W. G. and C. G. Sauer, Jr.: Payload Optimization for Power-Limited Vehicles. JPL Space Programs Summary No. 37-17, Vol. IV, October 1962.

IV-2. Hooke, R. and T. A. Jeeves: Direct Search Solution of Numerical and Statistical Problems. Journal of the Association of Computing Machinery, Vol. 8, No. 2, April 1961, pp. 212-229.

TABLE IV-1

SENSITIVITY OF PAYLOAD RATIOS TO "Γ SURFACE"

Nuclear Propulsion, I_{sp} = 800 sec α_w = 10 kg/kw
LV ⊕ 4215 AR ♂ 4375

		Γ Function			9 x 9 Table						5 x 5 Table					
β_1	β_2	ν_A	ν_B	μ_L	ν_A	ν_B	μ_L	% Diff ν_A	% Diff ν_B	% Diff μ_L	ν_A	ν_B	μ_L	% Diff ν_A	% Diff ν_B	% Diff μ_L
.15	.15	.7156	.4212	.3200	.7538	.4000	.3192	5.3	5.0	.25	.8000	.4000	.3191	11.8	5.0	.28
	.20	.7238	.3975	.3116	.7538	.4000	.3110	4.1	.63	.19	.8000	.4000	.3109	10.5	.63	.22
	.25	.7325	.3725	.3027	.7538	.4000	.3018	2.9	7.4	.30	.8000	.4000	.3016	9.2	7.4	.36
	.30	.7412	.3475	.2930	.7812	.3669	.2915	5.4	5.6	.51	.8000	.4000	.2910	7.9	15.1	.68
.20	.15	.6819	.4250	.3050	.6788	.4000	.3041	.45	5.8	.30	.7944	.4000	.3032	16.5	5.9	.59
	.20	.6894	.4012	.2969	.6788	.4000	.2963	1.5	.30	.20	.7944	.4000	.2954	15.2	.30	.51
	.25	.6981	.3762	.2883	.6788	.4000	.2874	2.8	6.3	.31	.7944	.4000	.2866	13.8	6.3	.59
	.30	.7069	.3506	.2790	.6950	.3788	.2775	1.7	8.0	.54	.7944	.4000	.2766	12.4	14.09	.86
.25	.15	.6438	.4294	.2882	.6062	.4000	.2876	5.8	6.8	.21	.7088	.4000	.2857	10.1	6.8	.87
	.20	.6519	.4050	.2806	.6062	.4000	.2802	7.0	1.2	.14	.7088	.4000	.2784	8.7	1.2	.78
	.25	.6600	.3800	.2723	.6062	.4000	.2718	8.2	5.3	.18	.7088	.4000	.2701	7.4	5.3	.81
	.30	.6681	.3544	.2635	.6131	.3900	.2623	8.2	10.0	.46	.7088	.4000	.2606	6.1	12.9	1.1
.30	.15	.6025	.4344	.2695	.6000	.4000	.2691	.41	7.9	.15	.6256	.4000	.2667	3.8	7.9	1.0
	.20	.6094	.4094	.2623	.6000	.4000	.2622	1.5	2.3	.04	.6256	.4000	.2599	2.7	2.3	.91
	.25	.6175	.3844	.2545	.6000	.4000	.2544	2.8	4.1	.04	.6256	.4000	.2522	1.3	4.1	.90
	.30	.6250	.3581	.2462	.6000	.3919	.2455	4.0	9.4	.23	.6256	.4000	.2433	.10	11.7	1.2

MARS PARKING ORBIT SUMMARY

PERIAPSIS = 1.28 MARS RADII

E-90262-6

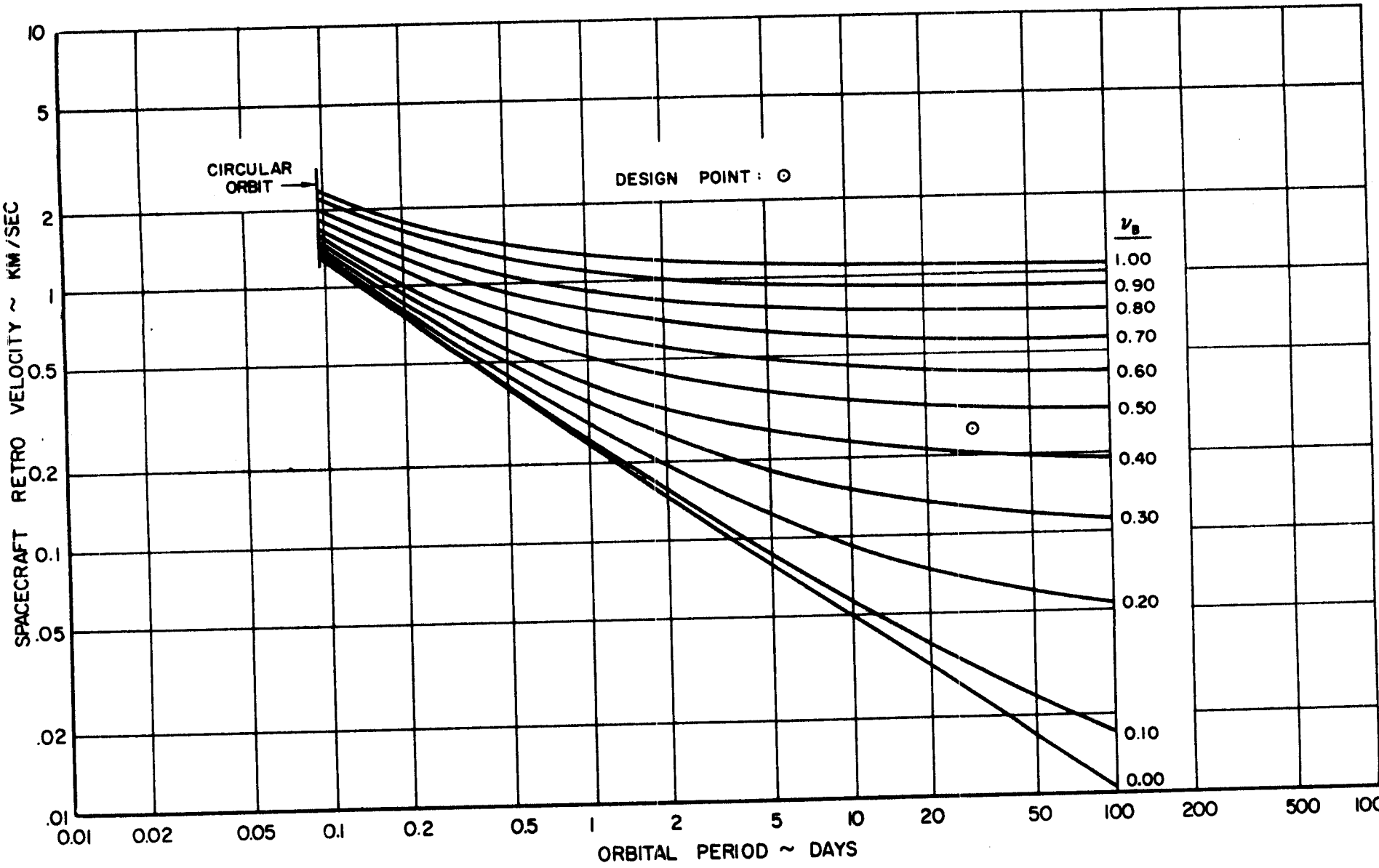

FIG. IV-1

MARS MISSION REQUIREMENTS
SINGLE - ELECTRIC SYSTEM

POWERPLANT CONFIG 8

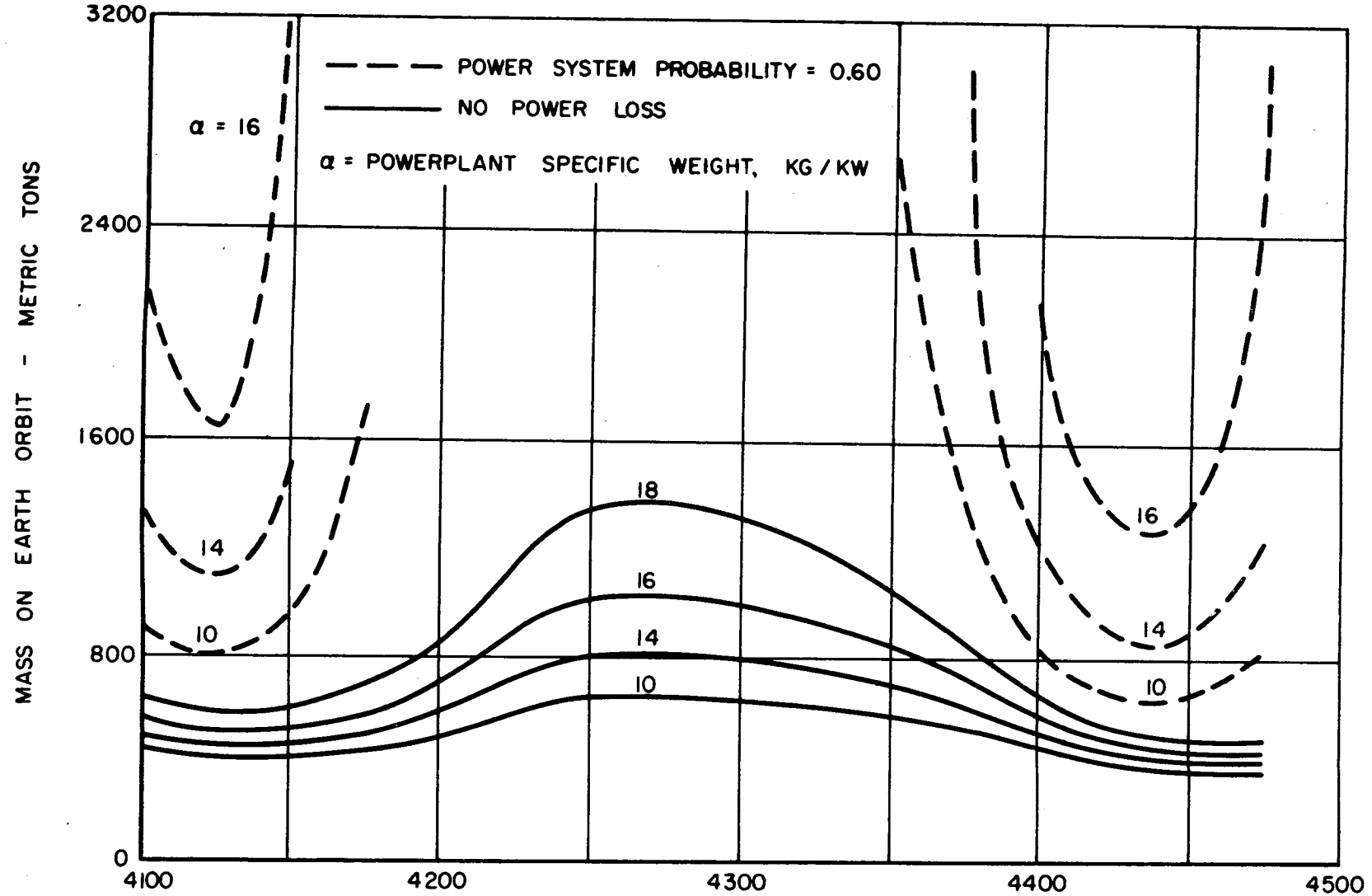

E-910262-6

FIG. IX-2

FIG. IV-3

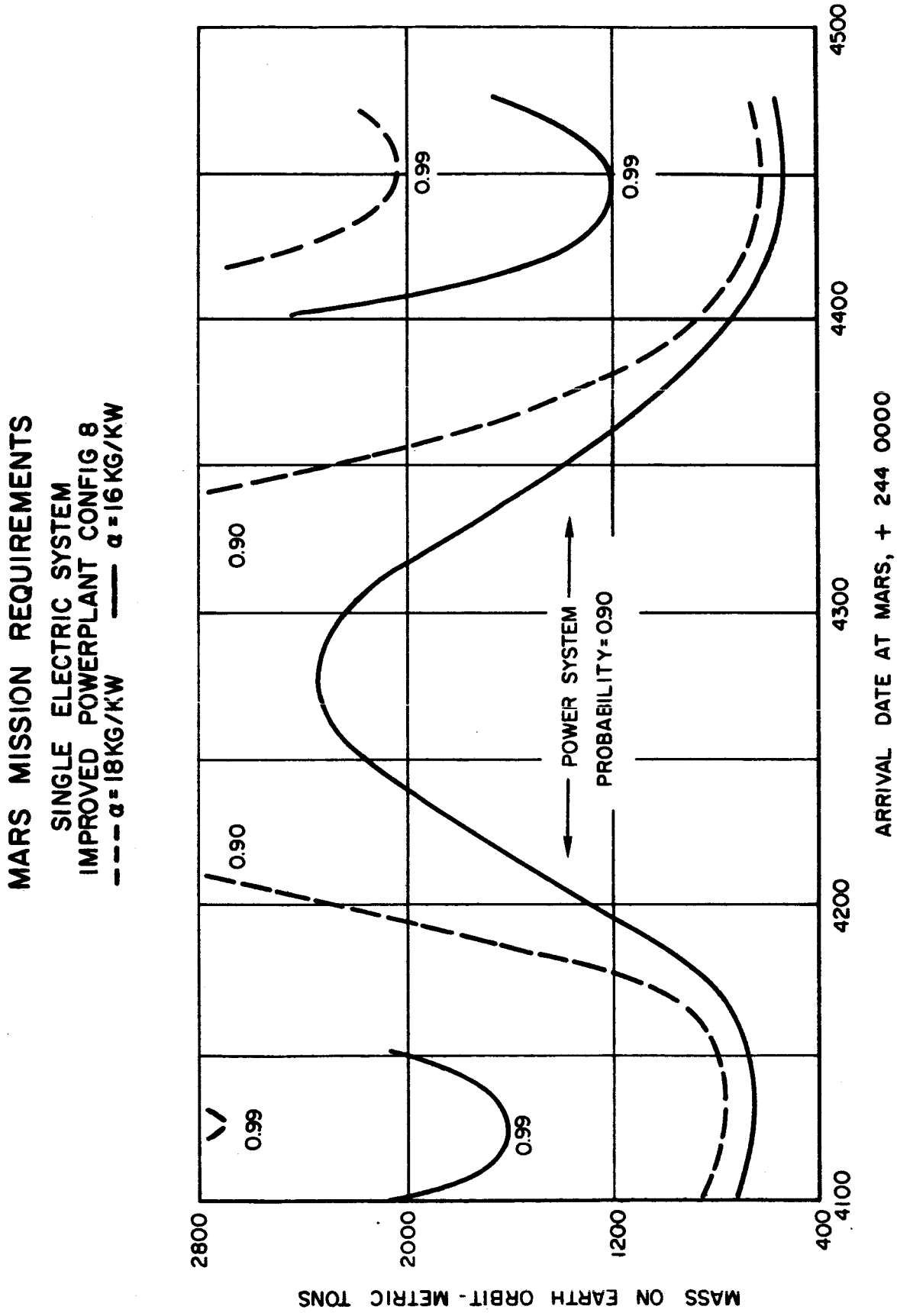
MARS MISSION REQUIREMENTS
SINGLE ELECTRIC SYSTEM
IMPROVED POWERPLANT CONFIG 8
---α=18KG/KW —— α=16KG/KW
MASS ON EARTH ORBIT - METRIC TONS
2800
2000
1200
400
4100
4200
4300
4400
4500
ARRIVAL DATE AT MARS, + 244 0000
POWER SYSTEM
PROBABILITY=0.90
0.90
0.99
0.90
0.99
0.99
0.99

MARS MISSION REQUIREMENTS
SINGLE ELECTRIC SYSTEM

POWERPLANT CONFIG 2

IMPROVED TECHNOLOGY

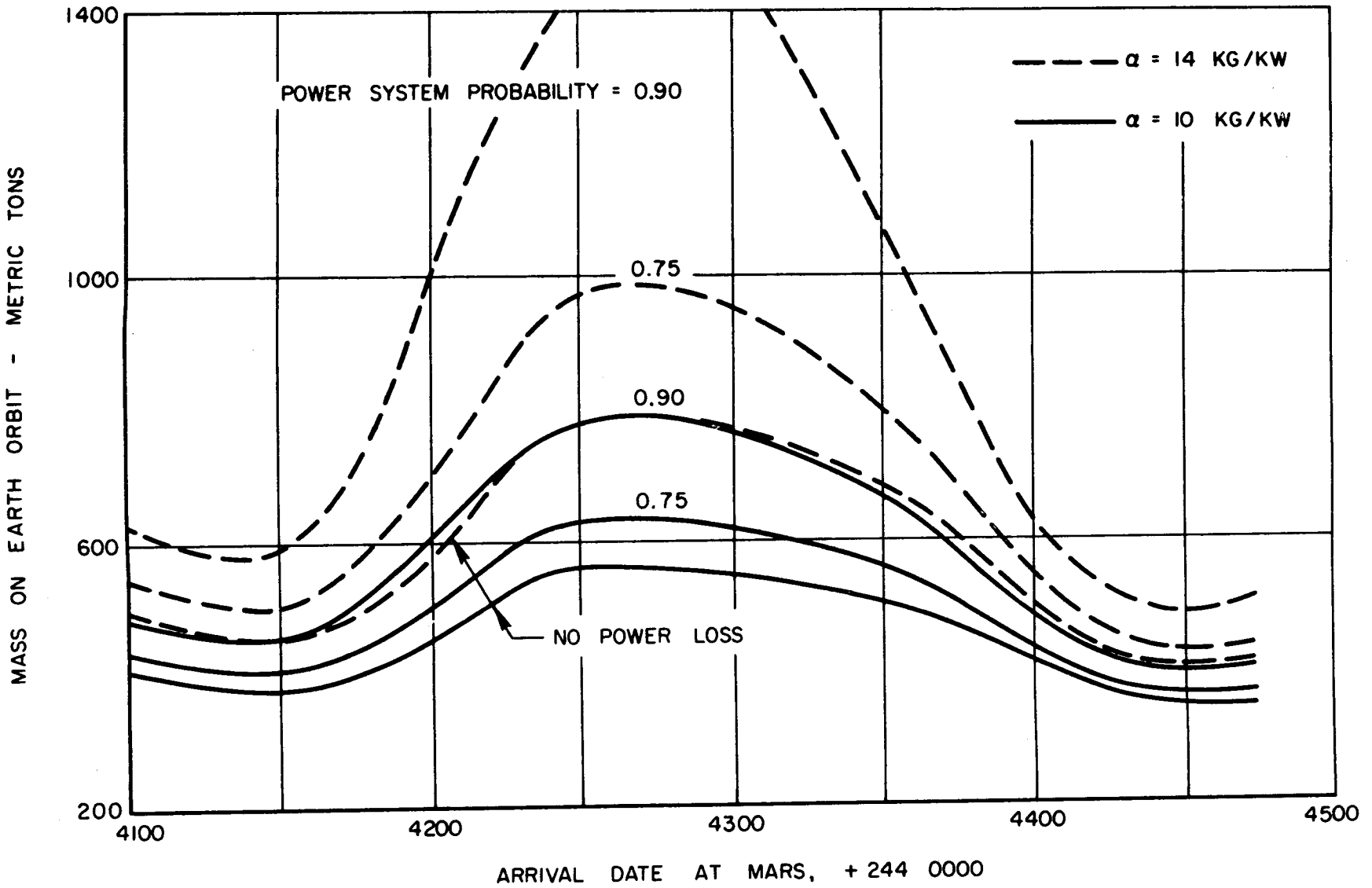

E-910262-6

FIG. IV-4

MARS MISSION REQUIREMENTS
DUAL ELECTRIC SYSTEM

POWERPLANT CONFIG 2

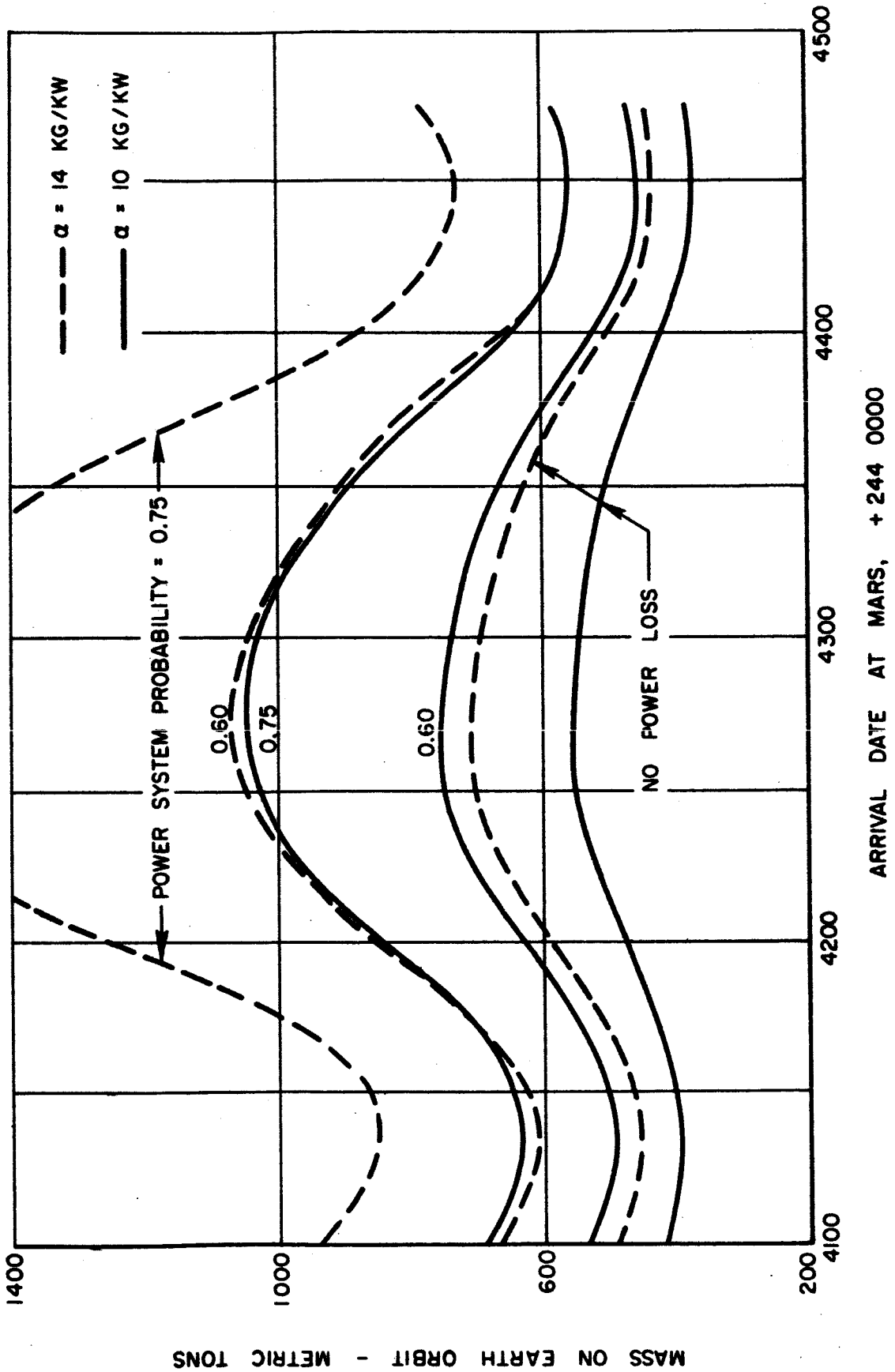

FIG. IV-6

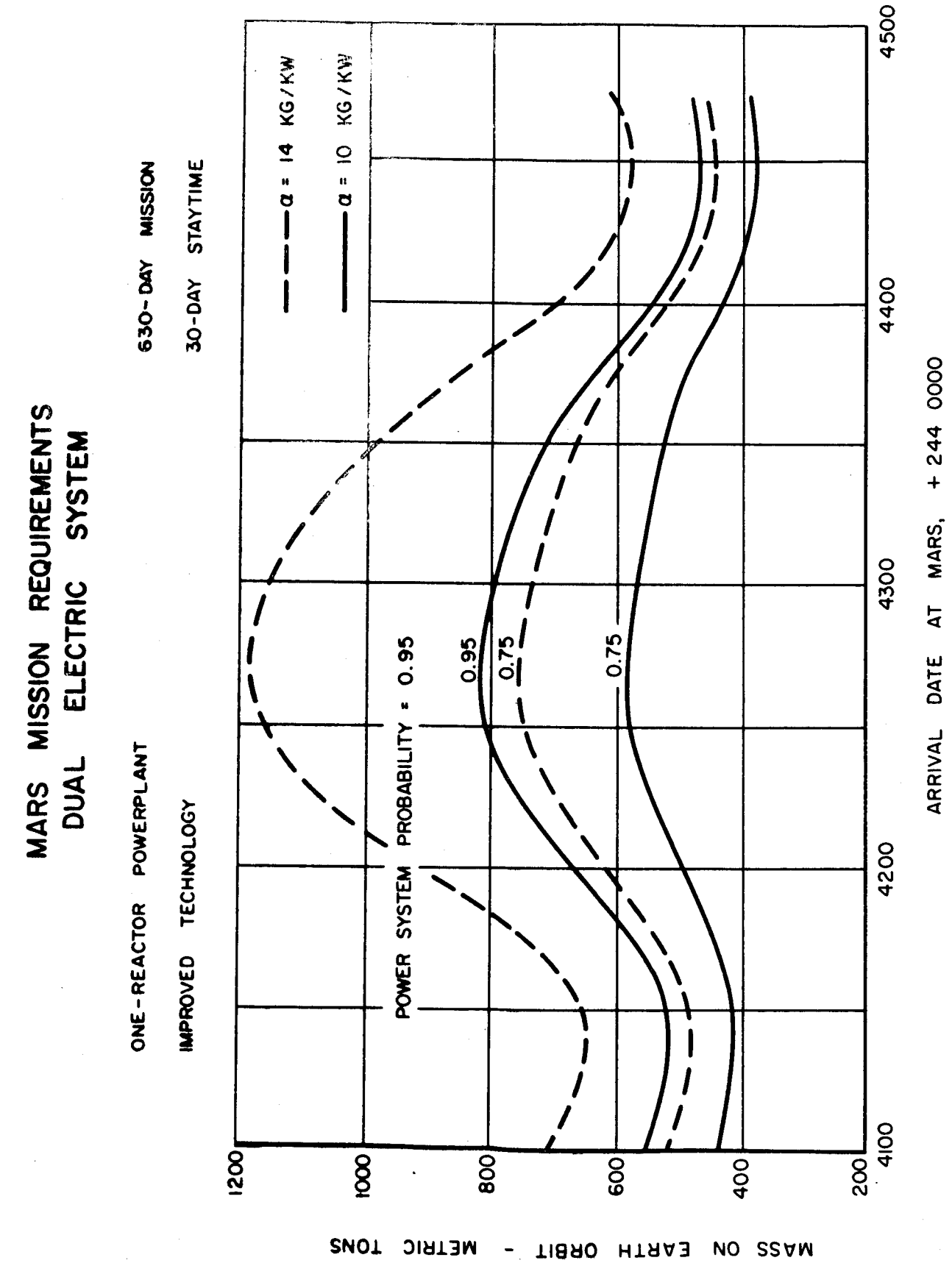
MARS MISSION REQUIREMENTS
DUAL ELECTRIC SYSTEM
ONE-REACTOR POWERPLANT
IMPROVED TECHNOLOGY
630-DAY MISSION
30-DAY STAYTIME
α = 14 KG/KW
α = 10 KG/KW
POWER SYSTEM PROBABILITY = 0.95
0.95
0.75
0.75
MASS ON EARTH ORBIT - METRIC TONS
1200
1000
800
600
400
200
4100
4200
4300
4400
4500
ARRIVAL DATE AT MARS, + 244 0000

E-910262-6

FIG. IV-7

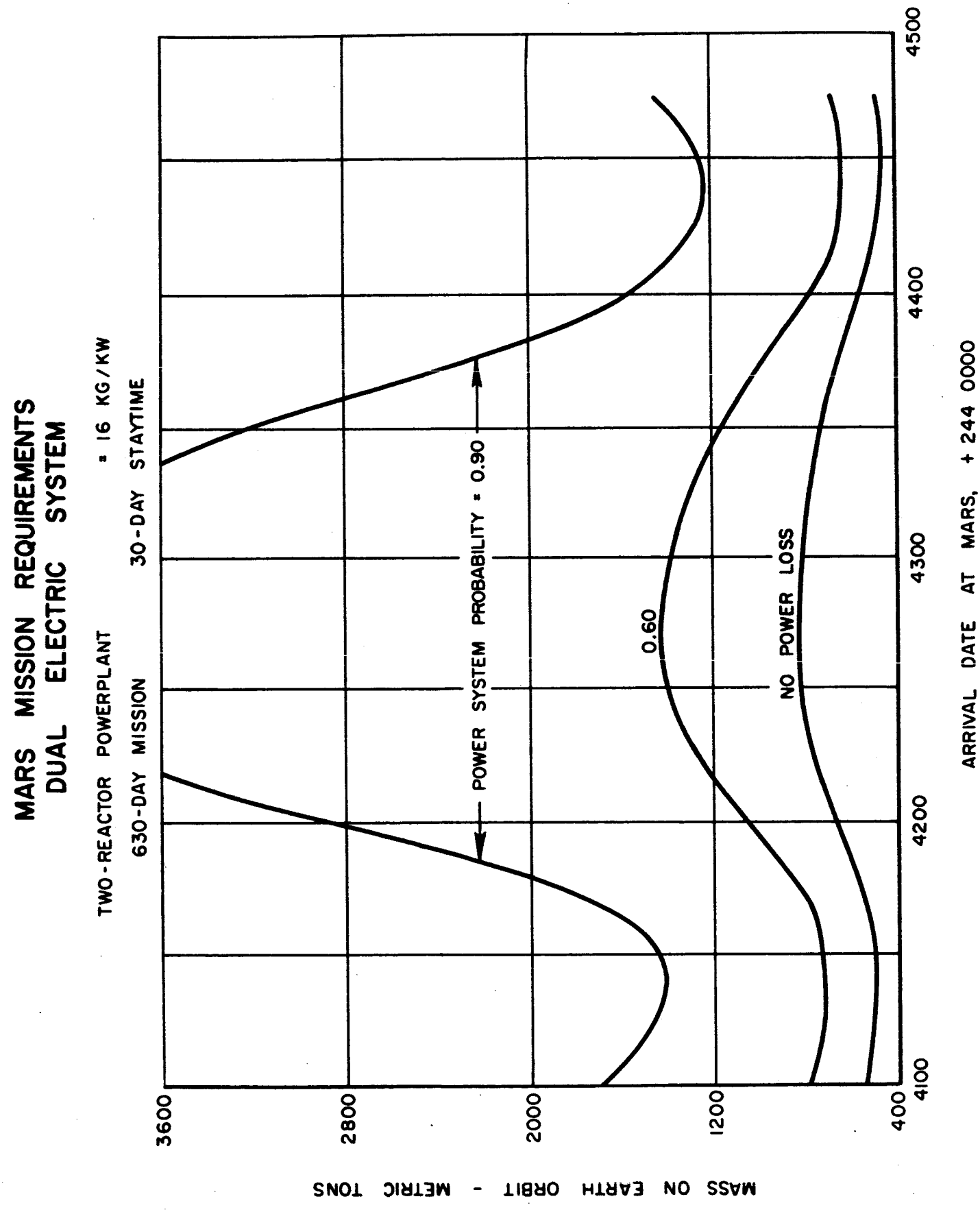

MARS MISSION REQUIREMENTS
DUAL ELECTRIC SYSTEM
POWERPLANT CONFIG 8 IMPROVED TECHNOLOGY

α = 18 KG / KW

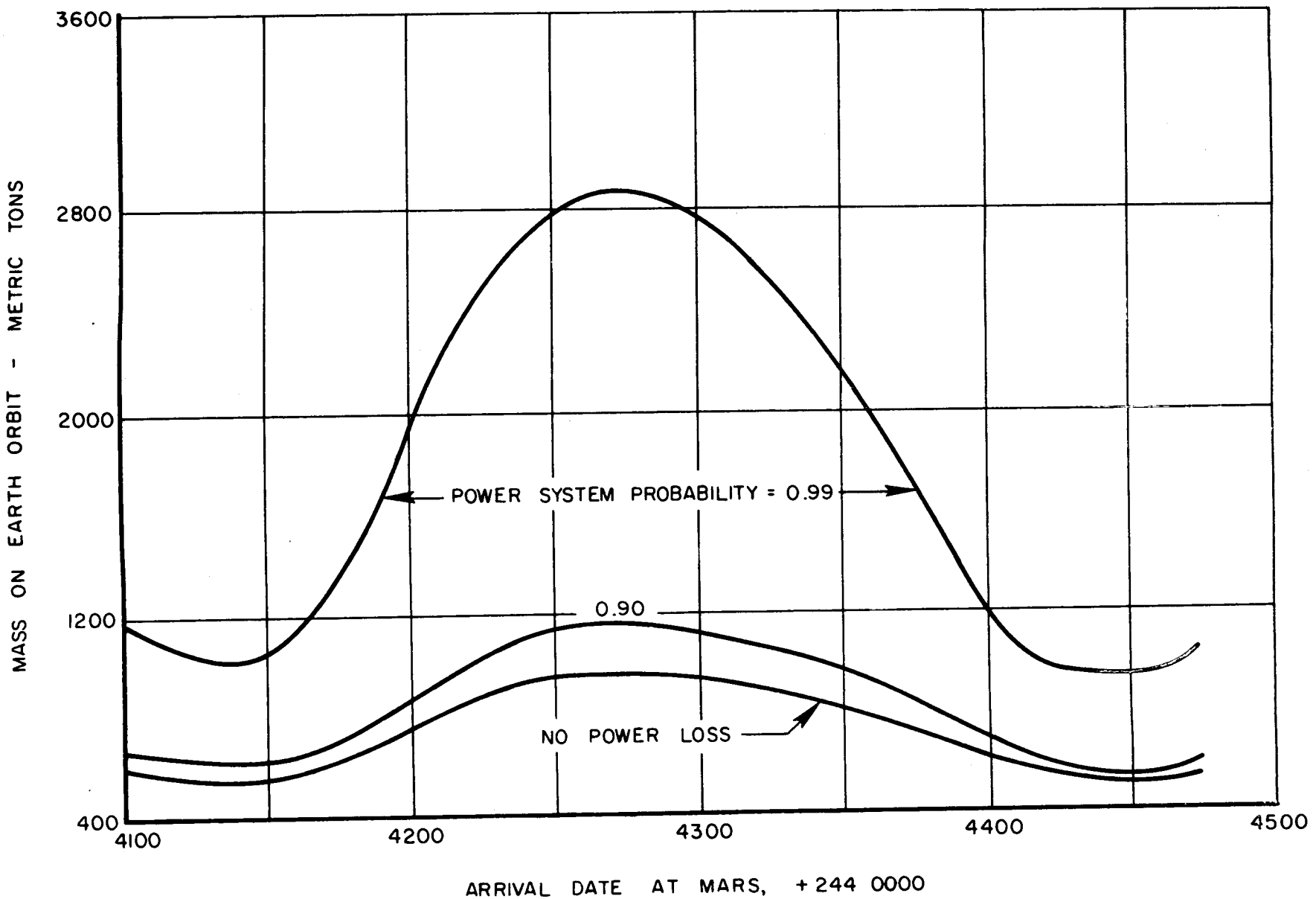

E-910262-6

FIG. IX - 8

E-910262-6

FIG. IV-9

COMPARISON OF SINGLE AND DUAL ELECTRIC SYSTEMS

POWERPLANT CONFIG 8
IMPROVED TECHNOLOGY
POWER SYSTEM
PROBABILITY = 0.90

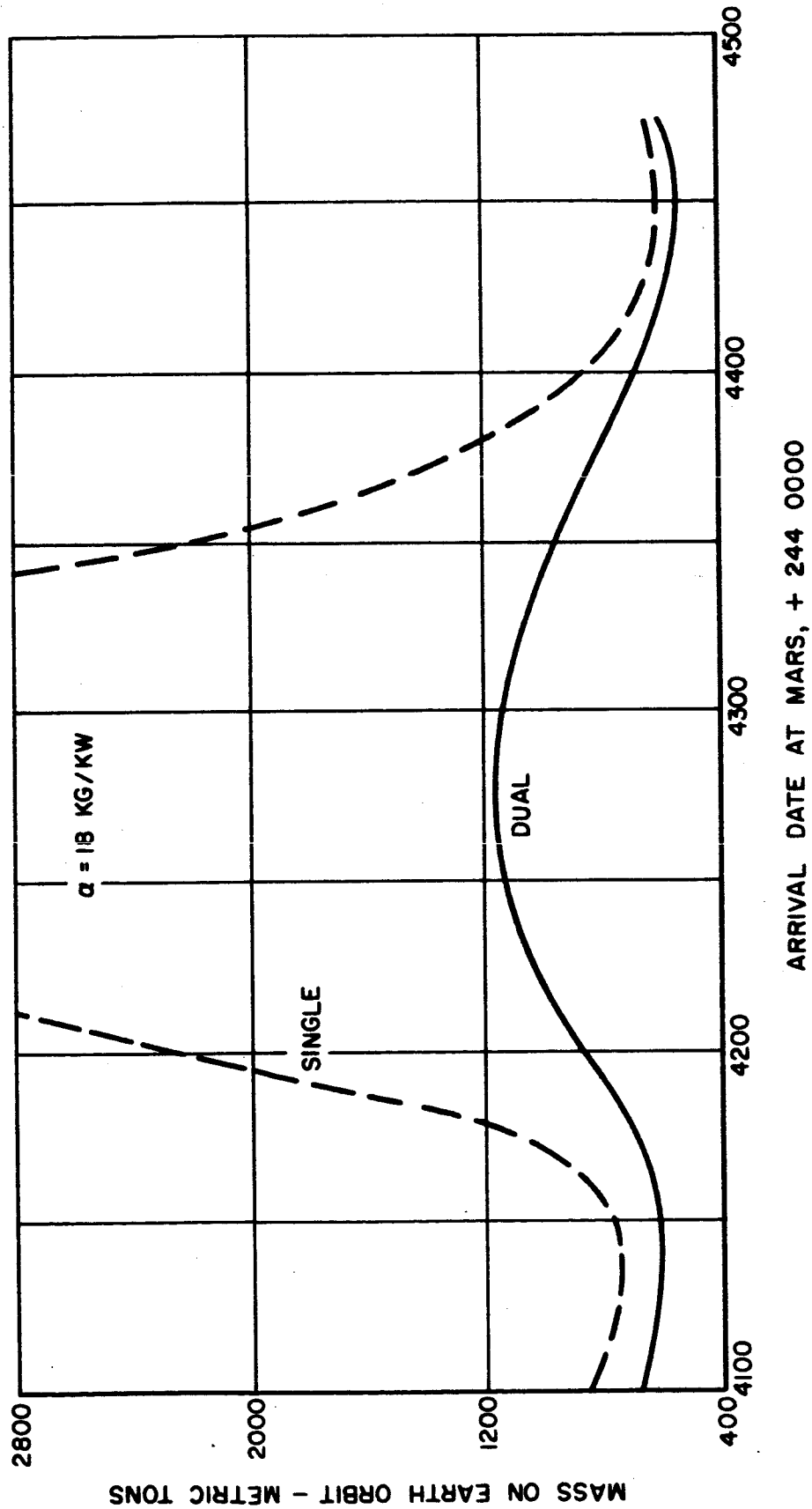

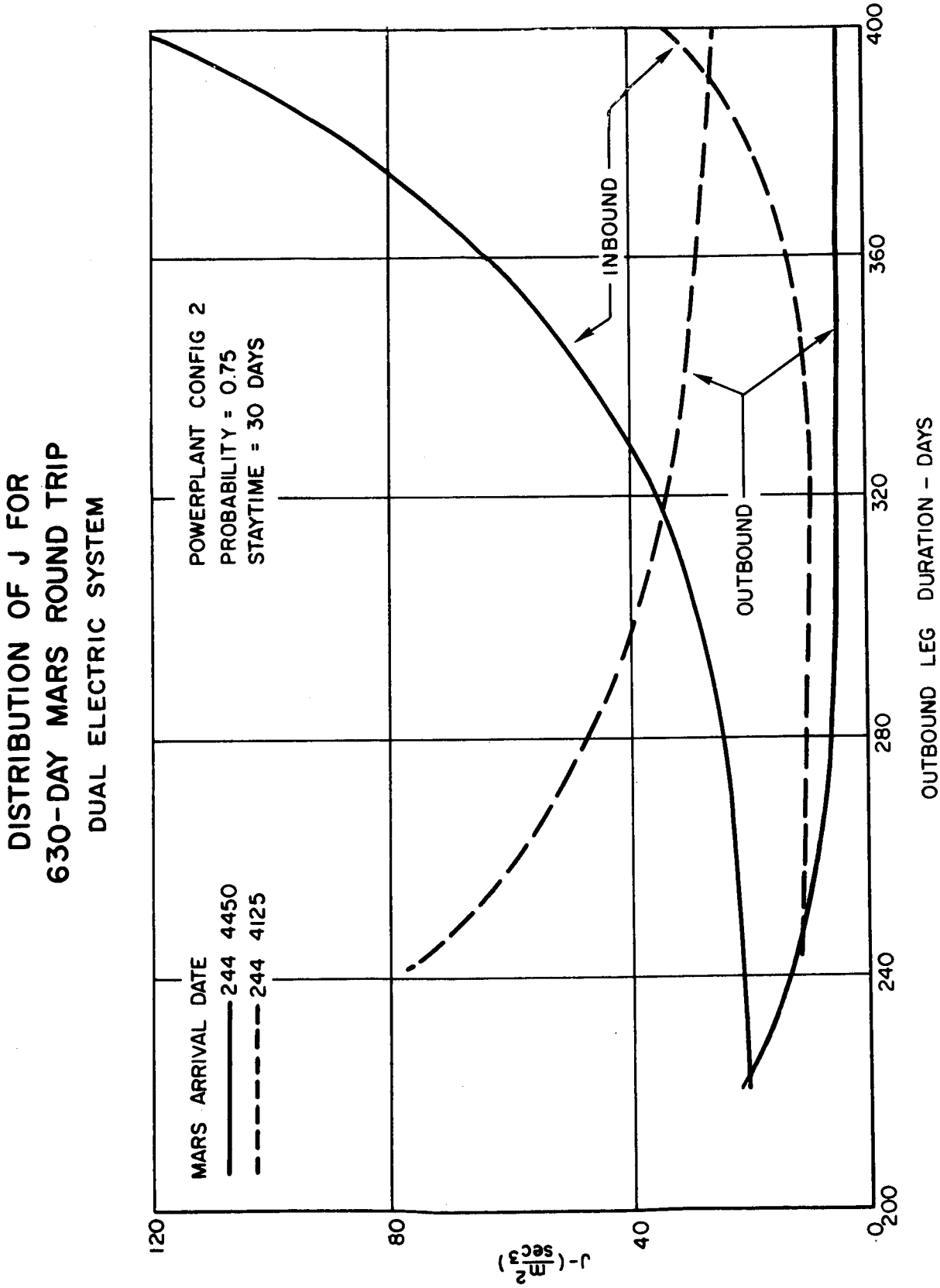
DISTRIBUTION OF J FOR
630-DAY MARS ROUND TRIP
DUAL ELECTRIC SYSTEM
POWERPLANT CONFIG 2
PROBABILITY = 0.75
STAYTIME = 30 DAYS
MARS ARRIVAL DATE
244 4450
244 4125
INBOUND
OUTBOUND
J-(km²/sec³)
120
80
40
0
200
240
280
320
360
400
OUTBOUND LEG DURATION - DAYS

COMPARISON OF MINIMUM TOTAL J TRIPS

DUAL ELECTRIC SYSTEM
POWERPLANT CONFIG. 2

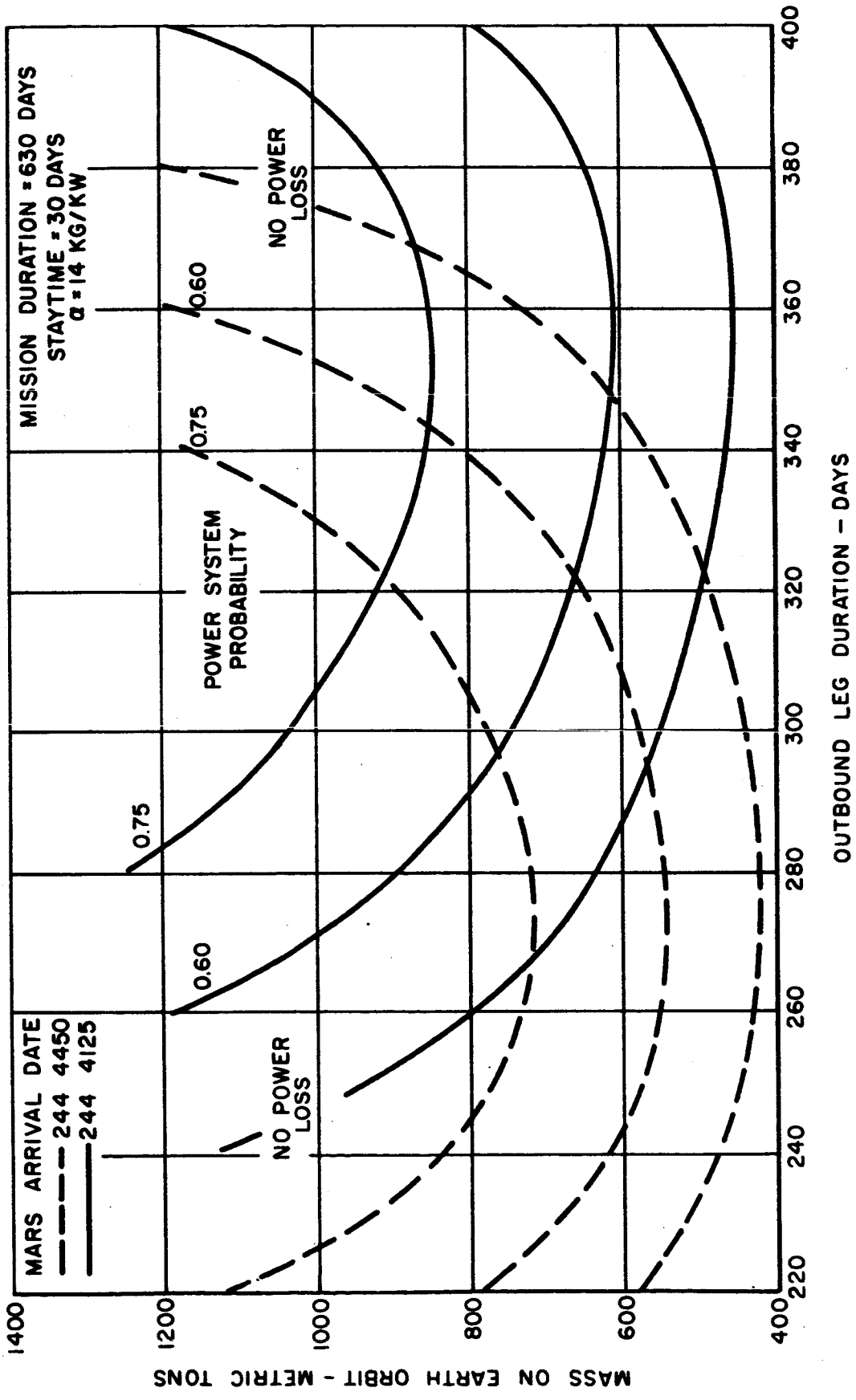

OPTIMIZATION OF HYBRID THRUST SYSTEMS

MARS 430 - DAY ROUND TRIP

MARS DEPARTURE = 0.10 EMOS
EARTH ARRIVAL = 0.50 EMOS
1980 OPPOSITION

DUAL ELECTRIC SYSTEM
IMPROVED POWERPLANT CONFIG 8
PROBABILITY LEVEL = 0.90

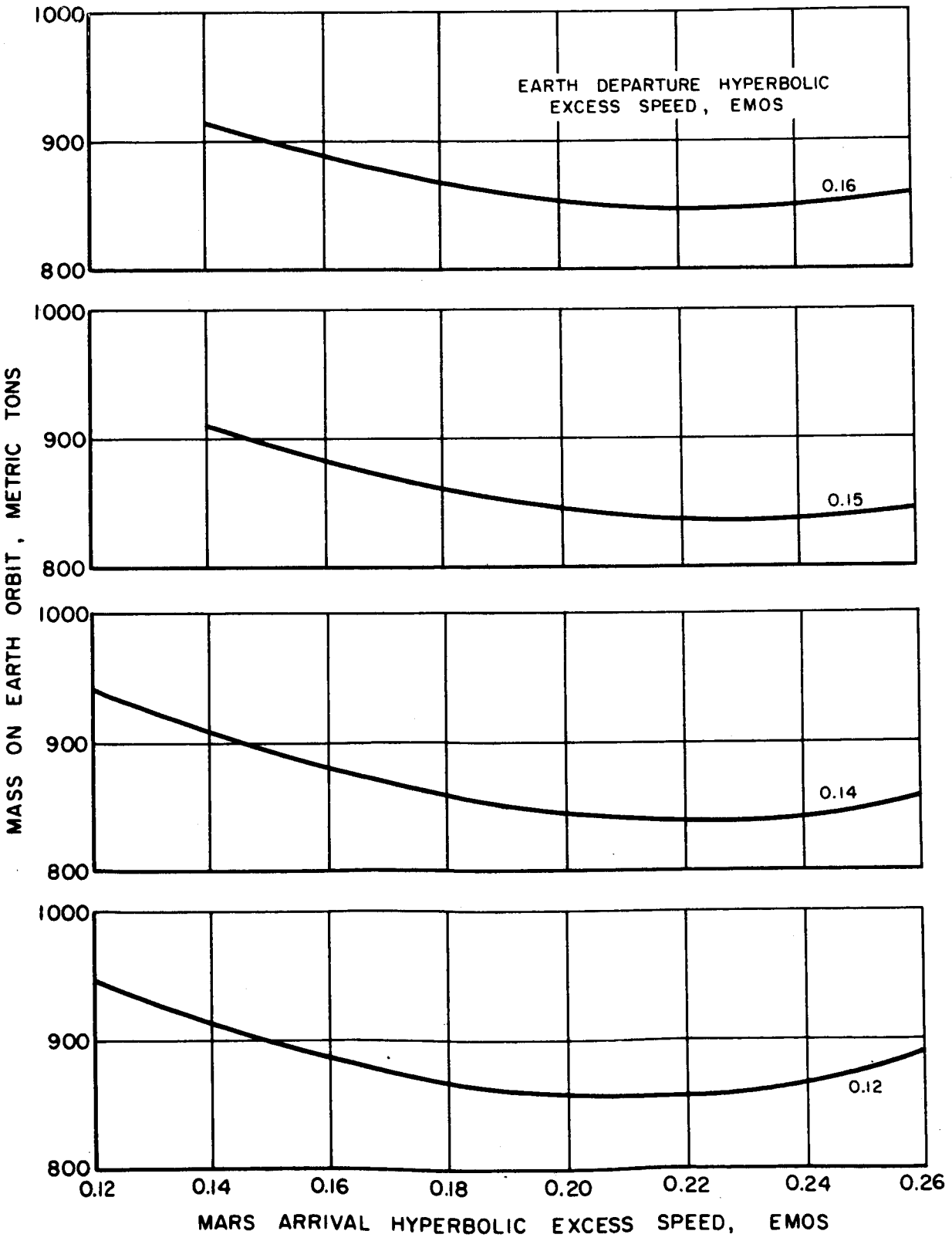

MINIMUM MASS HYBRID - THRUST SYSTEM

MARS 430 - DAY ROUND TRIP

MARS DEPARTURE = 0.10 EMOS
EARTH ARRIVAL = 0.50 EMOS
1980 OPPOSITION
DUAL ELECTRIC SYSTEM
IMPROVED POWERPLANT CONFIG 8
PROBABILITY LEVEL = 0.90

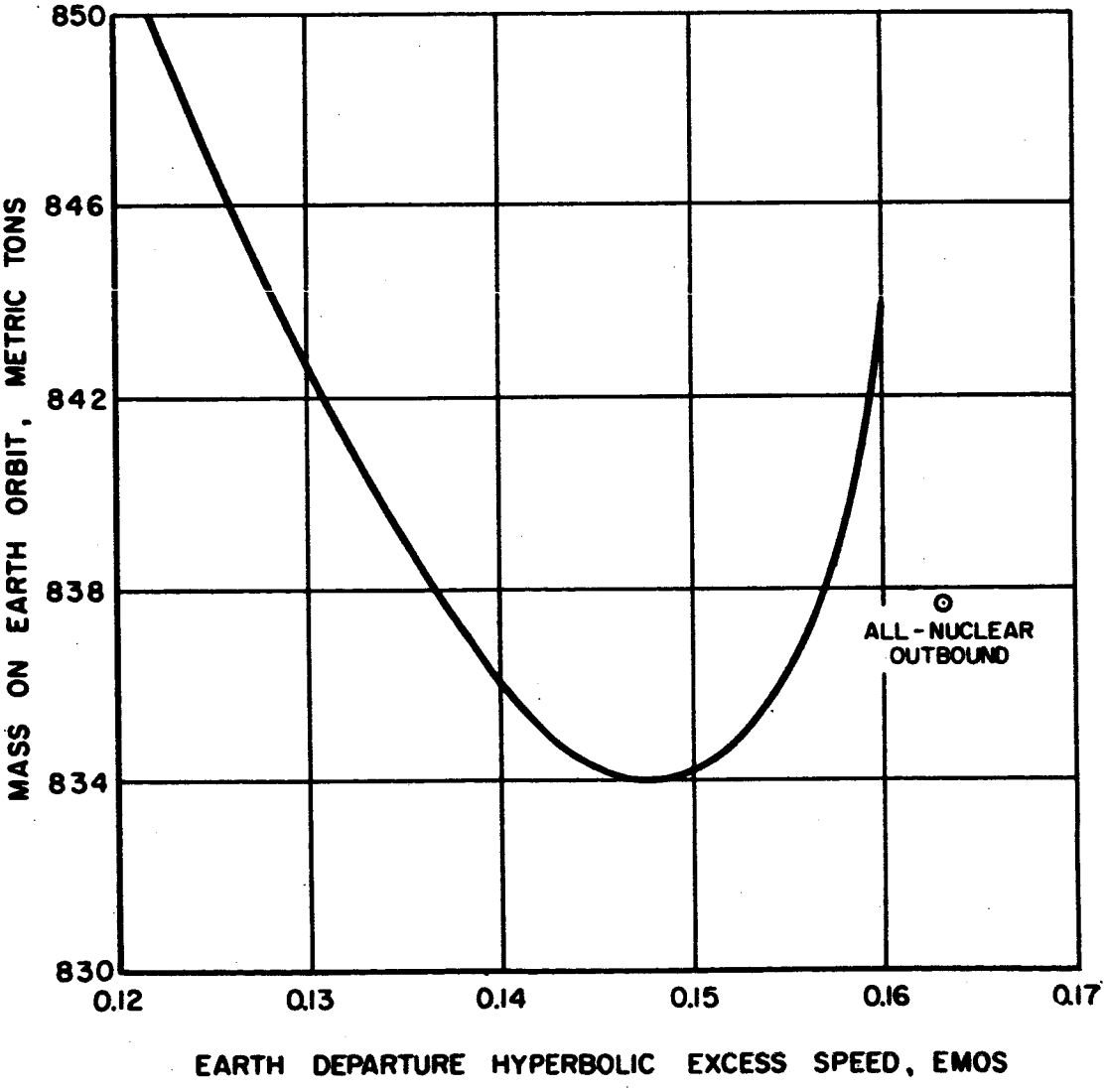

MIXED—THRUST EARTH—MARS TRANSFER

LV ⊕ 4215 AR ♂ 4375

$V_{\infty A}$ = 0.163 EMOS $V_{\infty B}$ = 0.260 EMOS

$J_m = 37.96\ m^2/sec^3$

$$\Gamma^2 = \frac{J}{J_m}$$

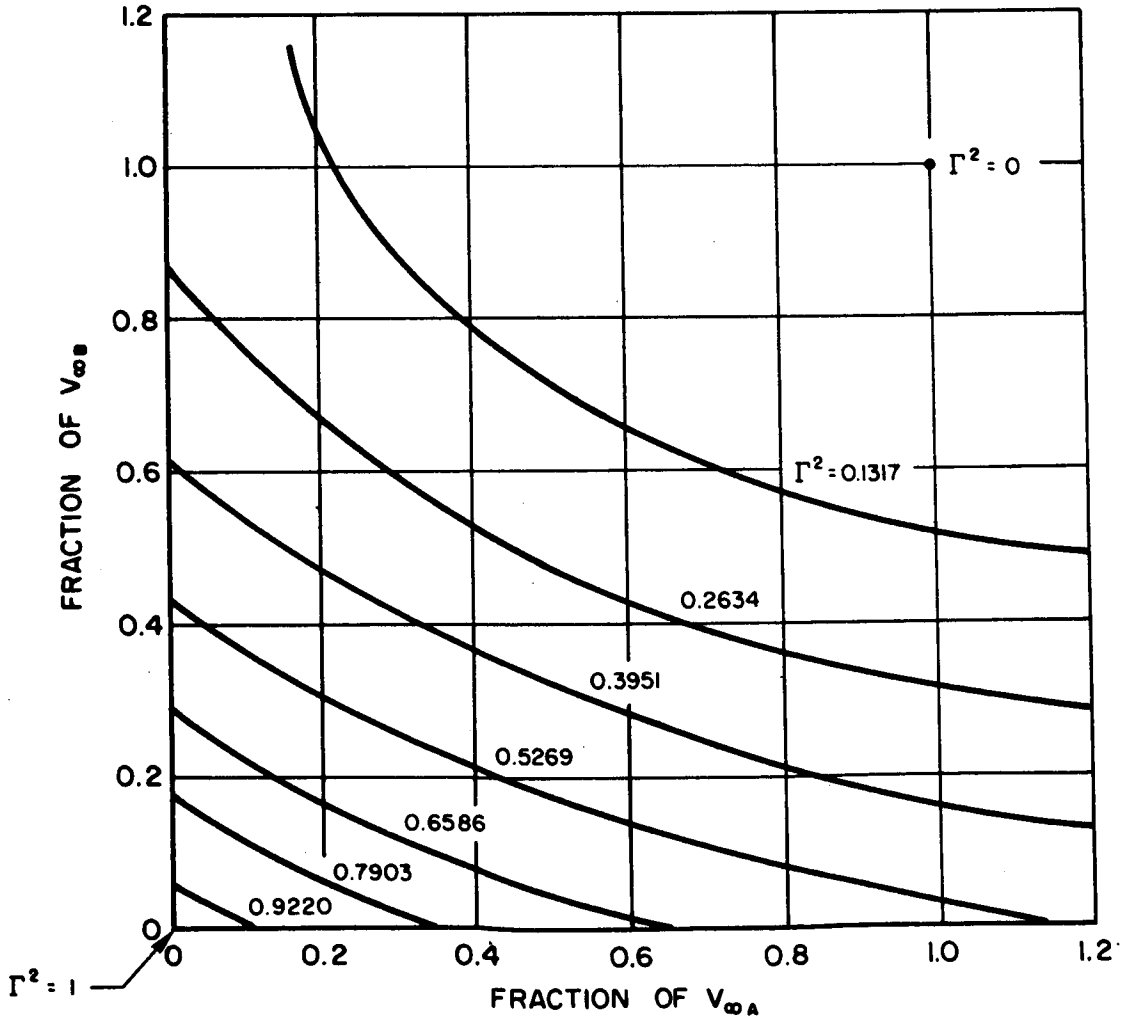

OPTIMIZATION OF HIGH - LOW - HIGH THRUST OPERATION

LV ⊕ 244 4215 $V_{\infty A}$ = 0.163 EMOS

AR ♂ 244 4375 $V_{\infty B}$ = 0.260 EMOS

β_2 = ARRIVAL STEP STRUCTURAL FACTOR

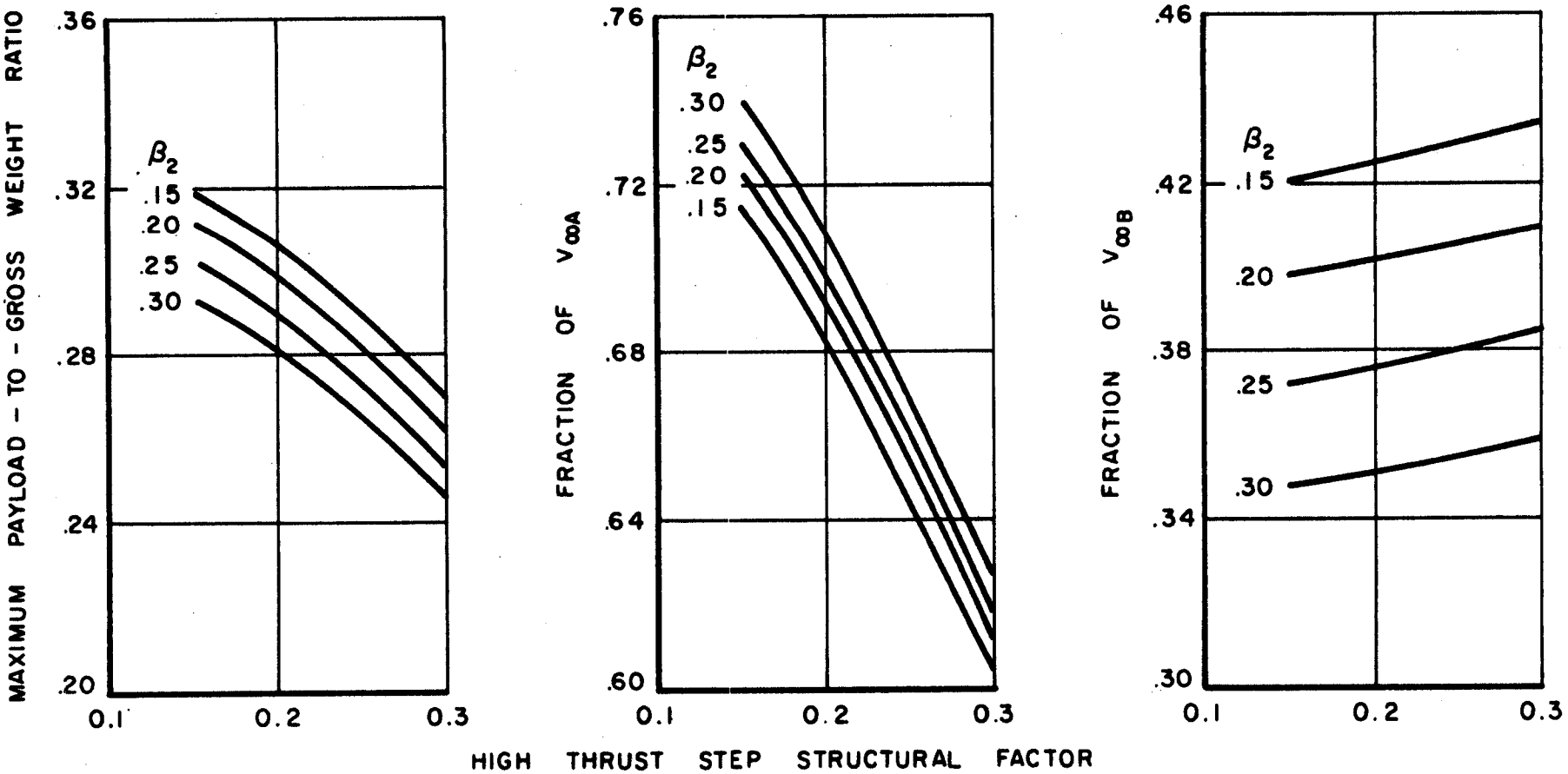

FIG. XII - 15

SECTION V
TRAJECTORY ANALYSES

The trajectory analyses were based upon approximating the n-body problem by a succession of two-body problems. This approach yields accurate results for propulsion requirements if the two-body solutions are properly matched. Failure to properly match the solutions had led to overestimation of the propulsion requirements in many low-thrust studies. An analysis of matching planetocentric and heliocentric trajectories is discussed in Appendix C.

At the beginning of the present study three important points pertaining to trajectories were realized: (1) for a meaningful mission study involving low-thrust propulsion it is important to optimize all interplanetary trajectories at least with respect to minimum propellant expenditure; (2) to achieve definitive results in a low-thrust manned Mars mission study requires the production of large amounts of optimum trajectory data; and (3) all the numerical computational methods for generating "exact" optimum low-thrust interplanetary trajectories known at the start of the study required too much machine time to be compatible with the second point above, and, furthermore, none of these were fully automated but required some artful guessing of such quantities as initial values of Lagrange multipliers, starting solutions, etc.

Taking account of the points just made, it was believed at the outset that only an accurate analytical approximation could possibly fulfill the arduous trajectory demands of the study. Throughout the initial phase of the study many analytical or semianalytical approximations were tried. None of these proved to be accurate enough to provide significant results. The characteristic length approximation (Ref. V-1) proved highly inaccurate for trip times greater than 180 days. The linearized analytic approximation set forth in Refs. V-2 and V-3 also lacked the accuracy required for the study.

Numerical Methods for Solving Two-Point Boundary Value Problems

Since none of the analytical approximations proved to be even marginally adequate for the mission study, the only alternative left was numerical analysis with the attendant requirements of lengthy computer operation. The numerical methods for the solution of trajectory optimization problems and the associated two-point boundary value problem can be divided into two classes, direct and indirect methods. Examples of the former are the gradient methods (Refs. V-4 and V-5) which have large domains of convergence but require the artistic choice of various parameters and tend to converge slowly as the solution is approached. The indirect methods are concerned with the numerical solution of the Euler-Lagrange equations of the calculus of variations (Refs. V-6 and V-7).

For the low-thrust interplanetary trajectory optimization problem these differential equations are nonlinear and must be solved subject to imposed two-point boundary values. The classical approach is to integrate these equations numerically as if they were defined as an initial-value problem. Sufficient initial conditions on the Lagrange multipliers must be assumed and iteratively improved until the two-point boundary conditions are satisfied. Unfortunately, the great sensitivity of the trajectories to the initial values of the multipliers and the small neighborhood in which they must be initially assumed continue to plague those who attempt to use this method.

The Finite-Difference Newton-Raphson Algorithm

Last year, a new approach to the solution of the two-point boundary value problem had been tried with some success (Refs. V-8 and V-9). This method is based upon an extension of Newton's method for finding roots of nonlinear equations applied to operator equations in Banach spaces (Ref. V-10). This generalized Newton-Raphson method (developed in Refs. V-11, V-12, and V-13) offers not only a wide domain of convergence, but also quadratic convergence to the solution. Like the gradient methods, it requires that an initial approximation to the solution be supplied, but it does not require the guessing or adjustment of any numerical constants. Moreover, because of the wide domain of convergence, the initial approximation to the solution need not be a sophisticated one.

The generalized Newton-Raphson method involves the iterative solution of a sequence of linear two-point boundary-value problems in place of the single nonlinear two-point boundary-value problem. At the start of the present study, the only application of this method to trajectory optimization problems was reported in Ref. V-8. The method employed was to numerically integrate the system of linear first-order differential equations, and to then construct the solution by solving an associated system of linear algebraic equations. This method of solving the linear boundary-value problem as an initial-value problem will break down if the equations are unstable or if the associated matrices become ill conditioned.

An improvement of the generalized Newton-Raphson method has been made for the present mission study through the introduction of an implicit finite-difference approach to the linear two-point boundary value problem which has been discussed in Ref. V-14 and others. This finite-difference approach eliminates the difficulties of unstable equations by using a one-step method to solve the boundary-value problem. This replaces the boundary-value system with a large system of linear algebraic equations. The unique feature of the approach taken in the present study is the combination of the generalized Newton-Raphson method with the finite-difference approach for the solution of a system of nonlinear, second-order differential equations. A detailed exposition of the finite-difference Newton-Raphson algorithm is presented in Refs. V-15 and V-16 and in Appendix A of this report.

The algorithm was initially written to solve the problem of optimal low-thrust interplanetary trajectories in two dimensions for the particular case of constant kinetic power in the exhaust jet and completely unconstrained specific impulse. In the past months, two efforts have been undertaken that have modified these underlying assumptions and correspondingly altered the algorithm. First, the equations of motion were rederived (in three dimensions) to represent the case of constant specific impulse flight with optimal coast periods. As indicated in Ref. V-17, the assumption of constant specific impulse implies that payload mass cannot be directly maximized by minimizing the fuel consumed during the flight. Accordingly, this modification of the Newton-Raphson algorithm is adjoined with a second, external routine necessary to extremize the powerplant characteristics; these two routines together iteratively converge to the optimal thrust and steering schedule and the optimal propulsion parameters for the mission. This method utilizes initial guesses for the thrust magnitude and mass flow rate to converge to the optimal values of constant specific impulse, mass flow rate, and the duration of the coast phase such that $J = \int_0^T a^2 dt$ is minimized and payload fraction is maximized. Secondly, the governing differential equations were rederived for the case of completely unconstrained specific impulse and a jet exhaust power possessing a generalized dependence upon time and the position of the vehicle. This algorithm is written in three dimensions and can represent a variety of power modes. The algorithm has utility in the comparison of power modes for various type missions. These two modifications of the original algorithm are discussed in detail in the analyses that follow.

Statement of the Problem and Assumptions

For power-limited propulsion systems the mass of propellant expended is given by Eq. (1).

$$\frac{1}{M_T} = \frac{1}{M_0} + J = \frac{1}{M_0} + \int_0^T \frac{[a(t)]^2}{2P(X,t)}\, dt \qquad (1)$$

where M_T and M_0 are the final and initial masses of the vehicle, respectively, $\vec{a}(t)$ is the thrust acceleration of the vehicle over the powered flight time, T, and $P(X,t)$ is the kinetic energy in the exhaust jet relative to the vehicle; X represents the vector of state and control variables. Minimum propellant expenditure, that is, J, as small as possible is required for optimal variable-thrust trajectories (Ref. V-17). The Newton-Raphson algorithm computes interplanetary transfer trajectories of a power-limited low-thrust space vehicle between two given planets with specified departure and arrival times that are optimum in the sense that the value of

$$J = \int_0^T \frac{[a(t)]^2}{2P(X,t)}\, dt$$

is a minimum (the nature of this minimum value is discussed below). In the machine program, the algorithm numerically solves the Euler-Lagrange necessary conditions for a minimum value of J coupled with the differential equations of the motion which constrain the optimal trajectory.

The trajectory optimization problem has been solved under the following assumptions:

1. The electric thruster of the spacecraft is capable of completely variable specific impulse operation. Although this assumption may seem unrealistic in terms of present-day thrusters which can operate only at constant I_{sp}, variable I_{sp} thrusters may be developed by the 1980's and, furthermore, variable I_{sp} operation may be approached by using a number of thrusters each designed to operate at a fixed value of specific impulse. At any rate the unconstrained trajectory data give an optimistic bound on performance which is generally within about 10% of constant-thrust operation.

2. The interplanetary trajectories are computed taking into account only the central-force gravitational field of the sun, while the departure and arrival planets are considered to be points in heliocentric space.

3. The heliocentric orbits of the departure and arrival planets are considered to be coplanar but have the correct eccentricity. (Where indicated in the analysis that follows, the algorithm is in three dimensions with the attendant eccentricities and inclinations incorporated into the ephemeris-generating subroutine. Three-dimensional solutions indicate that the above two-dimensional approximation is a very good one.)

4. The planetocentric and heliocentric trajectories are computed separately and matched such that the asymptotic velocity of the vehicle in the planetocentric frame is added vectorially to the heliocentric velocity of the planet to give the boundary value of velocity for the interplanetary trajectory.

Variable-Thrust, Constant-Power Trajectories

The work presented in this paragraph has been reported in greater detail before (Ref. V-18) and is summarized here as a preface to the modifications of

the basic algorithm that follow. The two-dimensional model is assumed, as is constant power in the jet exhaust. Coupled with assumptions (1), (2) and (4) above, the differential equations governing the optimal trajectory are (see Appendix B):

$$\ddot{x} - u + \frac{x}{R^3} = o$$

$$\ddot{y} - v + \frac{y}{R^3} = o \qquad (2)$$

$$\ddot{u} - \frac{u\,(2x^2-y^2) + 3vxy}{R^5} = o$$

$$\ddot{v} - \frac{v\,(2y^2 - x^2) + 3uxy}{R^5} = o$$

where x, y are the position coordinates of the vehicle, $R^2 = x^2 + y^2$ and u, v are the Lagrange multipliers associated with the x, y directions, respectively. Physically, u, v represent the thrust acceleration of the vehicle in the x, y directions, respectively.

The Newton-Raphson algorithm numerically determines the state and control variables as functions of time such that the above differential equations are satisfied subject to a prescribed set of boundary conditions on the state variables and the time. These boundary conditions are computed by a built-in ephemeris-generating subroutine from knowledge of the departure and arrival planets and the launch and arrival Julian dates as input quantities.

Starting Solutions and Multiple Stationary Trajectories

The finite-difference Newton-Raphson algorithm requires a starting solution of the problem which consists of N values for each of the position and control variables and the time between the given boundary values. In the current program, the N mesh points are evenly spaced in time. The efficiency of the program could probably be improved somewhat, however, through the introduction of a variable mesh point spacing depending upon the time rate of change of the state variables in the different regions of the trajectory. For the Earth-Mars trajectories of the current study, the number of mesh points employed has ranged between 100 and 500, depending upon the maximum rate of change of the state variables along the trajectory, but no systematic check of error versus the number of mesh points for a given problem has been made. Generally, cases of rapidly varying state variables correspond to close approaches to the sun.

Perhaps the power of the Newton-Raphson algorithm is best exemplified by the trivial starting solutions that easily converge in a small number of iterations. One of the most successful starting solutions is a circular orbit between the given initial and final longitudes. The radius of this circular orbit is determined to be such that a body coasting in the orbit would traverse the arc between the two given longitudes in the given trip time. Usually, convergence to trajectories which constitute short arcs can be made directly from this trivial starting solution. For longer arcs, where convergence difficulties arise, another less efficient starting scheme has been developed which is described subsequently.

If a number of sequential cases are to be run, the boundary conditions of each member of the sequence being not too far removed from the boundary conditions of its immediate neighbors, a procedure called "tracking" can be used in which the solution of a preceding case serves as the starting solution for the next case. This procedure is particularly suited to generating curves of J versus launch date for a fixed arrival date or vice versa.

Equations 2 satisfy the necessary condition of the calculus of variations due to Euler and Lagrange for a solution which locally minimizes J. Since the sufficiency conditions of Weierstrass and Jacobi have not been tested, the algorithm may converge on any one of a possible multitude of merely stationary solutions. For a given set of boundary conditions, the starting solution determines which of the set of stationary trajectories will be converged upon, or whether the algorithm will converge at all. In general, direct comparison is the only method of discriminating between the local minimum and stationary solutions and the global minimum that is sought. In practice, however, it is not necessary to make all possible comparisons, since the global minimum solution generally is unique in being a well-behaved trajectory and also usually has a much lower value of J than any other solution. For short arcs, the algorithm will almost always converge on the global minimum solution. For longer arcs, a starting scheme has been designed which, so far, has never failed to lead directly to convergence on the global minimum solution.

Trajectory Profiles

The algorithm was employed to generate a set of optimum Earth-Mars round trip trajectory data for the aphelion opposition year, 1980. Similar to plots presented in the Planetary Flight Handbook (NASA SP-35) for high thrust, Fig. V-1 shows contours of constant values of J plotted against departure and arrival Julian dates at Earth and Mars. To find the total J required by a certain round trip, it is simply necessary to sum the values of J indicated for the two legs determined by the given departure date at Earth, arrival date at Mars, departure date at Mars, and arrival date back at Earth. Note that the contours are spaced logarithmically in the figure. Round trips with values of total J greater than 50 m^2/sec^3 would probably not be feasible. It is seen from the figure that this limit sets the lower bound on round-trip time at about 500

days for an all-electrically propelled trip, not including waiting time at Mars.

Figure III-4 gives a less general but more precise picture of Mars round-trip trajectories. This figure shows J values for optimum round trips during 1980 plotted against the Julian date of arrival at Mars for total trip times of 430, 530, and 630 days. Each round trip includes a 30-day stopover at Mars. For each total trip time and each date of arrival at Mars, the best combination of outbound and inbound leg times was chosen so as to minimize the total J value.

For each value of total trip time, there are two points of minimum J separated by a maximum point at the date of opposition (244 4295). At opposition, the two legs of the round trip are very nearly mirror images of each other, each requiring half the total trip time (less the waiting time). The left-hand minimum corresponds to a long outbound leg and a short inbound leg, while the reverse is true for the right-hand minimum. Note that, for the 630-day trip, the J value corresponding to the maximum at opposition is about double that for each minimum. For shorter values of trip time, the difference is even larger, as is shown by the curve for 530 days.

Sample Round-Trip Trajectories

Corresponding approximately to the left-hand minimum of the curve for 630 days total trip time, the round-trip trajectory shown in Fig. V-2 arrives at Mars at 244 4125 after a 320-day outbound flight. After a 30-day wait the inbound trajectory departs for Earth, arriving at 4435 after a 280-day flight. Also shown in the figure are vectors representing the thrust acceleration magnitude and direction. These vectors are not shown in the middle sections of the trajectories since the magnitude of the thrust acceleration is very small in these regions.

For round trips in the vicinity of the symmetrical trip, the minimum-radius problem is alleviated somewhat, as is shown by the trajectory of Fig. V-3 for the round trip arriving at Mars on 244 4300, five days after opposition. This trip is close to the middle maximum point of the 630-day curve of Fig. III-4. Each leg of this round trip is 300 days.

Figure V-4 shows the trajectory corresponding to the right-hand minimum of the 630-day curve of Fig. III-4. Being approximately the mirror image of the left-hand minimum round trip, this one has a short (280-day) outbound leg and a long (320-day) inbound leg. Here the closest approach to the sun occurs on the inbound leg (0.451 AU).

For either of the unsymmetrical trips, one might expect to increase the radius of closest approach by employing a nonoptimum combination of leg times. Figure III-6 shows the effect of changing the distribution of leg times for the

630-day round trip arriving at Mars on 244 4450. The values of J and minimum radius are plotted against the inbound leg time. It is seen that the value of J increases sharply on each side of the optimum point, while the radius of closest approach to the sun is relatively unaffected.

Mixed High- and Low-Thrust Acceleration

As a result of using a high-thrust device in a low-altitude planetary orbit or of atmospheric entry at greater than parabolic speed, there arises an initial (or final) nonzero velocity of the vehicle with respect to the planet, usually called the hyperbolic excess velocity. Thus, for a given amount of high-thrust ΔV, the initial (or final) heliocentric velocity of the vehicle is given by the vector addition of the planetary velocity vector and the hyperbolic excess velocity vector. The direction of the latter vector must be chosen so as to minimize the resulting value of J. The transversality condition that accomplishes this states that the direction of the hyperbolic excess velocity vector must be parallel to the resulting optimum low-thrust acceleration vector on the boundary. The machine program has been extended by substitution of the transversality conditions corresponding to impulsive changes in velocity at the boundaries for the fixed boundary conditions on velocity. This analysis is presented in Appendix B.

To check this extension of the program, the following simple exercise was run: The initial and final orbits are circular with radii of 1.0 and 1.523 AU, respectively. The central angle between the initial and final longitudes is 180 degrees and the prescribed trip time is precisely that required for a Hohmann transfer (258.74 days). The exercise consisted of a sequence of problems, starting with the all-low-thrust case and ending with the all-high-thrust case. The intermediate cases have certain prescribed values of hyperbolic excess speed at the initial and final boundaries which are varied from zero to the Hohmann transfer values in concert.

In Fig. V-5 the value of J for the low-thrust contribution to the transfer is plotted against the fraction of high thrust employed. As would be expected, the curve is monotonically decreasing from a value of 4.4 m^2/sec^3, for the all low-thrust case, to zero for the all high-thrust case. At each point the directions of the hyperbolic excess velocity vectors have been optimized through the transversality condition.

The best division between high- and low-thrust propulsion with respect to minimum initial vehicle mass was determined for the 430-day round trip arriving Mars at 244 4375, including 160 days outbound, 240 days inbound (and a 30-day stopover). This combination is optimum for the all-low-thrust trip, but it is not necessarily optimum for the mixed-acceleration case.

The trajectory results for this case are shown in Figs. V-6 and V-7 for the outbound and inbound legs, respectively. In both figures the resulting

value of low-thrust J is shown as a function of the two values of hyperbolic excess speed on the initial and final boundaries in a three-dimensional plot where the J axis is perpendicular to the plane of the paper and the resulting J "surface" is characterized by a family of contours of constant value. At every point on these two figures the directions of the hyperbolic excess velocity vectors are optimized through the transversality condition.

Major Modifications of the Algorithm

Variable-Thrust, Variable-Exhaust Power Trajectories

Introduction

As was stated above (see Ref. V-17), for the case of completely unconstrained specific impulse, I_{sp}, minimizing the integral

$$J = \int_0^\tau \frac{[a(t)]^2}{2P(X,t)}\,dt$$

leads directly to maximization of payload mass and minimization of powerplant mass. It is noted that, for this case, the thrusting and steering schedule, $\vec{a}(t)$, is completely independent of the powerplant characteristics during the minimization of J, but the selection of a powerplant and its associated propulsion parameters is contingent upon the condition that the chosen power source must have the capability of delivering the required time-varying thrust magnitude, $|M(t)\cdot a(t)|$, where M(t) is the vehicle mass. Except for this coupling, the analysis leading to optimization of the powerplant characteristics and the analysis leading to optimal thrusting (in the sense that J is minimized) may be carried out independently.

Optimal low-thrust trajectories employing variable and unconstrained I_{sp} are not consistent with present propulsion system technology, and, therefore, steering and thrusting schedules obtained using this analysis cannot be used in actual missions. Yet, such solutions do have practical value in that they yield upper bounds on attainable payload masses for the missions considered and are therefore valuable in the evaluation of the performance of vehicles powered by constant-thrust or constant-I_{sp}, variable-thrust engines. References V-19, 20, 21 and 22 have demonstrated that important comparisons can be made between the optimal variable-thrust and optimal constant-thrust trajectories and propulsion parameters, where the engines are operating at constant power. The present analysis makes comparisons of the trajectories and the associated propulsion parameters for vehicles which have basically different propulsive power sources but operate at completely variable thrust magnitude. Again, the conclusions that might be arrived at as a result of such comparisons (as to which power mode is most advantageous for a particular

mission) could not be implemented by actual thrusters; but it is possible that such analysis may assist the systems engineer to more easily match powerplant requirements to over-all mission requirements where the flights are made by means of the more feasible constant I_{sp}, variable low-thrust propulsion system.

The four assumptions listed above continue to hold for this analysis with these exceptions:

1. The analysis is performed in three dimensions; the x, y plane coincides with the ecliptic plane.

2. The functional form of the exhaust power, P(X,t), is chosen to represent constant power, radioisotope power, or solar power. Implicit in the functional form of P(X,t) is a postulated constant efficiency of the process of converting electrical energy at the thrusters into kinetic energy in the exhaust jet.

The governing differential equations for the optimal trajectory are:

$$\ddot{x} - \frac{P_o u}{e^{\gamma t} R^n} + \frac{x}{R^3} = o$$

$$\ddot{y} - \frac{P_o v}{e^{\gamma t} R^n} + \frac{y}{R^3} = o$$

$$\ddot{z} - \frac{P_o w}{e^{\gamma t} R^n} + \frac{z}{R^3} = o$$

$$\ddot{u} + \frac{mP_o\lambda^2 x}{e^{\gamma t} R^{n+2}} - \frac{u(2x^2-y^2-z^2) + 3x(vy + wz)}{R^5} = o$$

$$\ddot{v} + \frac{mP_o\lambda^2 y}{e^{\gamma t} R^{n+2}} - \frac{v(2y^2-x^2-z^2) + 3y(ux + wz)}{R^5} = o$$

$$\ddot{w} + \frac{mP_o\lambda^2 z}{e^{\gamma t} R^{n+2}} - \frac{w(2z^2-x^2-y^2) + 3z(ux + vy)}{R^5} = o$$

where $\lambda^2 = u^2 + v^2 + w^2$, $2m = n$.

These equations and the attendant transversality conditions for rendezvous, flyby, and solar probe missions are derived in Appendix B; the explicit form that these equations take on in the algorithm is also presented there.

Power Modes

1. The constant-power mode for low-thrust interplanetary transfer has been treated extensively in the literature (Refs. V-17, 19, 20, 21, and 22). In

particular, this problem has been recently investigated through the use of the Newton-Raphson algorithm in Refs. V-23 and V-24, and the optimal trajectories and mass fractions generated for several missions are set forth there. Therefore, the constant-power, variable-low-thrust transfers are used as the nominal optimal transfers in this analysis, and the trajectories and system parameters of the other power modes are compared to them.

2. The use of radioisotope fuels for auxiliary power supply has been treated in the literature, e.g., Refs. V-25 and V-26, and actually implemented in satellites; the use of radioisotope fuel for the propulsive power supply in interplanetary low-thrust vehicles has been strongly promoted recently in Ref. V-27. The dominant problem in constructing such a propulsion system is the lack of availability, in the necessary amounts, of radioisotopes that satisfy these basic criteria:

a. The isotopic source should be of minimum size and weight; that is to say, the specific power, kilowatts per kilogram, should be large.

b. The half-life should be such that power flattening requirements are a minimum.

c. Radioisotope cost should be low.

d. Necessary shielding should be low.

e. The isotope must be chemically compatible with its containment material.

f. The isotopic form must be compatible with mission safety requirements.

That low-thrust missions carried out with radioisotope power propulsion are feasible can be demonstrated by a brief example. Consider the 300-day Mars flyby or impactor mission depicted in Fig. V-8. The value of J is 1.225 x 10^{-3} kw/kg; the radioisotope is Po^{210} with a half-life of 0.38 years (Ref. V-26). The rocket equation for power-limited systems given above may be rewritten

$$\frac{M_0}{M_T} = 1 + \frac{M_0}{M_W}\,\alpha \int_0^T \frac{[a(t)]^2}{2e^{-\gamma t}}\,dt$$

$$= 1 + \frac{M_0}{P_0}\,J$$

where $P_0 = M_W/\alpha$ is the electrical power delivered to the thruster at time $t = 0$, M_W is the mass of the power supply and power conversion machinery, and

α is the powerplant specific mass, kilograms per kilowatt, (Ref. V-17). The thruster efficiency, $\eta(I_{sp})$, is assumed equal to 100%. Then

$$P_0 = M_0 J \left[\frac{1}{M_0/M_T - 1}\right]$$

Assuming that $M_0 = 10^3$ kg and $M_T = 9.5 \times 10^2$ kg, then $P_0 = 23.3$ kw. Further assuming that the efficiency of conversion of thermal energy to electrical energy is 30% the heat energy generated by the power source must be equivalent to 77.7 kw. The Po^{210} compound has a specific power of 134 kw/kg; therefore 77.7/134 = 0.58 kg or 580 grams of isotopic fuel are required. Po^{210} is available in these amounts and has modest shielding requirements with a large specific power rating; further, its half-life of about 100 days meets minimum requirements. However, it is very costly - about $26,500 per gram or a $15,400,000 fuel bill for this mission. If the cost of this fuel can be brought down, as is envisioned for the future, it is seen that such a primary propulsion system is both feasible and desirable for a number of applications.

No attempt is made in this analysis to choose a "best" radioisotope fuel, but a comparison of various fuels was made for a particular Mars rendezvous as illustrated in Fig. V-9. The following fuels were used:

Radioisotope	Half-Life, yr	Decay Constant, γ
(Constant Power)	∞	0.0
Pu^{238}	89.0	0.124×10^{-2}
Tl^{204}	4.0	0.276×10^{-1}
Cs^{144}	0.78	0.141
Tm^{170}	0.35	0.315

Since the vehicles flown with power sources possessing long half-lives compared to the trip time operate at very nearly constant power throughout the mission, the resultant trajectories (and fuel consumptions) are very close to the constant-power case. For this reason, only the envelope of these five trajectories is given. As the power source half-life is decreased, the trajectories "drift" outward from that of the constant-power mode. This implies that as the half-life decreases further, the mission will not be physically possible to perform. That this is so is seen by a consideration of the vehicle at its encounter with the destination planet. The thrusting requirements for matching the planet's velocity could not be met where, in the case of radioisotopes with very short half-lives, the power available becomes vanishingly small.

Finally, there is a feature of the radioisotope power mode that considerably simplifies mission analyses, as was illustrated above in a cursory fashion. The exhaust power, as a function of time, obtainable from a particular radioisotope

is directly proportional to its mass at time t = 0. Hence, the mission thrusting requirements embodied in J lead directly to power-source mass and shielding requirements. The result is a quick and reliable feasibility survey for missions utilizing this power mode.

3. The use of the sun's energy as a source of propulsion power for interplanetary vehicles has been discussed and investigated in the literature (Refs. V-28, 29, 30, and 31). The present analysis has postulated that the power in the exhaust jet is proportional to $1/R^n$ where $R^2 = x^2 + y^2 + z^2$. The literature has shown that high temperatures greatly decrease the efficiency of solar cells (e.g., Ref. V-28). Therefore, solar power expressed in this fashion gives generality to the solution that allows for the degradation of the power delivered to the exhaust jet during close passage by the sun. Figure V-10 illustrates the form of the exhaust jet power in the solar power mode for various values of n, normalized such that the power is unity at Earth departure. The heavier profile represents the case where n = 2 for R ≥ 1.0 AU and n = 1 for R < 1.0 AU. It is seen that n can change values at R = 1.0 AU, only, while still maintaining continuity in the power profile. In actuality the power derived from the solar cell would drop off markedly at about 0.65 AU, and this power profile would not be valid. However, it is felt that by inclining the cells to the sun's rays, the effect of temperature on energy conversion efficiency would be lessened and the power level could be maintained at some constant level in the close environs of the sun. No attempt was made in this analysis to choose a "best" value for n in the region R < 1.0 AU; the value n = 2.0 was used for the power mode comparisons that follow.

Power Mode Comparisons for Mars Missions

As set forth in detail in Refs. V-17 and V-20, for the variable low-thrust missions considered here, extremization of the payload fraction and the powerplant fraction is implicit in the operation of minimizing the integral J. For any J obtained in this analysis, whether or not it be the global minimum for the trajectory mode, power mode, and destination planet under consideration, the payload fraction and powerplant fraction are given by

$$\mu_w \equiv \frac{M_w}{M_0} = \delta - \delta^2$$

$$\mu_{pl} \equiv \frac{M_{pl}}{M_0} = (1-\delta)^2$$

where M_{pl} is the mass of actual payload plus vehicle structure mass and $\delta^2 \equiv \alpha J$. These ratios are presented here and considered in the evaluation and comparison of the power modes. Further, these results are qualitative only, since the power in the exhaust jet at Earth departure, P_0, has been set equal to unity in

all numerical calculations. This does not affect the formal minimization of J, but merely implies that the rating of the power source is arbitrary. The comparisons are done without the addition of excess velocities at the boundaries, although the algorithm can handle this case (see Appendix B). All trajectory profiles are projections on the ecliptic plane.

Figures V-11, 12, and 13 illustrate a comparison of the power modes for a Mars rendezvous trip of 300 days. The differences in the three trajectories are negligible as might be expected, since this particular set of departure time and trip time is that of an optimum impulsive transfer, and therefore the J's associated with these trajectories are in the neighborhood of the global minimum value of J. Inspection of the mass fractions indicates that constant power is best for this mission in the sense that, for acceptable values of α ($\alpha < 20$), the powerplant and payload fractions are the minimum and maximum, respectively. As indicated above, at the encounter of the destination planet, thrust magnitude requirements are increasing; yet, for the radioisotope power (the fuel is Po^{210} which has a half-life of 0.38 years) and the solar power vehicles, the exhaust power is decreasing, indicating that these power modes do not suit this trajectory mode as well as the constant-power mode.

Figures V-8, 14, and 15 illustrate the comparison of the power modes for a Mars flyby or impactor mission for the same trip time and departure date. Again the differences among the three trajectory profiles are negligible. The transversality conditions for this trajectory mode cause the thrust magnitude to vanish at the final time (see Appendix B). This result indicates that the decreasing power modes would be best suited to the flyby mode, but this particular example does not bear this out. J_c, the J for the constant-power mode, is the smallest and, again, leads to the best powerplant and payload fraction for acceptable values of α.

Further insight into these comparisons is obtained if one investigates a trip that is not in the neighborhood of an optimum impulsive transfer. Figures V-16, 17, and 18 illustrate such a comparison for a Mars rendezvous. The radioisotope fuel used here has a half-life of 9.5 years; the power gained from its decay is essentially constant over the duration of the trip, approximately 0.45 years. Hence, the trajectories and corresponding J's of the constant-power and radioisotope-power modes very nearly coincide. It is interesting to note that the solar-power trajectory for this mission moves inward toward the sun from the constant-power trajectory during the early portion of the trip and outward during the final portion. If such a maneuver is to be performed to obtain an increase in power, a larger increment of energy is gained by "dipping" toward the sun at the smaller distances from the sun precisely as is depicted in this example.

Figures V-19, 20, and 21 illustrate a comparison of the power modes for a Mars flyby for the same trip time and departure date as the preceding example.

Of significance here is the fact that the radioisotope power mode (with Cs^{144} as fuel with a half-life of 0.78 years) yields the minimum value of J, $J_R = 2.15 \times 10^{-3}$ kw/kg; correspondingly, the best values for the powerplant and payload fractions are produced by this power mode. Additional insight into this fact is gained from Fig. V-22. This figure gives comparisons of the exhaust power with the thrust acceleration over the trip duration for each power mode. Clearly, the area under the thrust acceleration curve in the radioisotope power mode is the smallest of the three modes, a strong indication that this mode would yield the minimum value of J.

Summary

The comparisons made above are not complete enough to warrant a statement as to which power mode is the best one for a particular mission. However, the indications are that the constant-power mode is best for the Mars rendezvous and that the radioisotope-power mode is best for the Mars flyby trajectory (see Ref. V-27).

Constant-Exhaust-Power, Constant-Thrust-With-Coast Trajectories

Introduction

The analyses and computations thus far have yielded optimal variable-I_{sp}, low-thrust interplanetary trajectories. The more practical and useful case of constant-thrust, constant-exhaust-power trajectories is investigated in the following paragraphs. The detailed analysis is presented in Appendix B; presented below are the salient points of that analysis and an examination of the results of the numerical computations of some typical Mars rendezvous missions.

As has been shown in Ref. V-17, the solutions for (1) optimal thrusting and steering schedules and (2) optimal propulsion parameters cannot be uncoupled for the general case of power-limited, constant-I_{sp} interplanetary flights. Clearly, when the exhaust power, P, and the thrust magnitude, $|T|$, are specified for a particular mission, i.e.,

$$P = \tfrac{1}{2} \dot{m} c^2 \equiv \beta_1$$

$$|T| = \dot{m} c \equiv \beta_2$$

the jet exhaust velocity, c, and the (outward) mass flow rate, $\dot{m}$, are completely defined throughout the mission. Further, $P = M_w/\alpha \equiv \beta_1$; that is, for a given powerplant specific mass, the powerplant mass is also specified. (Implicit in this statement is the assumption that the power available at the powerplant

is converted with efficiency $\eta_c = 100\%$ into kinetic energy at the thruster nozzle. If η_c is other than 100%, its value could be reflected in a modified value for α; thus, this equality is generally applicable.) In addition, the choice of β_1 and β_2 directly affects the value of the integral $\int_0^T [a(t)]^2\, dt$. In short, specification of β_1 and β_2 for a mission admits a solution for optimal control during the flight, but this solution will not, in general, lead to a maximization of payload mass, the ultimate goal.

However, an approximate method has been presented in the literature (Ref. V-32) that allows the two operations of (1) optimizing the control and (2) optimizing the propulsion parameters to be uncoupled for the purpose of numerical computation of constant-exhaust-power constant-thrust-with-coast trajectories that are optimal in the sense that payload mass is maximized. The basic assumptions of this method are:

(a) The minimum value of $\int_0^T [a(t)]^2\, dt$ is invariant with respect to μ_W.

(b) The average thrust acceleration, $\bar{a}$, over a trajectory with minimum $\int_0^T [a(t)]^2\, dt$ also is invariant with respect to μ_W.

The validity of these assumptions is borne out by actual trajectory solutions, and it will be seen that these approximations lead to very good comparisons with exact results.

Analysis

From Appendix B it is seen that the governing differential equations are

$$\ddot{x} - \frac{\dot{m}c\alpha_p}{1-\dot{m}t}\frac{u}{p} + \frac{x}{R^3} = 0$$

$$\ddot{y} - \frac{\dot{m}c\alpha_p}{1-\dot{m}t}\frac{v}{p} + \frac{y}{R^3} = 0$$

$$\ddot{z} - \frac{\dot{m}c\alpha_p}{1-\dot{m}t}\frac{w}{p} + \frac{z}{R^3} = 0 \qquad (3)$$

$$\ddot{u} - \frac{u(2x^2-y^2-z^2) + 3x(vy + wz)}{R^5} = 0$$

$$\ddot{v} - \frac{v(2y^2-x^2-z^2) + 3y(wz + ux)}{R^5} = 0$$

$$\ddot{w} - \frac{w(2z^2-x^2-y^2) + 3z(ux + vy)}{R^5} = 0$$

over the interval $0 \leq t \leq T$ with

$$\alpha_p = \begin{cases} 1, & 0 \leq t \leq t_1 \text{ and } t_2 \leq t \leq T \\ 0, & t_1 \leq t \leq t_2 \end{cases} \tag{4}$$

where t_1, t_2 are the thruster switch-off and switch-on times, respectively, $p = (u^2 + v^2 + w^2)^{1/2}$ and $R^2 = x^2 + y^2 + z^2$. In addition, the following equations define the scaling of the Lagrange multipliers and the determination of the switching times

$$[p(o)]^2 = 1 \tag{5}$$

$$[p(t_1)]^2 = [p(t_2)]^2 \tag{6}$$

It is noted that for a rendezvous mission, when Eqs. (3) and the appropriate boundary conditions are expressed as central difference equations at each of n mesh points, Eqs. (3), (5), (6), and the boundary conditions represent $6n + 2$ equations in the $6n + 2$ unknowns x_k, y_k, z_k, u_j, v_j, w_j, t_1, t_2; $k = 0, 2, 3 \ldots n-1, n+1$, $j = 1, 2 \ldots n$.

In addition, the following two equations define the approximate values of μ_w and c such that the payload mass is maximized (Ref. V-32):

$$\mu_w \left[1 - \left(\frac{2\mu_1}{1+\mu_1}\right)\left(\frac{\eta' c}{\eta}\right)\right] - \mu_1(1-\mu_1) = o \tag{7}$$

$$\bar{a}\alpha c - 2\mu_w \eta - \frac{\alpha J}{2} = o \tag{8}$$

where

$$\frac{1}{\mu_1} = 1 + \frac{\alpha J}{2\eta\mu_w}$$

$$\eta = \frac{1}{1+(d/c)^2}$$

$$\frac{d\eta}{dc} \equiv \eta'$$

Thus, the solution to the coupled problem may be computed in parts through the use of two computer routines. Assuming the initial values for $\dot{m}c$ and c and specifying the parameters α and d, Eqs. (3), (5), (6), and expressions representing

the boundary conditions are solved by the modified Newton-Raphson algorithm thereby yielding values for $J = \int_0^T [a(t)]^2 \, dt$ and $\bar{\bar{a}}$. These two values are submitted to the second algorithm, a search routine for finding the c and μ_w that simultaneously satisfy Eqs. (7) and (8). This solution is then utilized to up-date the values of $\dot{m}c$ and c:

$$m = \frac{2\mu_w^* \eta}{\alpha(c^*)^2} \quad , \quad \dot{m}c = \frac{2\mu_w^* \eta}{\alpha c^*}$$

where here $\eta = \frac{1}{1+(d/c^*)^2}$ and c^* and μ_w^* are the updated values of c and μ_w.

These values, in turn, are resubmitted to the Newton-Raphson routine, which then computes up-dated values of J and $\bar{\bar{a}}$. This process is repeated until the changes in μ_w and c between successive iterations satisfy an appropriate convergence criterion. This process has proven to be very strongly convergent for the cases considered; so much so, in fact, that the values of J and $\bar{\bar{a}}$ may be up-dated after each iteration internal to the modified Newton-Raphson algorithm (not requiring that J and $\bar{\bar{a}}$ converge to definite values for each up-dated guess of $\dot{m}c$ and c), thus considerably shortening computation time. That this up-dating procedure can be efficiently carried out after each internal iteration leads to the conviction that this problem can be solved in an even more economical fashion by incorporating the propulsion parameter equations [Eqs. (7) and (8)] into the Newton-Raphson algorithm. In this regard, see Appendix D.

A brief description is useful to explain the method of attaining a first guess for the state, control, and propulsion variables required in order to initiate the computations. As is well documented in the literature (e.g., Ref. V-22) the value of J_v for an optimal constant power, variable I_{sp} trajectory is approximately 10% to 15% less than the J_c for the corresponding optimal constant-power, constant-I_{sp} trajectory. This correlation is the basis for the initial guess of $J_c : J_c = 1.15 \, J_v$. The initial guess for $\bar{\bar{a}}$ is the geometric mean of the thrust acceleration for the variable-thrust solution,

$$\bar{\bar{a}} = \left(\frac{J_v}{T}\right)^{1/2}$$

The initial guesses on the switching times t_1 and t_2 are then obtained in this manner: Letting T_p be the powered time for the constant-thrust case, $T_p = T - (t_2 - t_1)$, one can write

$$T_p = \frac{J_c}{\bar{a}^2}$$

utilizing the expression for the geometric mean thrust acceleration for the constant-thrust case. Then, T_{min} is determined as the time at which the magnitude of the thrust acceleration of the variable thrust case attains a minimum value; centering the coast phase, $t_2 - t_1$, about $t = T_{min}$, one has

$$t_1 = T_{min} - \frac{T - T_p}{2}$$

$$t_2 = T_{min} + \frac{T - T_p}{2}$$

The initial guesses of the state and control time histories are taken from the corresponding variable-thrust solution. Although these initial approximations seem rather gross (the possibility of better starting solutions certainly cannot be discounted), the numerical results presented in the next paragraphs required only 10 sec or less of computing time for the cases studied; the program is presently operational only for Earth-Mars and Mars-Earth rendezvous missions.

Computations and Results

Figure V-23 is a projection on the ecliptic plane of an Earth-to-Mars rendezvous trajectory using the constant-thrust, constant-power mode. In this case the values of I_{sp} and initial thrust acceleration, a_0, are held fixed; hence, the resultant payload fraction is not a maximum. The values of I_{sp} and a_0 are given in the figure and yield these values for the mass fractions with $\alpha = \eta = 1.0$: $\mu_{pl} = 0.8460$ and $\mu_W = 0.0232$. Although the figure does not illustrate this fact, it was found that the constant-thrust, constant-power trajectory profile differed to only a very small degree from the variable thrust profile. The value of J_v for the variable thrust case was 5.78 m^2/sec^3. This yields the mass fractions, $\mu_{pl} = 0.9010$ and $\mu_W = 0.0508$. It is noted that the variable-thrust case, while requiring the larger powerplant, yields a 6.1% increase in payload over the constant-thrust case. Figure V-24 is a graphical representation of the optimal thrusting and steering schedule for this case. The coasting phase is represented on the thrust direction curve by a dotted line; during this period the thruster must be reoriented for engine restart at t = 166 days.

Finally, a comparison is made in Table V-I of the vehicle parameters generated by Melbourne and Sauer in Ref. V-32 and those generated by the

modified Newton-Raphson algorithm coupled with the external routine to maximize payload mass. The results of the former are obtained through a rigorous analysis utilizing the calculus of variations throughout and are considered to be exact numerical solutions to the problems considered. The solutions generated by the Newton-Raphson algorithm are the results of the approximate analysis presented in Ref. V-32 and repeated above.

One factor has had an effect on the numerical solutions (although to what extent the values have been altered cannot be determined). The dates of Earth departure are not set forth explicitly for the trips cited in Ref. V-32. Hence, these dates were approximated as well as possible through interpolation of curves depicting J versus Earth launch date which are presented by Melbourne and Sauer elsewhere (Ref. V-22). It is felt that this fact has contributed, to a small degree, to the differences noted in the figure. The modified Newton-Raphson algorithm yields an exact value of the integral $\int_0^T [a(t)]^2\, dt$ for the mass flow rate and specific impulse to which the routine converges. Therefore, the best comparison between these two methods is obtained at those trip times for which the respective values of J are most nearly equal. As an example, for T = 180 days and α = 1 kg/kw, the values of this integral differ by just 2 parts in 8080, and the corresponding mass fractions illustrate very good comparison. In fact, the two methods illustrate good to excellent comparison over all of the missions that were examined.

Summary

The analysis and results presented above and in Appendix B bring together two strong methods in the realm of optimal trajectory and propulsion parameter investigations. The Newton-Raphson algorithm, on the one hand, modified to yield constant-thrust-with-coast trajectories, optimal in the sense that $\int_0^T [a(t)]^2\, dt$ is minimized, contributes to the solution the optimal control schedule and optimal positioning (in time) and duration of the coast phase plus its inherent rapid computing time. On the other hand, the approximate method of maximizing the payload fraction for various ranges of propulsion parameters (a la Melbourne and Sauer) contributes its excellent comparison to the results of the complete calculus of variations analysis and also imparts the uncoupling (for the purposes of numerical computation) of the optimal control portion and the optimal propulsion parameter portion of optimal constant-exhaust-power, constant-thrust-with-coast trajectory investigations.

Future Activities

There are certain areas in the analyses presented in this section that appear capable of bearing more useful and interesting results with the application of additional, concentrated effort. They are discussed briefly here.

• Experience has shown that the periods of optimal coast in constant-thrust trajectories correspond very closely to those periods in the unconstrained I_{sp} trajectories where the thrust acceleration magnitude attains its minimum value. Further, trajectories have been computed at the Research Laboratories utilizing unconstrained I_{sp} thrusting where the thrust acceleration magnitude has experienced two or more periods in which it has attained locally minimum values with respect to time, i.e.,

$$\left.\frac{d\left|\frac{\dot{m}\vec{c}}{m}\right|}{dt}\right|_{t = t_i} = 0, \quad i = 1, 2, \ldots.$$

A logical conclusion is that the corresponding optimal control for the constant-thrust trajectories may possess more than one coast period with attendant reductions in the propellant requirement. Additional effort on investigations of this nature would be a natural extension of the work presently being done at the Research Laboratories.

• The analysis in Appendix D sets forth an extension of the work presented in this section on constant-power, constant-thrust-with-coast trajectories. Essentially, it mathematically defines the coupling of the thrust control optimization and the powerplant parameter optimization under the assumption that the specific impulse is specified, a feasible restriction based upon present propulsion technology. The algorithm presented above can be easily modified to represent the equations of this analysis. The resultant solutions would be constant-power, constant-thrust-with-coast trajectories that are optimum in the sense that the payload fraction is maximized subject to specified values for these powerplant parameters: specific mass, specific impulse, and thruster efficiency.

• It appears that radioisotope fuel as the primary propulsion power source may be the best power mode for Mars flyby missions. However, many isotopes qualify as candidates for the fuel; consequently, a search is necessary to find the optimum fuel required for this trajectory mode and to make a more practical comparison of constant and radioisotope power based upon shielding requirements, availability, cost, etc. Such an investigation would be straight-forward since the required computer program is already written.

REFERENCES

V-1. Zola, C. L.: Trajectory Methods in Mission Analysis for Low-Thrust Vehicles. AIAA Preprint No. 64-51, January 1964.

V-2. Gobetz, F. W.: Optimal Variable-Thrust Transfer of a Power-Limited Rocket Between Neighboring Circular Orbits. AIAA Journal, Vol. 2, No. 2 February 1964.

V-3. Gobetz, F. W.: Optimal Variable-Thrust Rendezvous of a Power-Limited Rocket Between Neighboring Low-Eccentricity Orbits. Contract NAS8-11099 Final Report. UA Research Laboratories Report C-910098-12, October 1964.

V-4. Kelley, H. J.: Method of Gradients. Optimization Techniques, G. Leitmann, ed. Academic Press, New York, 1962, Chap. 6, pp. 206-252.

V-5. Bryson, A. E. and W. F. Denham: A Steepest Ascent Method of Solving Optimum Programming Problems. J. Appl. Mech. 29, 247-257, 1962.

V-6. Breakwell, J. V.: The Optimization of Trajectories. SIAM J. 7, 215-247, 1959.

V-7. Melbourne, W. G.: Three-Dimensional Optimum Thrust Trajectories for Power-Limited Propulsion Systems. ARS J. 31, 1723-1728, 1961.

V-8. McGill, R. and P. Kenneth: Solution of Variational Problems by Means of a Generalized Newton-Raphson Operator. AIAA J. 2, 1761-1766, 1964.

V-9. Kopp, R. E., et al: Several Trajectory Optimization Techniques. Computing Methods in Optimization Problems, Balakrishnan and Neustadt, ed. Academic Press, New York, 1964.

V-10. Kantorovich, L. V. and G. P. Akilov: Functional Analysis in Normed Spaces. Chap. XVIII, Pergamon Press, 1964.

V-11. Hestenes, M. R.: Numerical Methods of Obtaining Solutions of Fixed End Point Problems in the Calculus of Variations. Rand Corp. Report RM-102, August 1949.

V-12. Kalaba, R.: On Nonlinear Differential Equations, The Maximum Operation, and Monotone Convergence. J. Math. Mech. 8, 519-574, July 1959.

V-13. McGill, R. and P. Kenneth: A Convergence Theorem on the Iterative Solution of Nonlinear Two-Point Boundary Value Systems. XIV International Astronautical Federation Congress, Paris, France, September 1964.

REFERENCES (Contd.)

V-14. Varga, R. S.: Matrix Iterative Analysis. Chap. 6, Prentice-Hall, 1962.

V-15. Van Dine, C. P.: An Application of Newton's Method to the Finite Difference Solution of Nonlinear Boundary Value Systems. United Aircraft Research Laboratories Report UAR-D37, March 1965.

V-16. Van Dine, C. P., W. R. Fimple and T. N. Edelbaum: Application of a Finite-Difference Newton-Raphson Algorithm to a Problem of Low-Thrust Trajectory Optimization. Vol. 17, Progress in Astronautics and Aeronautics, Methods of Astrodynamics and Celestial Mechanics. Edited by R. L. Duncombe and V. G. Szebehely, Academic Press, May 1966.

V-17. Irving, J. H.: Low-Thrust Flight: Variable Exhaust Velocity in Gravitational Fields, Chap. 10, Space Technology, Edited by H. Siefert, John Wiley and Sons, Inc. 1959.

V-18. Ragsac, R. V.: "Study of Low-Acceleration Space Transportation Systems". United Aircraft Research Laboratories Report D-910262-3.

V-19. Melbourne, W. G.: "Interplanetary Trajectories and Payload Capabilities of Advanced Propulsion Vehicles"; Technical Report No. 32-68, Jet Propulsion Laboratory, Pasadena, 1961.

V-20. Melbourne, W. G. and C. G. Sauer, Jr.: "Optimum Thrust Programs for Power-Limited Propulsion Systems", Technical Report No. 32-118, Jet Propulsion Laboratory, Pasadena, 1961; also Astronautica Acta, Vol. VIII, 1962, FASC4.

V-21. Melbourne, W. G., D. E. Richardson, and C. G. Sauer, Jr.: "Interplanetary Trajectory Optimization with Power-Limited Vehicles", Technical Report No. 32-173, Jet Propulsion Laboratory, Pasadena 1961.

V-22. Melbourne, W. G. and C. G. Sauer, Jr.: "Optimum Interplanetary Rendezvous with Power-Limited Vehicles", Technical Report No. 32-226, Rev. 1, Jet Propulsion Laboratory, Pasadena 1962; also AIAA Journal, Vol. 1, No. 1 January 1963.

V-23. Van Dine, C. P.: "An Application of Newton's Method to the Finite Difference Solution of Nonlinear Boundary Value Systems". United Aircraft Research Laboratories Report UAR-D37, March 1965.

V-24. Van Dine, C. P., W. R. Fimple and T. N. Edelbaum: "Application of a Finite-Difference Newton-Raphson Algorithm to a Problem of Low-Thrust Trajectory Optimization". Presented at the AIAA-ION Astrodynamics Specialist Conference, Monterey, California, September 1965.

REFERENCES (Contd.)

V-25. Streb, A. J.: "Radioisotope Power Systems for Manned Space Stations", Presented at the Third Biennial Aerospace Power Systems Conference, Philadelphia, September 1964. AIAA Preprint No. 64-711

V-26. Rohrmann, C. A. and E. D. Sayre: "Radioisotope Space Power-Prospects and Limitations", Presented at 1st AIAA Annual Meeting, Washington, D.C., July 1964. AIAA Preprint No. 64-453.

V-27. Romero, J. B.: "Potentialities of Radioisotope Propulsion for Space Probes", J. Spacecraft, Vol. 3, No. 4, April 1966.

V-28. Loferski, J. J.: "The Photovoltaic Effect and Solar Energy Conversion", ARS Preprint 1288-60, September 1960.

V-29. "Research on Solar-Energy Conversion Employing Cadmium Sulfide", Technical Documentary Report No. ASD-TDR-62-69, Flight Accessories Laboratory, Wright-Patterson Air Force Base, Ohio, June 1962.

V-30. Wenzinger, C. J. and H. Carleton: "The Solar Power Supply System for the Orbiting Astronomical Observatories" ARS Preprint No. 63-217, June 1963.

V-31. Lamorte, M. F.: "Solar Cells Designed for Operation in the Inner Regions of the Solar System", ARS Preprint No. 2568-62, September 1962.

V-32. Melbourne, W. G. and C. G. Sauer, Jr.: "Payload Optimization for Power-Limited Vehicles", Vol. 9, Progress in Astronautics and Aeronautics, Academic Press, 1963.

TABLE V-1

COMPARISON OF VEHICLE PARAMETERS FOR MARS RENDEZVOUS MISSION:

RESULTS OF MELBOURNE AND SAUER VS RESULTS OF THE MODIFIED NEWTON-RAPHSON ALGORITHM

T (days)	α (kg/kw)	μ_{pl}		μ_w		μ_l		C x 10^{-2} (km/sec)		$\int_0^T a^3\,dt$ (m^3/sec^3)	
		M-S	N-R	M-S	N-R	M-S	N-R	M-S	N-R	M-S	N-R
270	1	0.935	0.931	0.033	0.035	0.967	0.965	1.847	1.620	2.178	2.450
	5	0.854	0.844	0.075	0.081	0.928	0.924	0.834	0.730	2.180	2.450
	10	0.791	0.775	0.110	0.122	0.901	0.897	0.602	0.526	2.185	2.450
	20	0.695	0.668	0.171	0.194	0.866	0.863	0.443	0.387	2.199	2.450
240	1	0.922	0.920	0.039	0.040	0.961	0.960	1.653	1.480	3.085	3.240
	5	0.826	0.820	0.089	0.094	0.915	0.914	0.751	0.668	3.090	3.240
	10	0.750	0.740	0.133	0.143	0.834	0.883	0.546	0.483	3.103	3.250
	20	0.634	0.613	0.208	0.232	0.842	0.845	0.408	0.359	3.136	3.250
210	1	0.904	0.904	0.048	0.048	0.952	0.951	1.488	1.358	4.758	4.840
	5	0.784	0.781	0.111	0.114	0.895	0.895	0.682	0.613	4.772	4.830
	10	0.690	0.682	0.166	0.176	0.856	0.859	0.500	0.444	4.804	4.830
	20	0.545	0.525	0.262	0.290	0.807	0.815	0.376	0.331	4.889	4.830
180	1	0.876	0.875	0.063	0.062	0.939	0.937	1.398	1.242	8.082	8.080
	5	0.722	0.719	0.144	0.147	0.866	0.866	0.632	0.561	8.118	8.100
	10	0.600	0.591	0.214	0.228	0.814	0.819	0.459	0.407	8.205	8.120
	20	0.413	0.386	0.338	0.379	0.750	0.764	0.347	0.304	8.420	8.150

MINIMUM J EARTH-MARS ROUNDTRIPS

VARIABLE LOW-THRUST RENDEZVOUS TRAJECTORIES

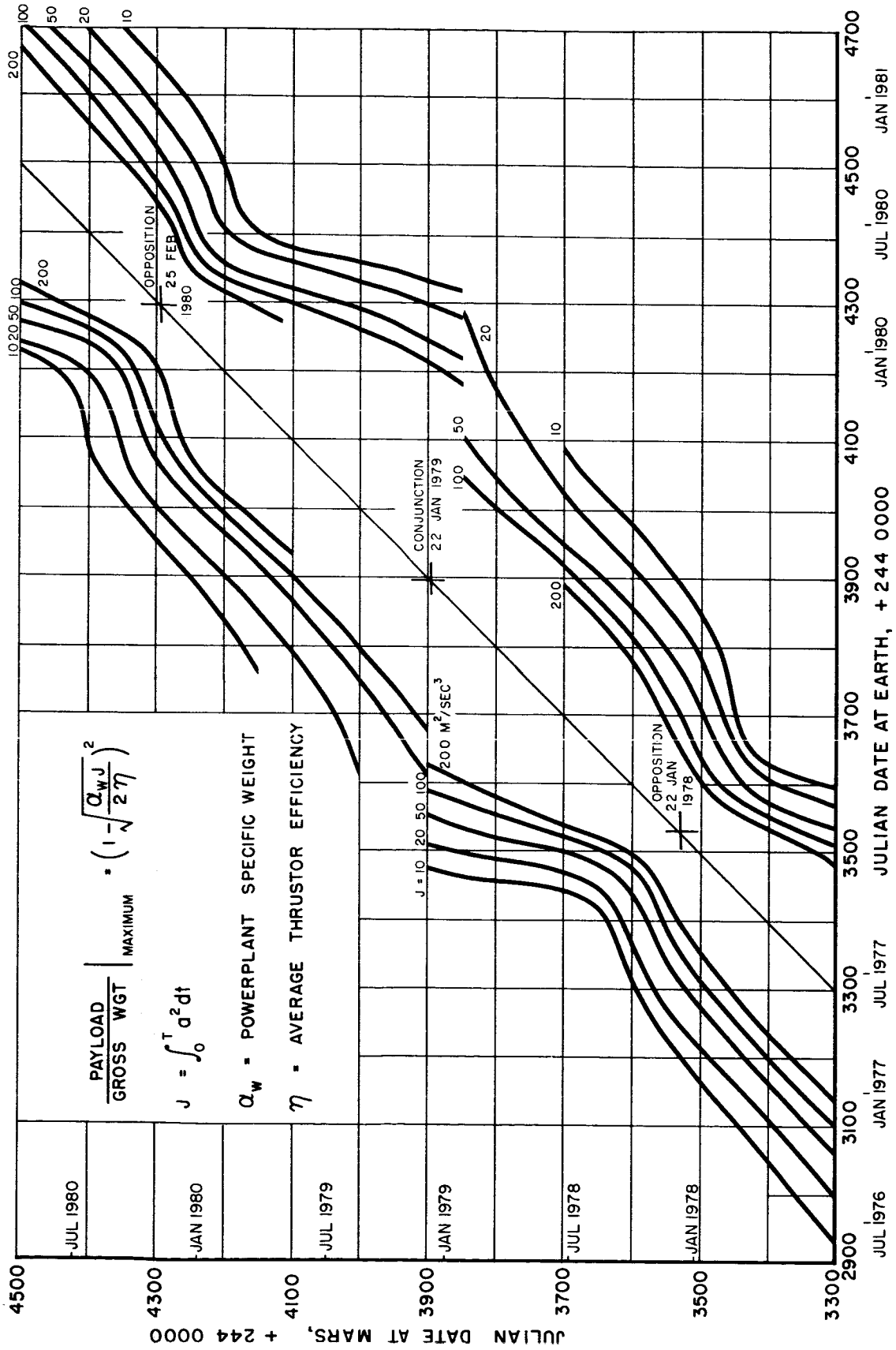

MARS ROUND TRIP ARRIVING BEFORE OPPOSITION

TOTAL TRIP TIME = 630 DAYS

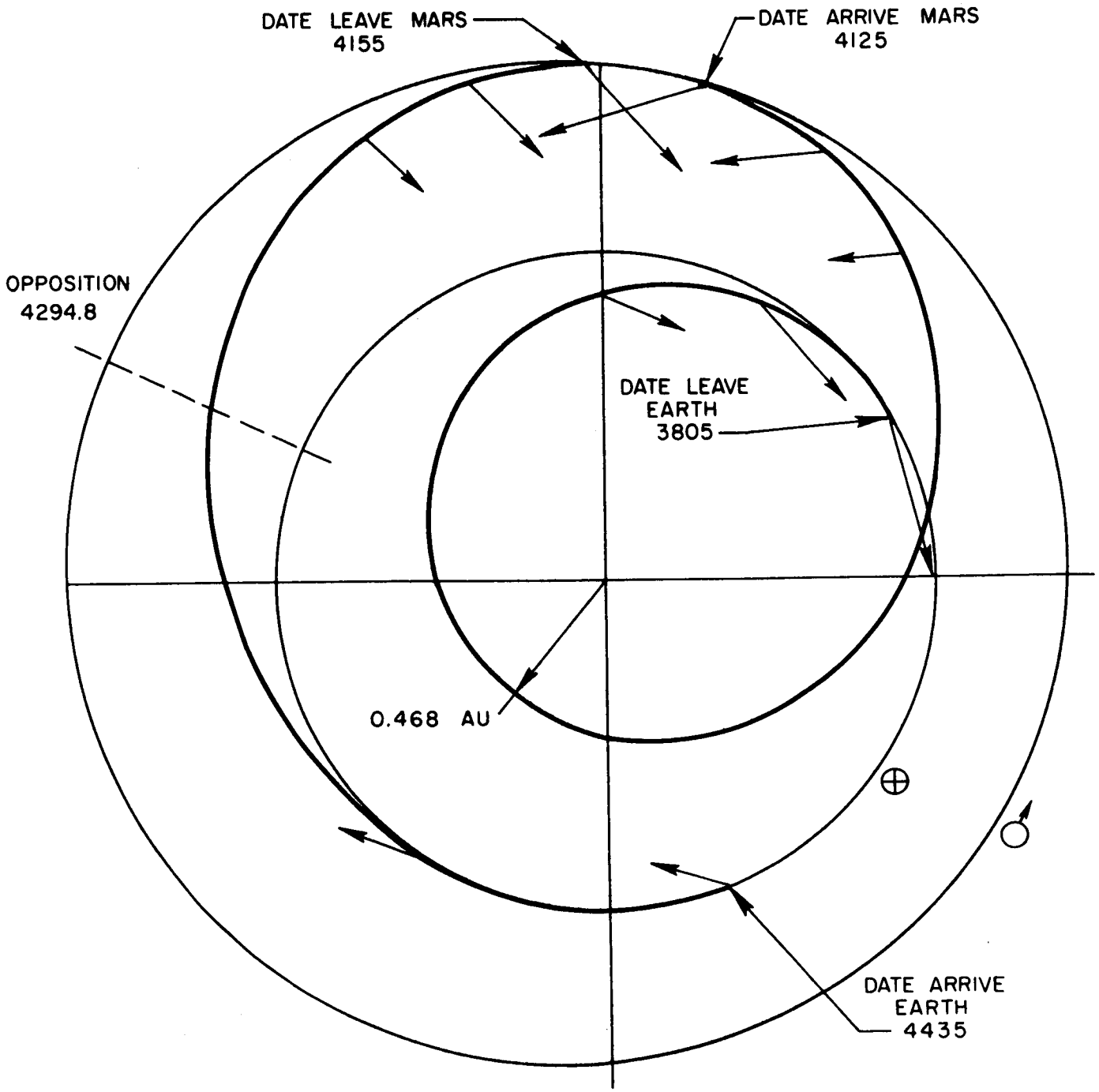

MARS ROUND TRIP ARRIVING NEAR OPPOSITION

TOTAL TRIP TIME = 630 DAYS

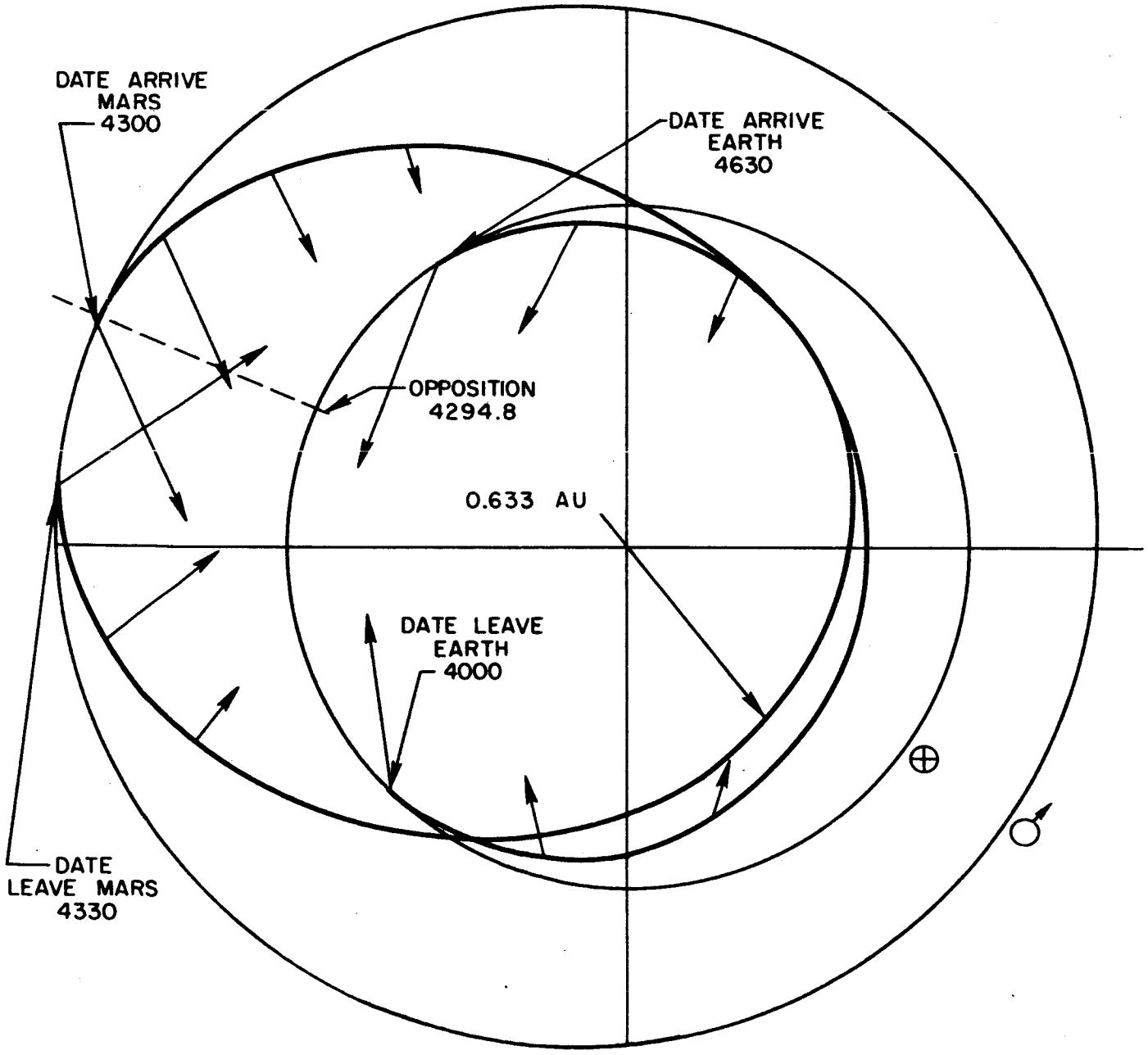

MARS ROUND TRIP ARRIVING AFTER OPPOSITION

TOTAL TRIP TIME = 630 DAYS

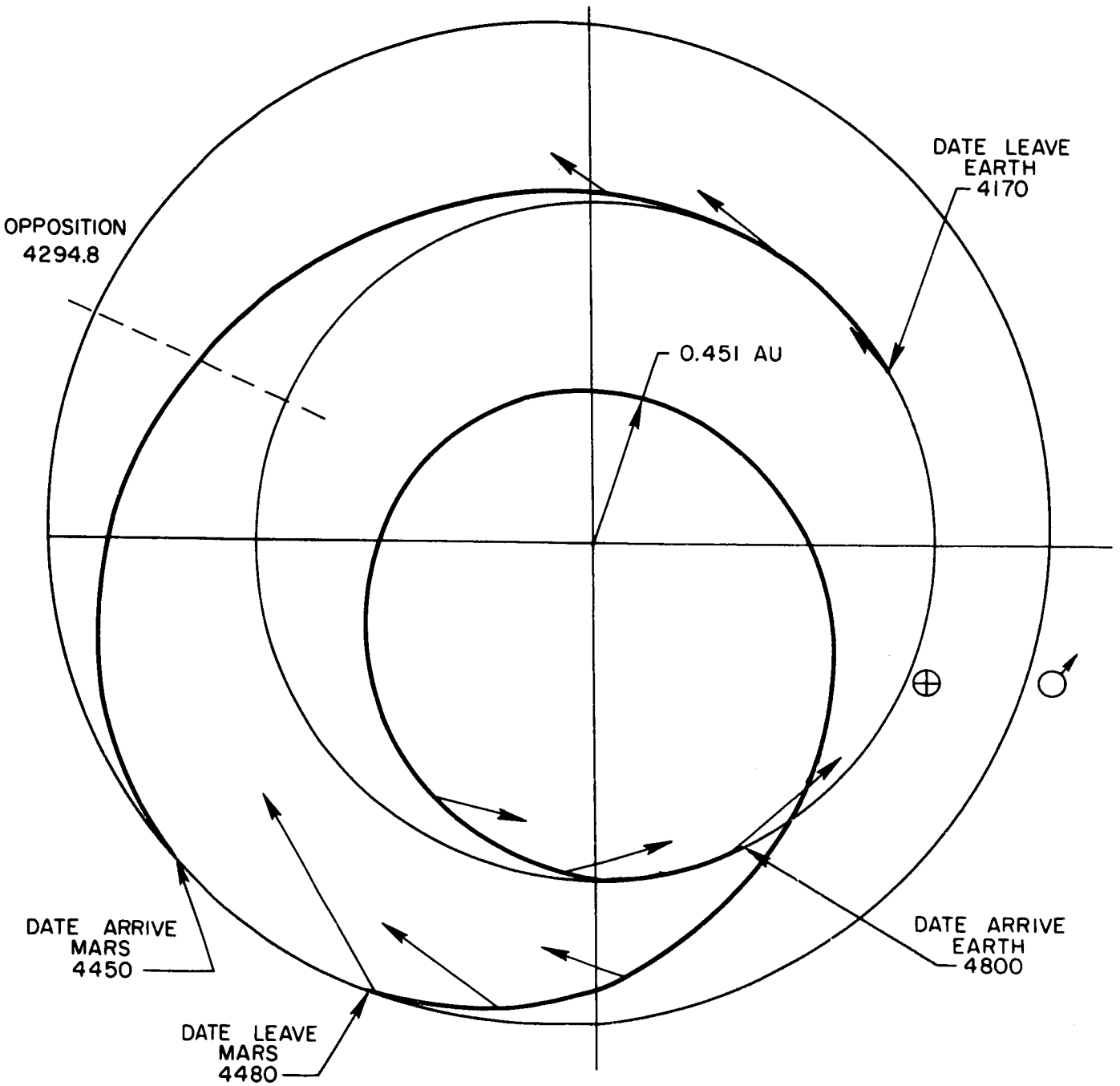

FIG. V-5

MIXED-THRUST HOHMANN TRANSFER

INITIAL CIRCULAR ORBIT RADIUS = 1.0 A.U.

FINAL CIRCULAR ORBIT RADIUS = 1.523 A.U.

TRANSFER TIME = 258.74 DAYS

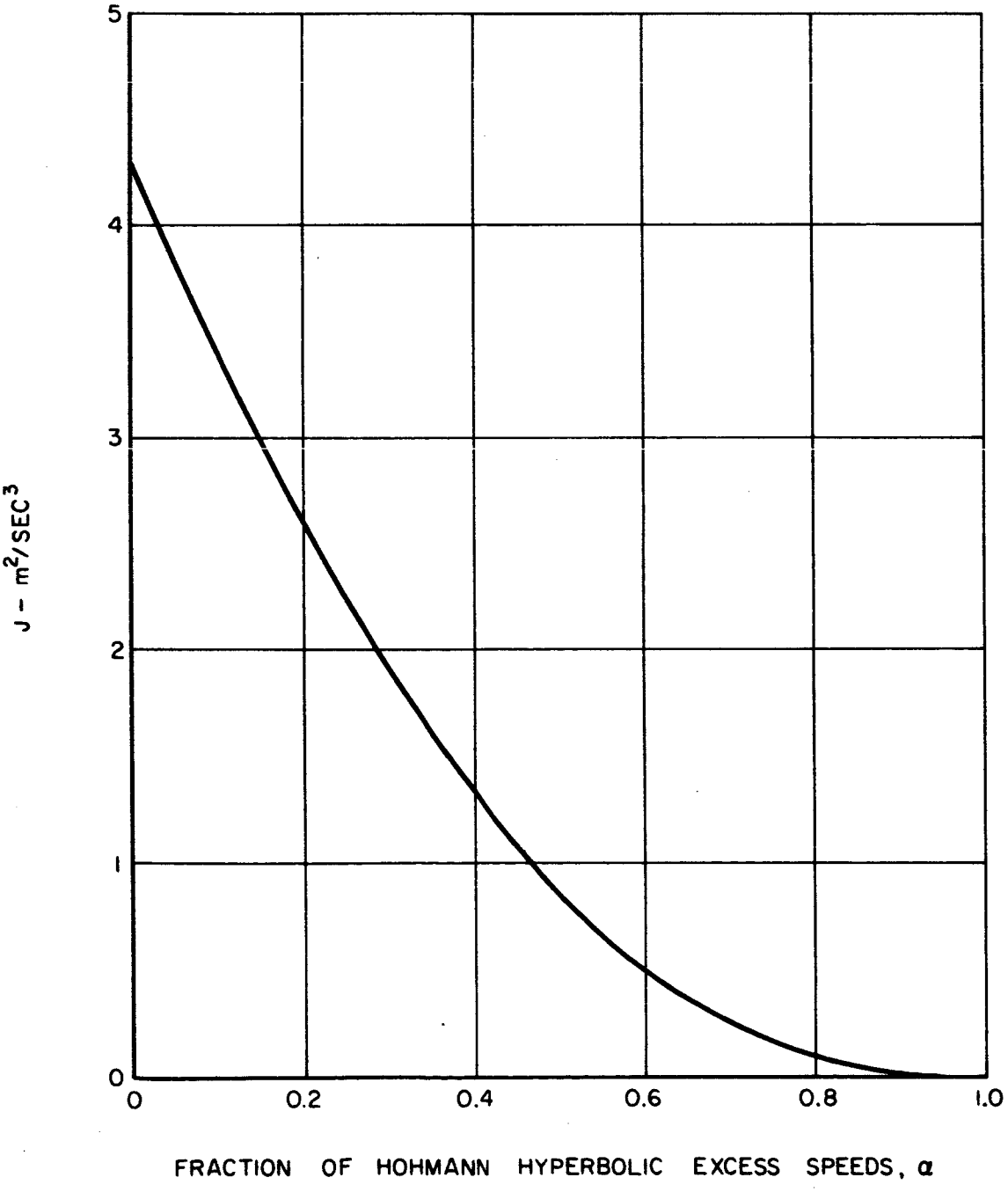

MIXED-THRUST EARTH-MARS ROUND TRIP

OUTBOUND LEG (160 DAYS)

TOTAL TRIP TIME = 430 DAYS

LEAVE EARTH 244 4215 ARRIVE MARS 244 4375

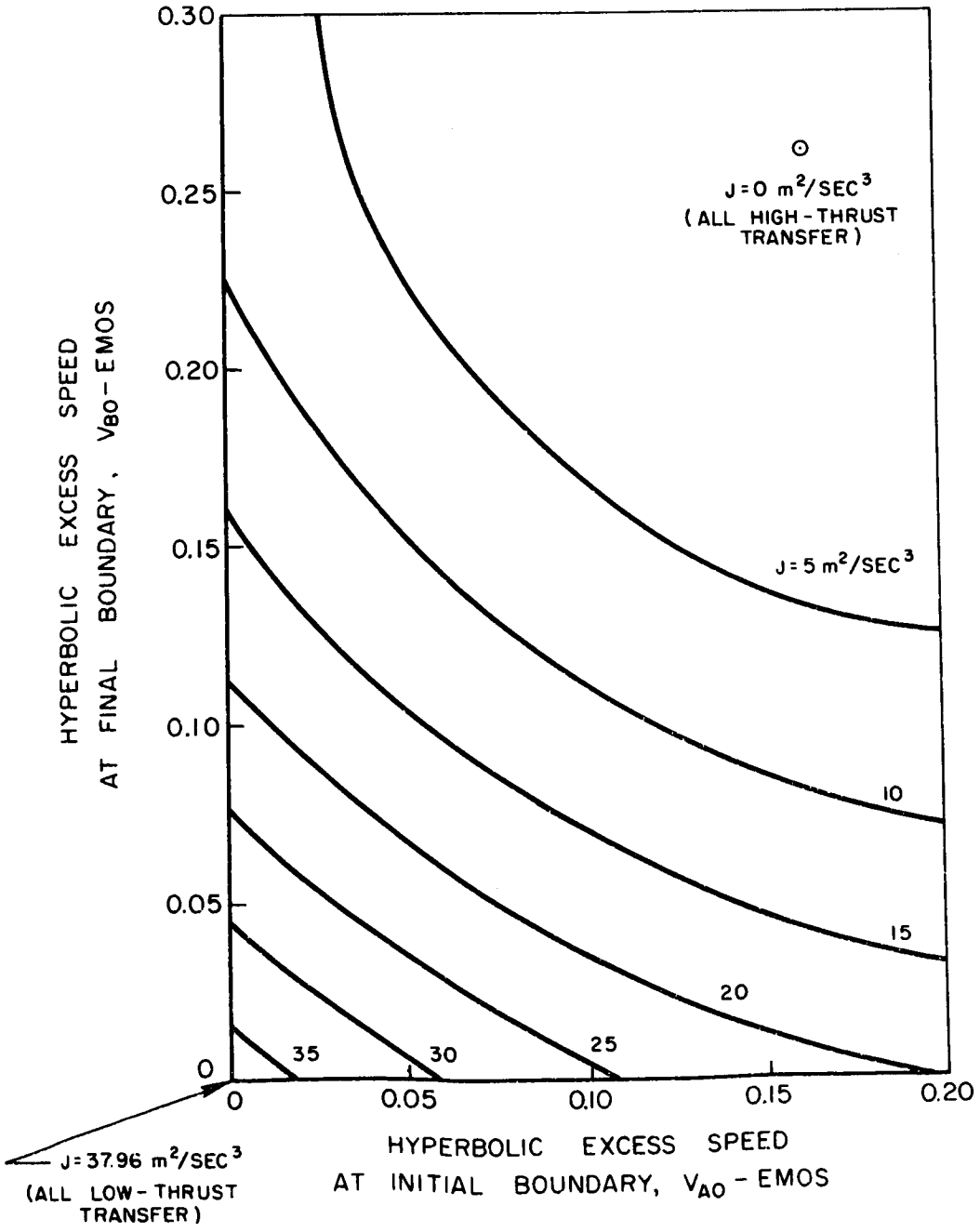

MIXED-THRUST EARTH-MARS ROUND TRIP

INBOUND LEG (240 DAYS)

TOTAL TRIP TIME = 430 DAYS

LEAVE MARS 244 4405 ARRIVE EARTH 244 4645

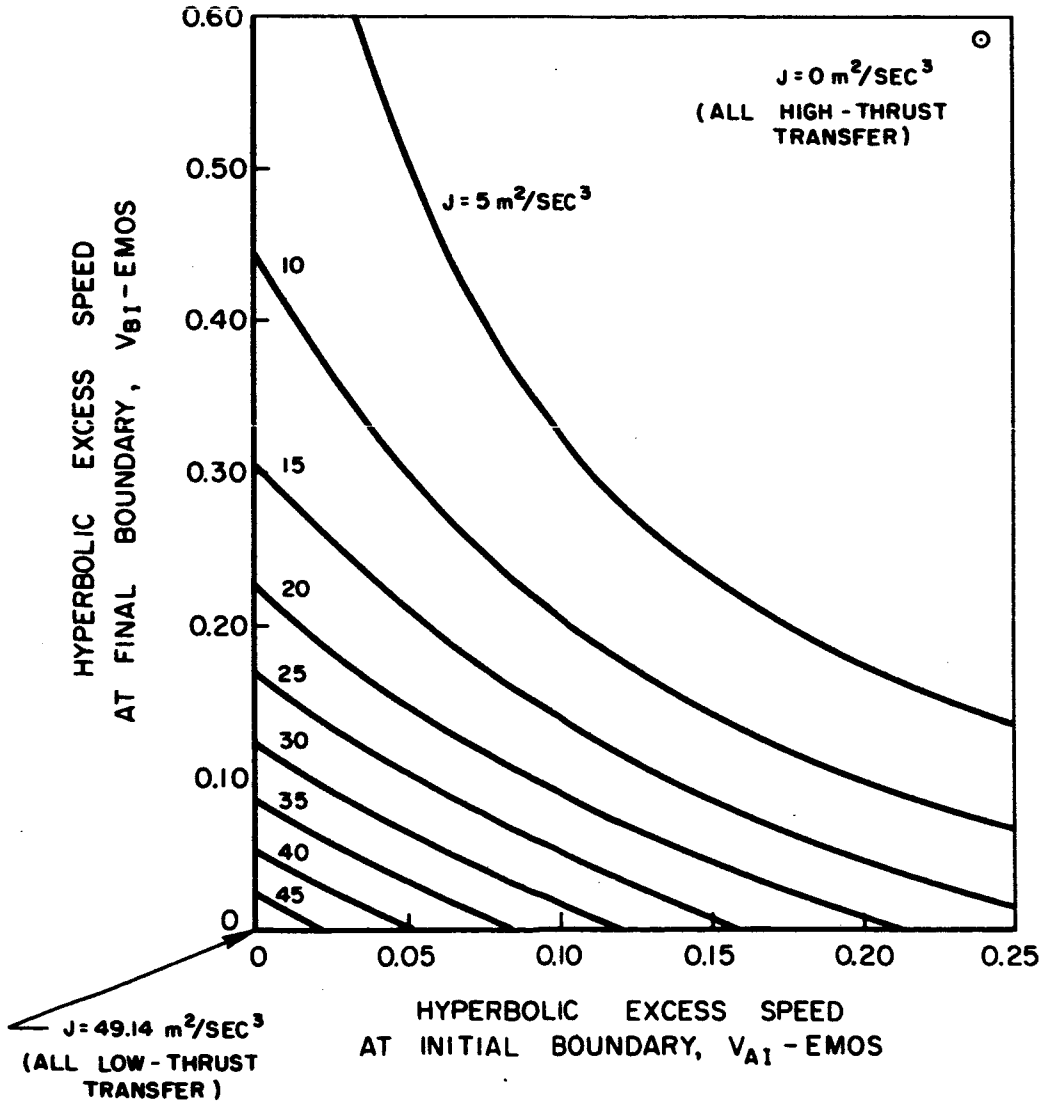

E-910262-6

FIG. V-8

OPTIMAL LOW-THRUST TRAJECTORIES

MARS FLYBY

NOTE: THE TRAJECTORIES ARE REPRESENTED HERE BY ONE CURVE AS THERE ARE ONLY SLIGHT DIFFERENCES AMONG THEM

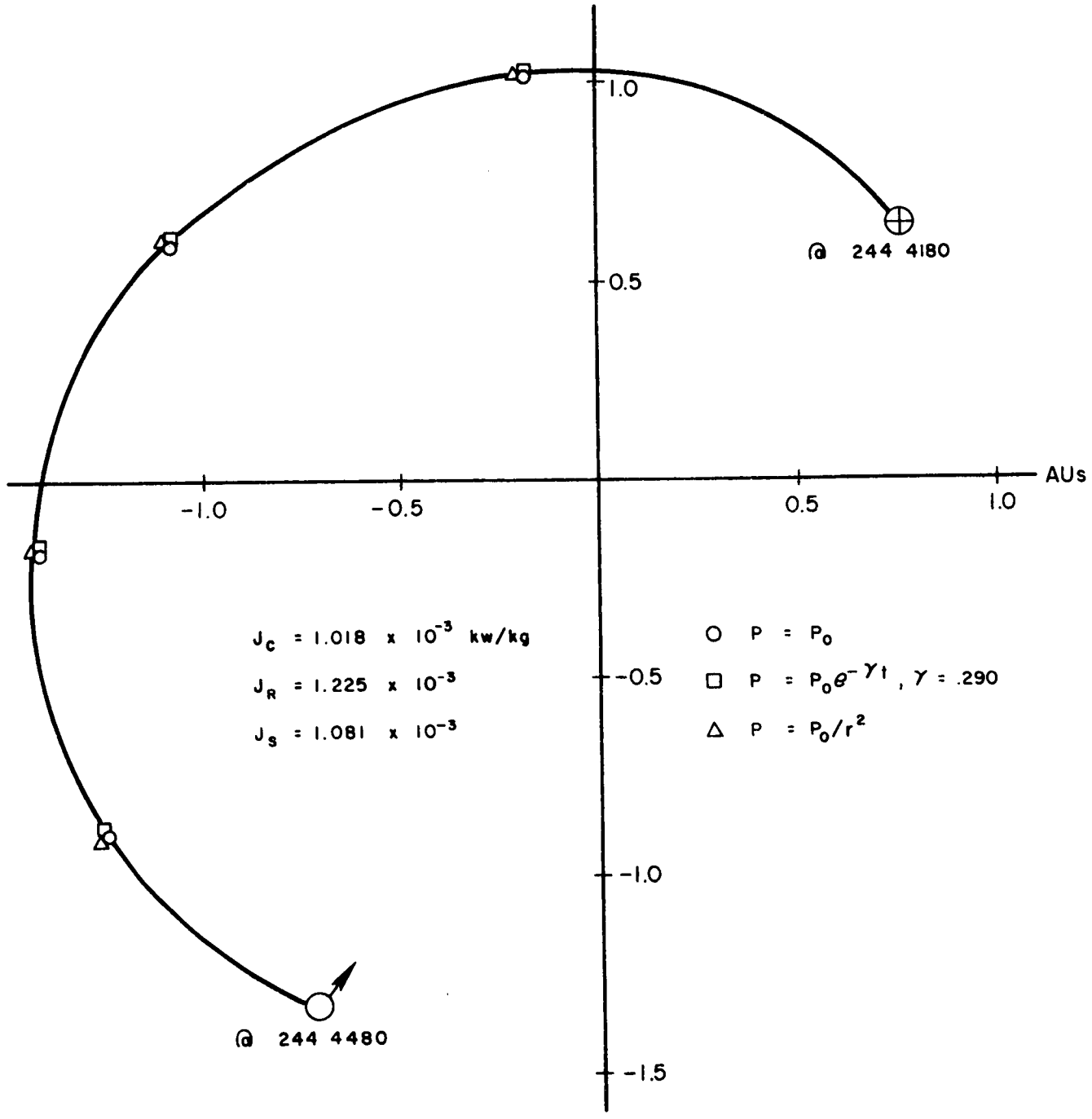

FIG. V-9

COMPARISON OF TRAJECTORIES FOR CONSTANT POWER AND RADIOISOTOPE POWER

O – CONSTANT POWER , P_O

Δ – RADIOISOTOPE POWER , $P_O / e^{\alpha t}$ (Tm_{170} , .35 YR. HALF-LIFE)

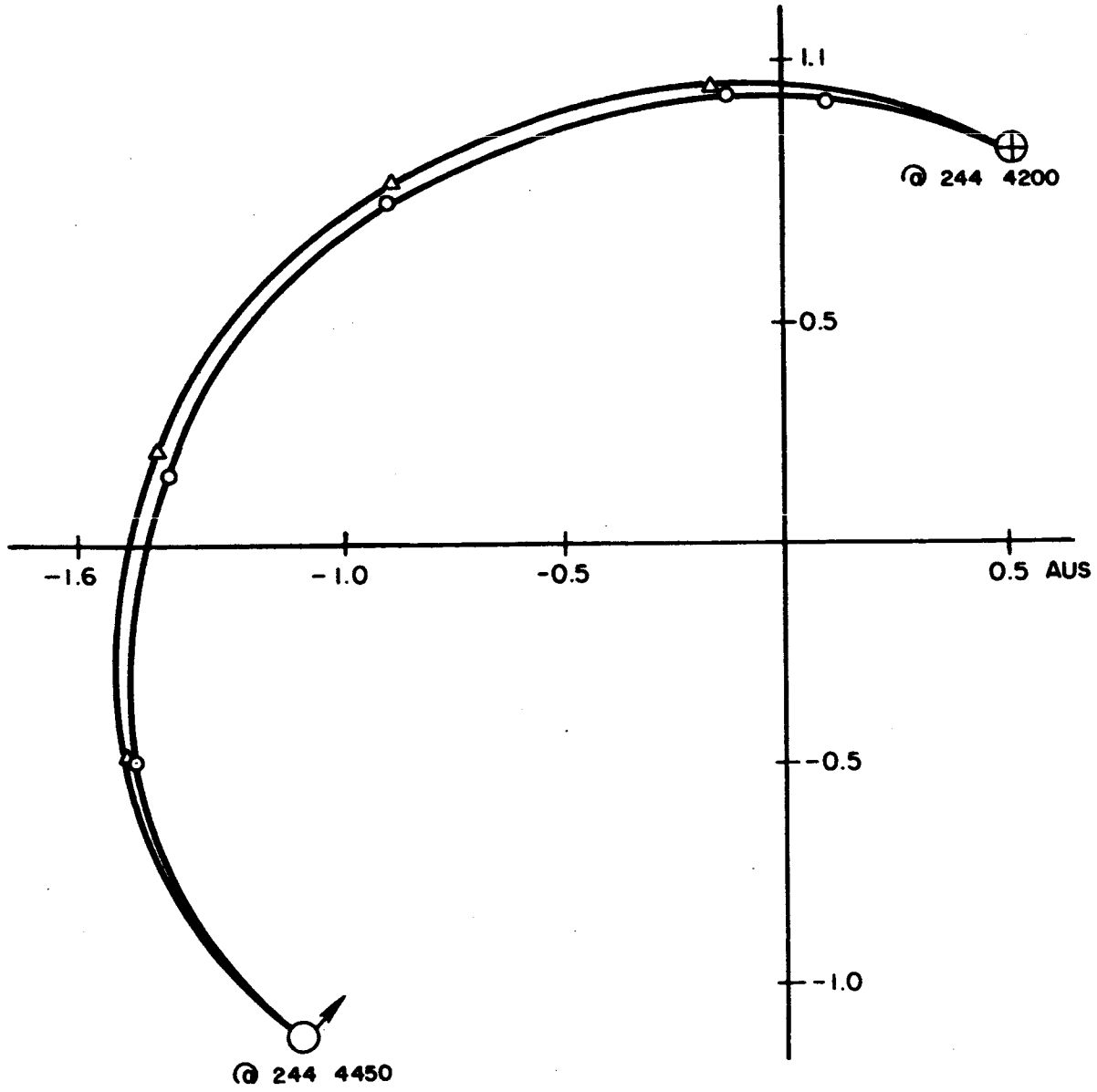

FIG. V-10

NORMALIZED POWER OF SOLAR CELL POWER SOURCE VS DISTANCE FROM SUN

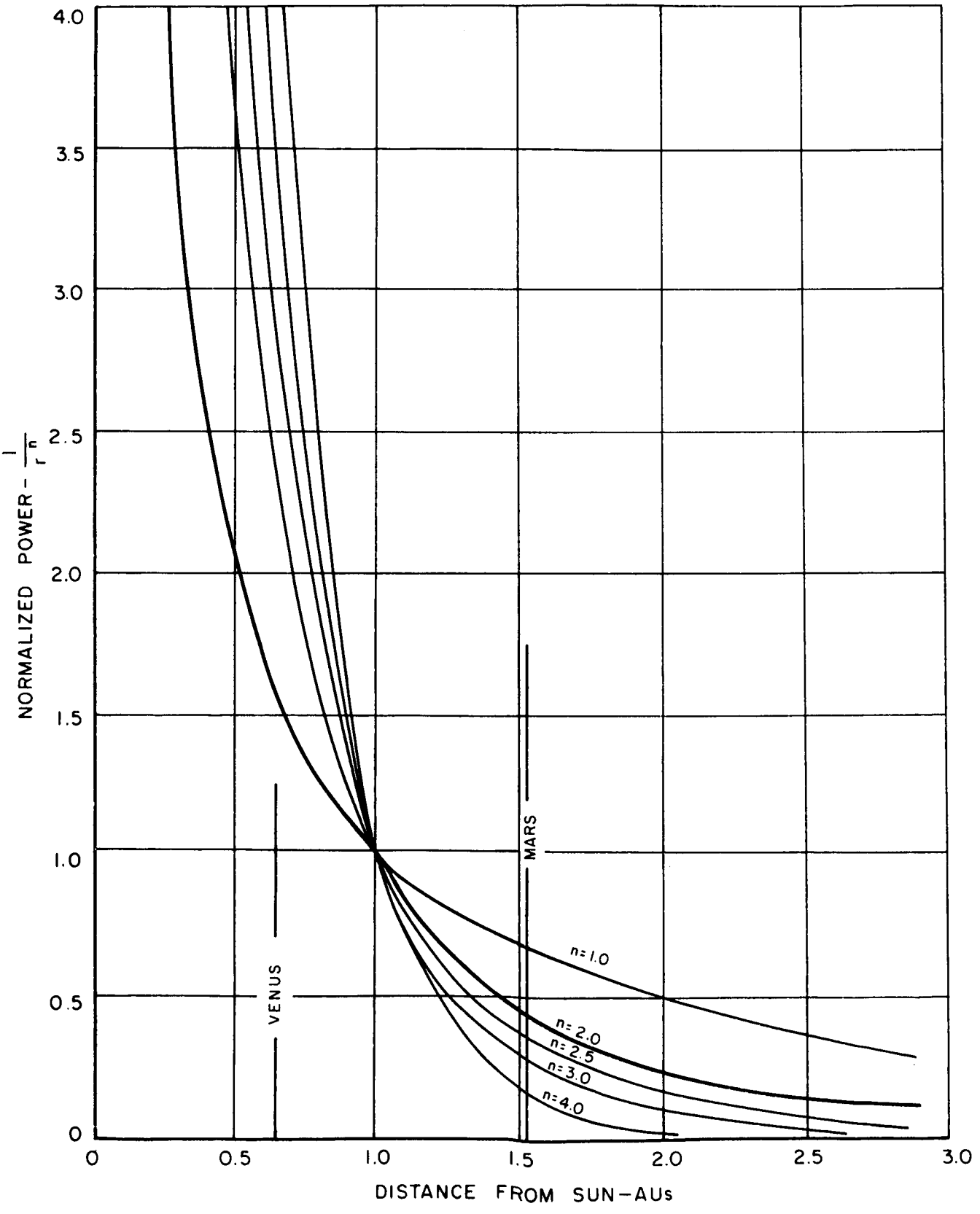

OPTIMAL LOW-THRUST TRAJECTORIES

MARS RENDEZVOUS

NOTE: THE TRAJECTORIES ARE REPRESENTED HERE BY ONE CURVE AS THERE ARE ONLY SLIGHT DIFFERENCES AMONG THEM

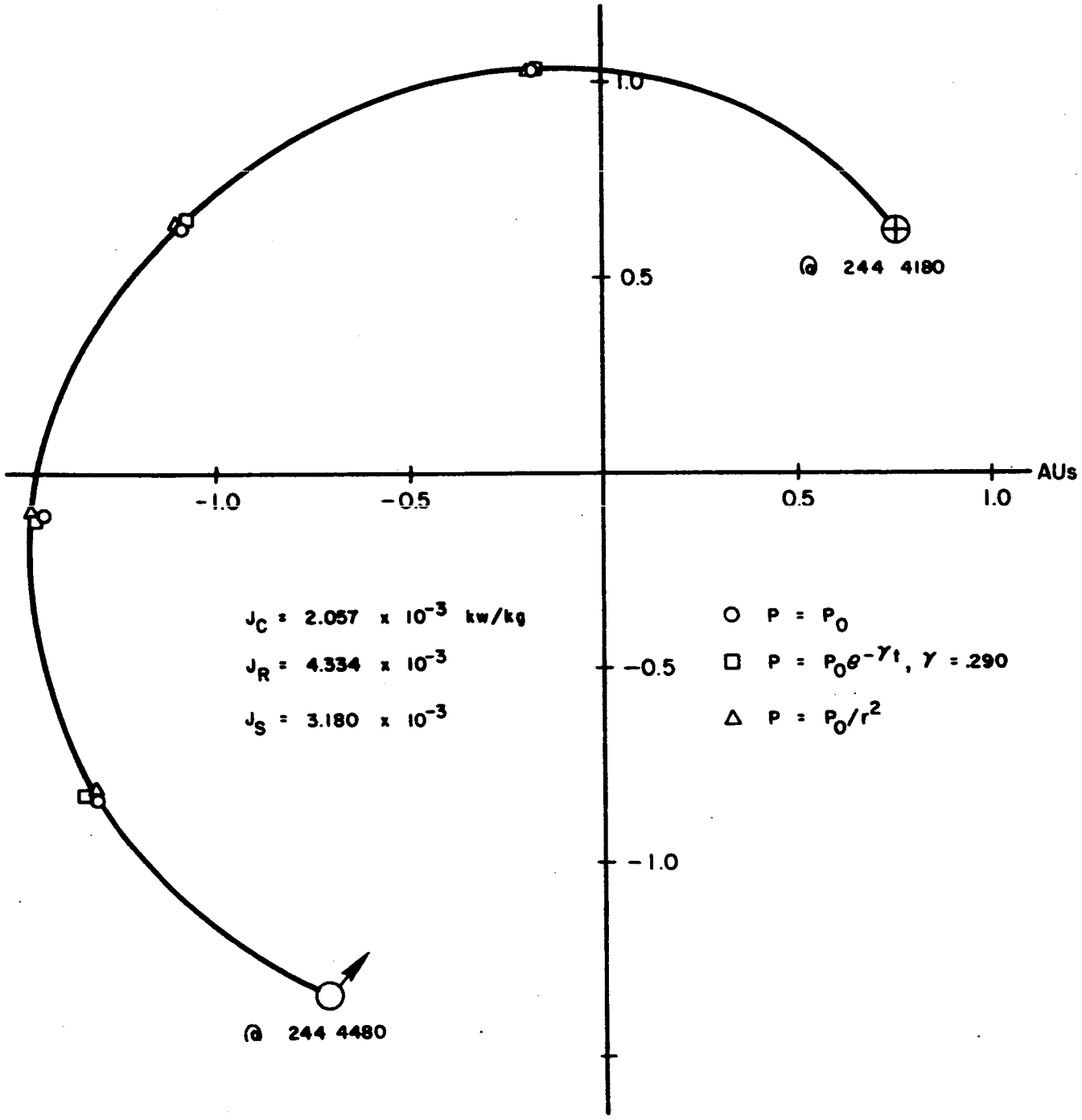

FIG. V-12

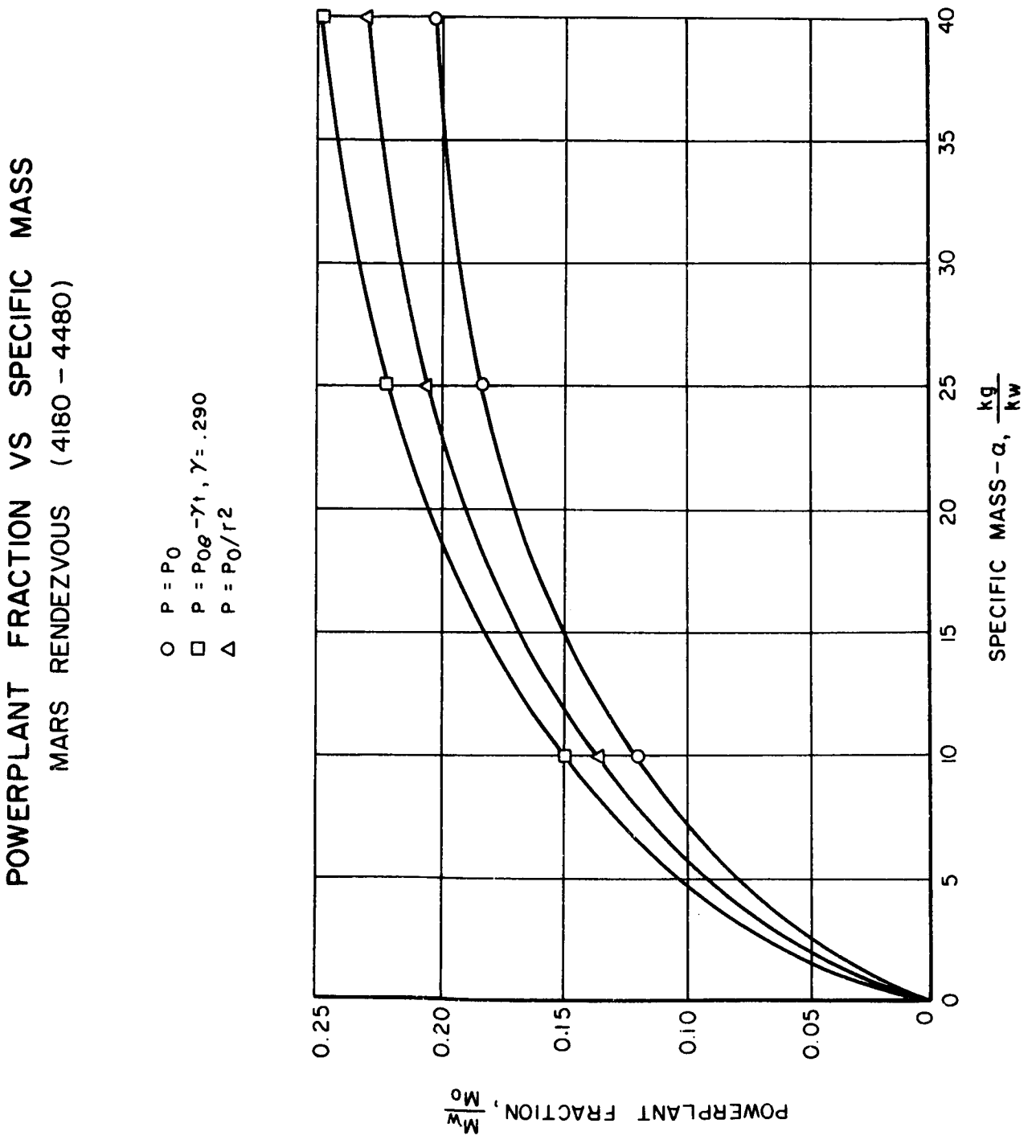
POWERPLANT FRACTION VS SPECIFIC MASS
MARS RENDEZVOUS (4180 - 4480)
O P = P0
□ P = P0e^-γt , γ = .290
Δ P = P0/r2
POWERPLANT FRACTION, Mw/M0
0.25
0.20
0.15
0.10
0.05
0
0
5
10
15
20
25
30
35
40
SPECIFIC MASS - α, kg/kw

PAYLOAD FRACTION VS SPECIFIC MASS

MARS RENDEZVOUS (4180-4480)

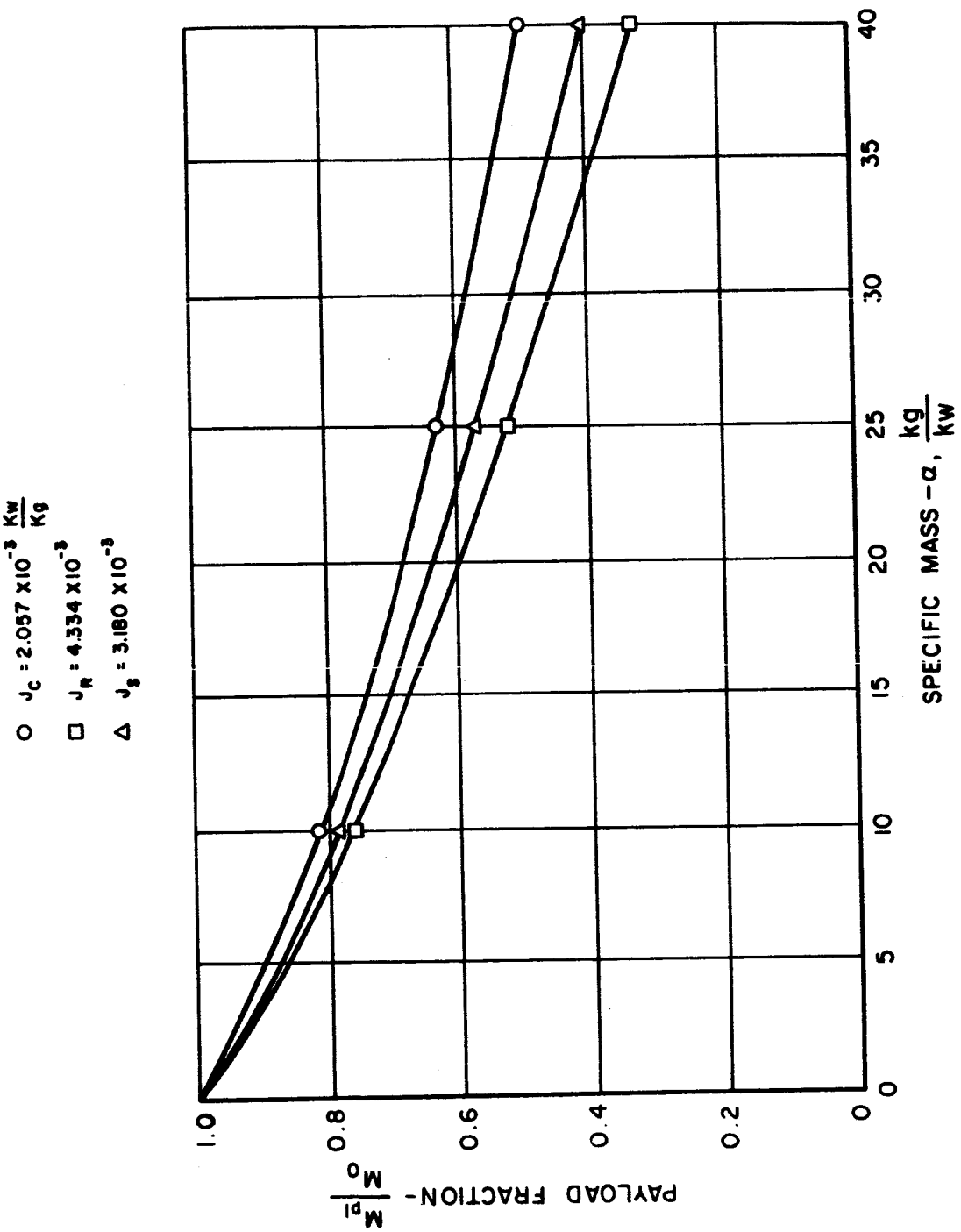

FIG. V-14

POWERPLANT FRACTION VS SPECIFIC MASS

MARS FLYBY (4180 - 4480)

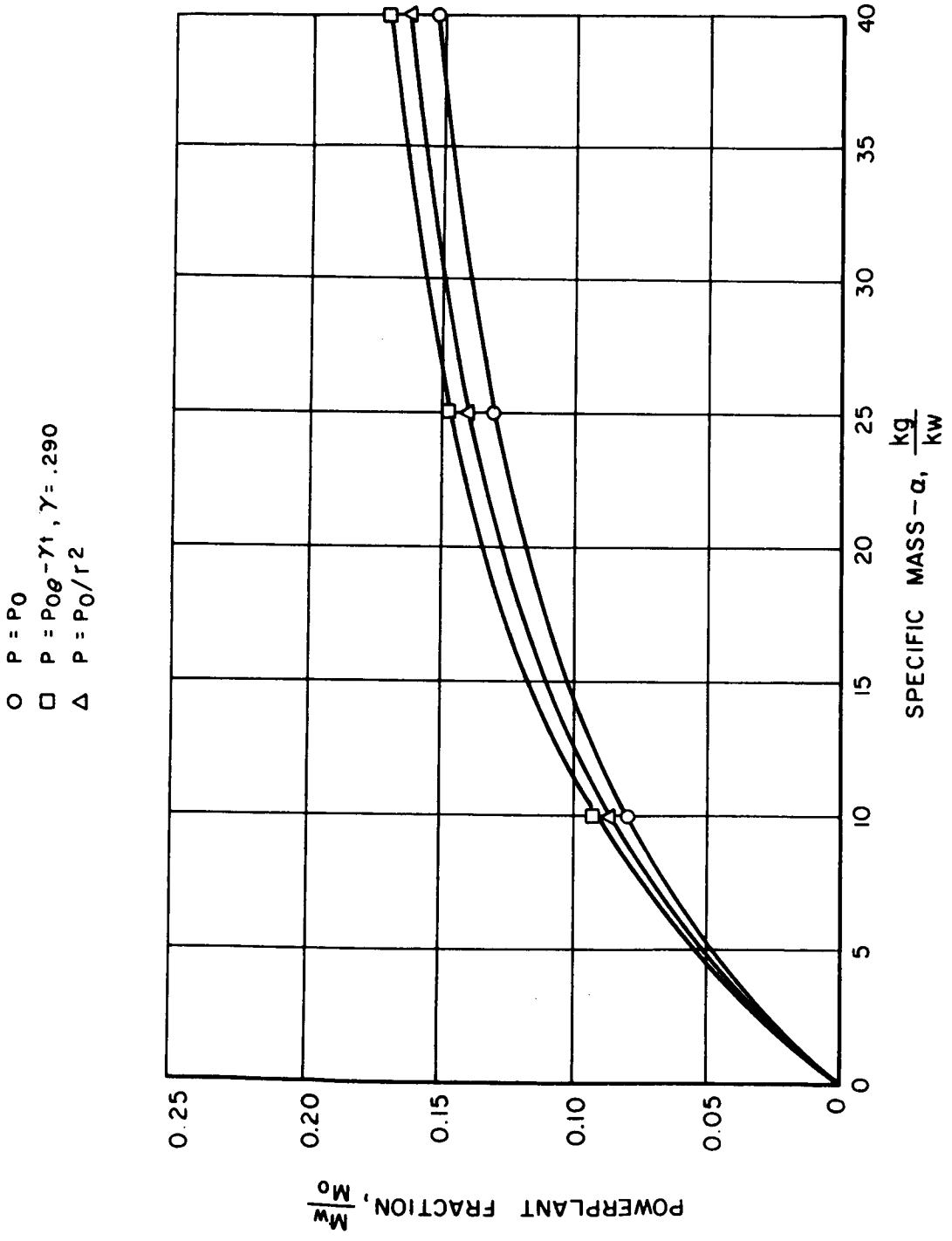

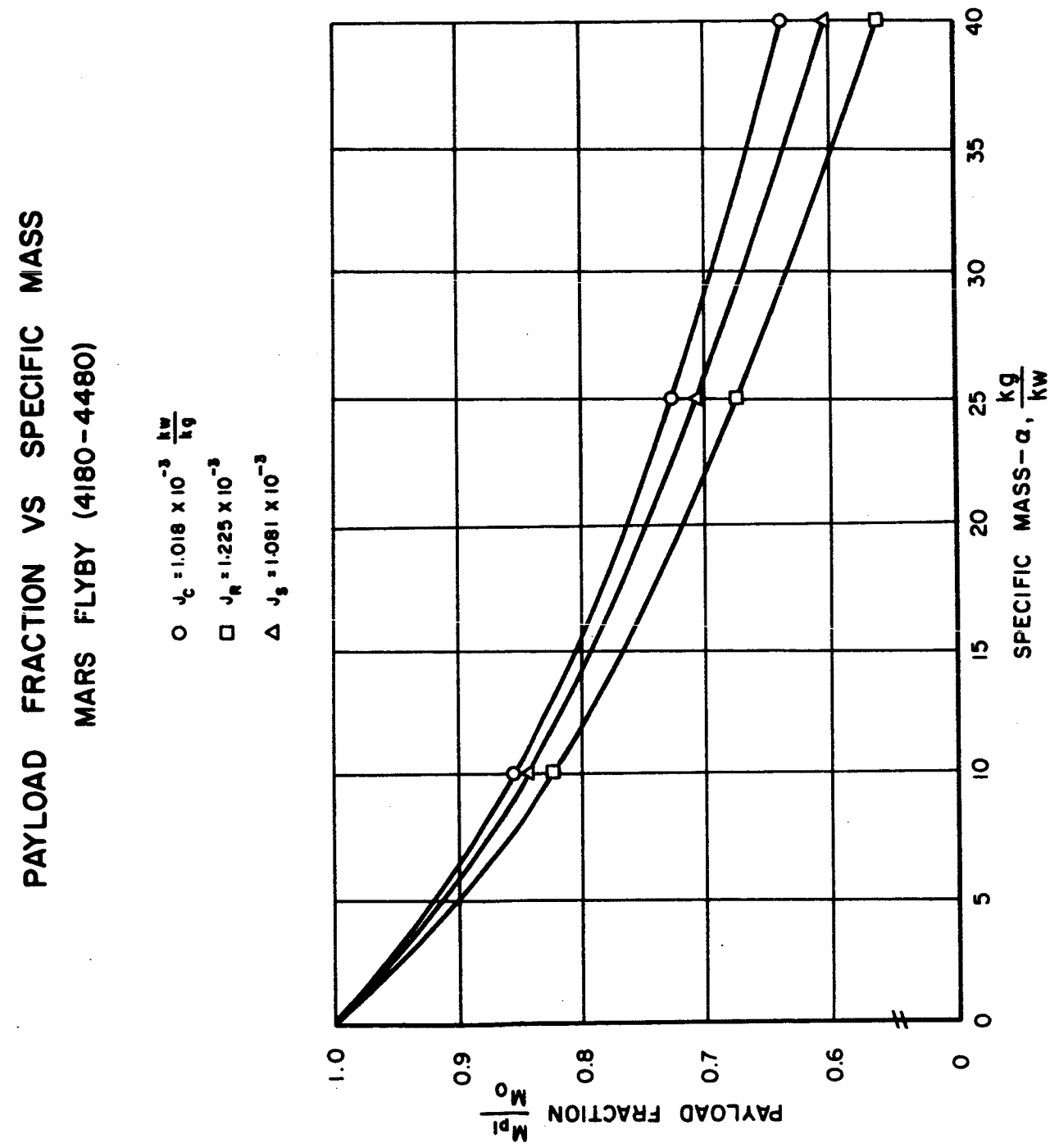
PAYLOAD FRACTION VS SPECIFIC MASS
MARS FLYBY (4180-4480)
○ $J_c = 1.018 \times 10^{-3}$ kw/kg
□ $J_R = 1.225 \times 10^{-3}$
△ $J_s = 1.081 \times 10^{-3}$
PAYLOAD FRACTION $\frac{M_{pl}}{M_o}$
1.0
0.9
0.8
0.7
0.6
0
0
5
10
15
20
25
30
35
40
SPECIFIC MASS-α, kg/kw

OPTIMAL LOW-THRUST TRAJECTORIES

MARS RENDEZVOUS

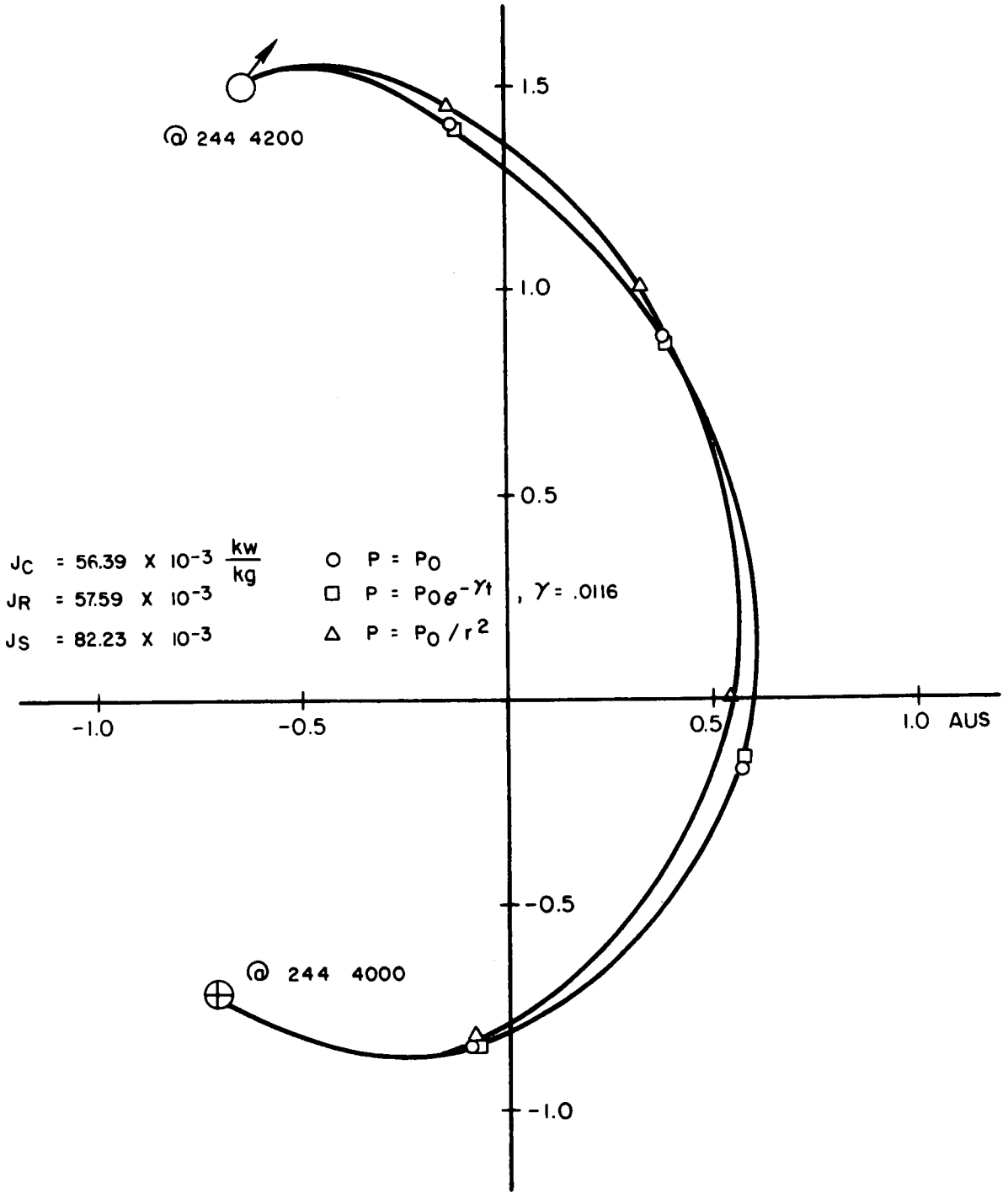

POWERPLANT FRACTION VS SPECIFIC MASS
MARS RENDEZVOUS (4000-4200)

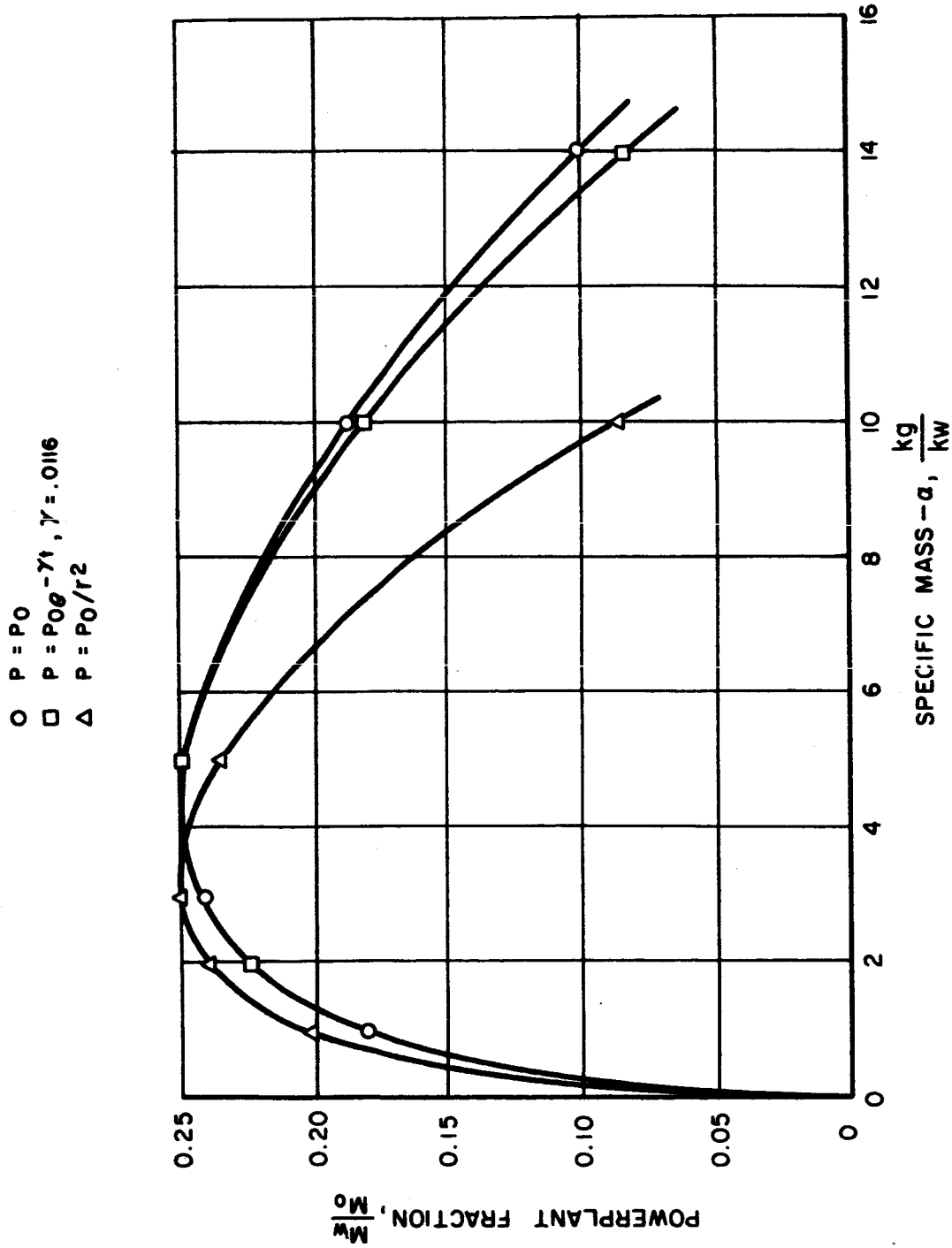

PAYLOAD FRACTION VS SPECIFIC MASS

MARS RENDEZVOUS (4000-4200)

$J_C = 56.39 \times 10^{-3}$ $\frac{kw}{kg}$

$J_R = 57.59 \times 10^{-3}$

$J_S = 82.23 \times 10^{-3}$

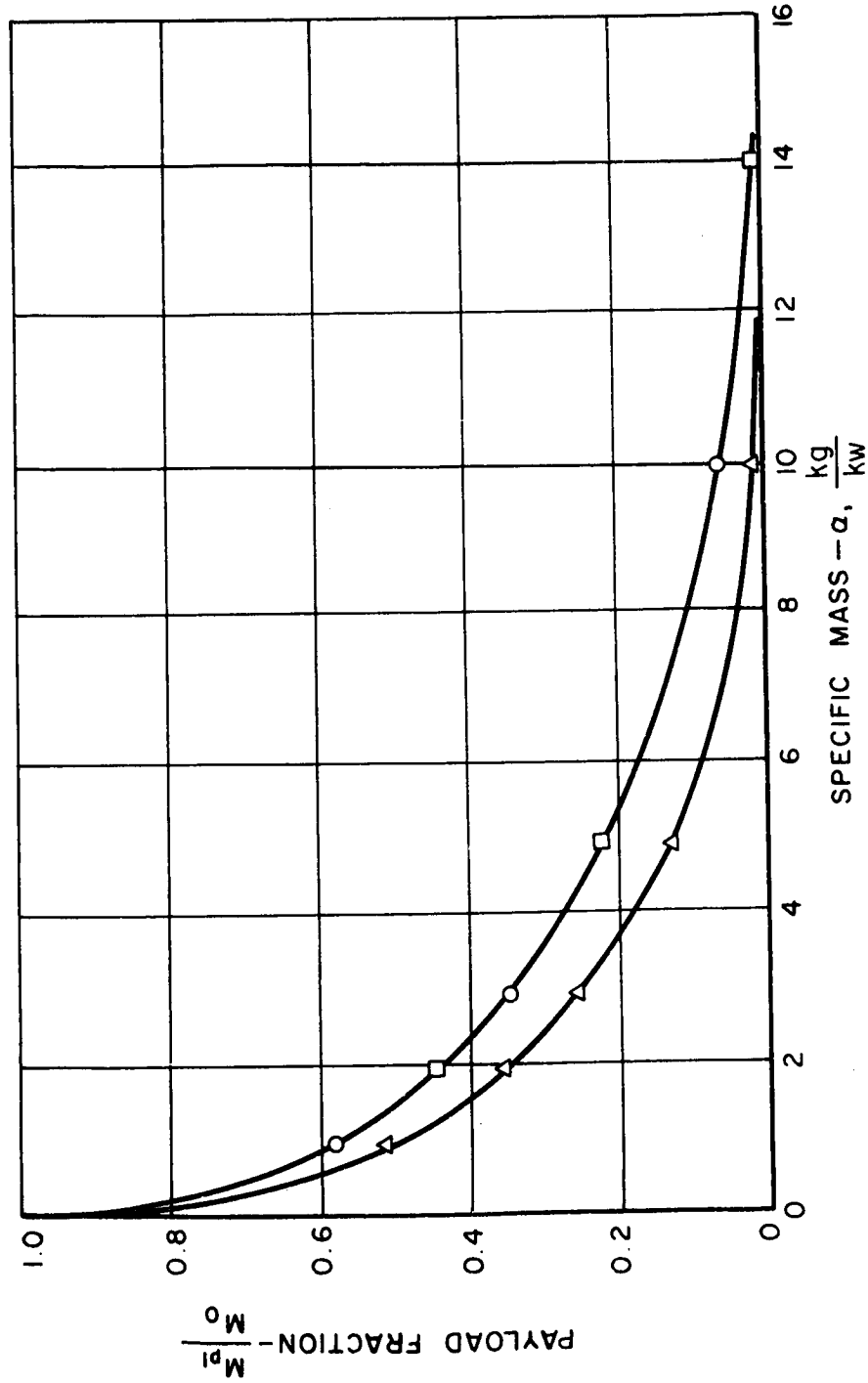

E-910262-6

FIG. V-19

OPTIMAL LOW-THRUST TRAJECTORIES

MARS FLYBY

NOTE: THE CONSTANT POWER AND RADIOISOTOPE POWER TRAJECTORIES COINCIDE WITH SMALL ERROR

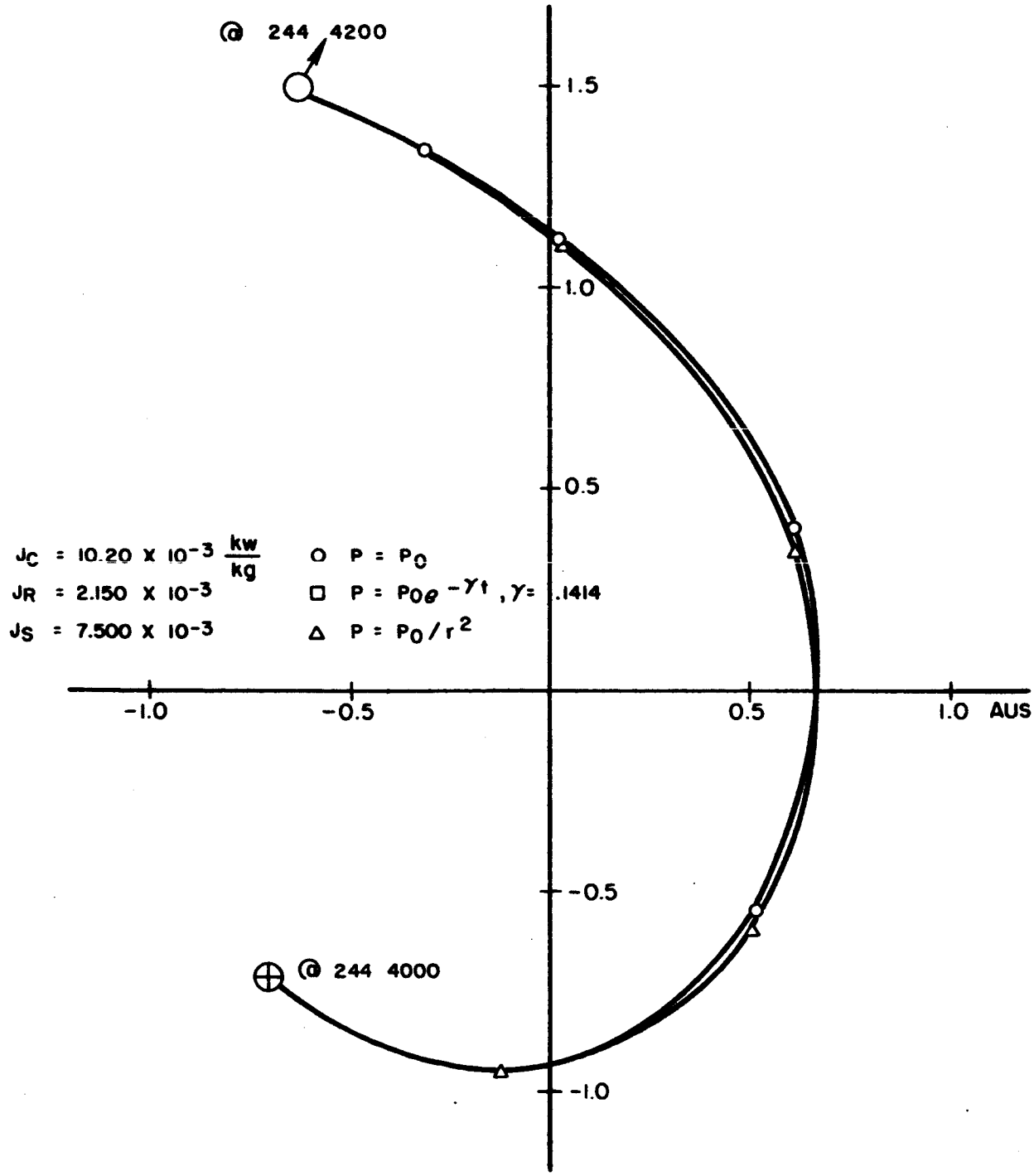

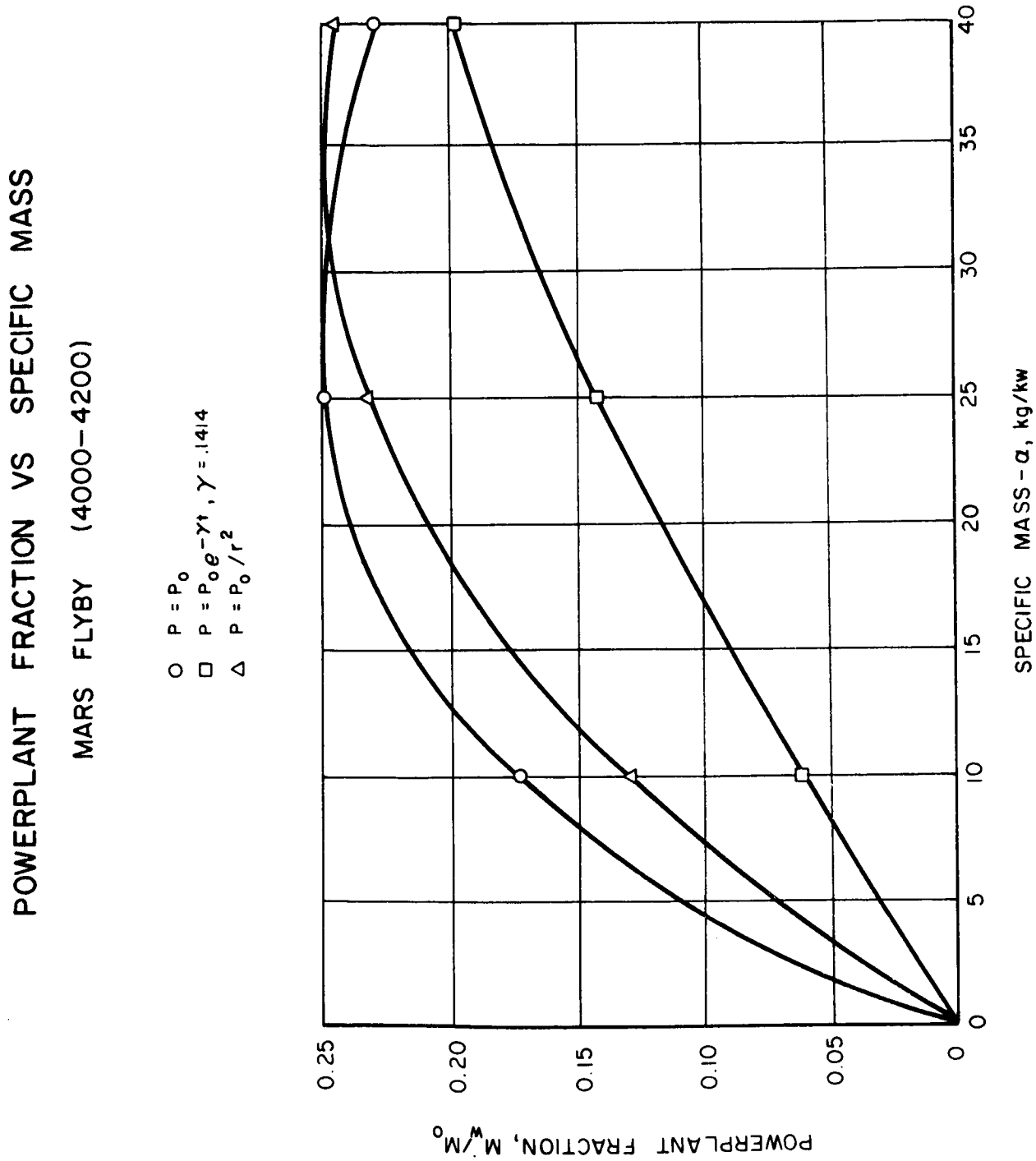
POWERPLANT FRACTION VS SPECIFIC MASS
MARS FLYBY (4000-4200)
○ P = P0
□ P = P0e^-γt, γ = .1414
△ P = P0/r^2
POWERPLANT FRACTION, Mw/M0
0.25
0.20
0.15
0.10
0.05
0
0
5
10
15
20
25
30
35
40
SPECIFIC MASS - α, kg/kw

FIG. V-21

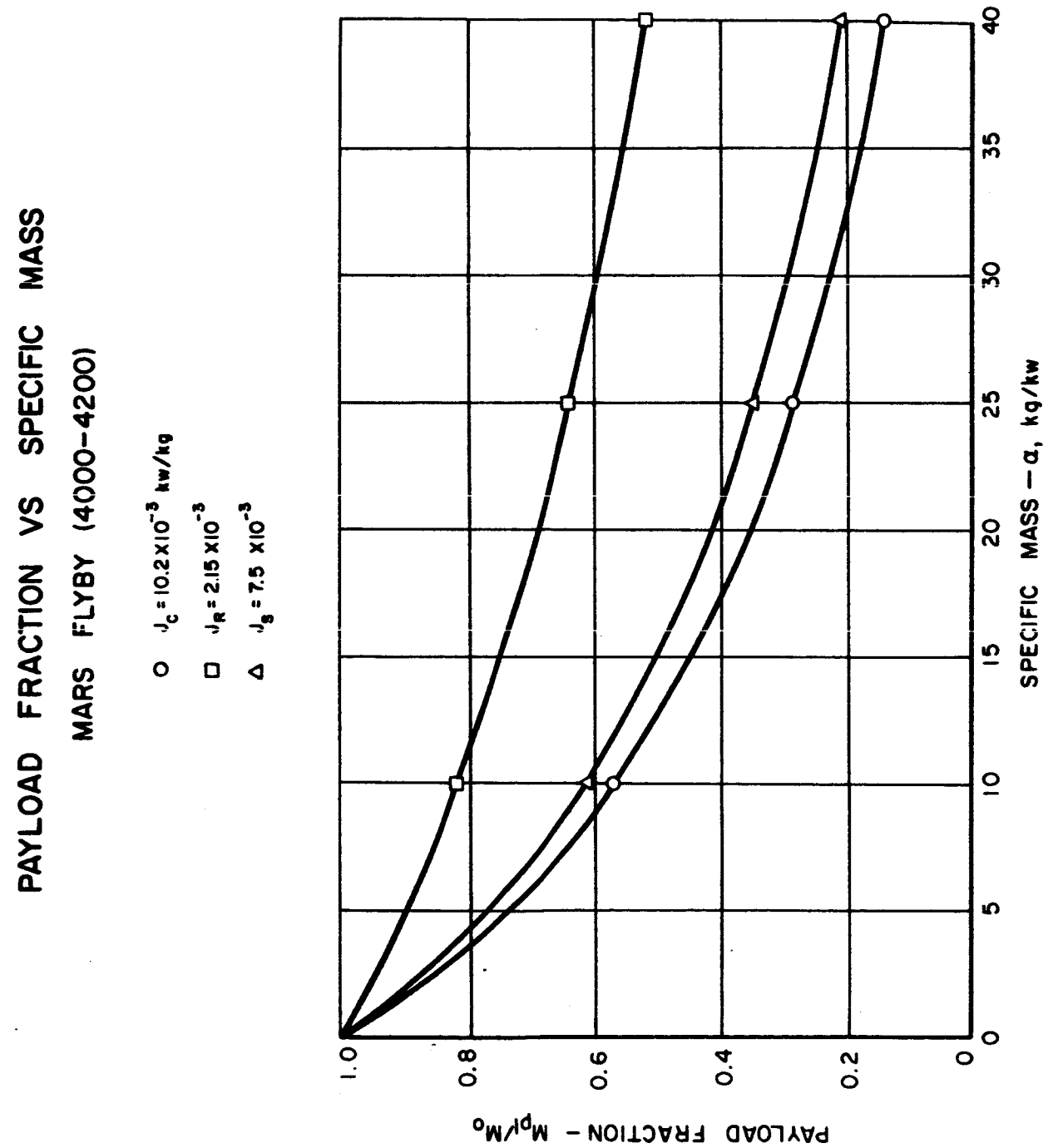
PAYLOAD FRACTION VS SPECIFIC MASS
MARS FLYBY (4000-4200)
O $J_c = 10.2 \times 10^{-3}$ kw/kg
□ $J_R = 2.15 \times 10^{-3}$
Δ $J_s = 7.5 \times 10^{-3}$
PAYLOAD FRACTION - M_{pl}/M_o
1.0
0.8
0.6
0.4
0.2
0
SPECIFIC MASS - α, kg/kw
0
5
10
15
20
25
30
35
40

NORMALIZED POWER AND THRUST ACCELERATION VS TIME FOR MARS FLYBY

(4400-4200)

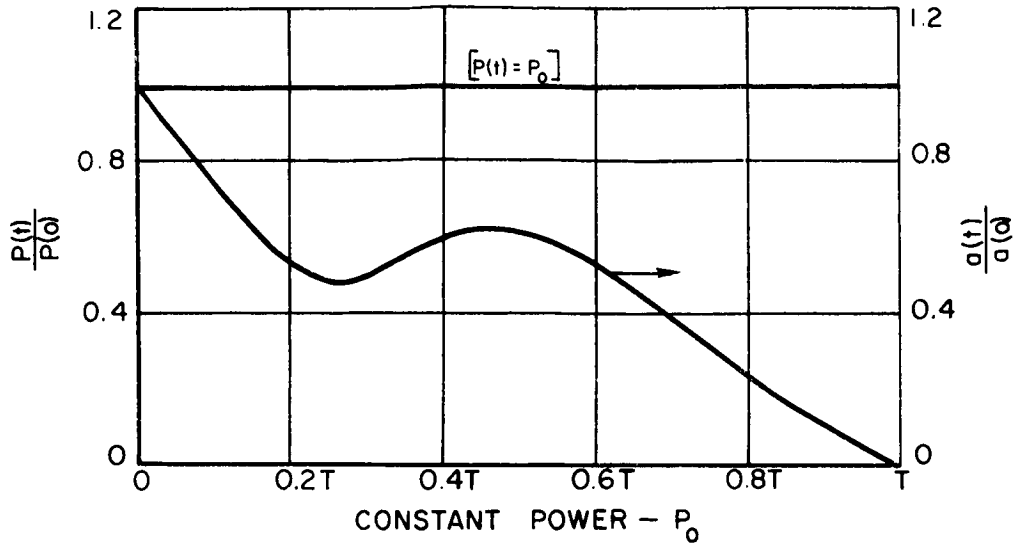

CONSTANT POWER – P_0

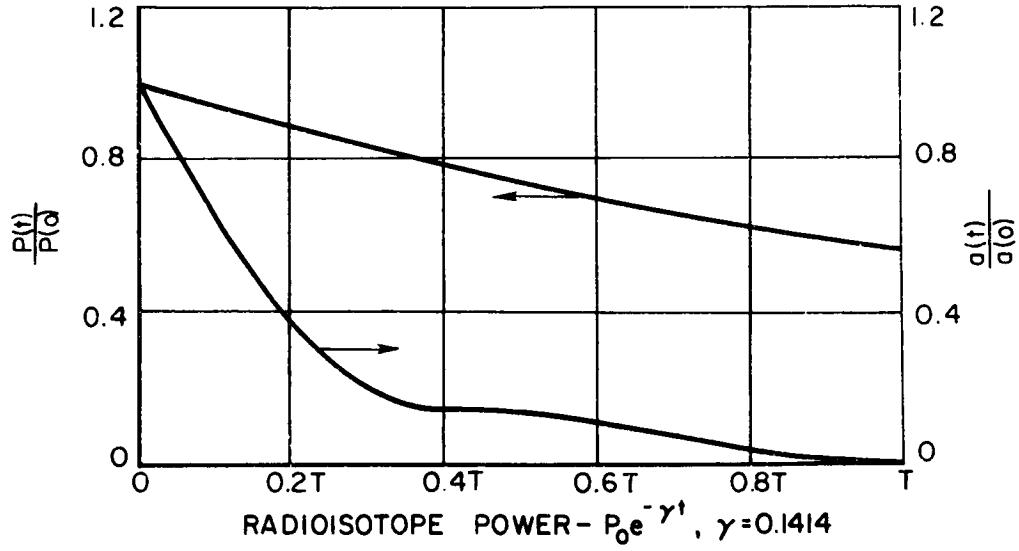

RADIOISOTOPE POWER – $P_0 e^{-\gamma t}$, $\gamma = 0.1414$

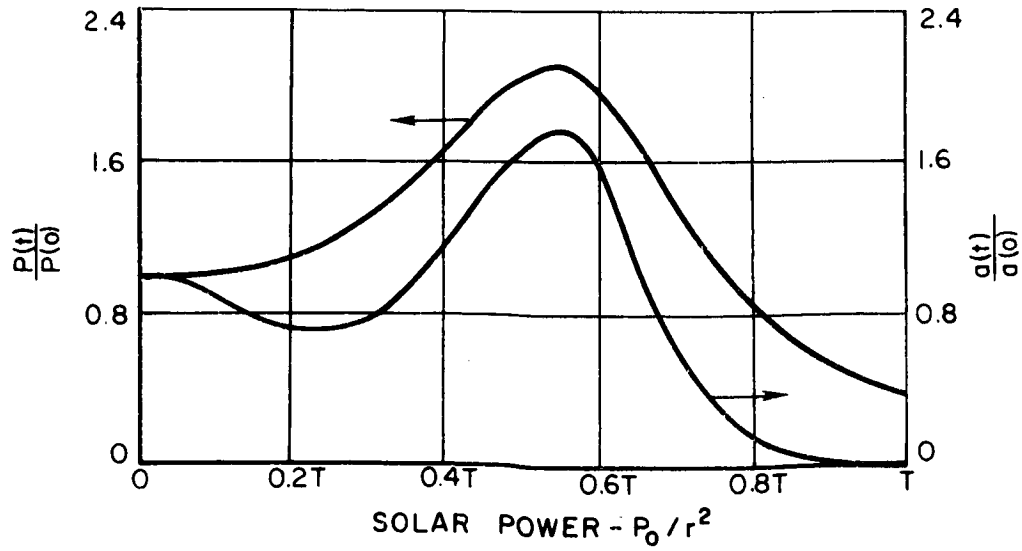

SOLAR POWER – P_0 / r^2

CONSTANT THRUST WITH COAST TRAJECTORY

I_{SP} = 8000 SEC

$a_0 = 0.593 \times 10^{-3} M/SEC^2$

$J = 6.976\ M^2/SEC^3$

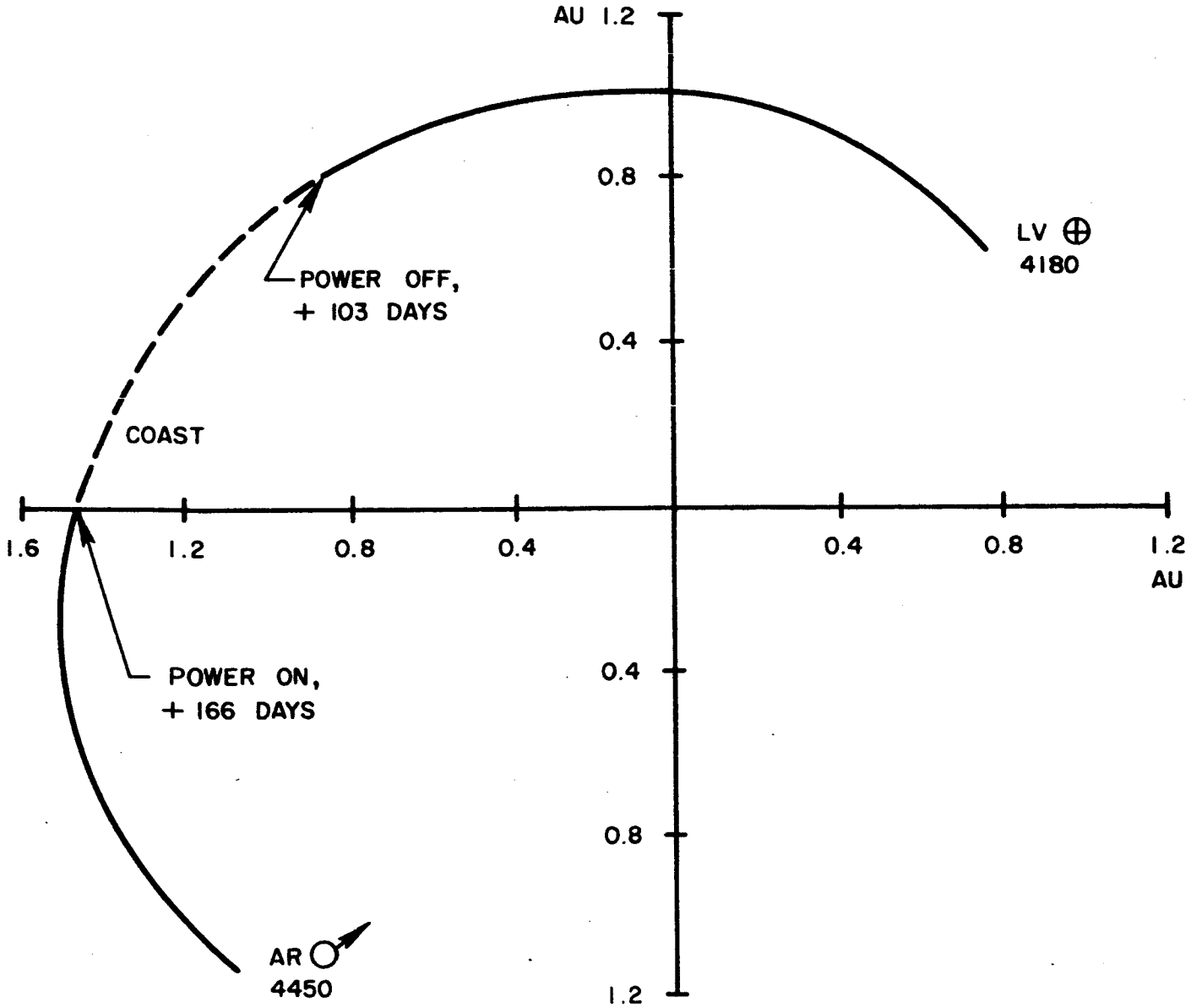

CONSTANT THRUST CONTROL TIME HISTORY

LV ⊕ 4180 AR ♂ 4450

I_{SP} = 8000 SEC

$a_0 = 0.593 \times 10^{-3}$ M/SEC^2

J = 6.976 M^2/SEC^3

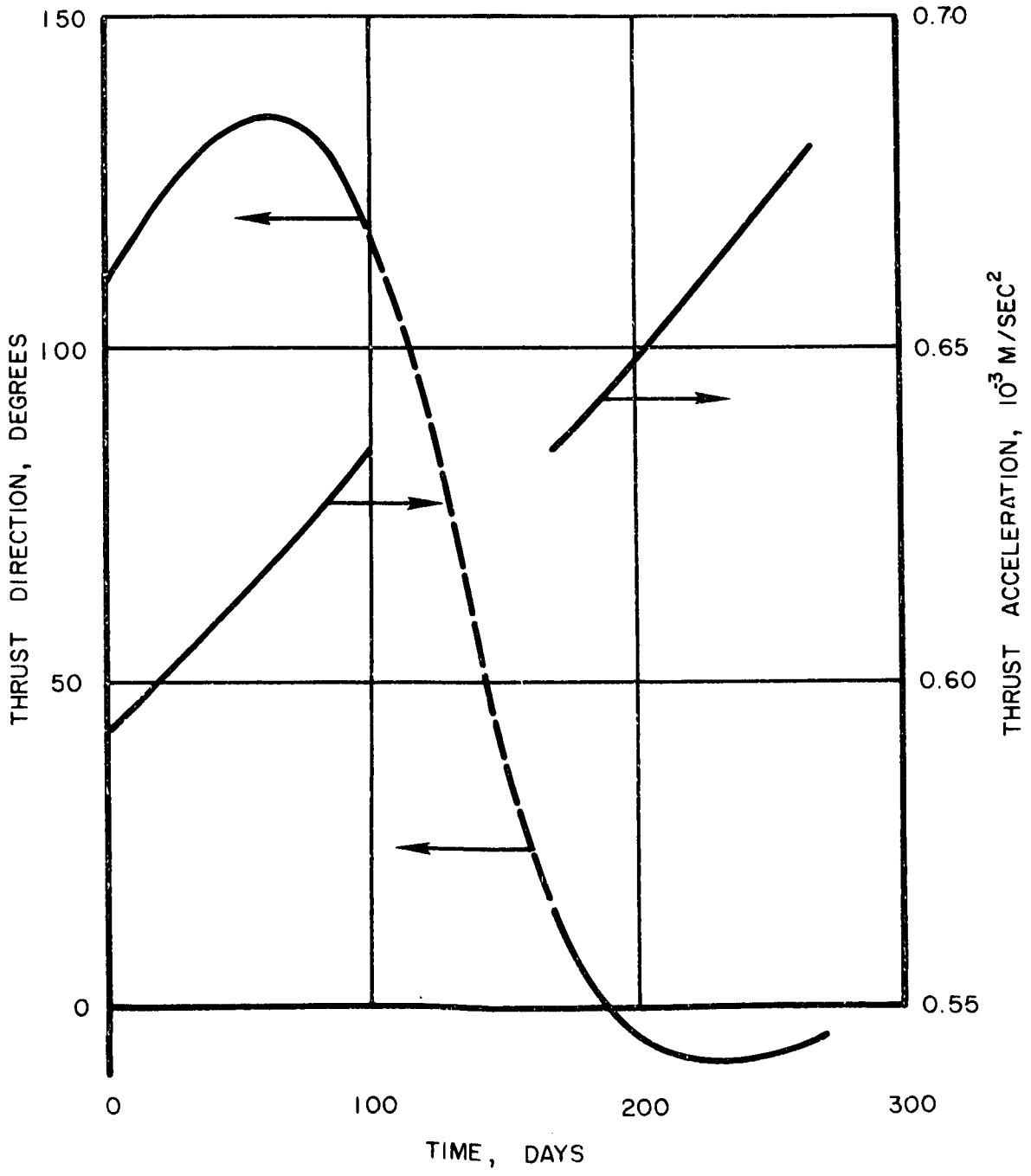

SECTION VI
POWER SYSTEMS STUDY

Introduction

The objectives of the power systems study are to:

1. Determine the required characteristics of nuclear Rankine-cycle space powerplants for low-acceleration manned Mars missions;

2. Determine the technological areas which can most significantly affect the powerplant characteristics through successful advanced research and technology requirements.

Previous powerplant studies reported under this contract (Ref. VI-1 included:

1. Powerplant design

2. The development of a method for relating component failure rates to the availability of system power during the mission

The work reported here is an extension of this earlier work and includes:

1. More detailed powerplant design,

2. An evaluation of powerplant reliability including the determination of powerplant redundancy and the effects of being able to maintain the powerplant,

3. The determination of mission requirements (as measured by mass on Earth orbit - MEO) as a function of various powerplant characteristics,

4. An evaluation of the development program required for a nuclear Rankine cycle space powerplant.

The classical method for relating powerplant and mission performance has been by means of powerplant specific weight. The great significance of the work reported here is the identification of an additional powerplant characteristic and the development of methods for relating this characteristic to trajectory and mission requirements. This additional characteristic is the probable change of available system power output with time.

This change in available system power output with time is determined by a statistical analysis of the failure probability of the system components. The basis of this statistical analysis is the assumption that the components can be developed to achieve some stated level of technology. In this study

two different levels of development were evaluated: the level of development of the aircraft gas turbine and the development corresponding to a factor of ten increase in the level of reliability. This technique allows the determination of the technological goals and the corresponding development required for the nuclear Rankine cycle system to perform the manned Mars mission. The goals which have been evaluated in this study are:

1. System design parameters - temperature, reactor fuel burnup, materials, etc.,

2. Component technology,

3. Component redundancy,

4. System and componenent maintenance program.

The mass required on Earth orbit can be determined using the two powerplant characteristics-specific weight and available power (as shown on Fig. VI-5). Thus the methods developed in this study allow the assessment of the mission effects of virtually all of the decisions which must be made during the course of a powerplant design and development program.

Powerplant Design

Description of Reference System

The powerplant concept which was used in this study is a three-loop liquid metal system as shown schematically on Fig. VI-1.

The powerplant module was:

a. designed to fit within the payload configuration of the Saturn V using the SII stage as the orbital injection stage, and

b. arranged to provide maximum maintenance access to the powerplant components.

The resulting powerplant arrangement is shown on Fig. VI-2. The reactor is located in the nose of the payload stage in order to maximize the distance between the crew and the reactor and to minimize the diameter of the reactor shield. The reactor shield is directly behind the reactor. The reactor control drum drive shafts pass through the shield to the drive mechanisms which are mounted on the rear face of the shield.

The primary system (boilers, pumps, accumulator, and piping) is placed in an enclosure just behind the shield. The power-conversion systems and the electrical systems are placed at the rear of the payload envelope in a

relatively cool, low-radiation-dose-rate region in order to improve maintenance access. The power-conversion systems are placed at the rear of the vehicle in four separate compartments. A shirtsleeve maintenance environment can be provided in any one compartment with the other three power-conversion systems operating. A closed breathing apparatus will be required for the maintenance personnel, however, because of the possibility of refractory metal corrosion by minute quantities of oxygen. In addition, environmental cooling of this compartment is required. Piping for the potassium vapor and condensate connects the primary system and the power-conversion systems. The vapor piping is placed in an insulated duct in order to reduce heat loss from the working fluid. Additional shielding is placed at the rear of the primary system enclosure in order to reduce the bremsstrahlung dose rate in the mission module, caused by lithium activation, to a reasonable level.

The heat rejection system has a conical-cylindrical configuration which has the same dimensions as the payload envelope. The radiator is used as structural support for the powerplant during launch and space flight. Additional support is supplied by a fairing which is attached to the radiator during launch and is ejected while the powerplant is in Earth orbit. P&WA studies reported in Ref. VI-6 indicate the desirability of disposing of this structure after the powerplant has attained Earth orbit. The forward group of main heat-rejection radiator segments is conical in shape. The remaining two groups of segments, as well as the auxiliary and low-temperature segments, are cylindrical in shape. The low-temperature radiator is at the rear of the powerplant, while the auxiliary radiator is between the aft main radiator segments and the low-temperature segments. A description of the major subsystems in the powerplant module is given below. It should be noted that the reference power system contains two 4 Mwe power modules.

Primary System

The primary system (shown schematically in Fig. VI-1) consists of the reactor and its control system, the primary piping of the lithium loop, the shield, four boilers and two reactor coolant pumps. The reactor is the heat source for the system and utilizes UO_2-50%W, clad in the tantalum alloy T-222, as the fuel. The columbium alloy D-43 was chosen as the vessel material because of a favorable compromise between strength and reactor control effects. The primary piping and boiler containment material is T-222. Lithium, the primary system coolant, is heated in the reactor from 2018 to 2200 F and pumped to the boilers where heat is transferred to the potassium coolant in the power-conversion system. Shielding for the powerplant is provided by a multilayer shield located directly behind the reactor. The shield is radiatively cooled and contains a layer of carbon (as a high-temperature capability neutron shield), layers of tungsten gamma shield, and a section of lithium hydride (for lightweight neutron shielding). The control drum motors are located directly behind the shield in order to allow for maintenance access. The boilers and primary pumps are grouped behind the shield with an additional shield located aft of the boilers to provide protection from bremsstrahlung radiation.

Power Conversion System (PCS)

There are four power-conversion systems. Each contains a turboalternator, a condenser, a pump, and interconnecting piping. The working fluid for this system is potassium which is vaporized and superheated to 2075 F in the boilers. The vapor from each boiler then flows to a turbine where work is extracted. The vapor is condensed and subcooled to 1162 F in the condensers and pumped back to the boilers. A jet pump is located upstream of the boiler feed pump in order to raise the pump inlet pressure to prevent cavitation. The motive power for the jet pump is provided by recirculating part of the condensate pump discharge.

The turboalternators, condensers, and pumps are located at the rear of the powerplant so that easy access can be gained to these components for maintenance operations. This arrangement requires long pipes between the boilers and turbines and additional superheating of the potassium working fluid in order to assure dry inlet conditions to the turbines. Expansion bends are contained in the piping to relieve the stress due to thermal expansion.

Main Heat Rejection System

The main radiator system consists of twelve radiator segments, the pumps used to circulate the radiator coolant, and the required liquid piping. The radiators are arranged in four bays around the circumference of the payload envelope. Each bay contains the three radiator segments associated with a single power-conversion system. The segments of each bay are arranged axially along the powerplant. The NaK coolant for this system is circulated through the condensers to remove waste heat from the power-conversion system. After leaving the condensers at a temperature of 1250 F the NaK is circulated through the radiator where heat is rejected to space at an average temperature of about 1100 F. The radiators are of tube-and-fin design with full meteoroid protection on the outer surface and partial protection on the inner surface. Stainless steel is the tubing material and beryllium the barrier and fin material.

Auxiliary Heat Rejection System

The auxiliary heat rejection system provides cooling and lubrication for the turboalternators and cooling for pump motors and other electrical equipment. There are four radiator segments for this system. The tubes are constructed of stainless steel and the barrier of beryllium. The segments are arranged to form a cylinder at the rear of the main radiator segments. The potassium coolant for this system is pumped to the cooling loads at 531 F and then to the radiator where heat is rejected at 550 F.

Low-Temperature Heat Rejection System

This system provides cooling for the rectifier and low-temperature instrumentation. The monoisopropylbiphenyl coolant for this sytem is pumped

to the radiator at 200 F and returned at 198 F. Aluminum is the containment material for the radiator, the barrier, and the fins. This radiator is located aft of the auxiliary heat rejection system and provides a relatively cool environment for the power-conversion system maintenance compartment.

A summary of the weight of the reference design powerplant is shown below, broken down to the subsystem level.

Powerplant Weight Summary

Primary coolant system	9,520 lb
Radiation shielding	61,700
Power-conversion system	15,670
Heat rejection systems	23,570
Electrical system	2,960
In-flight structure	6,000
Total powerplant weight in flight	119,420 lb
Powerplant specific weight	29.9 lb/kwe

A detailed weight breakdown by component is shown in Table VI-1.

Reliability Considerations

In order to plan the powerplant development it is necessary to have an understanding of the reliability requirements for the components and the system. An evaluation of powerplant reliability has been made which uses power availability as a measure of reliability. For any particular power system of interest, an estimate of available power as a function of time can be made and this estimate can be used as the basis of a calculation of the mass on Earth orbit requirements for the mission. Thus the reliability aspects of powerplant design can be evaluated on the basis of the effect of reliability on mission performance. In turn, powerplant development requirements are a measure of the technology required to achieve powerplant performance and reliability goals. In this study component failure rates are used as a measure of system development requirements.

This evaluation considers the following aspects of powerplant reliability:

a. The effect of component failure rate level,

b. The effect of multiple subsystems and systems,

c. The effect of being able to maintain, repair, or replace components,

d. The effect of providing reserve capacity in certain components.

The over-all method for evaluating these effects is as follows:

a. Estimate component failure rate,

b. Estimate power availability as a function of time associated with a particular powerplant arrangement, maintenance capability, and probability,

c. Using the power availability and an associated specific weight calculate the mass required on Earth orbit to perform the mission.

Failure Rate Study

The calculation of powerplant reliability requires the establishment of component failure rates. Insufficient data exist at this time to make a prediction of failure rates for nuclear Rankine-cycle space powerplant components. Therefore, the questions to answer are: what failure rates will result in acceptable powerplant performance? Approaching the question of powerplant reliability in this fashion will permit a determination of the relationship between powerplant performance and the development program which may result in a given powerplant performance. Thus component endurance goals can be specified. In order to provide a link with presently known technology, the failure rates used in the study were based on the extensive information available from Pratt & Whitney Aircraft gas turbine experience.

The failure rates used in the study were derived in a three-stage process:

a. The relative magnitude of the failure rate for each subsystem and component was established using available experience and engineering judgment.

b. Absolute predicted failure rates for a few components with well established reliability characteristics were determined. In establishing these rates, the in-flight shutdown experience with P&WA engines in commercial airline service was used. This experience is based on 70×10^6 engine hours of operation. In evaluating these data, prior experience of these components was examined to understand the duty cycle which resulted in the observed field failure. The failure rates used as the bases for the analysis are shown on Table VI-2.

c. Using the absolute failure rate values from Step b and the relative magnitudes from Step a, the predicted failure rates used in the study were determined. These values are listed in Table VI-3 through VI-7. The values shown in these tables are interpreted as the failure rates which will apply to a nuclear Rankine-cycle space powerplant if the components for this powerplant, when developed, have failure rates which correspond to current commercial

aircraft turbine failure rates. These failure rates are referred to in this report as the reference failure rate, λ. Further analysis was performed using failure rates corresponding to a failure rate level of $\lambda/10$.

The failure rates discussed here do not include the effects of meteoroid damage. These effects are included in the analysis and are based on the meteoroid barrier being sized so that the probability is 99% that at least 75% of the main radiator loops will be in operation at the end of the mission.

An important consideration regarding the failure rates is that the components are assumed to have sufficient endurance so that they do not enter the wear-out mode. The demonstration of the validity of this assumption is an important part of the powerplant development program.

Reliability Diagrams

Having assigned failure rate levels to the components, it is necessary to evaluate the amount of power generating capacity which is lost if a particular component fails. The logic involved in this evaluation is illustrated in Figs. VI-3 and VI-4. Figure VI-3 is a simplified schematic of the system which shows the reliability blocks for the subsystems (heavy dashed lines). The reliability blocks are defined by the loss of any other component in the block. For instance, in block R3 the failure of a turbogenerator results in the same decrease in power output as the failure of a condensate pump. As shown on this figure, the reliability blocks contain the following system components.

R1	Reactor
R2	Primary pump and motor
R3	Boiler
	Turbogenerator
	Condensate pump
	Jet pump
	Accumulator
	Auxiliary heat rejection system
	Low-temperature heat rejection system
	Electrical system
R4	Condenser
	Motor
	Pump
	Main heat rejection radiator segment

Figure VI-4 shows the logic involved in using the reliability block diagrams. The following illustrates the loss of power associated with the failure of any one of the various reliability blocks shown on Fig. VI-4.

Reliability Block	% Loss of Power	
R1	100	
R2	50	
R3	25	
R4	6.25	(for the first failure--% varies nonlinearly depending on the particular distribution of failures.)

Power Availability

Using the failure rates and the reliability block logic shown above, the variation in power output as a function of time can be calculated using the methods described in Appendix D of Ref. VI-1. The results shown on this figure correspond to the improved gas turbine failure rates ($\lambda/10$) for the reference system. As shown on the figure there is a probability associated with the power availability. The curve should be interpreted as showing the probability that the power available at any particular time is at least the value shown on the curve. For any powerplant with an assumed set of failure rates, there exists an infinite number of power availability curves each with an associated probability. As the probability increases the area under the power availability curve decreases as illustrated on Fig. VI-5 by the curves for 0.99 and 0.999 probability. This illustrates that the greater the desired degree of confidence the lower the power availability which must be used to plan the mission.

The concept of power availability is not a prediction of what the power availability will be but rather a method used to plan and evaluate the mission. Within limits, the mission can be flown using any pre-determined power availability probability. For the same mission constraints (launch date, payload, trip time) the higher probability is obtained by providing a greater amount of cesium propellant for the ion engines. Figure VI-5 for instance, shows the cesium requirements associated with the two probabilities shown (0.99 and 0.999). Thus the increased probability associated with a fixed set of failure rates represents a cesium propellant weight penalty.

Mass Required on Earth Orbit (MEO)

The power availability curve and the powerplant specific weight are used in the trajectory and mission analysis (as discussed in Sections III and V) to calculate the mass required on Earth orbit to perform a specified mission. The results of such a calculation are shown on Fig. VI-6 as a function of powerplant specific weight. As described before, the greater MEO associated with the higher probability is the result of the increased cesium propellant required for the higher degree of assurance in the power availability.

The procedures discussed above illustrate how both powerplant specific weight and power availability are characteristics of the nuclear-electric system. These characteristics have been used to evaluate the mission effectiveness (as measured by MEO) of various alternatives associated with powerplant design and development. Some of the alternatives will be discussed below as they apply to powerplant reliability.

Multiple Subsystems

One method of increasing system reliability is by providing a number of components which perform the same function. In the Rankine cycle powerplant this approach results in providing multiple subsystems. Ten different levels of subsystem multiplicity have been examined during this study (as discussed in Ref. VI-1). The results shown here are limited to the extremes of the range of systems evaluated. These extremes are presented by a single-thread system (Fig. VI-7) and the dual-reactor reference system (Fig. VI-8). The single-thread system represents the ultimate reduction in the number of components for a three-loop system (except for the multiple radiator segments). Loss of any component in the system, aside from one or two radiator segments, will result in a complete loss of system output.

The corresponding power availability curves for these two systems are shown on Fig. VI-9 for the reference failure rate, λ, and without any consideration of maintenance. In addition, the power availability is shown for the dual-reactor system with improved-technology ($\lambda/10$) failure rates. Two conclusions can be drawn from these results:

1. A single-thread system cannot provide sufficient power availability for the mission

2. Provision of multiple components improves power availability significantly. However, sufficient power availability is only achievable through a combination of multiple components and the lower ($\lambda/10$) failure rates (without considering maintenance).

Maintenance Effects*

Since the preceding results indicate the difficulty of obtaining significant power availability, it is of interest to examine the benefits which might be obtained if maintenance could be performed. The evaluation discussed here was limited to determining the potential benefits if it was assumed that maintenance operations are feasible. In addition, some of the more obvious aspects of maintenance, i.e., shielding, access, coolant

* Including maintenance, installed spares, replacement, or repair.

freezing, and thermal environments, were briefly examined. The over-all question of maintenance feasibility requires more detailed study.

As was pointed out in the powerplant description, the powerplant components have been arranged to maximize access to the components. In this configuration two powerplant modules (Fig. VI-2) are assembled with a mission module and an ion engine array to form the spacecraft assembly. Figure VI-10 illustrates that, with both power modules at full power, the radiation dose rate in the area where the power conversion and conditioning equipment is located is low enough to provide access for maintenance. However, the dose rate in the area immediately behind the shield is high enough, 2.5 rem/hr, to be of some concern as far as access at power is concerned. Access to this area will require either additional shielding or reactor shutdown.

A number of calculations has been made to determine how powerplant reliability is affected by the type of maintenance program which is chosen. The full-power level probabilities associated with the different maintenance programs considered are shown in Table VI-8 for both aircraft gas turbine (reference) and improved (1/10 reference) failure rate levels.

The first result shows that there is only a 3% probability of generating full power for the whole mission if no maintenance is performed and the components achieve the reference failure rate levels. The full-power probability is only 71% if 1/10 reference failure rate levels are achieved. These results show the desirability of maintenance. The second repair mode considered indicates that repairing all failures of the electrical system and the power-conversion system controls has a negligible effect on the probability of generating full power. Even if repairs to the reactor and primary system controls are added (such as in Maintenance Mode 3), the full-power probability is increased to only 5% for the basic failure rate or 74% for the reduced failure rate. In addition, 90,000 lb of shielding is required with this mode in order to gain access to this equipment while the reactor is operating. This shielding can be eliminated by complete reactor shutdown. Maintenance Mode 3 represents the limit of powerplant reliability improvement due to repair of nonliquid-metal components. It is clear that the capability to maintain liquid-metal components is required to assure a high probability of generating full power by means of maintenance.

The next level of repair capability considered (Mode 4) was repair of about 43 failures of all of the components in the system except the primary system components. This repair mode results in a considerable improvement in full-power probability (to 49 or 93% depending on the failure rates) with a required spares weight of 8400 lb. Repair of every failure of these components will not significantly improve the reliability (Mode 5). These modes do not require additional shielding nor reactor shutdown to reduce radiation dose rates.

However, partial reactor shutdown and isolation valves will be required for liquid-metal repairs, not only to provide a reasonable thermal environment, but also because of the reduction in electrical generating capacity of the portion of the system which is being repaired. Partial or complete shutdown to reduce the temperature of the working environment will cause a problem with liquid-metal freezing. Also, opening liquid-metal loops will result in some loss of fluid inventory. Therefore, a liquid-metal fill-and-drain system will be required to maintain the required liquid-metal inventory and to prevent coolant freezeup.

Increasing the repair capability to include all of the system components increases the reliability to over 90% for repair of 52 failures. That is, the probability of having more than 52 failures of a specific distribution (shown in Table VI-9) is 6% for the basic failure rate and 1% for the improved failure rate. However, this maintenance mode requires 9500 lb of spare parts. Also 90,000 lb of additional shielding is required to protect against bremmstrahlung from the activated primary coolant. The shielding can be completely eliminated if the reactor can be shut down during the repair operation. In any event, partial shutdown will be required if liquid-metal system repairs are made. This mode also requires a liquid-metal fill-and-drain system.

The final mode considered (Mode 7) includes the capability of repairing the reactor or the reactor control drum system. This additional capability will increase the reliability to either 99 or 99.9% depending on the failure rate. However, the weight penalty associated with this mode is greater than 100,000 lb. While not considered in detail, it is judged that the shielding requirements associated with reactor repair are prohibitive. Any further examination of reactor maintenance feasibility should include consideration of remote-handling techniques in order to reduce the shielding requirements.

The ability to perform inflight maintenance can result in a significant increase in the probability that the nuclear-electric system can operate at close to design power for the mission times required. In order to obtain the full increase in reliability that is possible with maintenance, the maintenance program must include the repair of components which contain liquid metals.

A detailed analysis of the relationship between access time, power level, reliability, dose rate, and spare parts weight is shown on Table VI-9 for one of many possible repair programs. The basis for this repair program is:

1. The total mission dose of 10 rem in the mission module has been increased to 20 rem to provide for maintenance capability.

2. The system power level may be reduced to provide either a lower temperature or a lower dose rate environment. For instance, system power level (and dose rate) was reduced to 50% in order to provide more time to work on the control drums and the primary coolant pumps. Power level is reduced to 120 kwe to reduce the radiator temperature level to 100 F for plumbing repairs to one of the four power-conversion systems.

The weight of spares given in Table VI-9 is not prohibitively heavy, and it appears reasonable to carry them aboard the powerplant. However, the desirability of providing shop facilities aboard the spacecraft should be evaluated. This evaluation should compare the reliability benefits due to the increased repair flexibility with the weight of the shop facilities. Such a facility may provide the flexibility to repair unanticipated failures of both system components and repair and maintenance equipment.

A number of conclusions can be drawn from this analysis. Some of them were anticipated in the discussion of Table VI-8 but are repeated here for emphasis.

1. About 43 component repairs or replacements (of all components except primary system) will give a 49 or 93% probability of maintaining full power capability for the duration of the mission. The weight of the spares required is about 8400 lb or 2.1 lb/kwe. Liquid-metal repair capability is required for this maintenance mode.

2. About 53 component repairs or replacements (of all components except the reactor) will give a 94 or 99% probability of maintaining full power. The required weight of spares for this mode is about 9500 lb (about 2.4 lb/kwe).

Also, 90,000 lb (about 22.5 lb/kw) of additional shielding will be required if it is desired to perform maintenance of the primary system components (including reactor control drum actuators) while the reactor is at any substantial power level. This shielding can be completely eliminated if the reactor can be completely shut down during repair of the primary system components.

3. Ample access time, about 4000 hr, is available for repair of the components associated with the reliabilities of 50 or 93%. The small number of significant components whose repair increases the reliability to 94 or 99% either have little access time (less than 100 hours with 90,000 lb of shielding) or require complete system shutdown in order to increase the access time.

4. System reliability is limited by the reactor to 0.948 in a single nonrepairable reactor system. A 99% or greater probability of

full-power capability throughout the mission requires either one, or some combinations, of the following:

a. A reactor and control drum reliability of greater than 99%. (This implies a requirement to develop the reactor to achieve the improved failure rate level.)

b. A redundant reactor (if the improved failure rate is not achievable and the reactor reliability is less than 99%).

c. Reactor repair capabilities (if one or two reactors are used whose separate or combined reliability is not greater than 99%).

There are a number of ways in which redundant reactors can be operated. For instance, two reactors can be operated simultaneously, each supplying 50% of the power. In this event the probability of one reactor being operational at the end of the mission is 0.9975. If a third reactor is added (each reactor producing 33.3% of the power) the probability of one surviving is 0.9999. An alternative strategy is to provide series operation of the reactors. In this event, one reactor would supply 100% power until it failed and then the second reactor would start up and supply 100% power. The probability of one reactor surviving is 0.9988 with this mode of operation. A choice between these alternatives requires analysis of mission effects to determine the influence of specific weight differences and to determine the influence of operating at part load. This is further discussed on page VI-15.

The third conclusion (regarding access time) is illustrated by Fig. VI-11 which shows the approximate equipment locations and the shielded and unshielded radiation dose rates. Sufficient time exists for maintenance to be performed at Locations 2 to 7. However, maintenance on the control drum drives at Location 1 is complicated by the bremsstrahlung dose rate from the primary system piping and components. Shielding is required around the primary system in order to perform maintenance on the drum drives without shutting down the reactor. The power-conversion system and the electrical components were placed at Location 7 in order to maximize the allowable maintenance access time. The weight penalty for placing the equipment at Location 7 is about 2600 lb for the additional piping and about 1100 lb for the additional power required to superheat the boiler exit vapor to account for the additional piping heat loss. The total specific weight penalty is about 1 lb/kwe.

Figure VI-12 gives the time allowed at specific locations in the powerplant as determined by the maximum total mission dose rate of 20 rem. For locations at the rear of the powerplant and for the reduced power levels more than enough time is allowed for one man to perform many operations. Figure VI-13 shows the variation in dose at a number of specific locations

for various power levels. The power levels correspond to the levels achieved due to the shutdown of the various failed components.

In order to more completely determine the potential benefits from maintenance it is necessary to evaluate:

a. The improvement in power availability,

b. The specific weight penalty associated with maintenance.

Both of these factors have been evaluated and used to determine MEO for a variety of situations. Figure VI-14 shows the improvements in power availability made possible by maintenance for the system demonstrating improved failure rates ($\lambda/10$). The specific components which are maintained are shown in Table VI-10 together with an estimate of spares specific weight. This information was used to determine the MEO requirements shown on Fig. VI-15 for maintained and nonmaintained situations.

This information points out a very significant aspect of being able to perform maintenance. The MEO requirements are the same for a nonmaintained powerplant with a specific weight of 20 lb/kwe as for a maintained powerplant with a specific weight of 32 lb/kwe (including 2 lb/kwe for spares). Thus, the same mission effectiveness can be obtained by either developing a low-specific weight powerplant (with the implication of an expensive development program) or by developing the heavier system with a maintenance capability (implying a cheaper development program).

Another aspect of performing maintenance is shown on Fig. VI-16. This curve shows that a maintenance program with a spares weight of 2 lb/kwe can increase the power availability probability from 0.99 to 0.999 and also reduce the MEO requirements by 5%. This may be a significant factor when determining the power system reliability requirements in the light of the manned mission requirements.

The power availability associated with a maintained, reference (λ) failure rate system is shown on Fig. VI-17. The MEO required for various levels of maintenance associated with this system is shown on Fig. VI-18. These results show that a more extensive maintenance program is required for the λ systems (120 rather than 42) in order to optimize the MEO requirements. A comparison of the MEO requirement for maintained λ level and $\lambda/10$ level systems are shown on Fig. VI-19. This information shows that the MEO penalty associated with the maintained λ level system is only 60,000 lb. This leads to the significant conclusion that the components achieving aircraft gas turbine development level are adequate if an extensive maintenance program can be developed. A complicating factor is that this level of maintenance will require a repair operation every four days. However, even if the maintenance level is the same for the

λ and the $\lambda/10$ cases (42) the penalty for the λ case causes a MEO difference of only 130,000 lb (less than one Saturn V launch vehicle). As will be shown later the development cost involved in improving component failure rates by a factor of ten is much greater than the cost of a Saturn V.

To perform maintenance on liquid-metal components, the equipment must be accessible, the crew must be protected from the thermal and nuclear environment so that it is safe to work on the equipment, and the equipment probably must be cooled and drained of liquid metal. In the event of an equipment failure, and resulting power reduction, about 1 to 2 hr are available for diagnosis and corrective action before the liquid-metal systems must be drained in order to avoid freeze-up in the radiators. If failure from meteoroid penetration should occur, even less time will be available to diagnose the fault and drain the failed system. Therefore a liquid-metal drain-and-fill system will be required in order to accomplish the repair of liquid-metal components. This system will have to incorporate many valves, controls and liquid-metal containment vessels. The question of the reliability of this system (including the required control system) requires examination to determine the real incentive for providing this system. No attempt was made to design such a system for the powerplant.

To repair the radiator segments, the radiator temperature must be fairly low. When a radiator segment fails, it will cool due to radiation from its outer surface. However, since the inner surface of the failed segment will be heated by radiation from the other operating segments, the temperature of the failed segment will cool to only 550 F, as shown in Fig. VI-20. This temperature is probably too hot to allow maintenance access. If the radiator segment is thermally insulated on its inner surface, it will cool in about an hour to a temperature that is low enough to allow maintenance, as shown in Fig. VI-21. However, in this event freezing of the NaK is a problem. The same holds true for the auxiliary radiator as shown in Figs. VI-22 and VI-23. The low-temperature radiator will take significantly longer to freeze (Figs. VI-24 and VI-25). It should be noted that the time required to freeze the radiator coolant depends on the effective sink temperature. The sink temperature used to develop Figs. VI-20 to VI-25 (0 R) represents a worse-case consideration and the time required to freeze the liquid metals may be somewhat greater than shown. This is not only true for the Earth and the Mars orbit modes but also in deep space. Since the powerplant will be part of a rotating spacecraft, most of the radiator faces the sun periodically and the effective sink temperature will be greater than 0 R.

Operating Mode Considerations

A number of methods have been proposed for improving power availability by scheduling the system operation in a number of different modes. The operating modes which have been evaluated are:

a. Sequential Reactor Operation

The flight is started with only one of the two reactors operating. At some time the second reactor is started.

b. Standby Power-Conversion Systems

The flight is started with some of the PCS's (R-3) shut down. As R3 failures occur the standby PCS's are started.

c. Reserve Capacity

The PCS's are initially sized so that they can provide excess power. As failures occur the remaining PCS's increase in power output.

Figure VI-26 shows the power availability with sequential reactor operation (solid line) compared with the reference case (dashed line). In this situation only one of the two power modules has been started at the beginning of the mission. When the power level decays to 25% of full power the second system is started. Operating the system in this manner makes a slight improvement during the later portions of the mission but not enough to offset the lower power availability during the early stages of the mission. Thus, it is concluded that this mission mode offers no benefit to mission performance.

The power availability for a similar sequential reactor operating mode is shown on Fig. VI-27. In this case the second powerplant starts up after 6000 hr have elapsed. Again, sequential operation (dashed line) has no significant advantages compared with the reference mode (solid line).

The power availability for the case where two of the eight power conversion systems are placed on standby at the beginning of the mission is shown on Fig. VI-28. When one of the operating PCS fails a standby is started up. The results indicate no benefit from this operating mode.

The results of the evaluation of the above operating modes tend to lead to the conclusion that the mission should be flown using all of the power that is available. However, a possible exception to this situation is shown on Fig. VI-29. In this case the power conversion systems have been designed to provide 25% in excess of the rated PCS capacity. In the event of failure of one PCS the power level of the remaining PCS is increased. As can be seen by Fig. VI-29 this excess capacity provision leads to an improvement in power availability. However, for the case which was examined here the powerplant specific weight increases by 3 lb/kwe as shown on Fig. VI-30.

This specific weight increase results from a requirement for providing reserve heat rejection capacity. The increase in capacity is gained by an increase in radiator effectiveness (with a consequent radiator weight

increase) since the Saturn V payload configuration is area-limited at 4 mwe. In order to determine the real benefit of this operating mode it is necessary to calculate the MEO for this situation to determine if the increase in power availability more than compensates for the increase in specific weight.

Another way to provide the required excess radiator capacity is to interconnect the radiator segments. This may make it possible to reduce the specific weight penalty. However, interconnection involves additional weight and unreliability because of additional piping, valves, and sensing and control equipment. This method of providing excess capacity requires further evaluation prior to reaching a conclusion.

Dependence of Powerplant Performance on Technology

Many choices must be made in the process of developing a nuclear Rankine-cycle powerplant. All of these choices depend on the technology which can be achieved during the development program. The range of choice is usually narrowly restricted by a number of technological considerations and the influence of the choice on system performance (specific weight) can usually be predicted. An extensive study has been made of the influence on specific weight of many of the powerplant parameters (Refs. VI-2 and VI-3). This study shows that most of the powerplant parameters have a relatively small influence on specific weight within a reasonable range of selection. However, three powerplant parameters stand out in terms of the effect which they have on specific weight. These are: (1) turbine inlet temperature, (2) reactor fuel burnup, and (3) radiator materials selection. These three factors will be discussed below.

Turbine Inlet Temperature

The selection of both reactor operating temperature and turbine inlet temperature is a very significant decision. While it is desirable to pick these temperatures as high as possible, recognition must be made of the physical limitation imposed by material properties, the development difficulties at high temperature, and the expected decrease in reliability as the temperature is increased. At the time a selection must be made a balance must be drawn between the improvements in performance which are possible at higher temperatures and the realities of hardware development. As a part of this study an attempt has been made to shed some sort of quantitative light on this selection.

Figure VI-31 shows the estimated decrease in powerplant weight as the turbine inlet temperature is increased. Also shown are corresponding values for reactor coolant exit temperature. It should be noted that there is an optimum combination of these two temperatures for any given

system. For the system under consideration a 200 F difference between reactor exit temperature and turbine inlet temperature is approximately optimum.

These results indicate a decreasing performance incentive for increasing the peak cycle temperature. Based on these results there is only a small weight incentive for increasing the reactor exit temperature above 2200 F. This is a result of the increase in reactor fission gas retention volume due to the decrease in reactor clad strength as the temperature is increased. The level of fuel burnup which can be achieved is also a function of temperature. In general, it may be expected that allowable burnup will decrease as the temperature increases. This provides a further incentive toward limiting cycle peak temperature. At the present time no information exists which will allow the interdependence of burnup and temperature to be expressed.

It is to be expected that component failure rates will increase directly with temperature. An attempt has been made to judge how the failure rate of the turbomachinery increases with temperature (Fig. VI-32). This curve represents a judgement based on analytical calculations of creep-limited machines and on limited data from aircraft gas turbine experience. It must be realized that this information is at best an approximation and probably has a fairly wide range of uncertainty.

The influence on MEO of turbine inlet temperature (as reflected by powerplant specific weight and failure rate) has been evaluated. Figure VI-33 shows this effect for two different assumptions. One assumption (probably optimistic) is that the failure rate of the high-temperature components does not depend on the turbine inlet temperature. The other assumption (probably pessimistic) is that the failure rate of the high-temperature components does depend on temperature as shown on Fig. VI-32. These results indicate that, regardless of which assumption is used the incentive for increasing turbine inlet temperature is not great. Indeed, using the optimistic assumption decreases MEO by only 10% when increasing the turbine inlet temperature from 1600 F to 2135 F. This is an insignificant weight change from an over-all mission standpoint for a 530-day mission. As the mission time decreases, the dependence of MEO on specific weight, and, therefore on turbine inlet temperature, increases. For instance, at 430 days the same change in turbine inlet temperature as above will change MEO by about 20%.

On the other hand, the dependence of MEO on specific weight is smaller for a maintained powerplant than a nonmaintained powerplant. All of these factors tend to lead to the conclusion that powerplant development risk can be decreased by choosing a relatively low turbine inlet (and therefore reactor outlet) temperature with only a small mission penalty.

Reactor Fuel Burnup

Past experience with nuclear systems indicates that development of the reactor fuel is usually the most technically difficult and costly item in the system. In addition, the burnup which can be achieved has a large effect on the weight of the system (as shown on Fig. VI-34). Therefore, the amount of burnup which can be achieved becomes a significant consideration in determining the development program requirements for the system under consideration. It is particularly significant that the high performance systems under consideration here assume a combination of burnup and fuel temperature which exceeds anything which has yet been demonstrated in an operational reactor.

Figure VI-35 shows the relationship between MEO and reactor fuel burnup for two different powerplant probabilities and for two different assumptions regarding powerplant maintenance. The conclusion which can be drawn is that reactor fuel burnup has a significant effect on MEO. Over the range evaluated burnup can change MEO by between 0.5 to 1.5 x 10^6 lb.

Effect of Mission Lifetime and Radiator Materials on System Weight

A large uncertainty exists regarding the effect of the interplanetary meteoroid environment and the effect on materials of meteoroid impact. This uncertainty may have a significant effect on mission performance since the selection of radiator fin and barrier material has a large effect on system weight (as shown on Fig. VI-36). The following summarizes how the materials choice affects powerplant specific weight and MEO for a mission time of 430 days:

Material	Specific Weight lb/kwe	MEO 10^6 lb
Beryllium	30	4.4
Copper Fins-Stainless Steel Barrier	34	4.8
Copper	37	5.4

It appears from these results that a copper stainless steel radiator presents a reasonable compromise selection.

Influence of Powerplant Technology on Weight

As indicated by some of these results, powerplant specific weight is very sensitive to the technological level, as reflected by temperature, burnup, radiator materials, etc., which can be achieved. This dependence is shown on Fig. VI-37 for a number of selected conditions. This illustrates

again that the influence of these systems parameters on specific weight is strong. It is also clear that there is a strong dependence between the level of technology and the cost of the required development program. This relationship is discussed in a later section. The effect on MEO of this variation in technology is shown on Fig. VI-38 for both 430- and 530-day missions.

These results are based on the optimistic assumption that the failure rate is not influenced by temperature. As the trip time increases the advantages of improving powerplant technology become smaller. Making the technology improvements shown reduces MEO by about 30% at 430 days and by about 10% at 530 days. These results indicate that further work is required in the area of mission parameter selection before firm conclusions can be drawn regarding powerplant parameter selection. However, the results indicate that the longer trip time (530 days) results in a significant reduction in MEO.

Reactor Shielding Considerations

In terms of the influence on power system weight and spacecraft design and integration complexity, the reactor shield represents the most important component in the system. In order to arrive at an optimum shield design many significant questions must be answered regarding over-all mission design and philosophy. Some of the questions are:

1. What is the total radiation dose which the astronauts may receive from all sources and what fraction of this can be from the powerplant?

2. What is the vehicle configuration?

3. What is the powerplant configuration?

4. How much of the allowable radiation dose may be received during maintenance operations?

5. What radiation dose may be received during rendezvous operations and what provisions should be made for accidental excursions outside of the scheduled rendezvous flight plan?

Answering these questions requires evaluation of the following shield design considerations:

1. Radiation dose

    a. direct
    b. scattered
    c. bremsstrahlung

2. Fission product release

3. Materials activation

4. Shield cooling

5. Reflector cooling

6. Maintenance access and reliability

7. Rendezvous shielding

The final shield design will require an iterative process which considers many alternatives. In addition, the system specific weight can vary by as much as 100% depending on the shield design criteria selected. It is for these reasons that shield design and development represents such a significant role in evaluating a nuclear powerplant.

Detailed shield design considerations have already been presented in Ref. VI-3. The work presented here will be limited to specific considerations which have been evaluated during this study.

The reference spacecraft configuration is shown in Fig. VI-10. Design of the reactor shield is closely integrated with the configuration of the spacecraft. In addition to direct radiation from the reactor to the mission module, the shield must adequately attenuate radiation which is scattered to the mission module by the material in the spacecraft. Further considerations are maintenance access and coolant activation.

The primary shield consists of three sections. One is a conically shaped shield which is placed in the cone of the spacecraft module to provide maintenance access to the powerplant components and to attenuate the radiation which is scattered by the radiator. Another shield section is a slab which projects from the conical portion of the module and attenuates radiation which is scattered by the other powerplant module. In addition, this section of the shield allows maintenance access to the adjacent powerplant module. Additional shielding may be required, depending on the powerplant arrangement, to attenuate radiation from coolant activation or contamination.

One of the shielding aspects which has been considered is that of shielding the primary system. There are two considerations involved. The first is the bremsstrahlung (X-ray) radiation due to the beta activity of the lithium primary coolant and the second is the neutron and gamma radiation involved with fission product contamination of the primary coolant caused by a leaking fuel element.

Figure VI-39 shows a simple schematic presentation of the alternative primary system shield configurations which have been studied. These are:

1. Secondary Shield - In this arrangement the boilers, primary pumps, accumulator, and associated piping are located to the rear of the primary shield. These components must also be shielded to attenuate bremsstrahlung radiation and radiation from radioactive contamination of the primary coolant.

2. Shielded Primary System - In this configuration the primary system components have all been moved behind the primary shield thus eliminating the requirement for additional bremsstrahlung shielding.

3. Intermediate Loop - In this arrangement an intermediate lithium loop has been placed between the reactor system and the power conversion system. This minimizes the coolant shielding required at the expense of system complexity. It should be noted that this arrangement requires the addition of a shield cooling loop as contrasted to the other arrangements which are cooled by direct radiation to space.

Each of these configurations are discussed below.

The secondary shield configuration (Fig. VI-40) requires tungsten shielding around the primary system components which are to the rear of the primary shield. The specific weight of this shield is about 30 lb/kwe. A large fraction (about 50%) of the shield weight is due to the requirement for the bremsstrahlung shield. The bremsstrahlung shield also provides protection for some degree of contamination of the primary system from fission products which may be accidentially released from the reactor. The advantages of this configuration are the ability to radiatively cool the primary shield and the accessibility of the primary system components for maintenance.

A major consideration in evaluating the secondary shield configuration is the effect of the accidental release of fission products from the reactor. These fission products release large amounts of gamma radiation and, under some conditions, neutron radiation. The following table shows the gamma ray dose which an astronaut in the mission module would accumulate if exposed to various amounts of released fission products for 10,000 hr.

Dose Due to Fission Product Release

% of Equilibrium Fission Products Released	Dose Accumulated in 10,000 hr-rem*	
	Reactor Operating	Reactor Shutdown
0.1	6.5	0.5
1.0	65	5.0
10.0	650	50

* Attenuated through bremsstrahlung shield and spacecraft wall

These results show that release of 1% of the core is probably tolerable. If the reactor which has the failed fuel element is shut down after the failure, as much as 10% of the core can be released without too much concern. The conclusion which may be drawn from these results is that a fuel element failure of some degree is not a limiting factor in establishing the design of this configuration.

In the shielded primary arrangement the entire primary system has been moved behind the primary shield in order to eliminate the bremsstrahlung shield, Fig. VI-41. However, the primary shield must be moved toward the rear of the powerplant module with a consequent increase in the weight of this shield. In addition, all of the primary system components become inaccessible for maintenance purposes. The shield weight for this arrangement increases to about 37 lb/kwe and the system weight to about 52 lb/kwe.

Figure VI-42 compares the power availability curve for a maintainable secondary shield powerplant with that for a maintainable shielded primary powerplant. In the first case the primary system is accessible for maintenance with the reactor shutdown. In the second case the primary system is not accessible for repair under any conditions. These results show that the effects of not being able to repair the primary system are significant. Because of the shield weight increase and because of the reduction in the maintenance access this arrangement does not appear to be of further interest.

In the intermediate-loop configuration (Fig. VI-43) the requirement for additional bremsstrahlung shielding for the lithium system is eliminated by placing an intermediate lithium loop between the reactor system and the potassium power conversion system. In addition, in the event of fission product release the fission products are shielded by the primary shield. Thus a fuel element failure does not impose a radiation hazard on the crew.

Figure VI-44 compares the power availability for a three-loop system with that of a four-loop system. The four-loop system requires the addition of the following nonmaintainable components:

1. shield cooling piping

2. shield cooling pumps

3. shield cooling radiator

4. intermediate loop piping

5. intermediate loop pumps

6. intermediate heat exchanger

7. accumulators

The results indicate that the difference in reliability between these two systems appears to be small and probably is offset by the lower weight of the intermediate-loop system.

The following table summarizes the results of the shielding configuration study. Reliability and maintenance capability considerations are ranked in the order of preference.

Shield Configuration Summary

	Shield Specific Weight lb/kwe	Reliability	Primary System Maintenance Capability
Secondary Shield	30	1	1
Shielded Primary System	37	2	3
Intermediate Loop	15	3	2

A tentative conclusion appears to be that the potential low weight of the intermediate loop offsets the lower reliability and decreased maintenance capability. However, the consequences of adding this additional complexity to the powerplant requires further study both from the standpoint of reliability and the potential development problem involved with this arrangement.

One of the many choices which must be made by mission planners is the radiation dose which the astronauts may receive during the mission. The shield weight can be decreased if the allowable dose is increased. Figure VI-45 shows how the reactor shield weight varies as the yearly dose rate in the mission module is changed. It seems probable that the allowable dose will be between 10 and 100 rem/yr. It is of interest to note that over this range the shield weight changes by only about 6%. Thus the selection of crew dose does not significantly affect the shield weight.

Another way in which the shield weight can be reduced is to increase the dose rate in the area in which the power conversion and power conditioning equipment is located. Figure VI-46 shows how this dose rate influences the shield weight. A critical question to be answered is "How much time is an astronaut required to be in this region?" As the results show, if the maintenance dose is limited to 10 rem, the shield weight changes by only about 10% between 100 and 1000 hr of access. Therefore, reduction of the access time from the design value of 1000 hr does not significantly affect the shield weight within the range of reasonable access times (100 hr or more). A definitive selection of the proper shield design requires a trade-off between maintenance capability (and the associated power availability), the time required for a particular capability, and the resulting shield weight.

Development Program

In order to place decisions regarding the powerplant in proper perspective, it is necessary to make an estimate of the powerplant development cost. A first-order analysis has been made of a development program for a nuclear Ranking-cycle powerplant. It should be recognized that the development program estimates for advanced systems are subject to large uncertainties because of a lack of experience with the particular system being estimated. This is particularly true for systems having development cycles lasting for 10 to 20 yr. With this qualification in mind, the study reported here has been made to give the approximate magnitude of the development program cost and time, some idea of the sensitivity of cost and time to the assumptions used, and some idea of cost trends related to technological goals.

The work reported here has been based on a Rand study reported by Pinkel (Ref. VI-4). The Rand work was based on a three-loop 2000 F reactor outlet temperature Rankine-cycle system similar to the baseline system used in this study. The Rand work consisted of estimating:

a. A reference development program schedule,

b. Ground and flight test requirements and costs,

c. Hardware costs for various types of subsystems,

d. Facility requirements and costs.

In addition, the Rand study evaluated the sensitivity of the program cost to various assumptions and alternatives. The study reported here used the aircraft gas turbine development experience to check various aspects of the Rand work. It should be noted that the resulting estimates substantially agree with comparative cost estimates given in Ref. VI-4.

In estimating an advanced program such as this, it is desirable to examine the information available from similar programs. Some advanced programs of a nature similar to the Rankine cycle are shown below together with an estimate of the cumulative spending to date and the development phase accomplished.

System	Development Cost - 10^6 to End of FY 1966	Development Status
SNAP-8	90	Tech. Demonstration
SNAP-10A	80	Tech. Demonstration
ANP	1000	Tech. Demonstration
Nuclear Rocket	870	Tech. Demonstration
Aircraft Gas Turbine	?	Operational

While this is not an all-inclusive list of advanced system development programs, it does include some of the more prominent systems. It is of interest to note that only the aircraft gas turbine has reached the operational stage. The other systems are in some stage of the technology demonstration phase of the development cycle. Because the aircraft gas turbine experience represents a complete development cycle and because of the relative accessibility of this information, the gas turbine experience has been used as a guide in preparing this estimate of the Rankine-cycle development program.

P&WA Aircraft Gas Turbine Development

The gas turbine experience has been based on a technology background which has been developed over the last 20 yr. During this time the development effort has taken two separate but related forms.

One is the effort spent directly on specific engine system projects. The other is the effort spent on general component technology acquisition and improvement. Both of these activities contribute to the attainment of the current performance and duration levels. The attainment of these levels has been a gradual process of increasing performance (as reflected by turbine inlet temperature) and reliability (as reflected by component failure rate). The achievement of these levels did not occur through development of a single system designed to meet the current requirements but was an evolutionary process which grew from an accumulation of technological experience. It should also be noted that the experience gained in over 70 million engine hours of flight operation also contributes substantially to the achievement of the present performance and endurance levels.

The general characteristics of gas turbine development time and cost experience are shown on Fig. VI-47. This figure shows the cumulative relative cost and the time required for developing three typical gas turbine engines. Superimposed on this information are lines showing failure rate milestones during the development program.

The cost curve for engine A indicates a gradual buildup in funds in the failure rate level of about 10 λ. This first phase is primarily intended to demonstrate engine performance. At about the 10-λ level the flight test program for the engine is started. The initial phase of the flight test program is usually performed on a test bed aircraft with the engine being developed not used for primary propulsion power. The ground test program continues in parallel and in combination with the flight test. The primary purpose of this development activity is to demonstrate the endurance, as well as the performance, of the engine in the operational environment. This phase of development culminates in the production qualification test which demonstrates that the engine has achieved both the required performance and reliability. It is of interest to note that the development program cost increased by a factor of 3 in decreasing the failure rate by a factor of 10. This development phase required about 4 years.

The trends for engine B (with the same turbine inlet temperature as engine A) are similar to engine A. However, due to the existence of a broader technological base and due to the greater experience in existence at this time, the cost increase in achieving λ level failure rates was less than a factor of 3 and required only about 3 years to achieve.

Engine C, despite a 100 F increase in inlet temperature, also required less than a factor of 3 increase in cost and less than 3 years to achieve lower failure rates. This again illustrates the benefits due to a broader technological base and to the existence of more experience.

This curve does not reflect two additional factors:

1. The money spent prior to these programs to develop the basic technology required to demonstrate jet engine feasibility and to develop earlier engines,

2. The money spent during these programs not specifically on engine development but on component technology improvement. This amounts to a factor of 8 greater than the cost to develop engine A to a failure rate level of 10 λ during the 12 years shown on this figure.

It is also of interest to examine a comparison of the characteristics of the nuclear Rankine-cycle system (RC) and the aircraft gas turbine (AGT). The significant items are:

	AGT	RC
1. Mission Duration	10 hours	10,000 to 15,000 hours
2. Duty Cycle	Extreme power & speed variation every 4-6 hr	Relatively uniform
3. Working Fluid	Air	Alkali liquid metals
4. Materials	Superalloys	Refractories
5. Energy Source	Chemical	Nuclear
6. Number of Missions	Large	Small

From the development program standpoint the most significant differences between the gas turbine and the Rankine cycle are the differences in mission duration and mission frequency. For the gas turbine application it is reasonable to test, prior to flight, many engines for durations many times the mission duration. Thus it is feasible to demonstrate that the probability is high that an engine will successfully complete the mission. In addition, the millions of hours of inflight operation contribute substantially to the development of the engines. The reverse situation applies to nuclear space powerplants (thermionics and Brayton cycle systems as well as the Rankine cycle). Because of the long mission durations it is not feasible to test powerplants for times greatly exceeding the mission duration. In addition, the inflight experience available for development purposes is limited. For these reasons large sample statistical demonstration that a desired reliability goal has been reached will not be available for any nuclear space powerplant.

Nuclear Rankine-Cycle Powerplant Development

A number of factors peculiar to nuclear space powerplants have been taken into account in estimating the development program requirements. Again it must be noted that these factors apply to the development of any type of high-performance, high-temperature nuclear space powerplant. The significant factors are:

1. Insufficient technology now exists to directly develop the components of the system. In addition, insufficient experience exists to now judge that the system is feasible. Therefore, the first stage of the development requires the establishment and the demonstration of the required technological base prior to initiation of full-scale development. Compared to full-scale development this initial phase of the program is characterized by a relatively low funding rate. The program is designed so that the investment required to demonstrate system feasibility is relatively low. Numerous milestones will

be built into this phase of the program to measure development progress and to continually evaluate the probability of achieving the program goals. The development risk is minimized until it has been demonstrated that a reasonable assurance exists that the program will be successful.

2. As mentioned above, the attainment of desired component or system reliability cannot reasonably be demonstrated. Assurance that the system is reliable enough to perform the mission will depend on the manner in which the development program is organized and operated. The following are characteristics of a development program designed to attain the desired system characteristics:

a. The program will be performed by an experienced team with a record of success in developing high-performance, high-temperature, high-reliability powerplants,

b. Sufficient program funding,

c. Clear and constant program goals,

d. Extensive testing of components and systems to eliminate sources of failure,

e. Extensive quality assurance program for design, materials, and manufacturing,

f. Selective assembly of systems,

g. Successful completion of specified system qualification tests.

3. It has been assumed that the initial acquisition and demonstration of basic technology will begin with an 1800-F reactor outlet temperature and a 1 a/o uranium burnup system. The process of technology acquisition and demonstration will proceed in increments of 200 F or 2 a/o burnup until the technology required for the operational systems has been demonstrated. At this point full-scale development will be initiated for the flight systems.

The reasoning outlined above led to the consideration of a three-phase development cycle:

a. Technology Demonstration

This phase will consist of accumulating and demonstrating that the necessary technology is available to achieve the required performance. In addition, a 2000-hr test will be made to demonstrate system feasibility and to pinpoint initial sources of wear-out failures.

b. System Development

This phase of the program will consist of extending the endurance of the multiple component system to that required for the flight.

c. Flight Test

This phase of the program will consist of demonstrating system operation, performance, and endurance in the space environment.

It is of interest to note the distinction between reliability (as measured by failure rate) and endurance. Figure VI-49 shows the variation of failure rate with time for a typical component. This illustrates that three different reliability periods exist.

These are:

1. Infant mortality - the failure rate decreases during this period as parts which are likely to fail are discovered by acceptance tests and/or green runs.

2. Service life - the failure rate is essentially constant during this period and the failures which do occur are of a random nature.

3. Wear-out - the failure rate increases during this period because of failures which occur because parts have begun to wear out.

Two factors illustrated on this curve have significant development program implications. These are:

1. The failure rate during the service life period is influenced by the quality of the development program. The random failures which may occur during this period may be reduced by stringent quality control, careful design of the components to account for variations in the design conditions (by careful specification of both the design requirements and acceptable design margins) and of anticipated operating conditions. By following these procedures a reasonable assurance exists that levels of failure rate previously attained in similar development programs can be attained for this system. However, it is difficult to predict that failure rates which are an order of magnitude less than previously obtained can in fact be achieved. In addition, as mentioned previously, it is not feasible to demonstrate the achievement of these failure rates nor can it be expected that significant improvement can be obtained from field experience with nuclear space powerplants.

2. The required system endurance can be achieved and demonstrated during the development program (assuming that system feasibility has been

demonstrated). The achievement and demonstration of the required endurance to a large extent sets the time and money requirements for the development program.

To summarize, the achievement of desired failure rate goals cannot rationally be planned directly but is an intangible result of a certain type of a development program. Conversely, the achievement of endurance goals can usually be accomplished by spending the required time and money.

1800 F, 1 a/o Burnup System

The over-all schedule for this system is shown in Fig. VI-49 to include the following:

a. A five-year Technology Demonstration program for this system (will consist of 3 years of subsystem and component development followed by a 2-year, 2000-hr demonstration test)

b. A six-year System Development program

c. A four-year Flight Test program

If all of these programs are conducted in series the total time required will be 15 years. One alternative would be to perform a portion of the programs in parallel as shown on Fig. VI-49. This would reduce the development time to about 13 years. The feasibility and degree of performing these programs in parallel depends on the degree of success achieved in the various stages of development.

It has been estimated that the Technology Demonstration phase of the development of this system will cost $60M/yr for 5 years. In addition, the facilities required for this program are estimated to cost $70M for a CANEL-type facility and an additional $70M for a nuclear system test facility.

Thus the total requirements for the Technology Demonstration phase are estimated to be 13 to 15 years and about $440M.

It is anticipated that the following areas of investigation will be emphasized during this phase:

1. Primary System

Reactor - fuel element design, control systems, fuel alloy development
Shield - thermal design, weight
Boiler - stability, low "g" heat transfer
Pumps - seals, bearings
Valves - materials, seals
Accumulator

2. Secondary Systems

Turboalternator	- materials bearings seals erosion electrical insulation bore seal
Condenser	- stability low "g" heat transfer
Pumps	- seals bearings
Valves	- materials, seals

3. Heat rejection systems - beryllium fabrication and bonding techniques

4. Maintenance - tool techniques, liquid-metal storage system development

The System Development phase includes the program required to demonstrate the performance and endurance level of the baseline system. The requirements for this phase of the program are estimated at 6 years and $4260M. This estimate was based on methods suggested by Pinkel (Ref. VI-4) with check-points based on aircraft gas turbine experience.

A breakdown of this cost estimate follows:

1.	Development Engineering	$ 180M
2.	Program Management (all 3 phases)	240
3.	Hardware	3080
4.	Instrumentation, Tooling, Test Equipment	230
5.	Facilities	215
6.	Ground Test Operations	315

The tests included are listed below and a test schedule is shown on Fig. VI-50.

Item	Yr of Testing on all Rigs	No. of Equivalent Test Units
1. Primary System		20
Reactor	11.25	
Pump	13.50	
Boiler	13.50	

Item	Yr of Testing on all Rigs	No. of Equivalent Test Units
2. Power Conversion		23
Turboalternator	13.5	
Secondary Pump	13.5	
Condenser	13.5	
Radiator Pump	13.5	
Radiator	13.5	
Secondary Loop Test	7.5	
Radiator Loop Test	7.5	
3. Power Conditioning	13.5	20
4. Complete Power Source	10.5	10
Total No. of Hours of Testing	1.3×10^6	

The facilities required are listed below (Ref. VI-4).

Item	No. Required
Test Cell (fuel element hot flow tests)	1
Critical Facility	1
Shielded Vacuum Chamber (reactor tests)	2
Hot-Laboratory Complex	1
Fabricating Plant	1
Vacuum Chamber (pump tests)	3
Hydro Test Cell (pump tests)	2
Vacuum Chamber (boiler tests)	3
Turbo-alternator Test Cell	3
Secondary Pump Test Cell	3
Condenser Test Cell	3
Vacuum Chamber (radiator tests)	3
Secondary Loop Test Cell	2
Heat Rejection Loop Test Cell	2
Nonnuclear System Test Cell	1
Mechanical Testing Laboratory	1
Shielded Vacuum Chamber (system test)	3
Power Conditioning Test Cell	3
Thruster Test Cell	3
Miscellaneous, including administrative buildings and research and fabrication laboratories	

The Flight Test phase of the program is intended to demonstrate that the system can achieve the required performance and endurance in space. The Flight Test program has been set up on the basis that it is cheaper

to accomplish almost any test objective on the ground. Therefore, the number of flight tests have been minimized. It is assumed that the flight tests will be performed on orbiting space stations.

The test schedule has been set up to include:

1. Three single-system tests to demonstrate operational characteristics, startup and shutdown, endurance, maintenance capability

2. Three 10,000-hr dual-powerplant endurance tests

The requirements for the Flight Test phase have been estimated at 4 years and $2070M.

A cost breakdown of the Flight Test program is shown below:

1.	Flight Test Hardware	$ 690M
2.	Launch Facilities and Operations	1120
3.	Electric Propulsion Operations	40
4.	Logistic Support & Space Station Operations	200
5.	Miscellaneous	20

The total development program requirements for the 1800-F, 1-a/o burnup system therefore are estimated to be about 13 to 15 years and $6780M. A cost breakdown by phase is shown below:

1.	Technology Demonstration	$ 440M
2.	System Development	4260
3.	Flight Test	2070

A curve of the rate of expenditure for this program is shown on Fig. VI-51. This shows the low level of funding during the Technology Demonstration phase and illustrates the relatively small commitment to the concept prior to demonstration of the feasibility of the system.

An obvious question which arises is: can reductions be made in the development time and money requirements? A number of possibilities are apparent; however, further evaluation is required before it can be concluded that significant reductions are possible. Some of these possibilities will be discussed below.

1. In order to place the development cost in proper perspective an estimate should be made of the number of missions to which the Rankine-cycle technology will be applicable. While the work reported here was concentrated exclusively on the manned Mars mission, the Rankine-cycle technology is obviously applicable to other programs. Thus the question of how the development costs should be apportioned or, alternatively, the

total range of benefits received from the development should be considered. As a simplified example Fig. VI-52 shows how the cost per trip varies with the number of manned Mars missions which are flown. This information illustrates that if enough missions can be flown the development program costs become relatively insignificant. Thus, an extensive space program which has a large number of Rankine cycle applications in addition to the manned Mars mission would make a large powerplant development program appear to be reasonable.

2. One possibility for reducing development costs is to perform most of the Technology Demonstration phase on lower-power level components. It is anticipated that this will reduce the cost of this phase of the program without a significant loss in assurance that the results are applicable to the larger systems. Since reactor size does have a significant influence on reactor control this aspect of system development must be considered at the power level of interest.

One aspect of the size effect is shown on Fig. VI-53. This information is taken from Ref. VI-4. It should be noted that the range of results obtained in this study bracket the extrapolated results from Ref. VI-4.

3. Some consideration might be given to a greater degree of paralleling of the various phases of the program. The degree to which this can be done is very uncertain. One consideration will be the degree of success actually achieved during the program. Adjustments due to this factor will not be apparent until the programs are underway. However, it must be recognized that, in general, estimates of development time and cost are usually optimistic and experience usually increases both time and cost. The base-line system development presented here has attempted to recognize this factor and to present a realistic situation. However, a more optimistic schedule has been estimated as 13 years. The "series" and "parallel" schedules are compared on Fig. VI-49. These two schedules may be viewed as presenting the uncertainty involved in estimating the development time requirements. There is no apparent reduction in development cost resulting from this paralleling process.

The selection of performance goals for any advanced system is an exercise of judgement which must take into account many factors. It is desirable to quantify as many of these factors as possible even though there is a large degree of uncertainty in this process. For this reason estimates of development program requirements which have been considered are:

a. Powerplant Maintenance
b. Component Failure Rate
c. System Temperature
d. Reactor Fuel Burnup
e. Radiator Materials

The final selection of the costs for various alternatives requires consideration of the cost trade-offs between development costs and mission costs. Some of the factors which influence the total cost are:

a. Cost of obtaining various levels of powerplant technology,

b. Cost of performing the mission with powerplants of different levels of performance; i.e., MEO, launch vehicle cost, and number of missions.

Some of these factors have been considered and will be discussed below.

1800-F Reactor Outlet, 3-a/o Burnup System

The initial step to extending system technology to 1800 F and 3 a/o consists of extending the Technology Demonstration phase past the point of demonstration of the 1800 F, 1-a/o burnup system. This additional step, as illustrated on Fig. VI-54, consists of an additional four-year program. Two years of this program are devoted to component development and two years to system demonstration. This results in a total development program length of 16 to 18 years (allowing for one year of paralleling in the Technology Demonstration phase).

The cost of the Technology Demonstration phase has been estimated using two rather extreme assumptions. These are:

a. $60M/yr for the entire duration of the Technology Demonstration

b. The annual cost doubles for the additional Technology Demonstration required for the 1800-F, 3-a/o burnup program. That is, the annual cost is $60M/yr for the 1800-F, 1-a/o program and $120M/yr for the 1800-F, 3-a/o program.

The resulting Technology Demonstration phase cost varies between $620M and $920M.

The System Development and Flight Test programs have been estimated to cost $4000M and $2060M, respectively.

Therefore, the total cost of the development program for the 1800-F and 3-a/o system is between $6680M and $6980M. The rate of expenditure for this program is shown on Fig. VI-55.

Consideration of these results reveals a number of interesting aspects of the development program. These are:

a. The assumption of expenditure rate for Technology Demonstration does not significantly affect the total cost of the development program for the technology increment shown here (2 a/o).

b. Decision points exist during the Technology Demonstration for redirecting the program. At the end of the fourth year (when the investment is about 10% of the total required for completion) three alternatives can be evaluated on the basis of the evidence accumulated at that point. These are:

   1. Cancel program because system is judged to be not feasible

   2. Begin the Technology Demonstration for 1800 F and 3 a/o burnup because results indicate that the changes of developing this system are good

   3. Reorient the program to develop the 1800-F, 1-a/o burnup system because the experience with this system has been good but the chances for developing the 1800-F, 3-a/o burnup system appear to be poor.

c. The total system development cost of between $6680M and $6980M is not significantly different than that of $6780M required for the 1800-F, 1-a/o burnup system. This is the result of two counteracting trends:

   1. As the burnup increases the cost of the Technology Demonstration phase increases.

   2. As the burnup increases the cost of the System Development and Flight test phases tends to decrease. This decrease is due to the reduction in system hardware weight with increasing burnup and the resulting decrease in hardware and launch costs.

Further Technological Advances

Development programs corresponding to further advances in technology have been evaluated. These programs have been assessed on the same basis as the previous example. That is, Technology Demonstration proceeds in 4-yr program increments. These increments consist of either 200-F increases in reactor outlet temperature or 2-a/o increases in uranium burnup. Again, two different assumptions have been made regarding the cost of Technology Demonstration:

a. $60M per year

b. Annual cost doubles for each new technology increment

That is:

1800 F, 1 a/o	$60M/yr
1800 F, 3 a/o	$120M/yr
2000 F, 3 a/o	$240M/yr
2200 F, 3 a/o	$480M/yr

Programs have been investigated for increasing both temperature and burnup and the results are presented in the accompanying table. A typical Technology Demonstration program schedule is shown on Fig. VI-56.

The results of both the temperature and the burnup influence on system development costs are plotted on Figs. VI-57 and VI-58 (normalized to a 2200-F, 3-a/o burnup system). These results indicate:

a. The total cost of the development program becomes extremely sensitive to the assumption of the cost for technology demonstration as the technology becomes more advanced.

b. Regardless of the cost assumption there is an incentive toward developing relatively low-level technology (1800 F to 2000 F and 1 to 3 a/o burnup).

These conclusions are further demonstrated by the information shown on Figs. VI-59 and VI-60 for the optimistic assumption of Technology Demonstration cost (assumption a).

These figures show:

a. The development cost as a function of temperature or burnup amortized over 1 mission and 10 missions.

b. The vehicle cost/mission as a function of temperature or burnup. The change in vehicle cost is a reflection of the change in MEO over the range of temperature and burnup examined (Saturn V cost has been assumed as $70M/vehicle).

These results illustrate that the total cost of the mission is not strongly affected by the powerplant technology. Thus, from the standpoint of development risk, there appears to be no strong incentive for developing the higher-level technology systems.

Reliability Improvements

As indicated previously, there is no clear way in which to perform a development program to achieve an improvement in component reliability. In addition, there is no feasible method for demonstrating the level of

PROGRAMS FOR INCREASING TEMPERATURE AND BURNUP

Temperature Variation (at 3 a/o burnup)

Assumption A	1800 F	2200 F	2400 F
Technology Demonstration	8 yrs - $620M	14 yrs - $98M	17 yrs - 1160M
System Development	6 - 4000	6 - 3460	6 - 334.
Flight Test	4 - 2060	4 1580	4 - 1490
Total	18 yrs - 6680M	24 yrs - 6020M	27 yrs - 5990M
Assumption B			
Technology Demonstration	920M	3170M	6290M
System Development	4000	3460	3340
Flight Test	2060	1580	1490
Total	18 yrs - 6980M	24 yrs - 8210M	27 yrs - 11120M

Burnup Variation (at 2200 F Reactor Outlet)

Assumption A	1 a/o	3 a/o	5 a/o
Technology Demonstration	11 yrs - 800M	14 yrs - 980M	17 yrs - 1160M
System Development	6 - 3840	6 - 3460	6 - 3330
Flight Test	4 - 1940	4 - 1580	4 - 1400
Total	21 yrs - 6580M	24 yrs - 6020M	27 yrs - 5890M
Assumption B			
Technology Demonstration	1610M	3170M	6290M
System Development	4000	3460	3340
Flight Test	2060	1580	1490
Total	21 yrs - 7670M	24 yrs - 8210M	27 yrs - 11120M

failure rate to which long mission time components have been developed. However, the reliability analysis indicates that one way in which to achieve reasonable power availability is to develop components to achieve an order of magnitude improvement in gas turbine reliability. Thus it is of interest to see if this is a reasonable goal.

A development program designed to achieve improved component reliability will require increased quality assurance provisions, special handling provisions, and testing. There is no existing data which directly correlates the resulting increase in development cost with the resulting reliability improvements. However, gas turbine experience suggests that the cost of an engine development program increases by a factor of three to obtain a factor of ten reduction in failure rate. In addition to the money spent directly on each program, general technology improvement funds also contribute to the reduction in failure rate. This amounts to about another factor of two increase in development program cost. Therefore, it has been assumed that improving the reliability of the Rankine cycle will increase the System Development and Flight Test cost by a factor of 3 to 6 to reduce the failure rate by a factor of ten. This will result in program costs of

a.	Technology Demonstration	$ 980M to $ 3,170M
b.	System Development	$10,400M to $20,800M
c.	Flight Test	$ 4,750M to $ 9,500M
	Total Cost	$16,000M to $33,000M

Thus, it is fairly clear that this estimate predicts a drastic increase in development cost to achieve $\lambda/10$ failure rate level. While this is a very crude estimate the implication is clear that, based on the assumptions that have been used, an inflight maintenance capability is undoubtedly a more attractive alternative for improving power availability.

Development of Maintenance Capability

The cost required to develop an extensive maintenance capability has been estimated to be $690M. This cost is distributed as follows:

a.	Technology Demonstration	$50M
b.	System Development	$250M
c.	Flight Test	$390M

These costs include the following factors:

a. Design and development of special tools, machinery, and procedures

b. System hardware for spares

c. Spacecraft logistics for maintenance development personnel

d. Launch costs for equipment, spares, and personnel

It has already been noted that a nonmaintained "λ" level system provides a high probability of reasonable power level for only a short period of time (less than the mission time of interest). Thus it becomes apparent that developing a maintenance capability makes the use of "λ" level system feasible with a large saving in development costs. This situation is summarized below for a 530-day mission:

	λ Level	λ/10 Level
	30 lb/kwe system 6 lb/kwe spares	30 lb/kwe systems 2 lb/kwe spares
Development Cost (average)	$7690M	$16,000M to 33,000M
Launch Vehicle Cost	398M	364M
Total Cost	$8000M	$16,000M to 33,000M

Thus the trend is clear that a maintained, aircraft gas turbine failure rate-level system represents a reasonable Rankine-cycle system development goal.

Alternative Radiator Materials

An evaluation has been made of the effect of the choice of radiator materials on the system development cost. The choice evaluated is between a radiator with beryllium barrier and fins and a radiator with copper fins and stainless steel barrier. The cost of the development program was estimated to be $6030M for the beryllium radiator and $5900M for the copper-stainless steel radiator. This estimate, while confirming an intuitive judgement that the copper-stainless steel development is cheaper, does not show a significant difference between these two choices.

REFERENCES

VI-1. Ragsac, R. V., et al: Study of Low-Acceleration Space Transportation Systems, Report D-910262-3. United Aircraft Research Laboratories, July 1965.

VI-2. Clausi, J. V., and J. W. Schmitt: Parametric Study of Large Rankine Cycle Nuclear Space Powerplants, Report PWA-2539 or NASA CR-54334, Pratt & Whitney Aircraft Division, February 1965.

VI-3. Schmitt, J. W.: Preliminary Design of 4 mwe Rankine Cycle Nuclear Space Powerplant, PWA-2673, Pratt & Whitney Aircraft Division, September 1965.

VI-4. Pinkel, B.: Electrical Propulsion In Space: Mission Comparisons, Development Cost, Reliability, and Their Implications for Planning, Memorandum RM-9056-NASA, August 1964.

VI-5. Pinkel, B.: The Impact of the High Development Cost of Advanced Flight Propulsion Systems on Development Policy, Memorandum RM-4560-PR, October 1965.

VI-6. Buatti, A. U. and J. W. Schmitt, Design Study of a High Power In-Pile Nuclear Thermionic Space Powerplant, Report PWA-2351 or NASA CR-54172, Pratt & Whiteny Aircraft Division, July 1964.

TABLE VI-1

DETAILED POWERPLANT WEIGHT BREAKDOWN

Item	No.	Weight, lbs	
Primary Coolant System			
reactor core, vessel, reflector	1	5,280	
primary coolant pump	2	380	
boiler	4	840	
piping and meteoroid barrier	-	3,020	
Subtotal			9,520
Radiation Shielding			
primary shield		48,700	
bremsstrahlung shield		13,000	
Subtotal			61,700
Power-Conversion System			
turboalternator	4	11,200	
condenser	12	1,210	
jet pump	4	190	
condensate pump	4	590	
piping	-	2,480	
Subtotal			15,670
Heat Rejection Systems			
main			
radiator panels	12	11,700	
piping	-	2,050	
pumps	12	1,070	
auxiliary			
radiator panels	4	4,380	
piping	-	1,210	
pumps	4	1,920	

TABLE VI-1 (Cont'd.)

Item	No.	Weight, lbs	
low temperature			
radiator panels	4	1,040	
piping	-	60	
pumps	4	140	
Subtotal			23,570
Electrical System			
alternator (included in turboalternator)			
transformer	4	2,140	
rectifier	4	600	
busbar	4	220	
Subtotal			2,960
Inflight Structure			6,000
Total Weight			119,420 lbs
Specific Weight			29.9 lb/kwe

TABLE VI-2

TYPICAL FAILURE RATES

Component	No. of Failures in 10^6 Hours	Reliability For 10^4 Hours
Gas Turbine	8.00	0.9231
Plumbing	1.30	0.9871
Fuel Oil Cooler	0.78	0.9922
Solenoid Valve	0.72	0.9928
Oil Pump	0.16	0.9984

TABLE VI-3

POWER SYSTEM FAILURE RATE SUMMARY

Subsystem	No. of Failures in 10^6 Hours λ	Reliability For 10^4 Hours λ	$\lambda/10$
R_1 - Reactor System	29.14	0.747	0.971
R_2 - Primary Pumps	16.32	0.849	0.985
R_3 - Power Conversion System	30.07	0.740	0.970
R_4 - Heat Rejection System	13.78	0.871	0.986
Total	89.31	0.409	0.915

TABLE VI-4

REACTOR AND PRIMARY SYSTEM

FAILURE RATES (R1)

Component	No. of Failures in 10^6 Hours
Reactor	5.04
Reactor Controls and Instrumentation	23.40
Accumulator and Piping	0.42
Meteoroid Barrier	0.28
Total	29.14

TABLE VI-5

PRIMARY PUMPS (R2)

Component	No. of Failures in 10^6 Hours
Pump	10.00
Pump Cooler	0.42
Motor Controls	3.80
Piping	2.10
Total	16.32

TABLE VI-6

POWER CONVERSION SYSTEM (R3)

Component	No. of Failures in 10^6 Hours
Boiler	2.10
Turbogenerator	10.00
Pumps	8.24
Electrical Equipment and Controls	1.95
Plumbing and Valves	3.05
Condenser	0.38
Auxiliary Heat Rejection Systems	4.10
Meteoroid Barrier	0.25
Total	30.07

TABLE VI-7

HEAT REJECTION SYSTEM (R4)

Component	No. of Failures in 10^6 Hours
Condenser	3.80
Pumps and Controls	4.41
Plumbing	0.21
Meteoroid Barrier	5.36
Total	13.78

TABLE VI-8

PROBABILITY OF GENERATING 100% POWER

	Maintenance Mode	At Reference Failure Rate	At 1/10 Reference Failure Rate	Weight* Penalty Lbs.
1.	No Maintenance	0.031	0.706	0
2.	Repair all electrical system & PCS control failures (Items 10, 11, 14, 27 of Table VI-9)	0.034	0.714	-
3.	Repair all electrical and control failures (Items 2, 5, 10, 11, 14, 27)	0.05	0.74	90,000
4.	Repair 43 failures of all except primary system components (Items 7 through 29)	0.49	0.93	8,400
5.	Repair all failures except primary system (Items 7 through 29)	0.50	0.93	-
6.	Repair 52 failues of all components except reactor (Items 2 through 29)	0.94	0.99	100,000
7.	Repair 53 failures of all components (Items 1 through 29)	0.99	0.999	100,000**

* Includes weight of spares plus shielding but not tools, equipment and facilities

** Detailed weight estimate not prepared

TABLE VI-9

BREAKDOWN OF A POSSIBLE REPAIR PROGRAM

Item No.	Primary System	Numbers of Repairs or Replacements	Max. Time[1] Allowable for Maintenance, hr	Powerplant[2] Power Level, %	Component[3] Reliability	Dose Rate of Equipment Location, rem/hr	Replacement Component Weight, lbs
1	reactor	0	0		0.948	-	-
2	drum controls and instrumentation	2	28	50	0.9982	0.756	200
3	accumulator	1	50	100	0.9999	0.5	100
4	primary coolant pump	2	75	50	0.999	0.5	240
5	cooler, controls and plumbing	2	75	50	0.9997	0.5	100
	Power-Conversion System						
6	boiler	2	60	75	0.9999	0.5	475
7	turboalternator	4	4000		0.9999	0.0036	5960 (1490x4)
8	condenser	2	4000		0.9999	0.0036	200
9	condensate pump	2	4000		0.9995	0.0036	100
10	transformer	2	4000		0.9999	0.0036	1060
11	rectifier	1	4000		0.9999	0.0036	150
12	accumulator	1	4000		0.9999	0.0036	50
13	plumbing	1	-	*120 kwe	0.9999	0.288-0.0036	-
14	motor controls	1	4000	75	0.9994	0.0036	-
15	control valve	2	4000		0.9999	0.0036	-
16	stop valve	1	4000		0.9999	0.0036	-
17	jet pump	1	4000		0.9994	0.0036	-
	Auxiliary Heat Rejection System						
18	pump	2	4000	75	0.9995	0.0036	50
19	pump motor	2	4000		0.9999	0.0036	100
20	accumulator	1	4000		0.9996	0.0636	50
21	plumbing	1	-	*120 kwe	0.9998	0.0045-0.0036	-
22	radiator	1	4000	75	0.9999	0.0045-0.004	-
23	Low Temperature Heat Rejection System	1	4000	100	0.9999		-
	Main Heat Rejection System						
24	condenser	4	4000	75	0.9999	0.0036	400
25	pump	4	4000	91.6	0.9999	0.0036	200
26	motor	2	4000	91.6	0.9999	0.0036	100
27	controls	2	4000	91.6	0.9999	0.0036	-
28	plumbing	1	-	*120 kwe	0.9997	0.288-.0045	-
29	radiator	4	67-4140	91.6	0.9995	0.288-.0045	-
	TOTAL	52			0.94		9535

[1]Estimated time allowed for one man to receive a mission dose of 20 rem if he remains at the location of the equipment for this time and stays in the mission module during the rest of the mission.

[2]Powerplant power level corresponding to time allowed.

[3]Probability that no more than the predicted number of failures will occur.

*Power reduced to very low level to allow radiator temperature to decrease to 100 F. Additional auxiliary power required for pumping power. More than 1000 hours of exposure are allowed for plumbing repairs at this power level.

TABLE VI-10

MAINTAINED POWERPLANT COMPONENTS

Component	Failure Rate 10^6 Hr.	Number Operating	Number of Spares	
Reactor	0.3040	2	0	0
Reactor Reflector Mechanism	0.4800	2	2	2
Reactor Control	1.0000	2	4	3
Reactor Outlet Temp. Controls	0.2900	2	2	1
Reactor Flux Sensor	0.2100	2	1	1
Integrating Cont. and Program	0.4200	2	2	2
Command Unit and Telemetry	0.4200	2	2	2
Accumulator	0.0420	2	1	0
Primary Coolant Pump	1.0000	4	4	3
Primary Coolant Pump Cooler	0.0420	4	1	0
Boiler	0.2100	8	1	1
Turbine-Generator	1.0000	8	4	3
Auxiliary Cooling Pump	0.3700	8	2	2
Condensate Pump	0.3700	8	2	2
Transformer	0.0740	8	1	0
Rectifier	0.0370	8	1	0
Accumulator	0.0380	8	1	0
Control Valve	0.2100	8	1	1
Stop Valve (9)	0.0190	8	1	0
Condenser	0.0380	8	1	0
Jet Pump	0.0840	8	1	0
Low Temp. Accumulator	0.0400	8	1	0
Low Temp. Pump Motor	0.3700	8	2	2
Condenser	0.3800	32	2	2
Main Radiator Pump-Motor	0.4200	32	2	2
Radiator - Auxiliary	0.1250	8	0	0
Radiator - Low Temp.	0.0250	8	0	0
Radiator - Main	5.3600	32	0	0
TOTAL		240	42	29
Specific Weight - Lb/kwe			2	1.4

4 MW(e) NUCLEAR RANKINE CYCLE SPACE POWERPLANT
SYSTEM SCHEMATIC

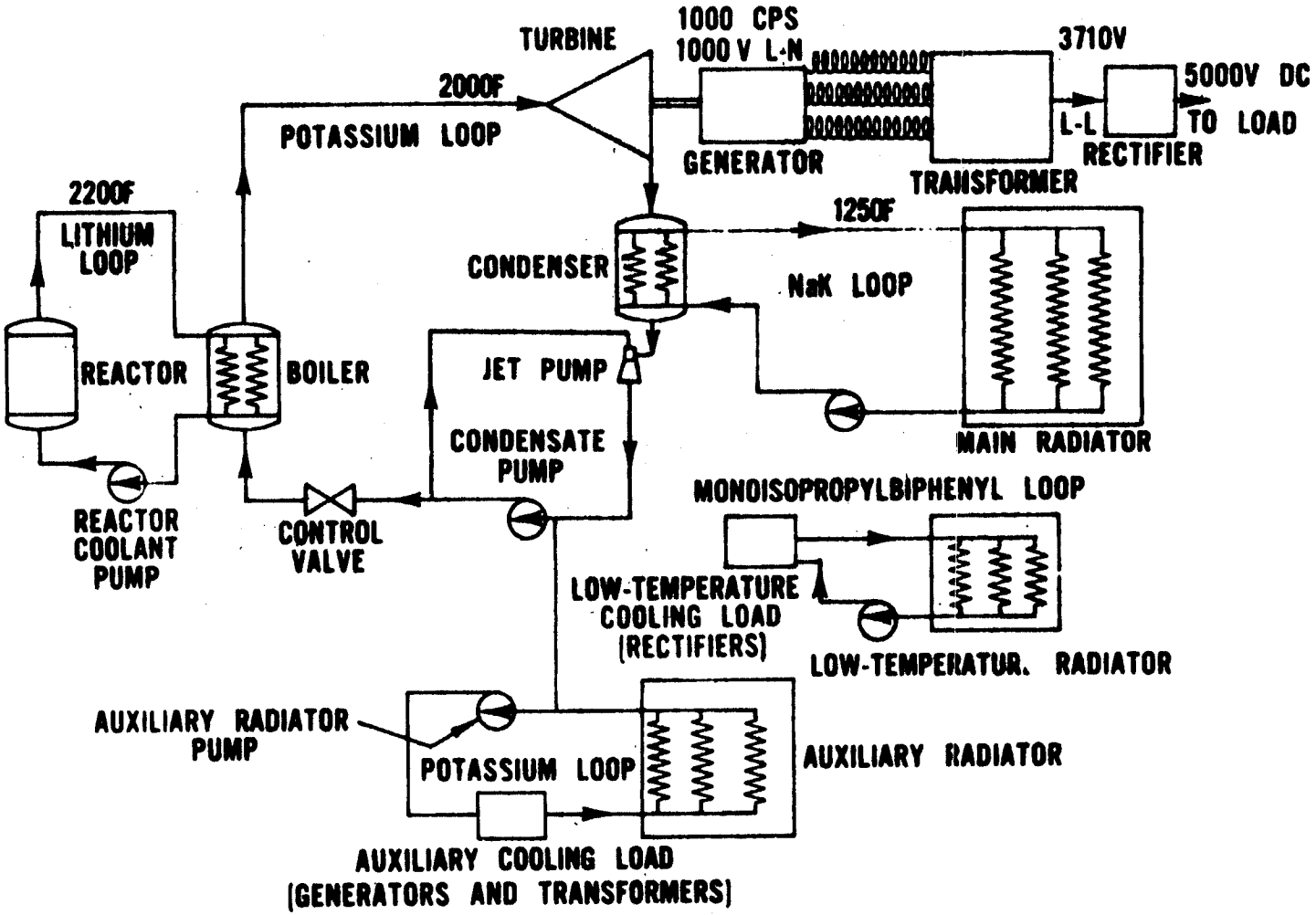

Pratt & Whitney Aircraft
DIVISION OF UNITED AIRCRAFT CORPORATION

M-34046
650809

E-910262-6

Figure No. VI-1

4-MW NUCLEAR POWER SYSTEM
Pratt & Whitney Aircraft — UA

4 MW(e) RANKINE CYCLE NUCLEAR SPACE POWERPLANT

POWERPLANT RELIABILITY SCHEMATIC

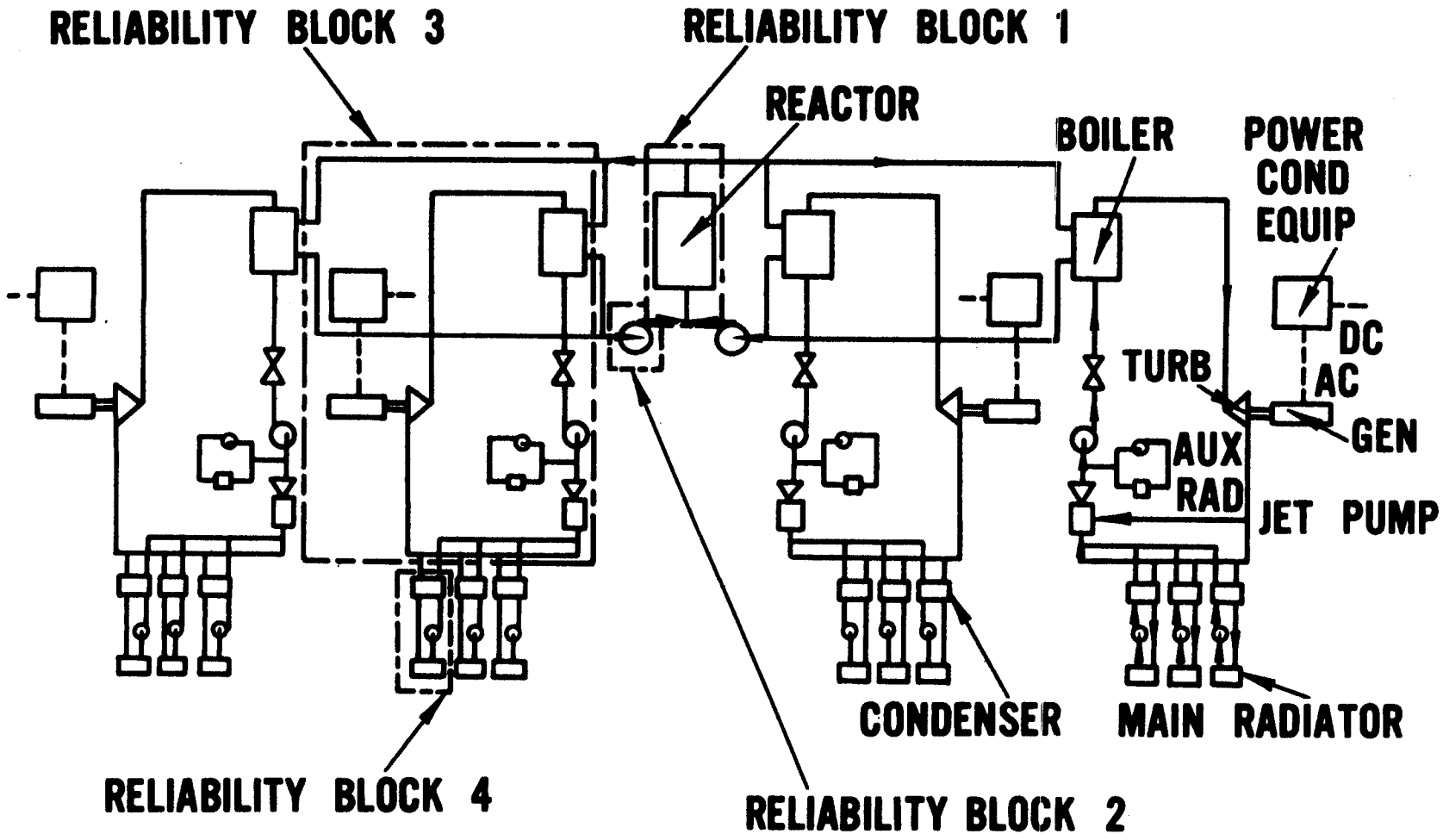

Pratt & Whitney Aircraft

DIVISION OF UNITED AIRCRAFT CORPORATION

M-35430
651111

E-910262-6

Figure No. VI-3

LOW ACCELERATION SPACE TRANSPORTATION

RELIABILITY BLOCK DIAGRAM

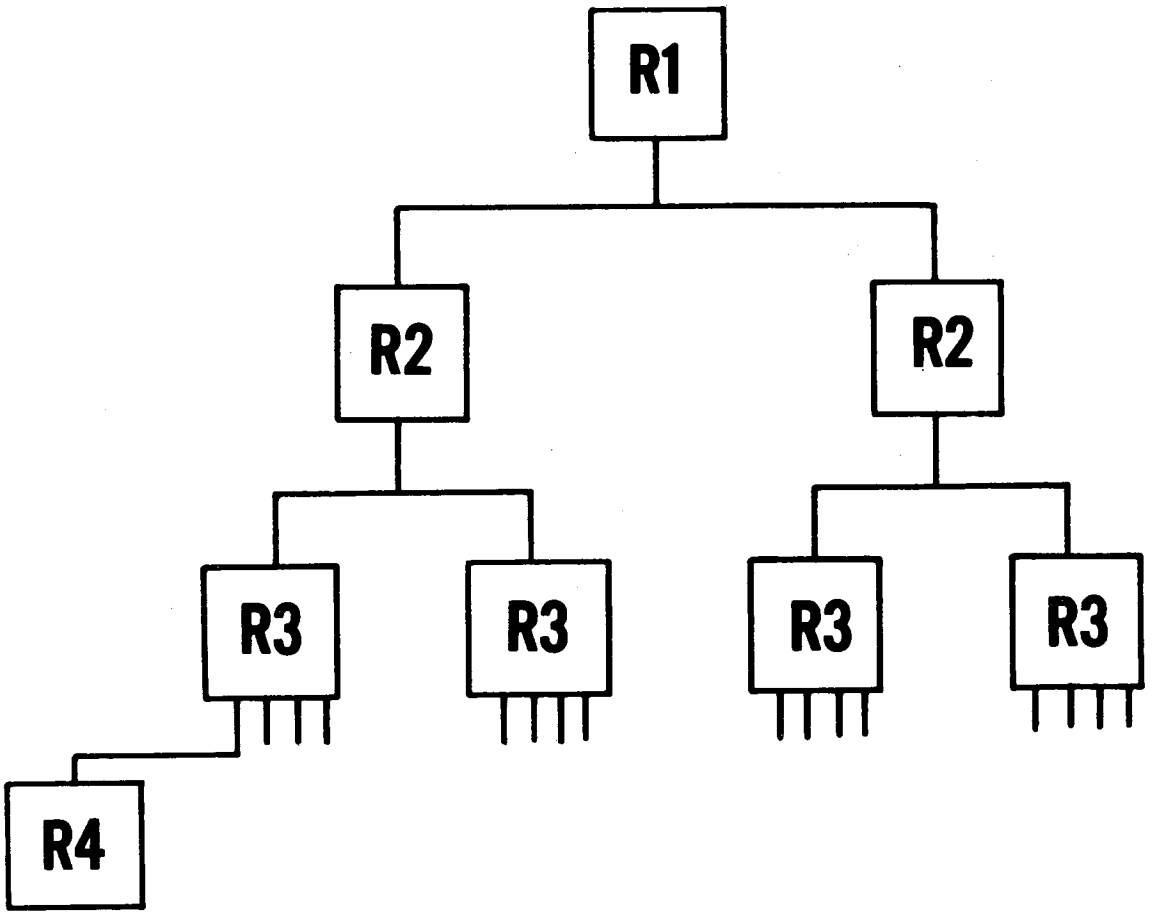

Pratt & Whitney Aircraft

DIVISION OF UNITED AIRCRAFT CORPORATION

M-38908
662006

E-910262-6

Figure No. VI-4

LOW ACCELERATION SPACE TRANSPORTATION

PROBABLE POWER vs MISSION TIME

IMPROVED TECHNOLOGY TWO REACTOR SYSTEMS

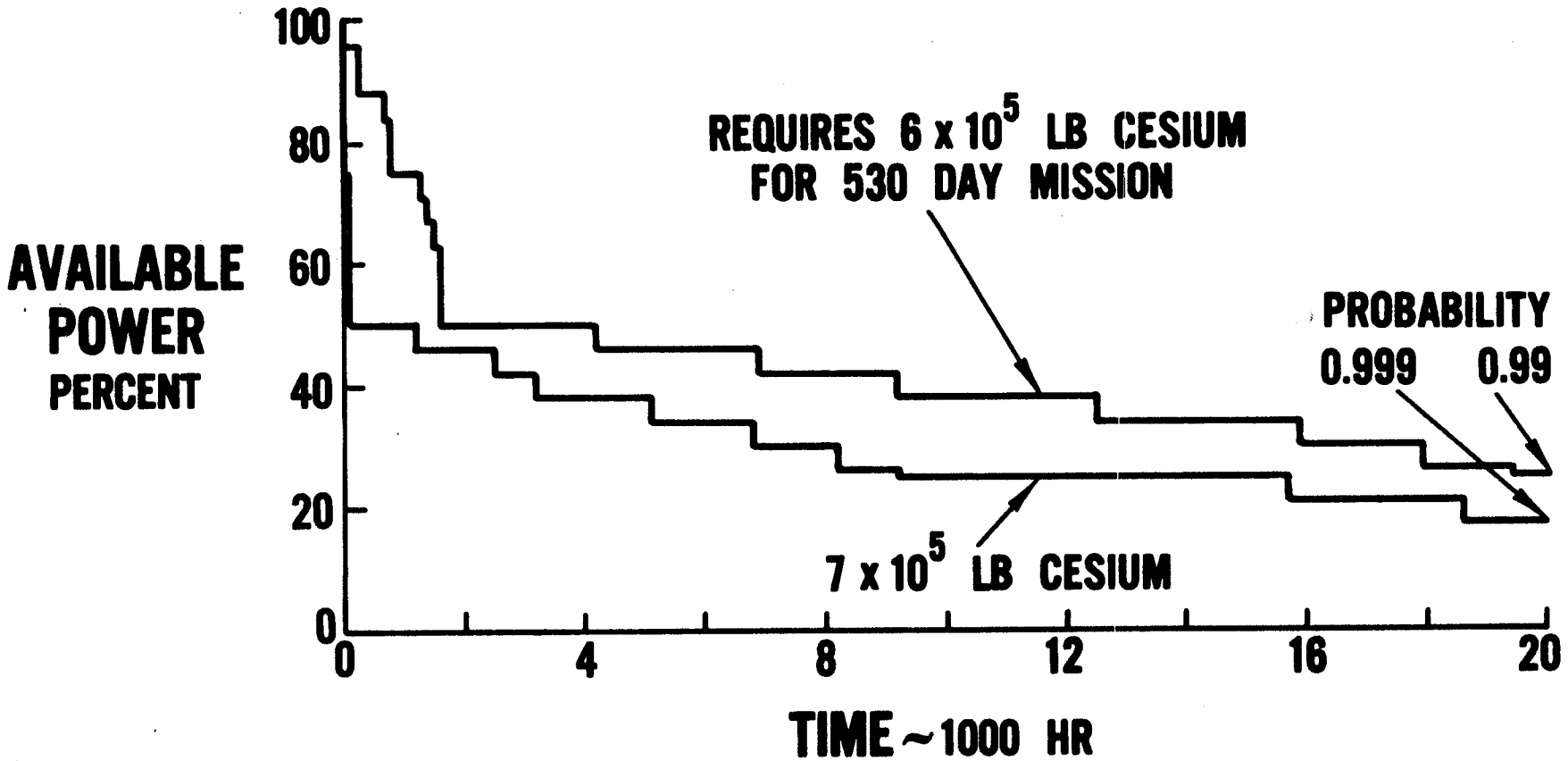

Pratt & Whitney Aircraft
DIVISION OF UNITED AIRCRAFT CORPORATION

M-38730
660906

E-910262-6

Figure No. VI-5

LOW ACCELERATION SPACE TRANSPORTATION

EFFECT OF POWERPLANT ON VEHICLE MASS

OPTIMUM NUCLEAR ROCKET AND ELECTRIC PROPULSION OPERATION

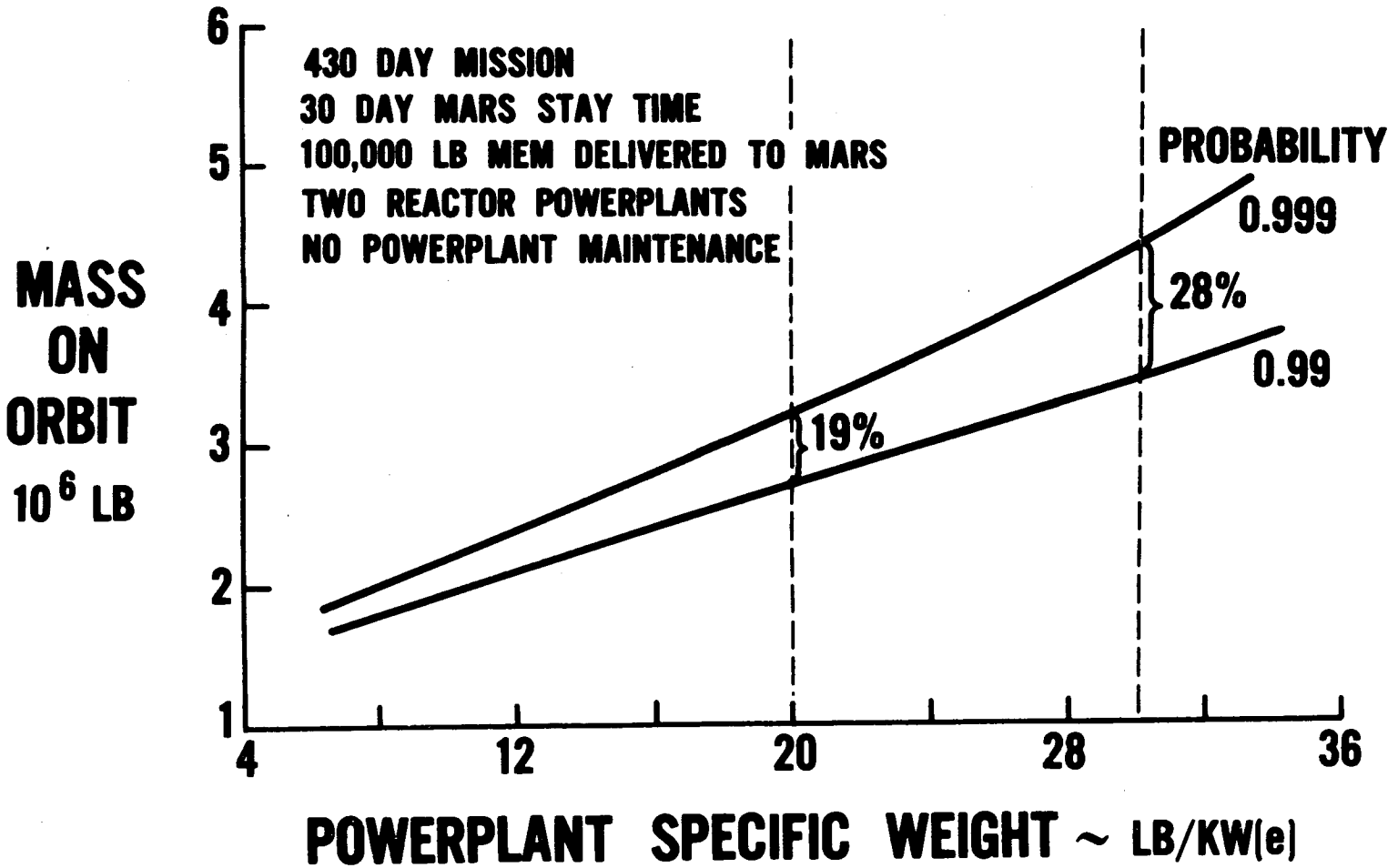

Pratt & Whitney Aircraft

DIVISION OF UNITED AIRCRAFT CORPORATION

M-38726
660906

E-910262-6

Figure No. VI-6

LOW ACCELERATION SPACE TRANSPORTATION
RELIABILITY BLOCK DIAGRAM
SINGLE THREAD SYSTEM

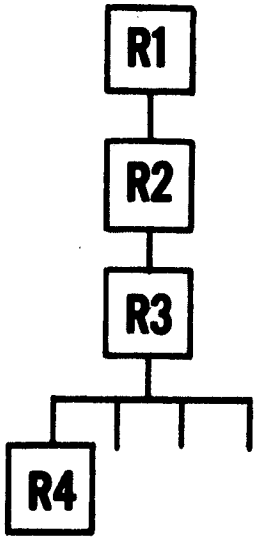

LOW ACCELERATION SPACE TRANSPORTATION

RELIABILITY BLOCK DIAGRAM

TWO REACTOR SYSTEM

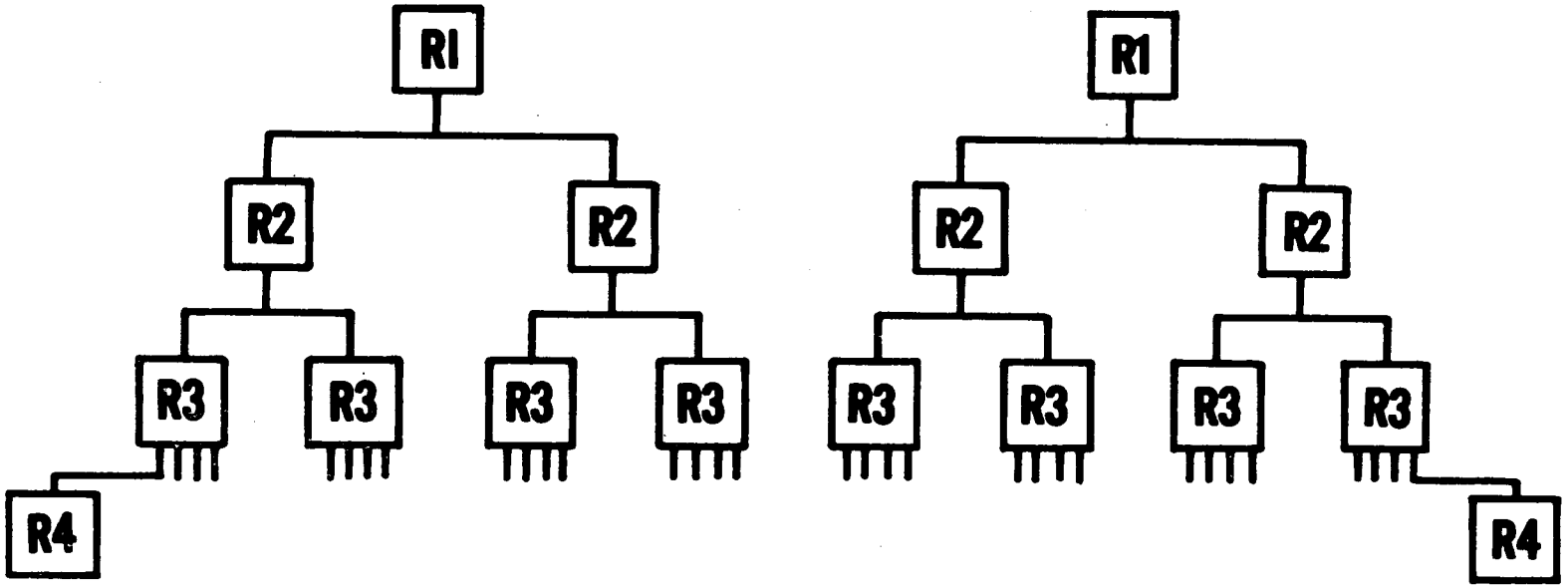

Pratt & Whitney Aircraft
DIVISION OF UNITED AIRCRAFT CORPORATION

M-37445
661003

E-910262-6

Figure No. VI-8

LOW ACCELERATION SPACE TRANSPORTATION

PROBABLE POWER vs MISSION TIME

PROBABILITY = 0.99

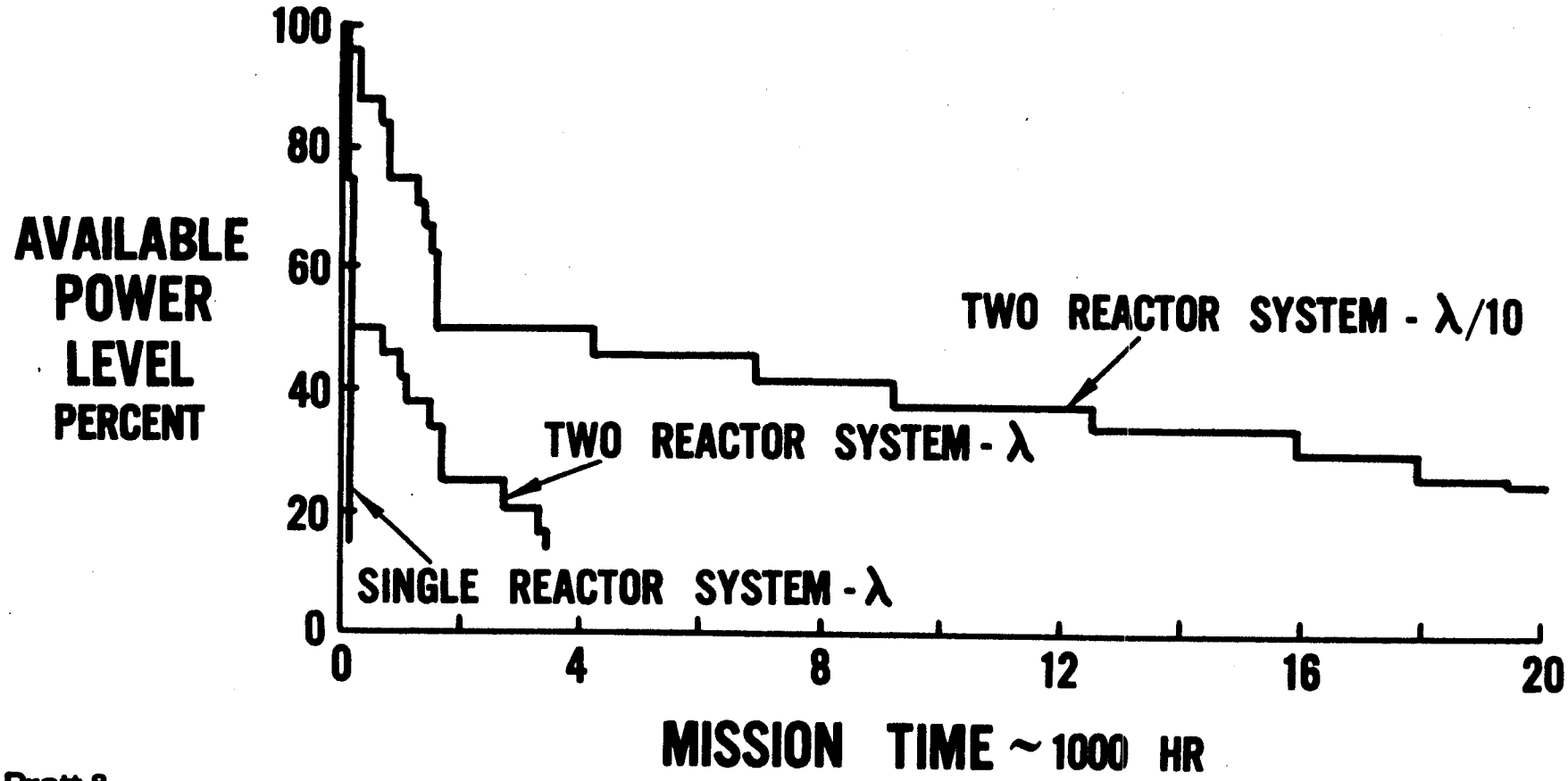

Pratt & Whitney Aircraft

DIVISION OF UNITED AIRCRAFT CORPORATION

M-37441
661003

E-910262-6

Figure No. VI-9

LOW ACCELERATION SPACE TRANSPORTATION
VEHICLE CONFIGURATION

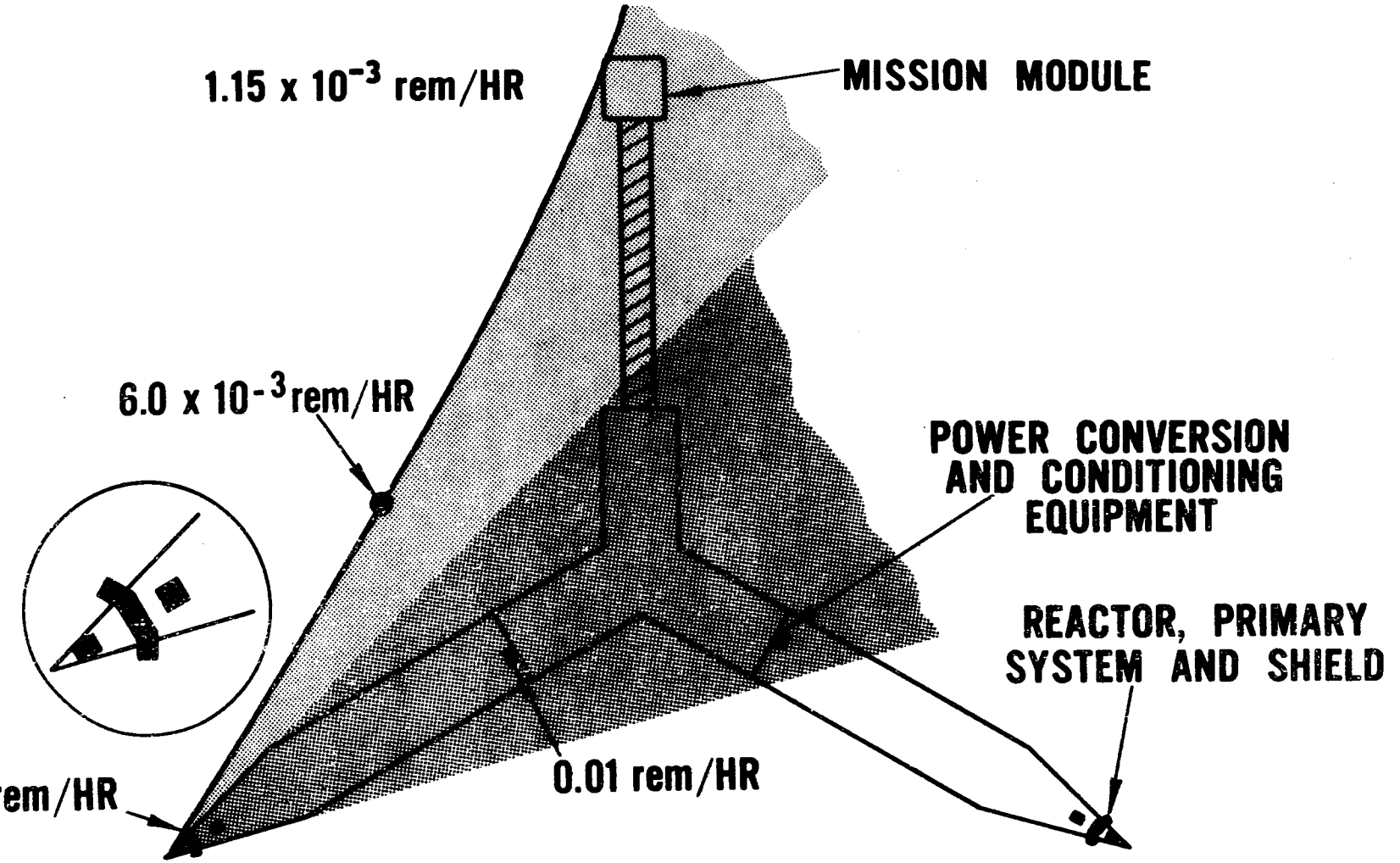

DOSE RATES SHOWN ARE FOR BOTH REACTORS AT FULL POWER

Pratt & Whitney Aircraft
DIVISION OF UNITED AIRCRAFT CORPORATION

M-37444
661003

E-910262-6

Figure No. VI-10

Fig. No. VI-11

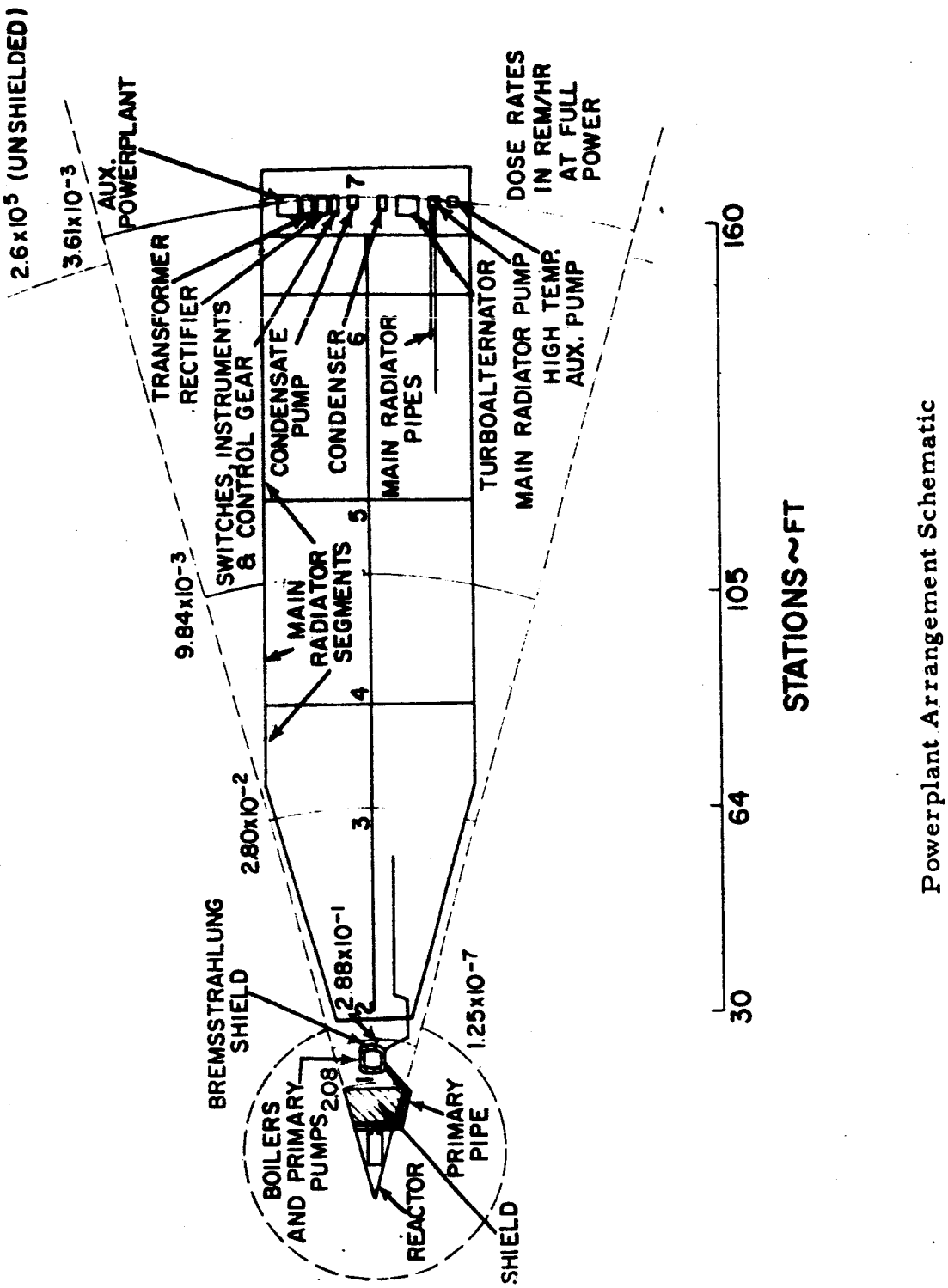

Powerplant Arrangement Schematic

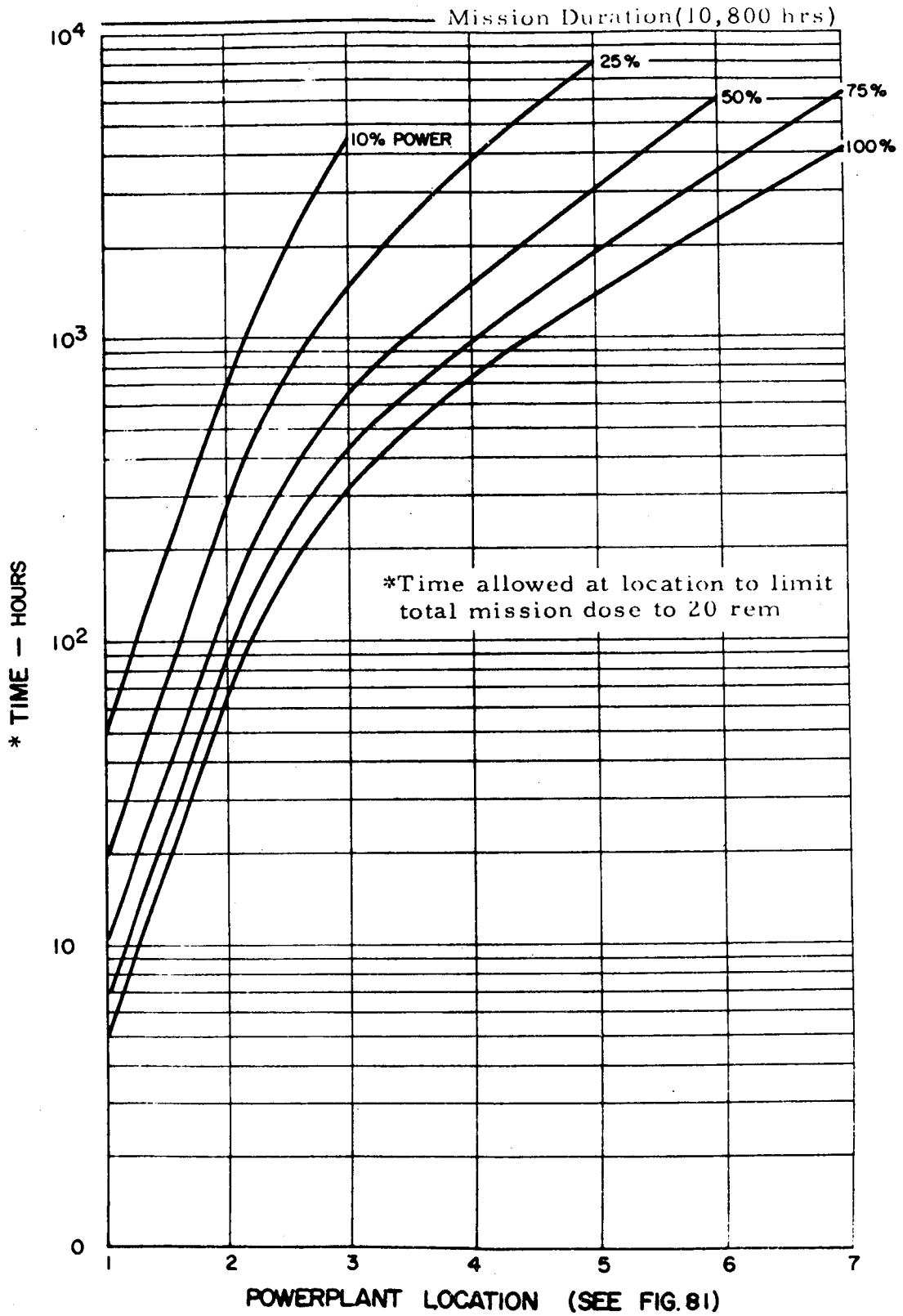

Maintenance Time vs Powerplant Location

4 MW(e) RANKINE CYCLE NUCLEAR SPACE POWERPLANT

POWERPLANT DOSE MAP

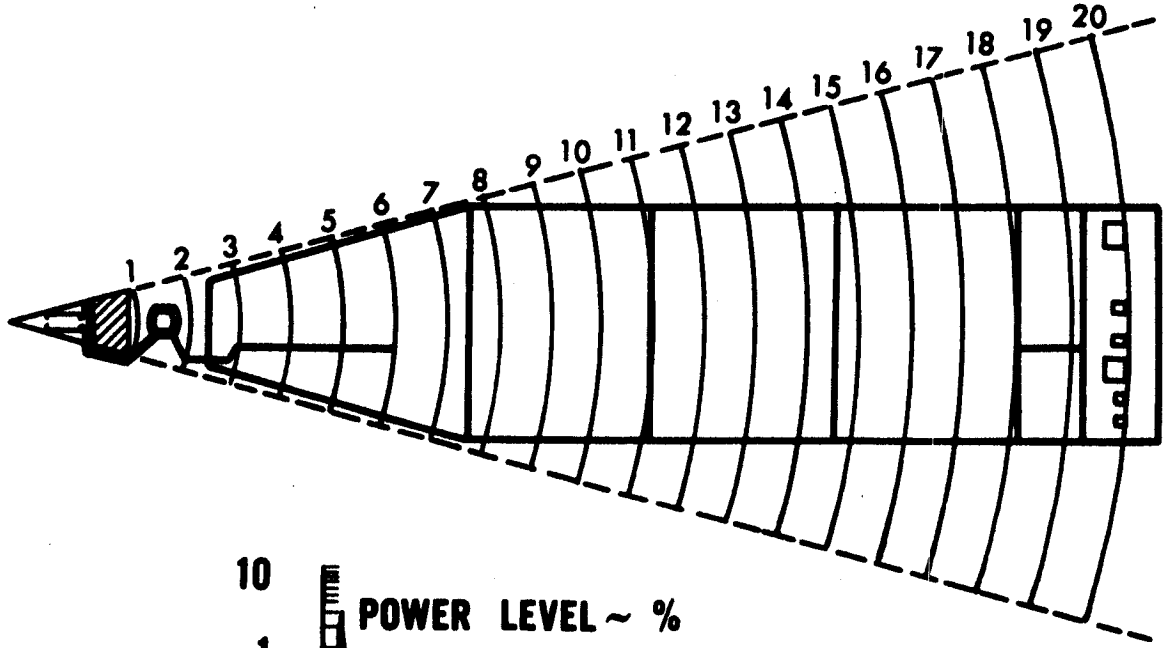

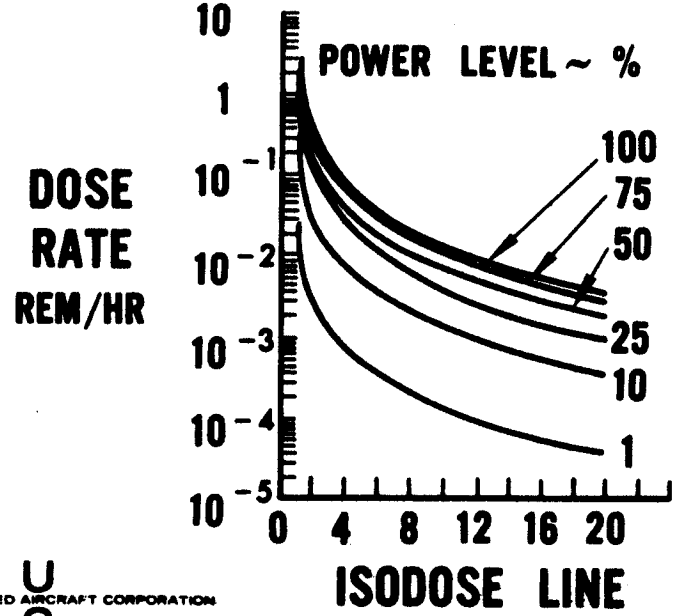

Pratt & Whitney Aircraft

DIVISION OF UNITED AIRCRAFT CORPORATION

M-35413
651211

E-910262-6

Figure No. VI-13

LOW ACCELERATION SPACE TRANSPORTATION

EFFECT OF MAINTENANCE ON AVAILABLE POWER

IMPROVED FAILURE RATES PROBABILITY = 0.99

ALL COMPONENTS MAINTAINABLE EXCEPT REACTOR

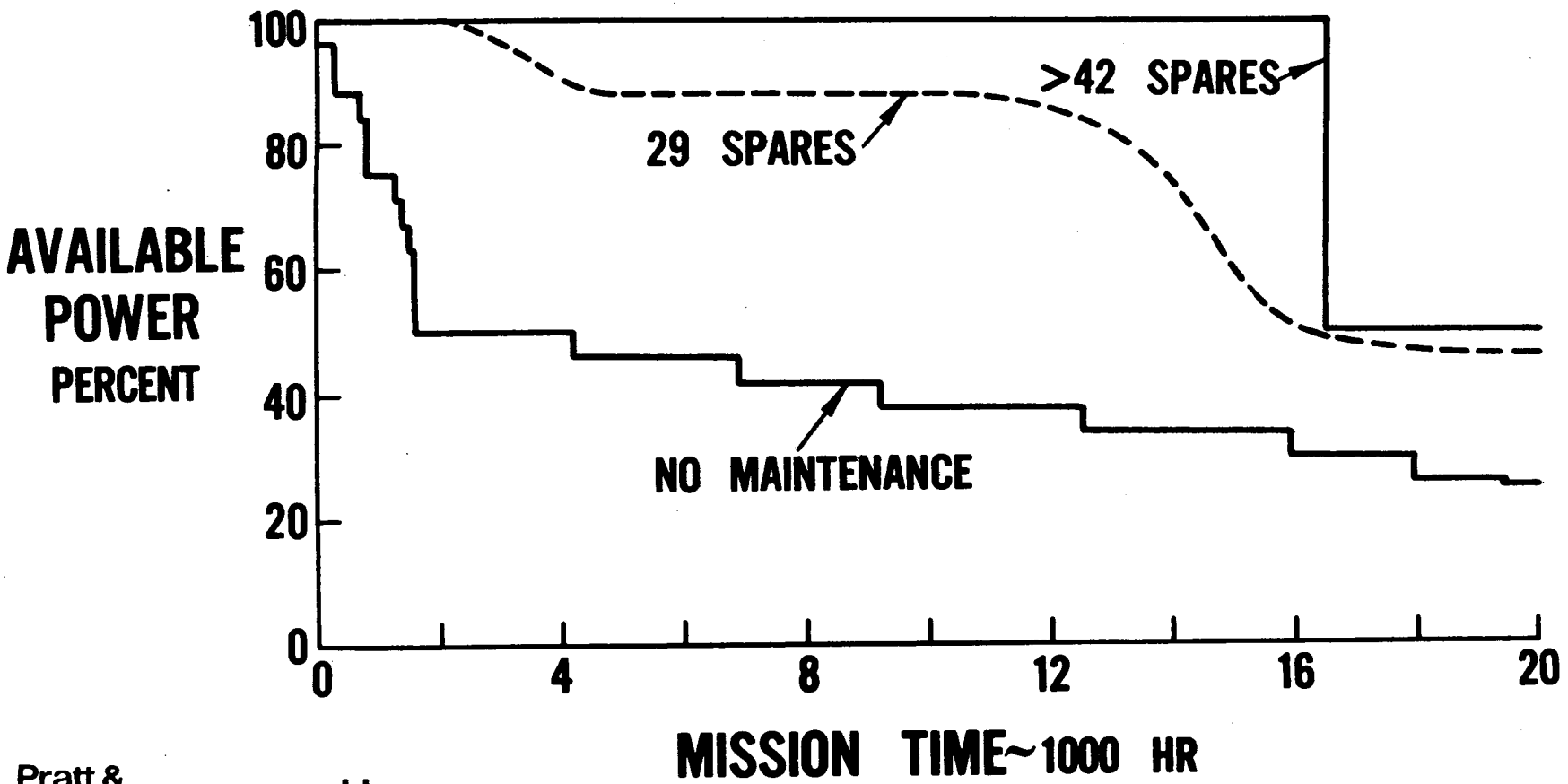

Pratt & Whitney Aircraft

DIVISION OF UNITED AIRCRAFT CORPORATION

M-37440
R662006

E-910262-6

Figure No. VI-14

LOW ACCELERATION SPACE TRANSPORTATION

EFFECT OF POWERPLANT ON VEHICLE MASS

OPTIMUM NUCLEAR ROCKET AND ELECTRIC PROPULSION OPERATION

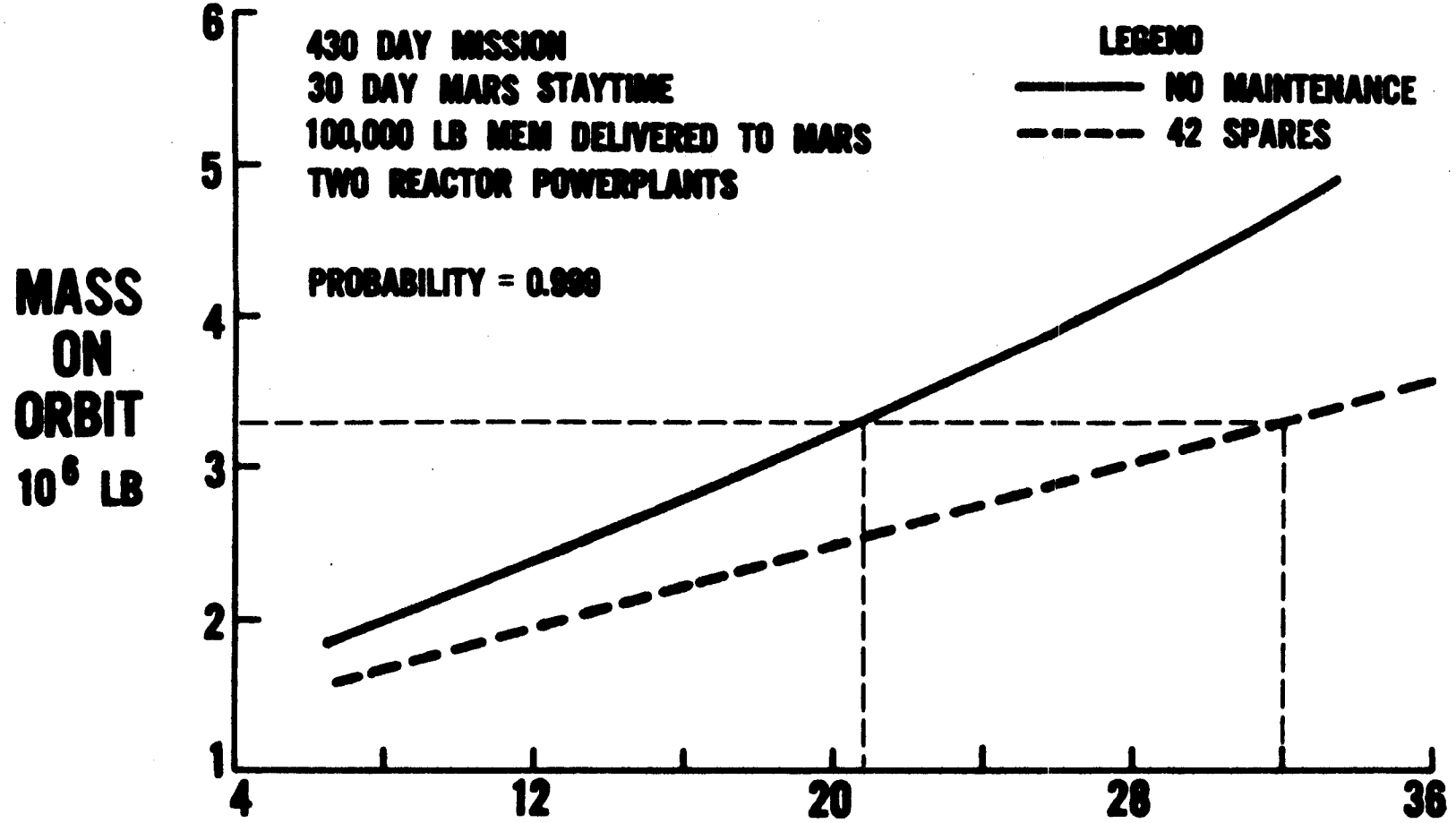

Pratt & Whitney Aircraft
DIVISION OF UNITED AIRCRAFT CORPORATION

M-38729
660906

Figure No. VI-15

LOW ACCELERATION SPACE TRANSPORTATION

EFFECT OF POWERPLANT ON VEHICLE MASS

OPTIMUM NUCLEAR ROCKET AND ELECTRIC PROPULSION OPERATION

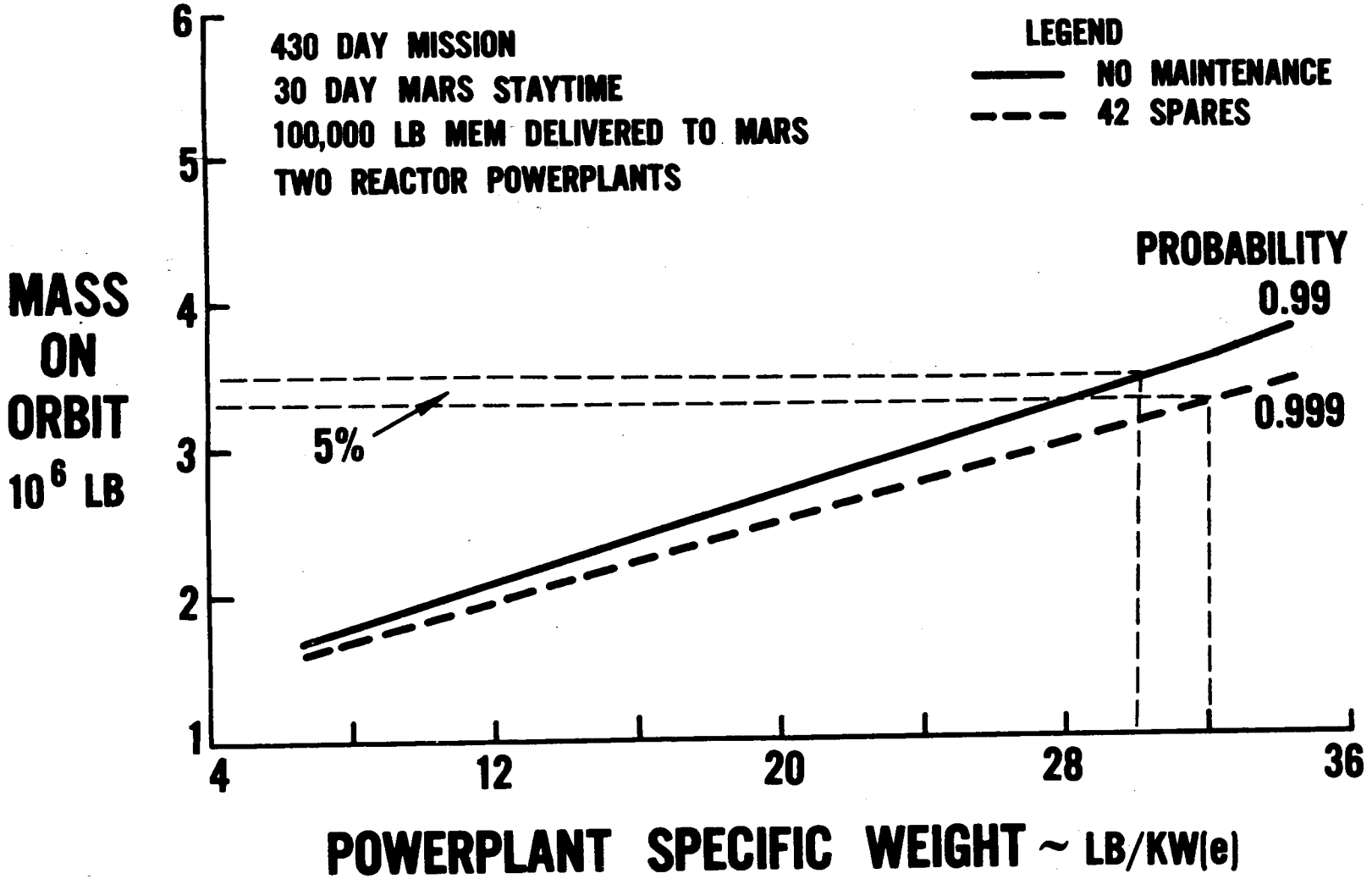

Pratt & Whitney Aircraft

DIVISION OF UNITED AIRCRAFT CORPORATION

M-38727
660906

E-910262-6

Figure No. VI-16

LOW ACCELERATION SPACE TRANSPORTATION

EFFECT OF MAINTENANCE ON AVAILABLE POWER

AIRCRAFT GAS TURBINE FAILURE RATES PROBABILITY = 0.99

ALL COMPONENTS MAINTAINABLE EXCEPT REACTOR

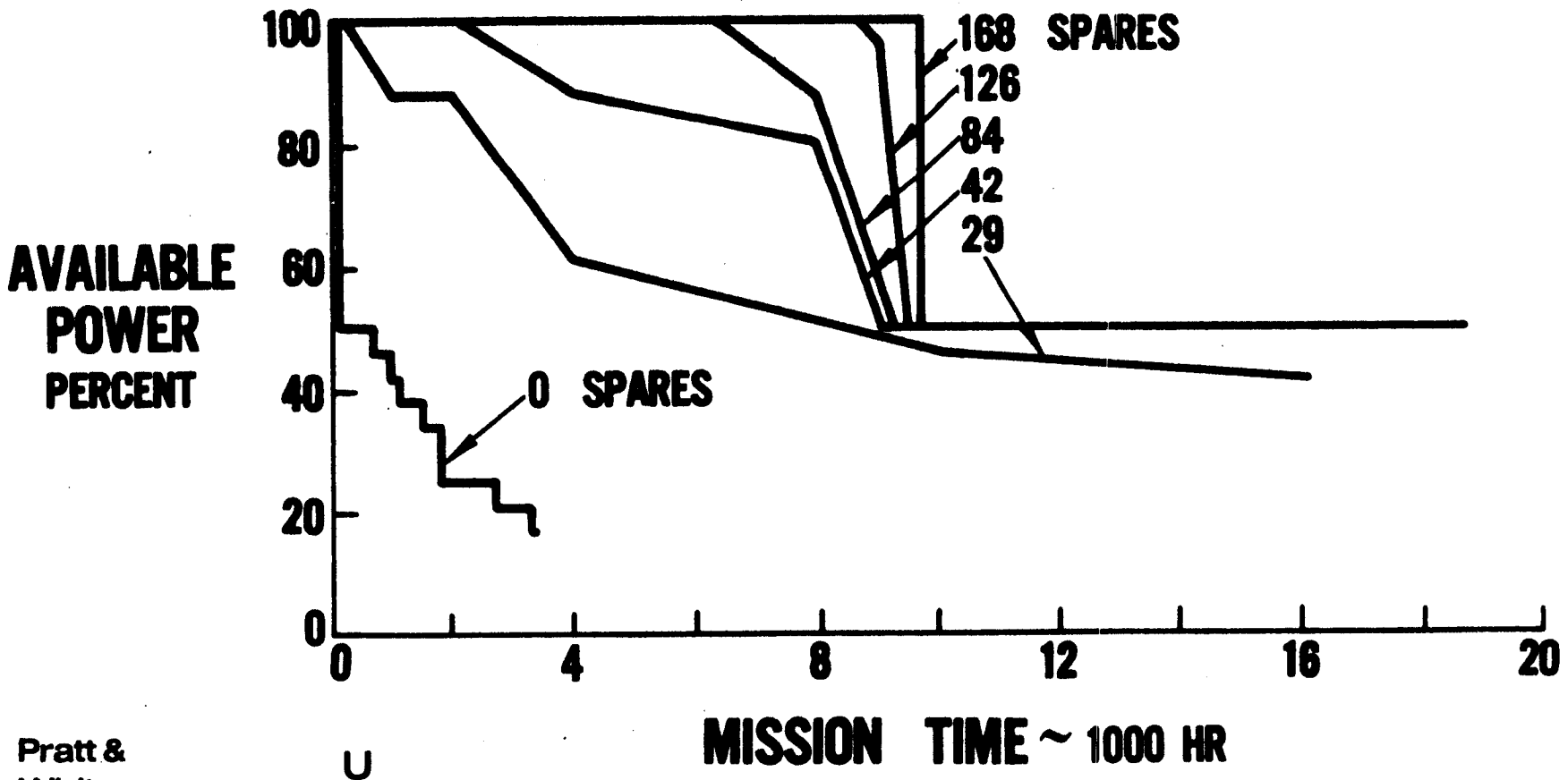

Pratt & Whitney Aircraft

DIVISION OF UNITED AIRCRAFT CORPORATION

M-38903

E-910262-6

Figure No. VI-17

LOW ACCELERATION SPACE TRANSPORTATION

EFFECT OF MAINTENANCE ON MIEO

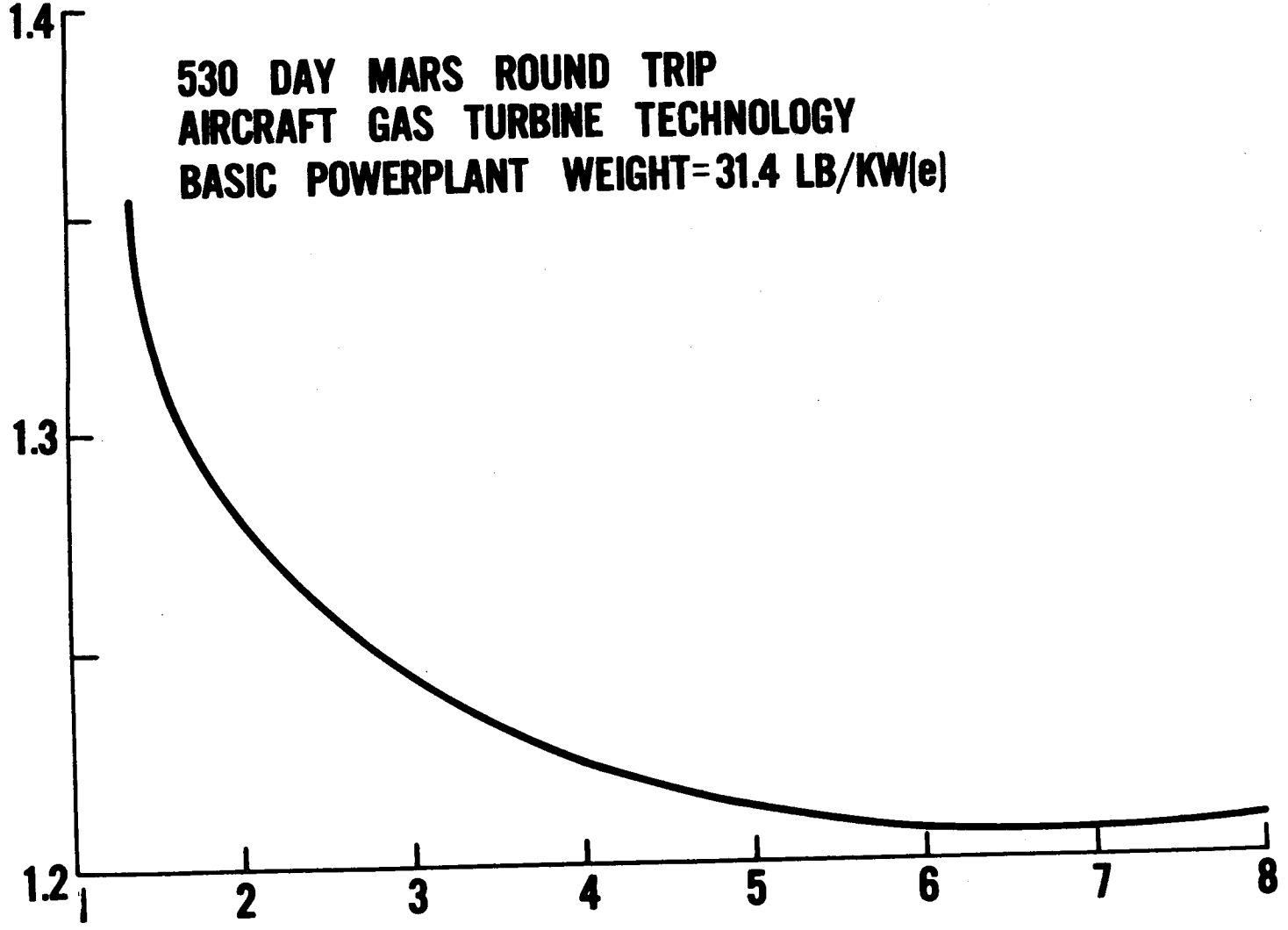

Pratt & Whitney Aircraft

DIVISION OF UNITED AIRCRAFT CORPORATION

M-38904
662006

E-910262-6

Figure No. VI-18

LOW ACCELERATION SPACE TRANSPORATION

EFFECT OF COMPONENT TECHNOLOGY ON MIEO

MAINTAINED SYSTEMS
530 DAY MARS ROUND TRIP
0.99 PROBABILITY
POWERPLANT SPECIFIC WEIGHT 31.4 LB/KW(e)

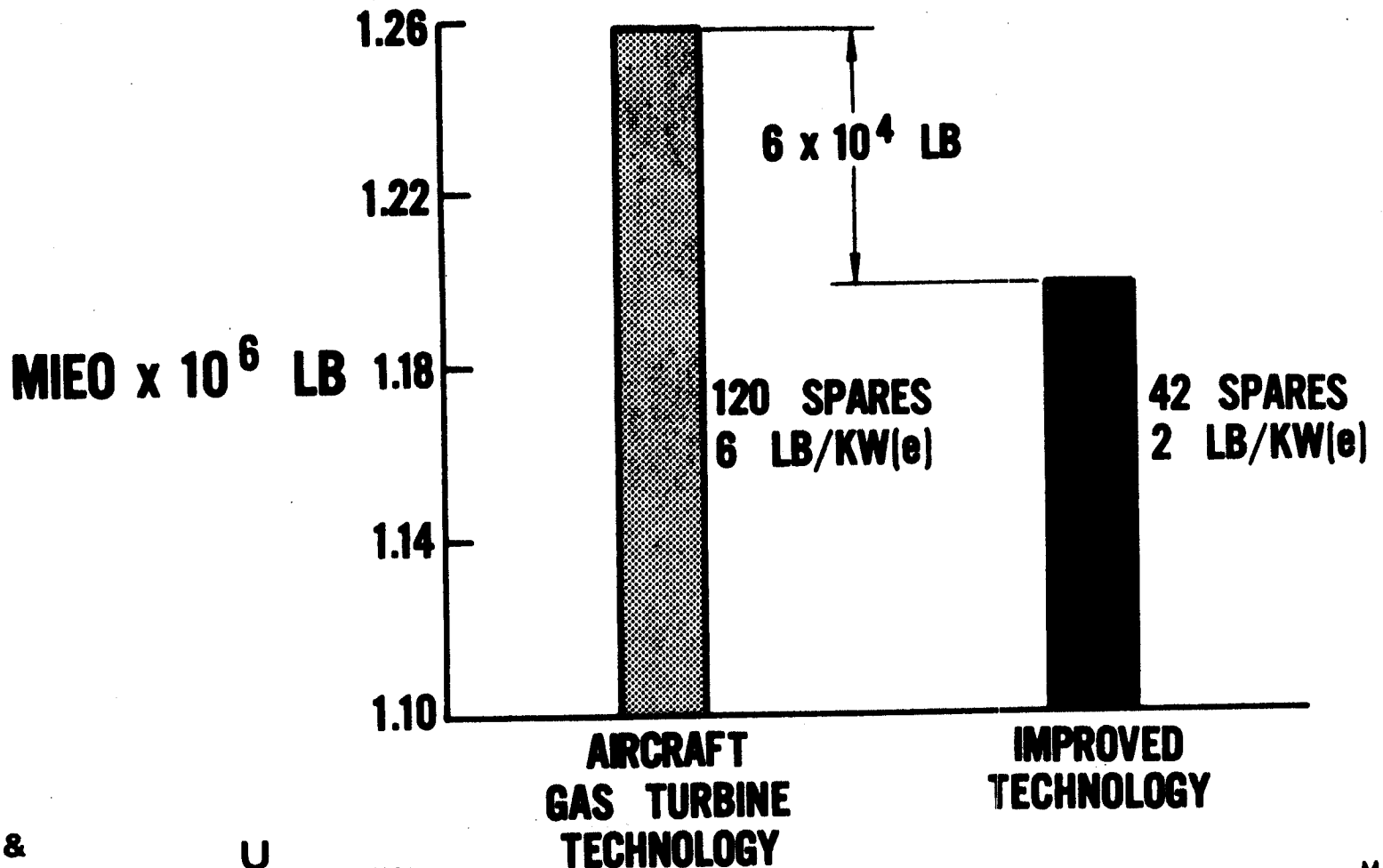

Pratt & Whitney Aircraft
DIVISION OF UNITED AIRCRAFT CORPORATION

M-38731
661006

E-910262-6

Figure No. VI-19

4 MW(e) RANKINE CYCLE NUCLEAR SPACE POWERPLANT

MAIN RADIATOR COOLDOWN

(ONE PCS SHUTDOWN)

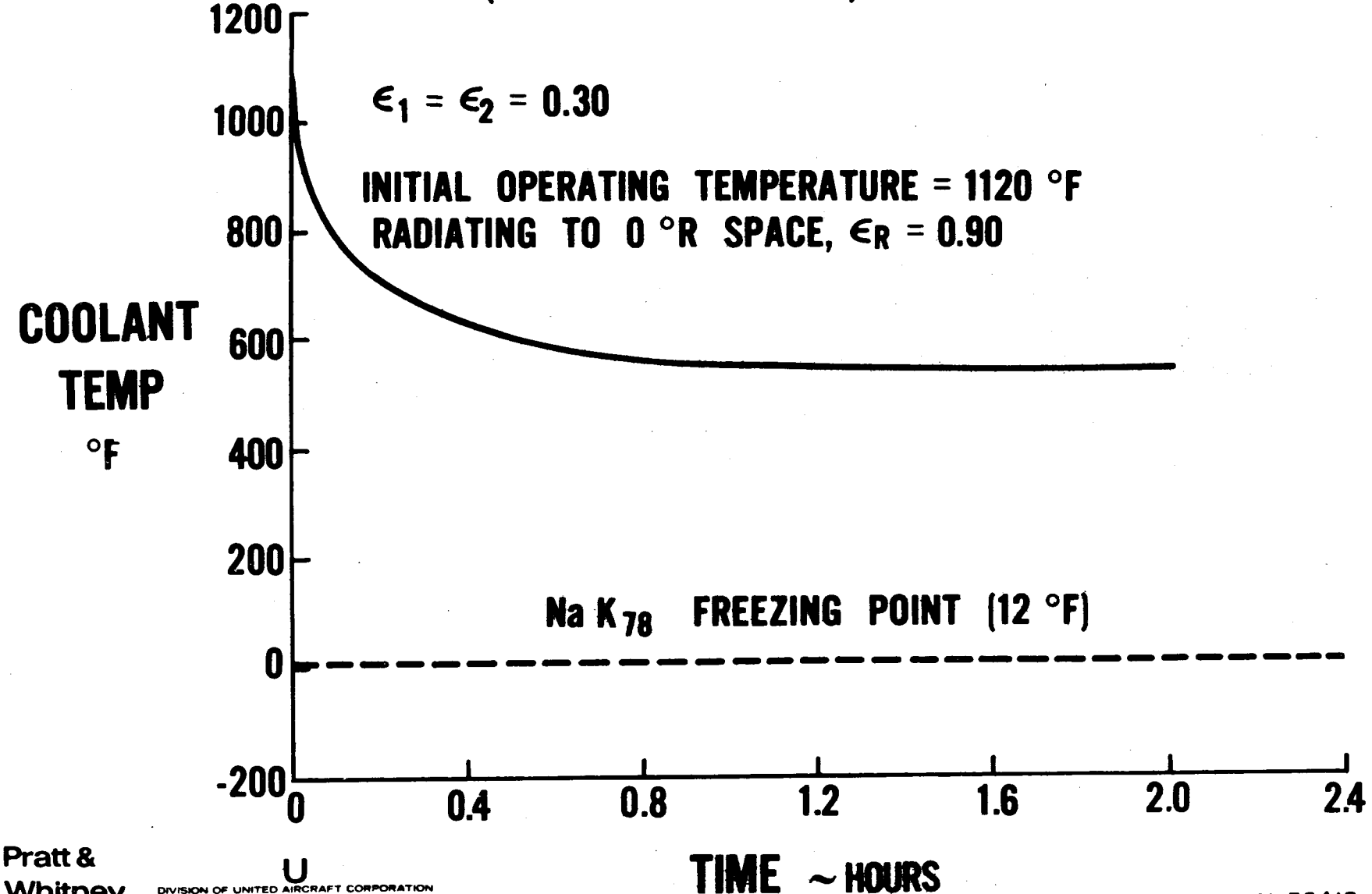

Pratt & Whitney Aircraft

DIVISION OF UNITED AIRCRAFT CORPORATION

U A.

M-35415
651111

E-910262-6

Figure No. VI-20

4MW(e) RANKINE CYCLE NUCLEAR SPACE POWERPLANT
MAIN RADIATOR COOLDOWN
(POWERPLANT SHUTDOWN)

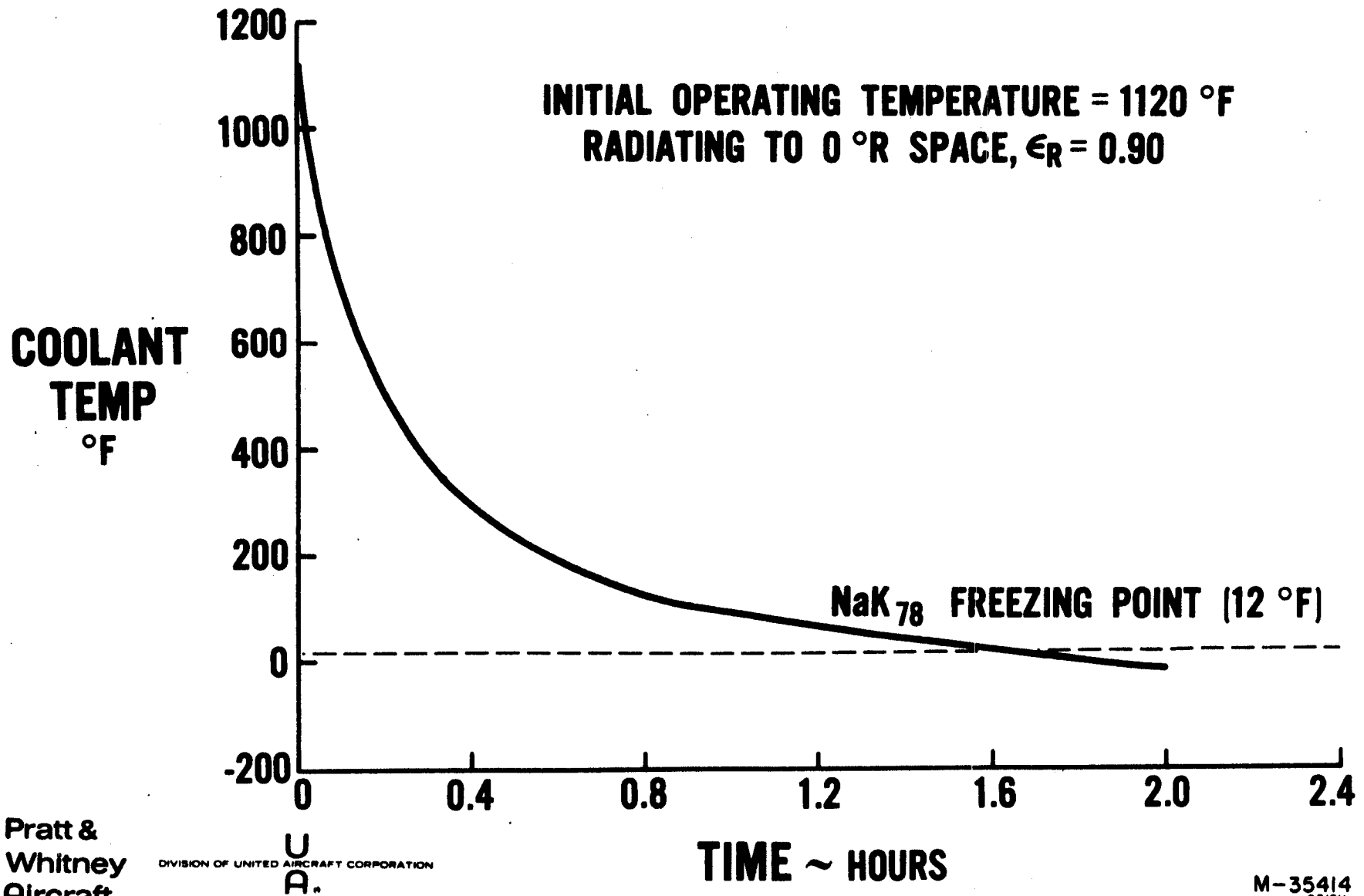

Pratt & Whitney Aircraft
DIVISION OF UNITED AIRCRAFT CORPORATION
U A.

M-35414
651211

E-190262-6

Figure No. VI-21

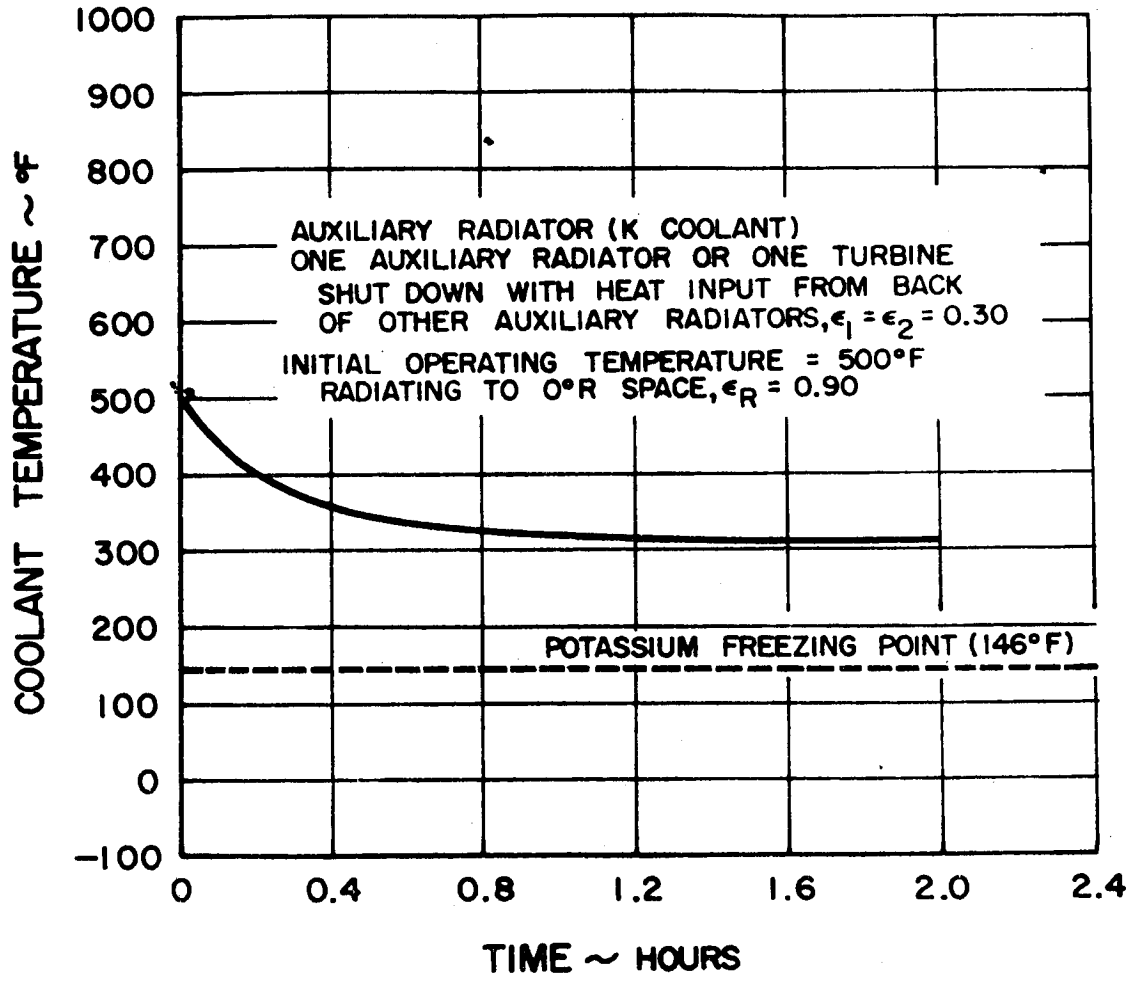

Auxiliary Radiator Coolant (K) Temperature vs Time

Figure No. VI-23

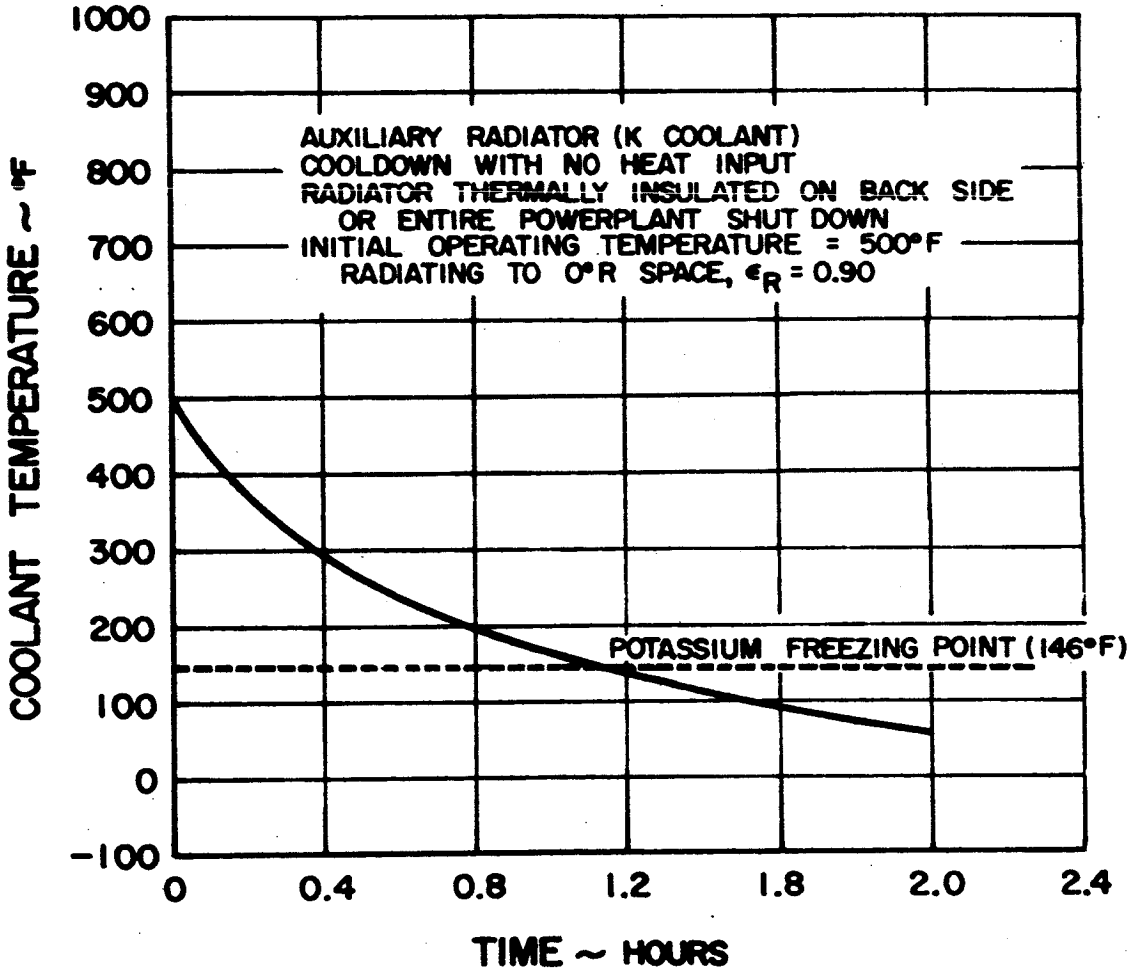

Auxiliary Radiator Coolant (K) Temperature vs Time

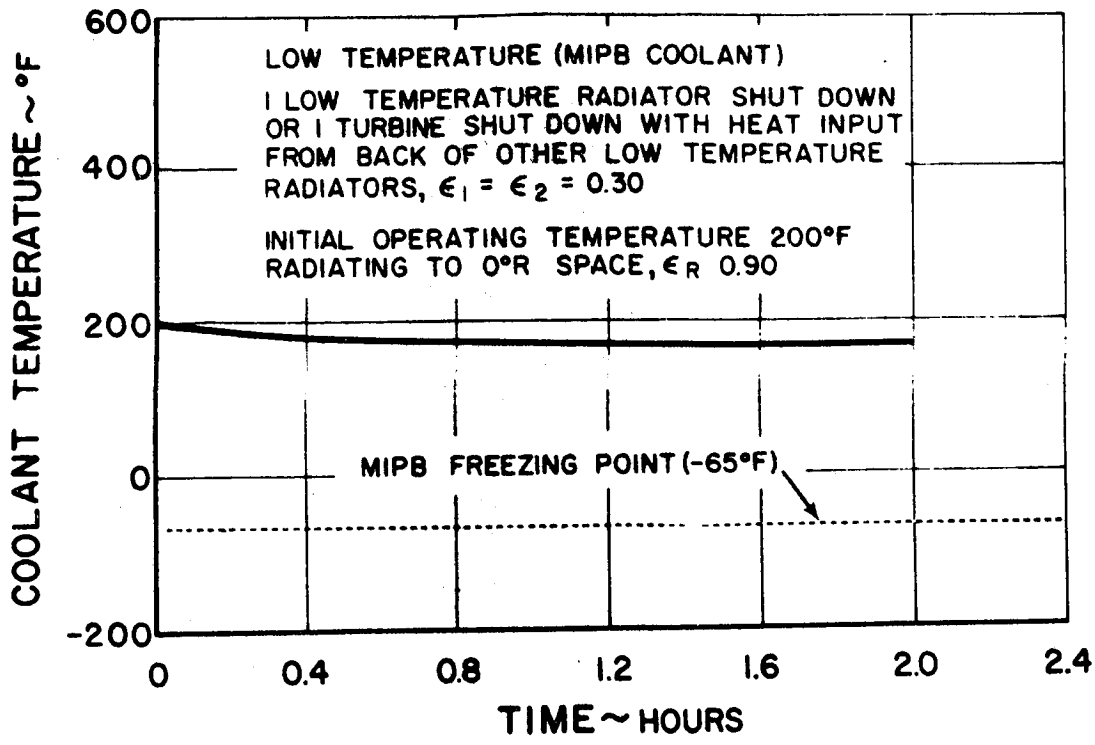

Low-Temperature Radiator Coolant (MIPB) Temperature vs Time

Fig. VI-25

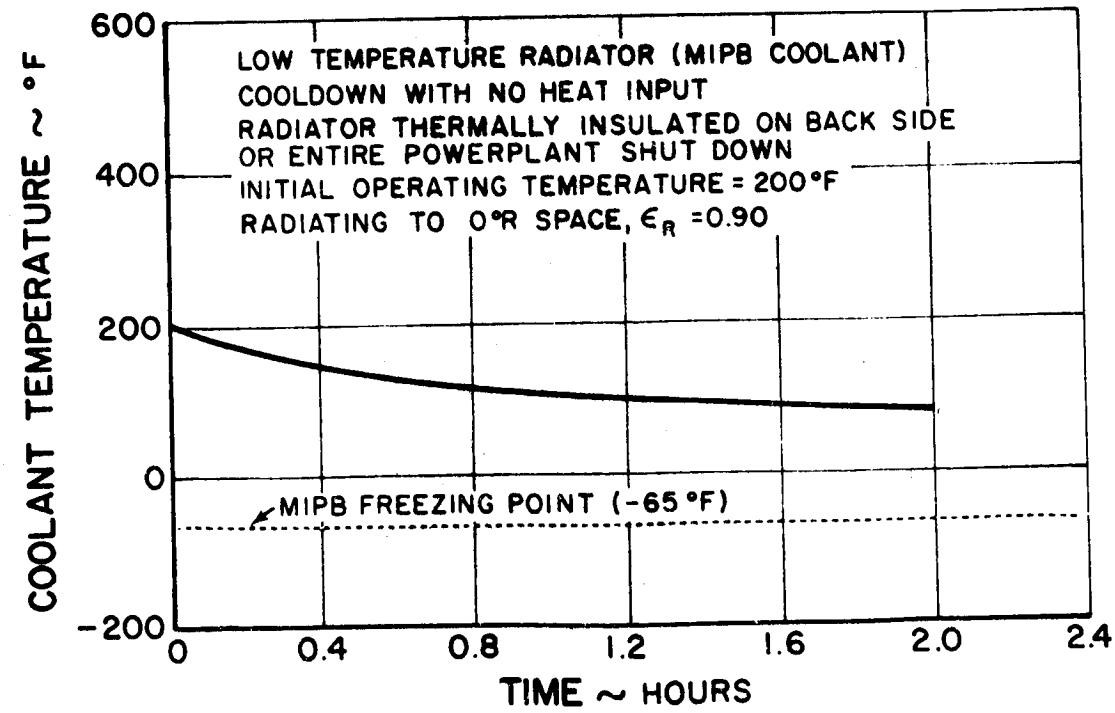

Low-Temperature Radiator Coolant (MIPB) Temperature vs Time

LOW ACCELERATION SPACE TRANSPORTATION
EFFECT OF OPERATING MODES ON AVAILABLE POWER
SEQUENTIAL REACTOR OPERATION

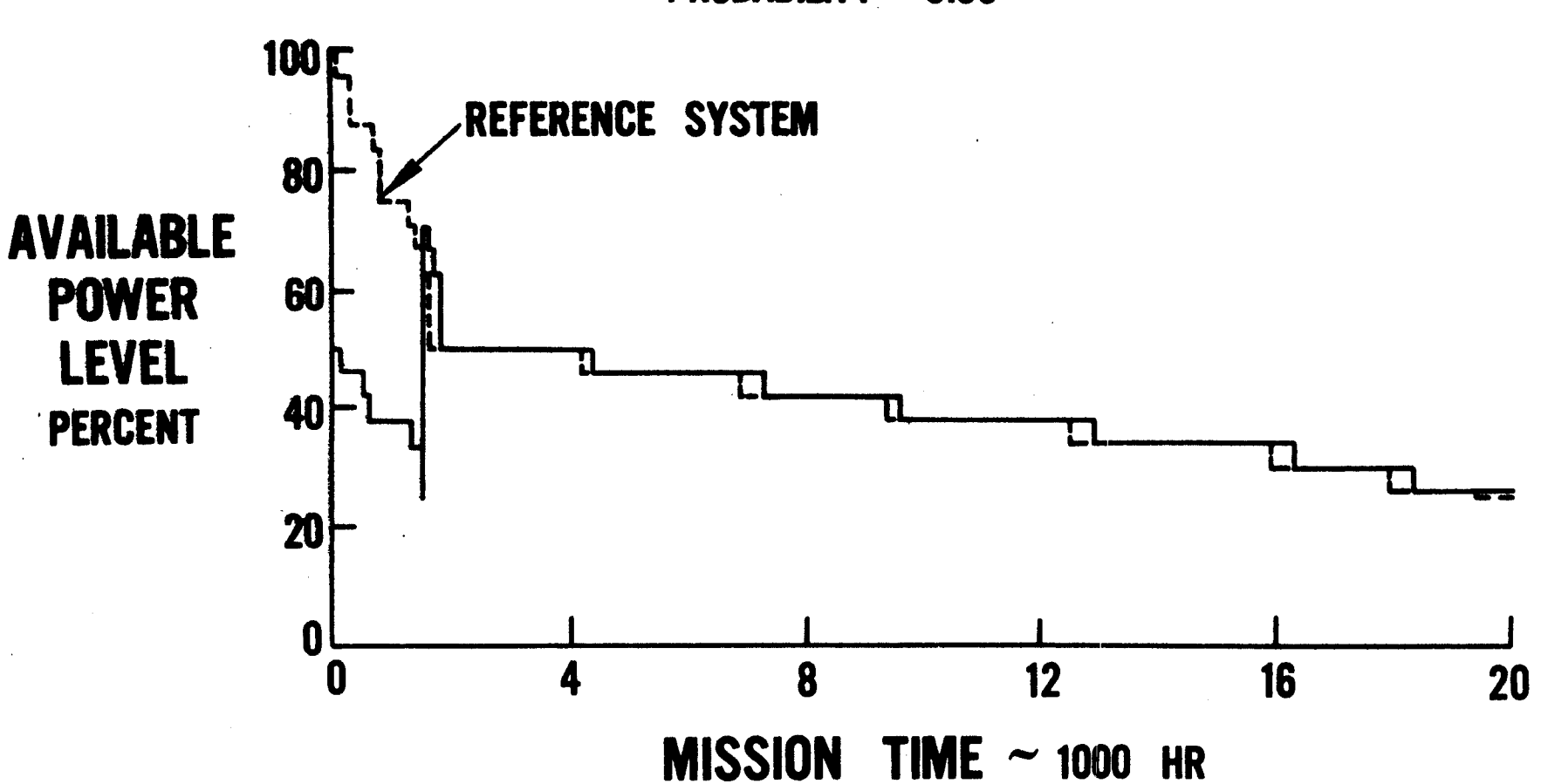

Pratt & Whitney Aircraft
DIVISION OF UNITED AIRCRAFT CORPORATION

M-37469
661003

E-910262-6

Figure No. VI-26

LOW ACCELERATION SPACE TRANSPORTATION
EFFECT OF OPERATING MODES ON AVAILABLE POWER
STARTUP STANDBY REACTOR AT 6000 HR
PROBABILITY=0.95

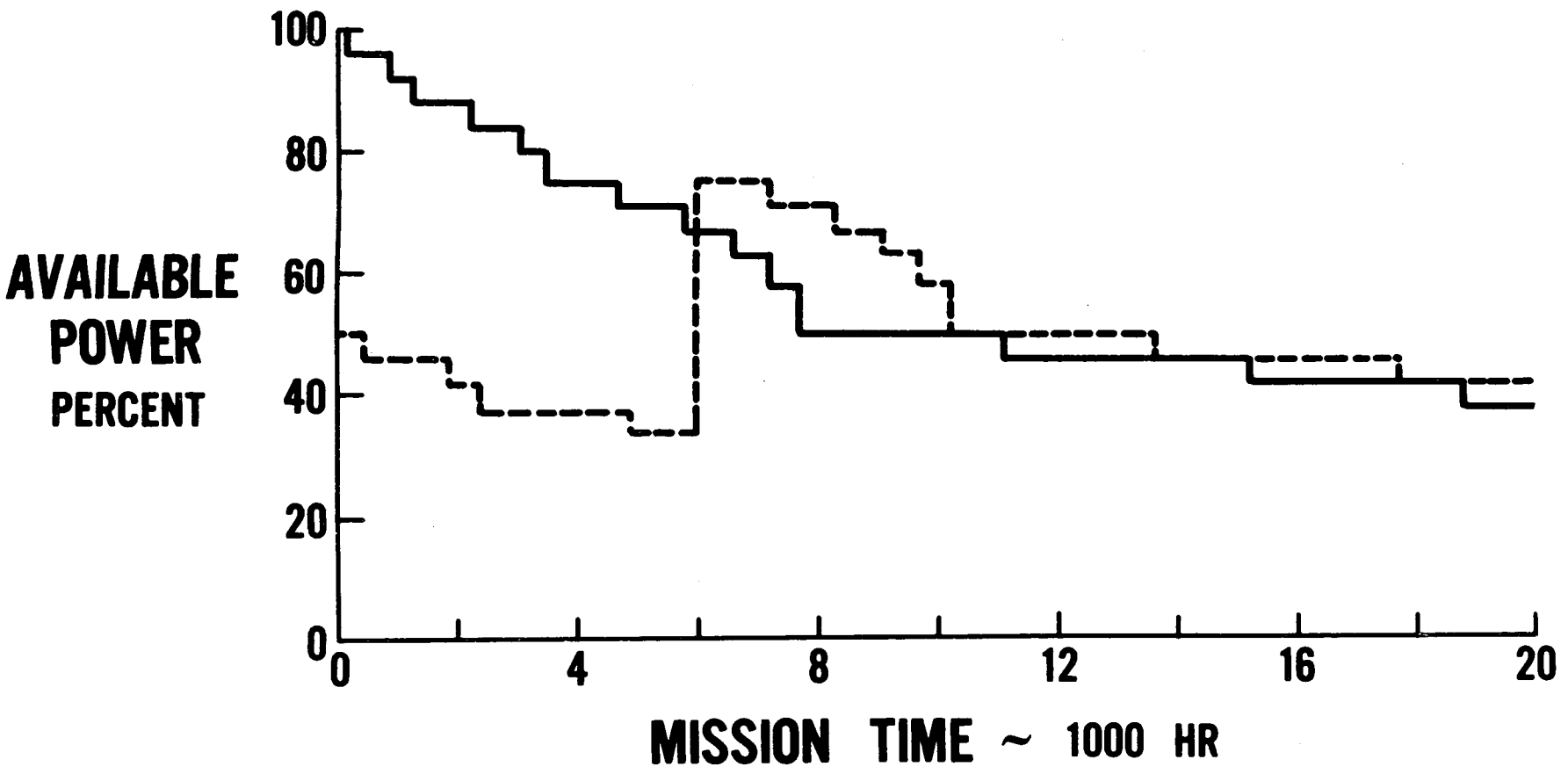

Pratt & Whitney Aircraft
DIVISION OF UNITED AIRCRAFT CORPORATION

M-37514
661503

E-910262-6

Figure No. VI-27

LOW ACCELERATION SPACE TRANSPORTATION

EFFECT OF OPERATING MODES ON AVAILABLE POWER

TWO STANDBY PCS

PROBABILITY = 0.99

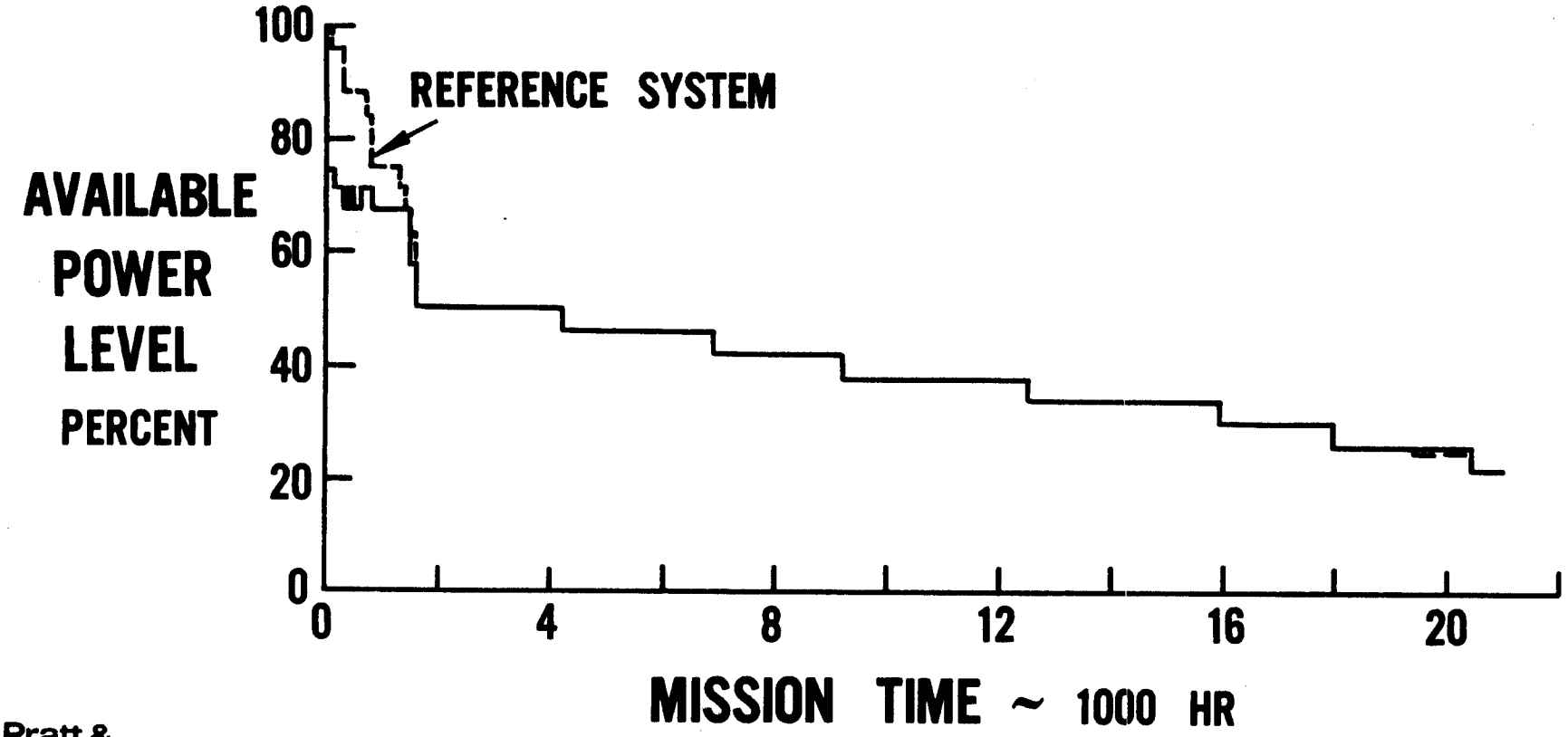

Pratt & Whitney Aircraft
DIVISION OF UNITED AIRCRAFT CORPORATION

M-37470
661003

E-910262-6

Figure No. VI-28

LOW ACCELERATION SPACE TRANSPORTATION
EFFECT OF OPERATING MODES ON AVAILABLE POWER
25 PERCENT RESERVE PCS CAPACITY

PROBABILITY = 0.99

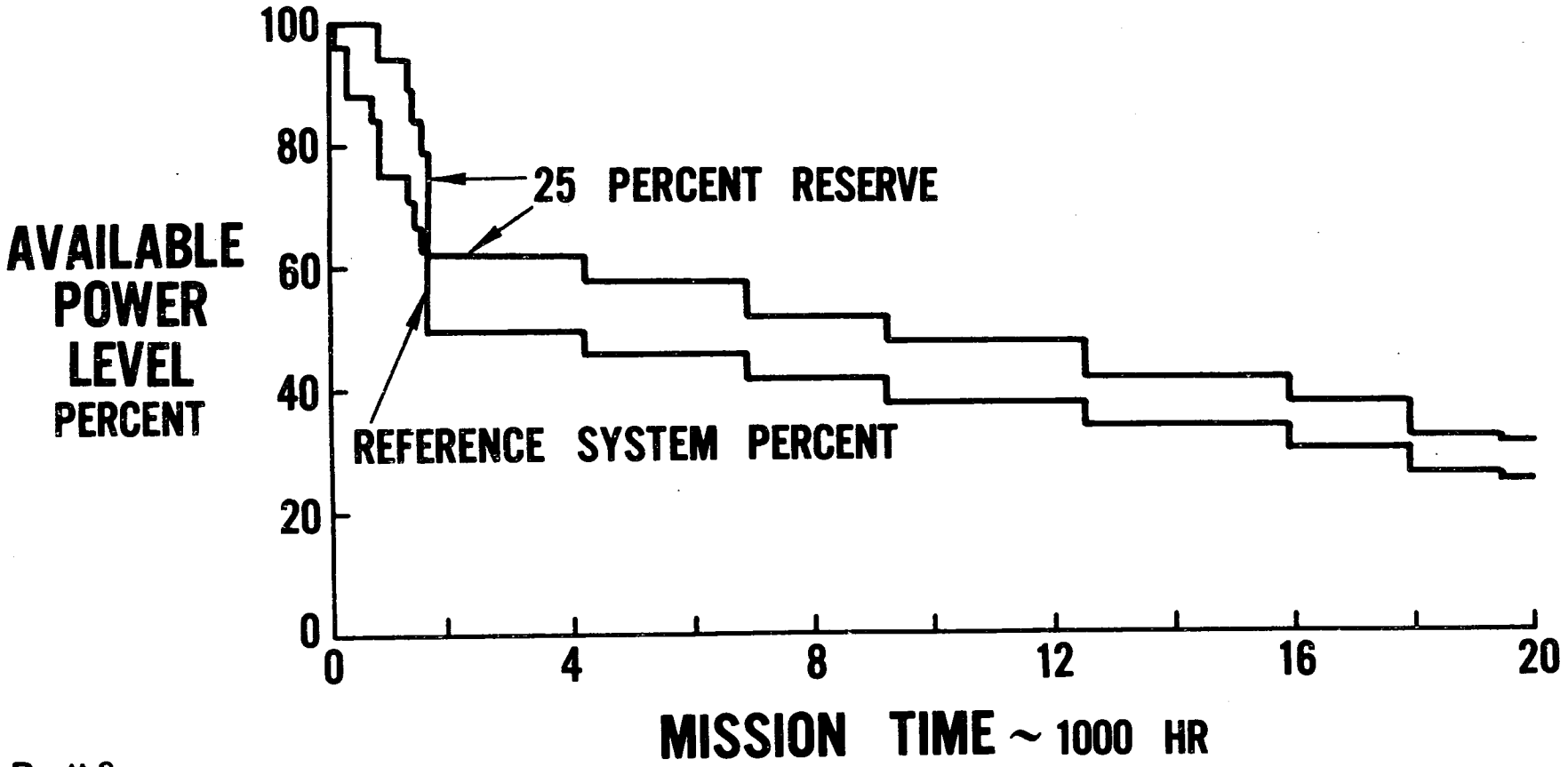

Pratt & Whitney Aircraft
DIVISION OF UNITED AIRCRAFT CORPORATION

M-37471
661003

E-910262-6

Figure No. VI-29.

LOW ACCELERATION SPACE TRANSPORTATION
RESERVE CAPACITY WEIGHT REQUIREMENTS

AN EXAMPLE

	RESERVE CAPACITY CONFIGURATION			REFERENCE CONFIGURATION	
		RATING MW(e)	WEIGHT 10^3	WEIGHT 10^3	RATING MW(e)
REACTOR SHIELD & PRIMARY SYST		4	70.4	70.4	4
BOILERS		5.2	1.0	0.8	
TA		5.2	13.7	11.2	
AR		5.2	7.6	7.5	
MR		5.2	19.7	14.8	
PC		5.2	5.4	4.2	
	4mw(e)				
OTHER		–	12.5	10.5	
	TOTAL		130.4	119.4	
	SP WT LB/KW		32.6	29.9	

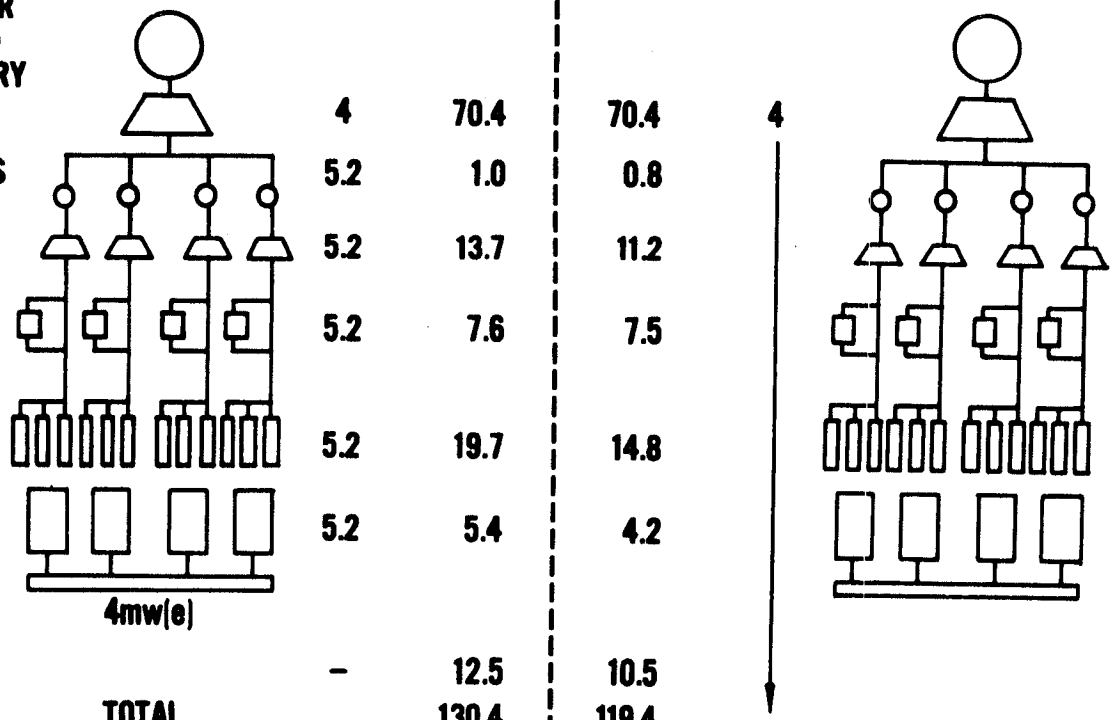

Pratt & Whitney Aircraft
DIVISION OF UNITED AIRCRAFT CORPORATION

M-37538
661403

E-910262-6

Figure No. VI-30

LOW ACCELERATION SPACE TRANSPORTATION

EFFECT OF TURBINE INLET TEMPERATURE ON SYSTEM WEIGHT

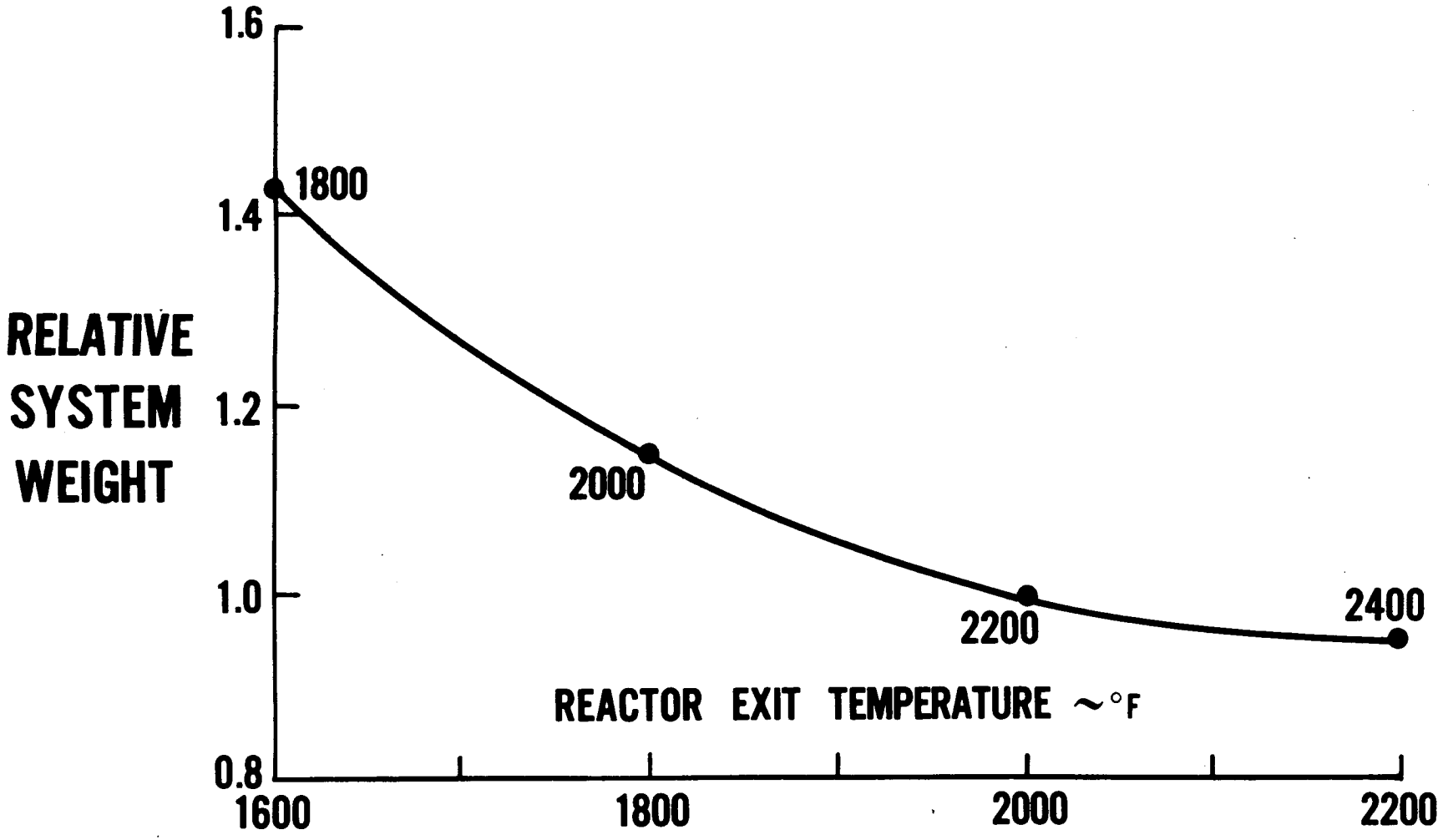

Pratt & Whitney Aircraft

DIVISION OF UNITED AIRCRAFT CORPORATION

M-37453

661003

E-910262-6

Figure No. VI-31

LOW ACCELERATION SPACE TRANSPORTATION

EFFECT OF TEMPERATURE ON FAILURE RATE

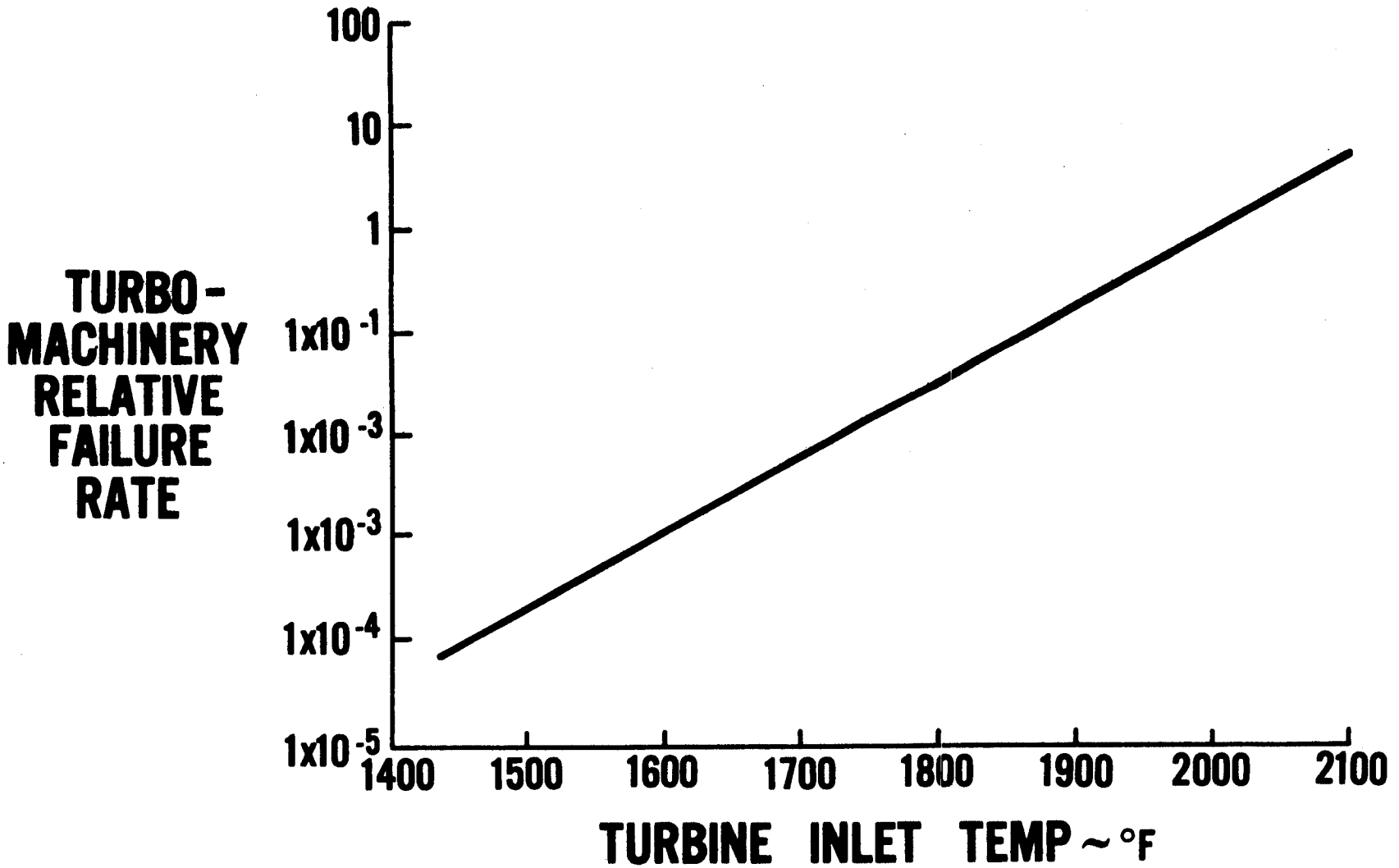

Pratt & Whitney Aircraft
DIVISION OF UNITED AIRCRAFT CORPORATION

M-37509
661503

E-910262-6

Figure No. VI-32

LOW ACCELERATION SPACE TRANSPORTATION

EFFECT OF TURBINE INLET TEMPERATURE ON VEHICLE REQUIREMENTS

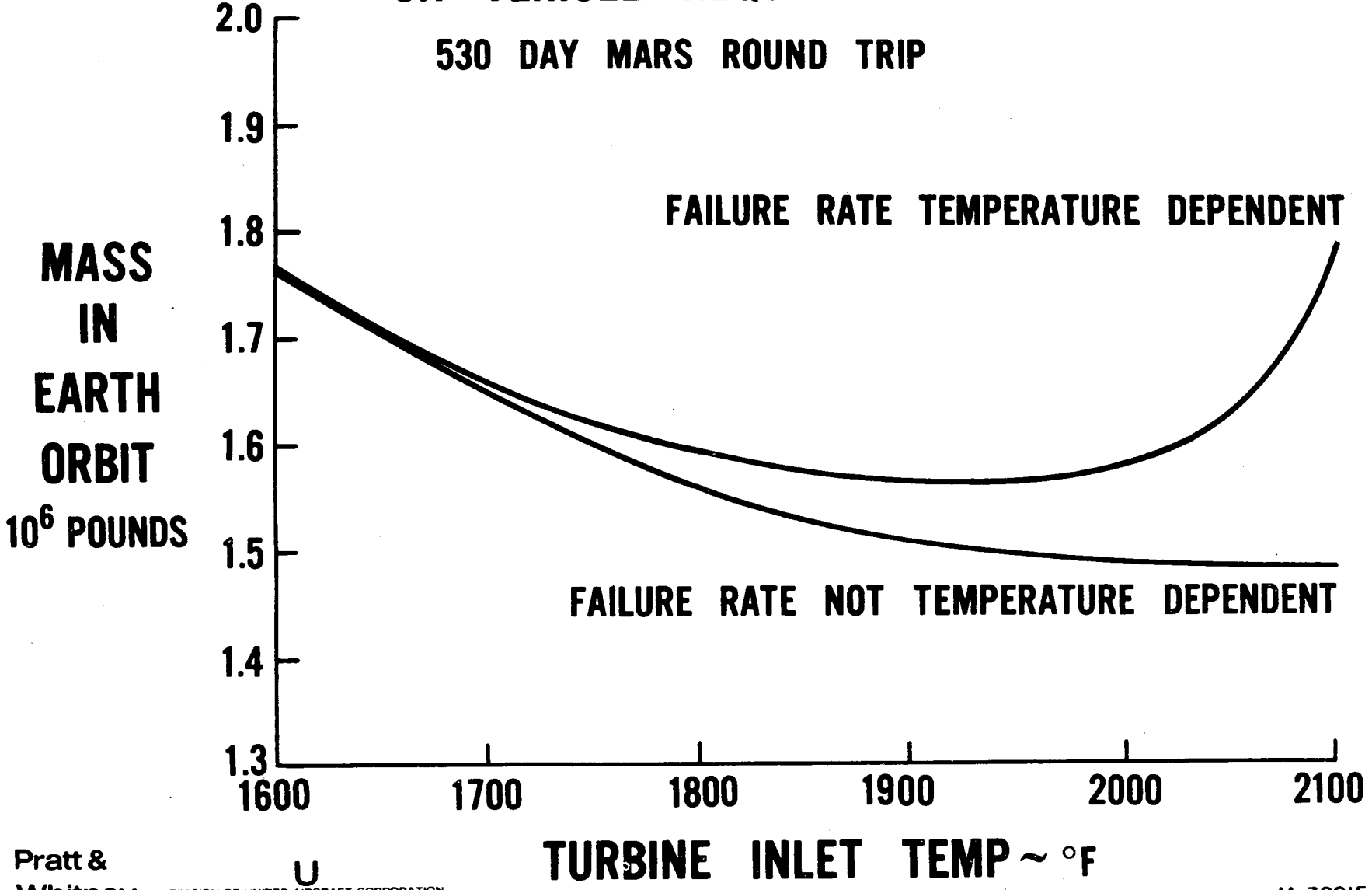

Pratt & Whitney Aircraft

DIVISION OF UNITED AIRCRAFT CORPORATION

M-39015

Figure VI-33

LOW ACCELERATION SPACE TRANSPORTATION

EFFECT OF REACTOR FUEL BURNUP ON SYSTEM WEIGHT

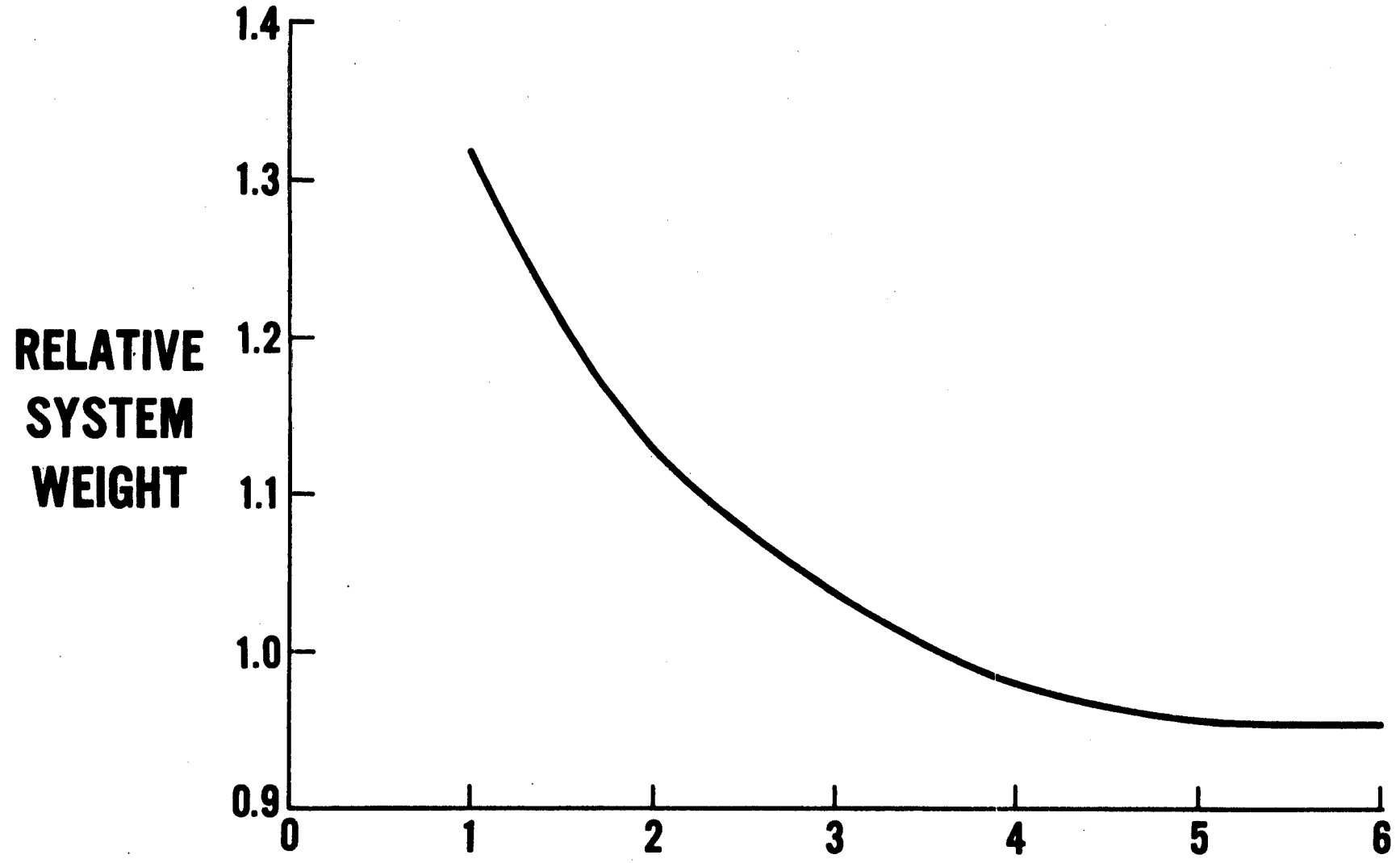

Pratt & Whitney Aircraft

DIVISION OF UNITED AIRCRAFT CORPORATION

M-37452
661003

E-910262-6

Figure No. VI-34

E-910262-6

LOW ACCELERATION SPACE TRANSPORTATION
EFFECT OF BURNUP ON MIEO

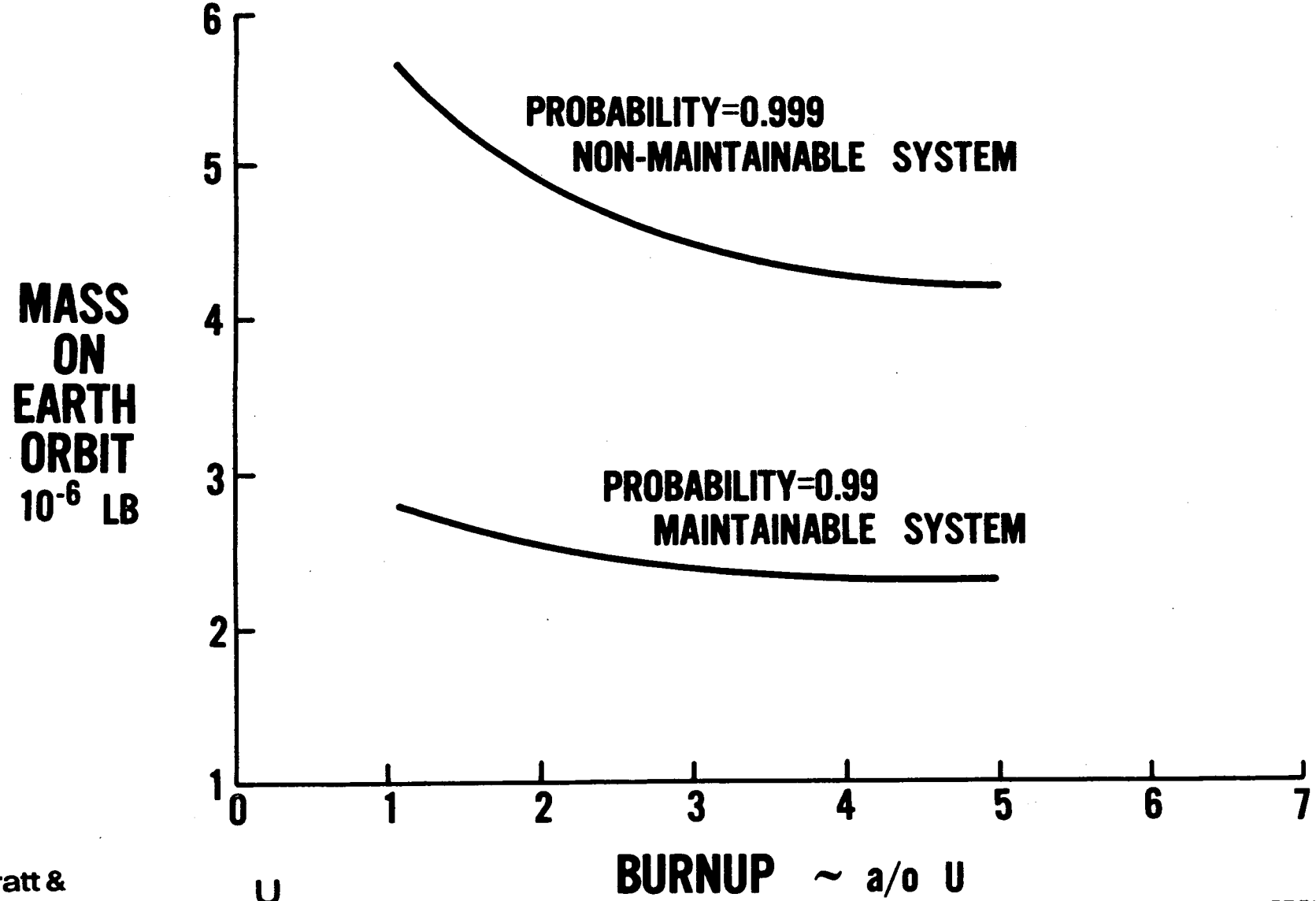

Pratt & Whitney Aircraft
DIVISION OF UNITED AIRCRAFT CORPORATION

M-37513
681403

Figure No. VI-35

LOW ACCELERATION SPACE TRANSPORTATION
SYSTEM RELATIVE WEIGHT vs LIFETIME

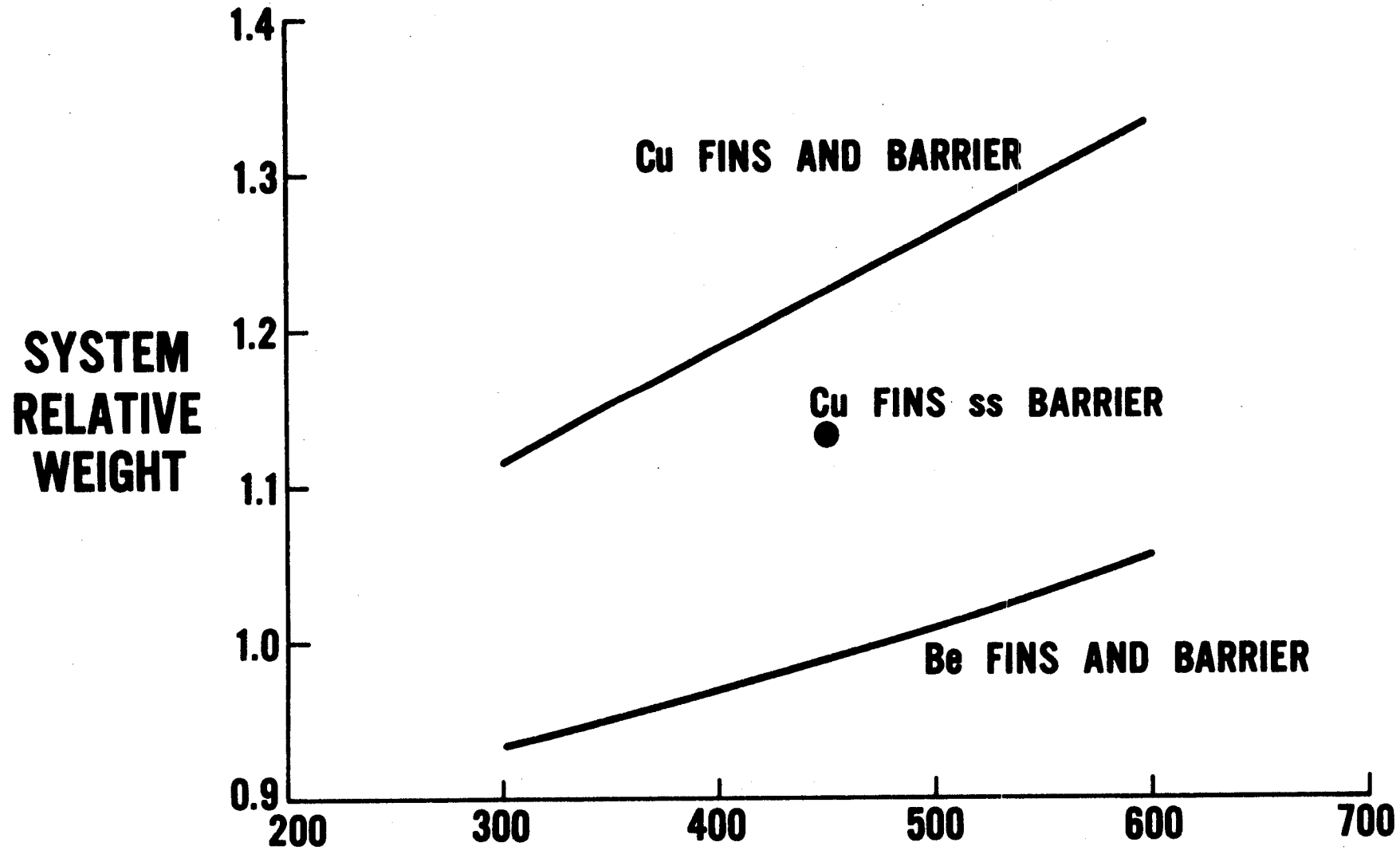

Pratt & Whitney Aircraft
DIVISION OF UNITED AIRCRAFT CORPORATION

M-37473
661003

E-910262-6

Figure No. VI-36

LOW ACCELERATION SPACE TRANSPORTATION
VARIATION IN SPECIFIC WEIGHT WITH MAJOR POWERPLANT PARAMETERS

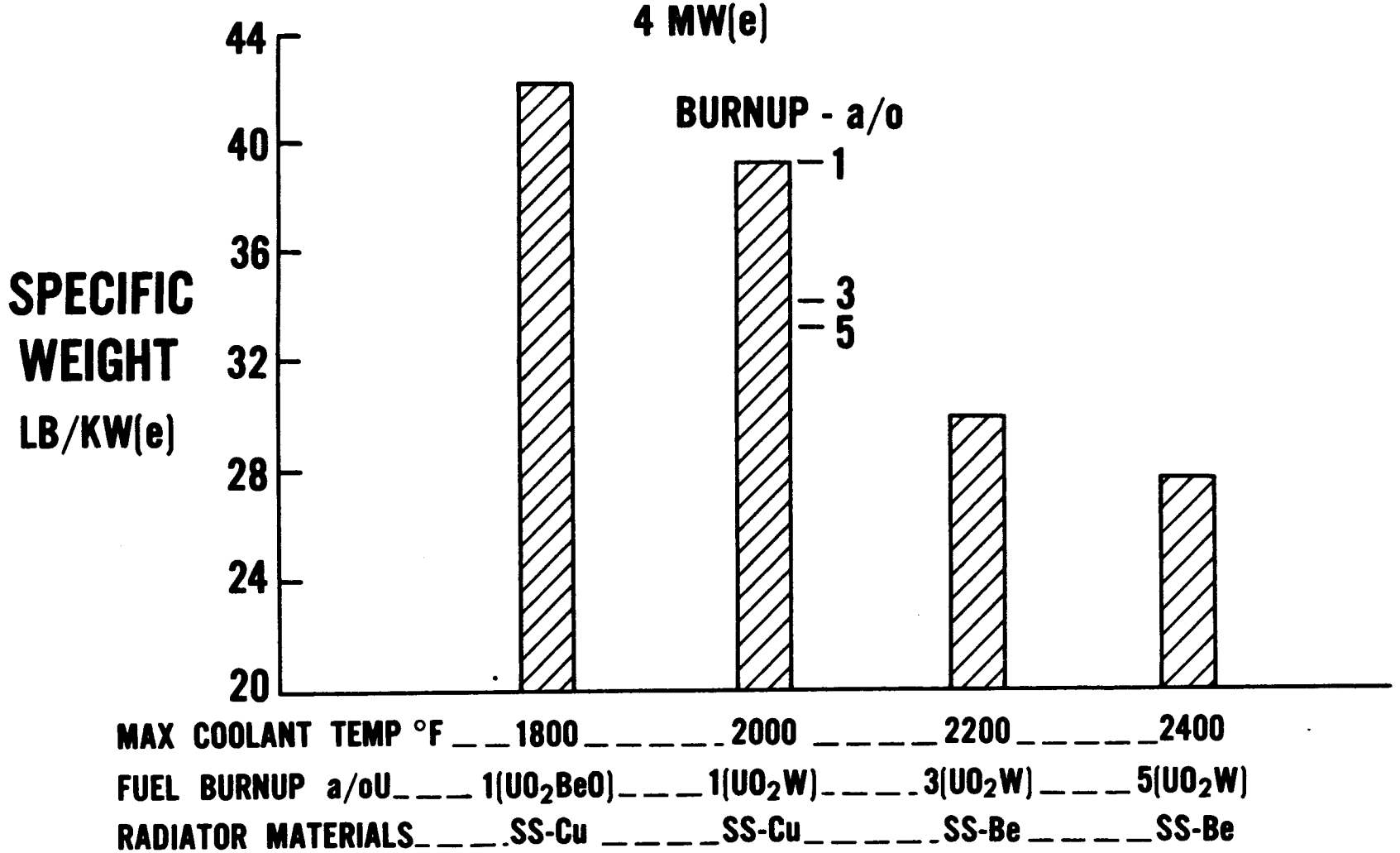

Pratt & Whitney Aircraft
DIVISION OF UNITED AIRCRAFT CORPORATION

M-37474
661003

E-910262-6

Figure No. VI-37

LOW ACCELERATION SPACE TRANSPORTATION

VARIATION IN MIEO WITH MAJOR POWERPLANT PARAMETERS

4 MW(e), 0.99 PROBABILITY, IMPROVED FAILURE RATES

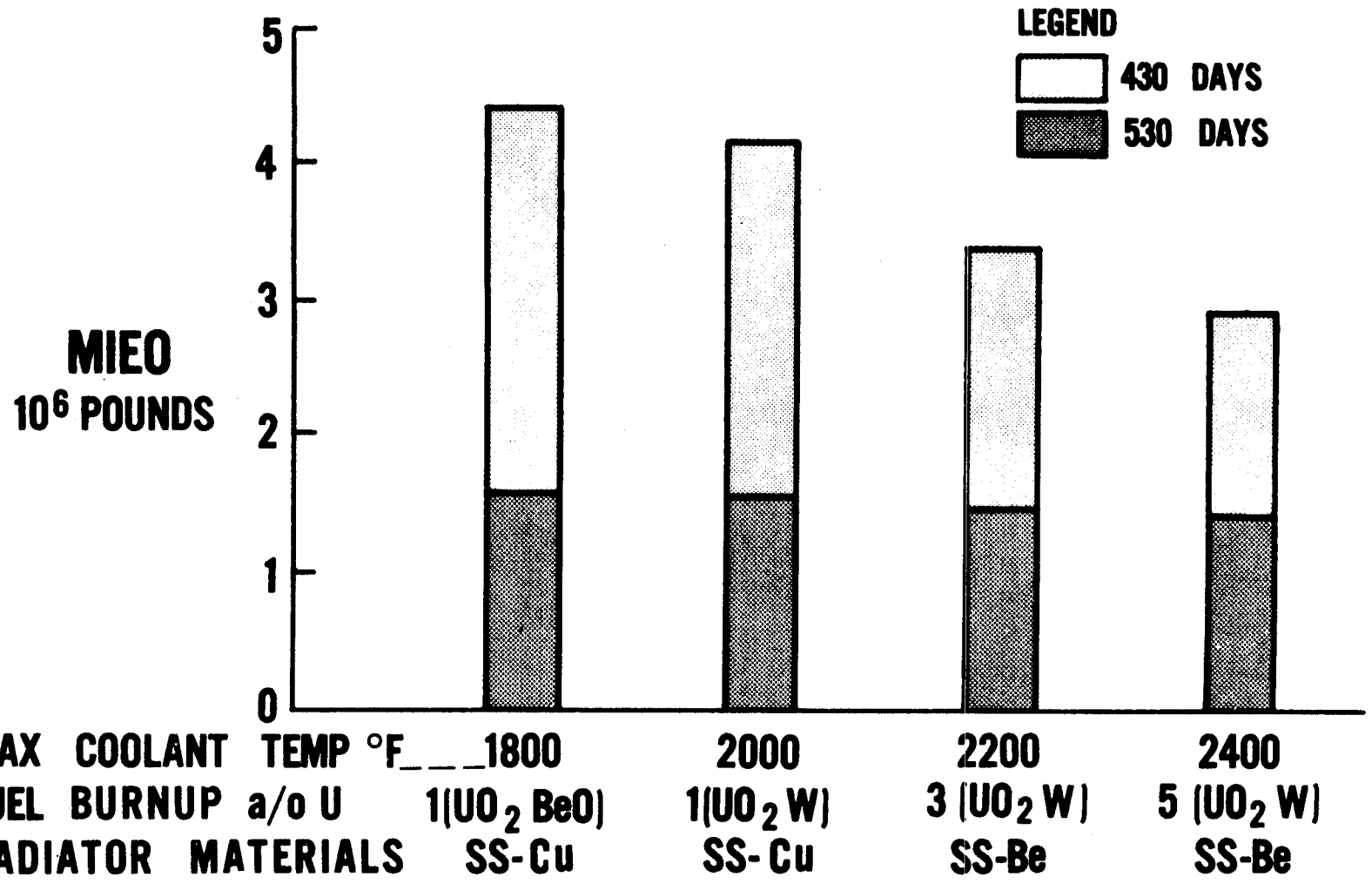

Pratt & Whitney Aircraft
DIVISION OF UNITED AIRCRAFT CORPORATION

M-38936
R660108

Figure VI-38

LOW ACCELERATION SPACE TRANSPORTATION

SYSTEM ARRANGEMENTS AND SHIELDING

SECONDARY SHIELD

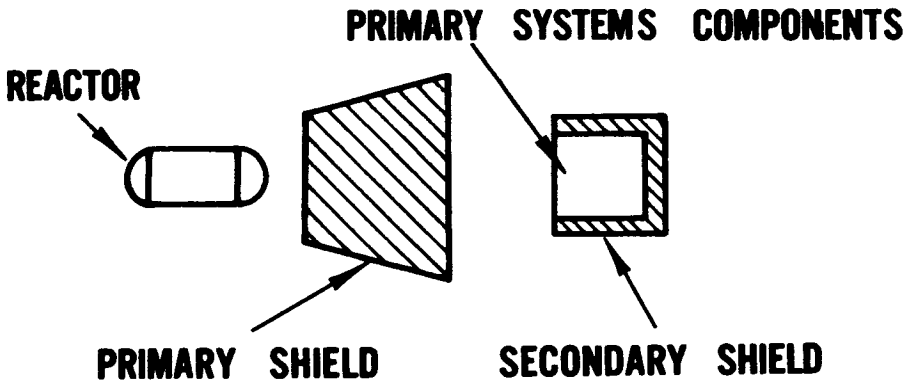

SHIELDED PRIMARY

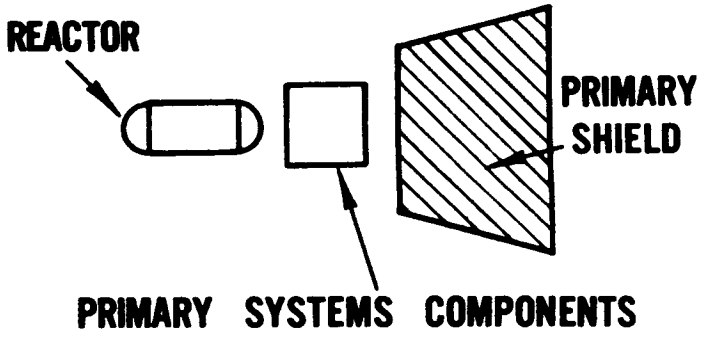

INTERMEDIATE LOOP

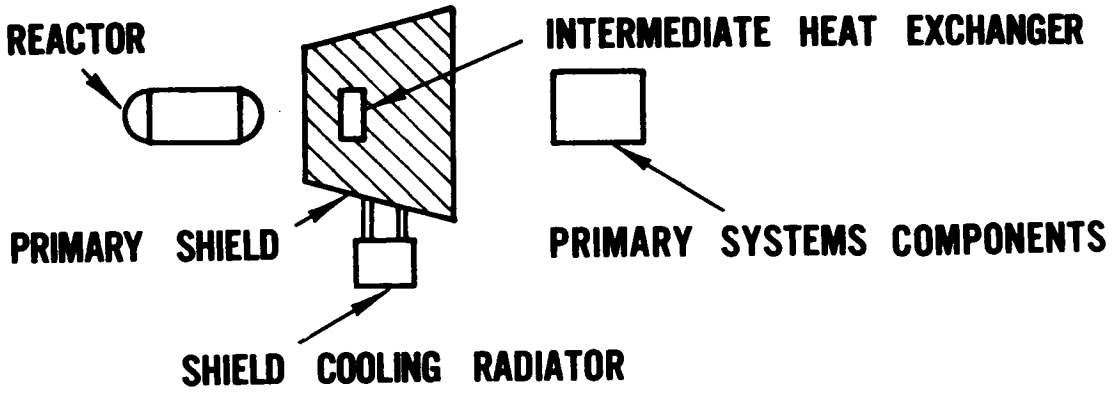

E-910262-6

Figure No. VI-39

Pratt & Whitney Aircraft
DIVISION OF UNITED AIRCRAFT CORPORATION

M-37526

661103

LOW ACCELERATION SPACE TRANSPORTATION
SECONDARY SHIELD

E-910262-6

SHIELD SPECIFIC WEIGHT 30 LB/KW(e)

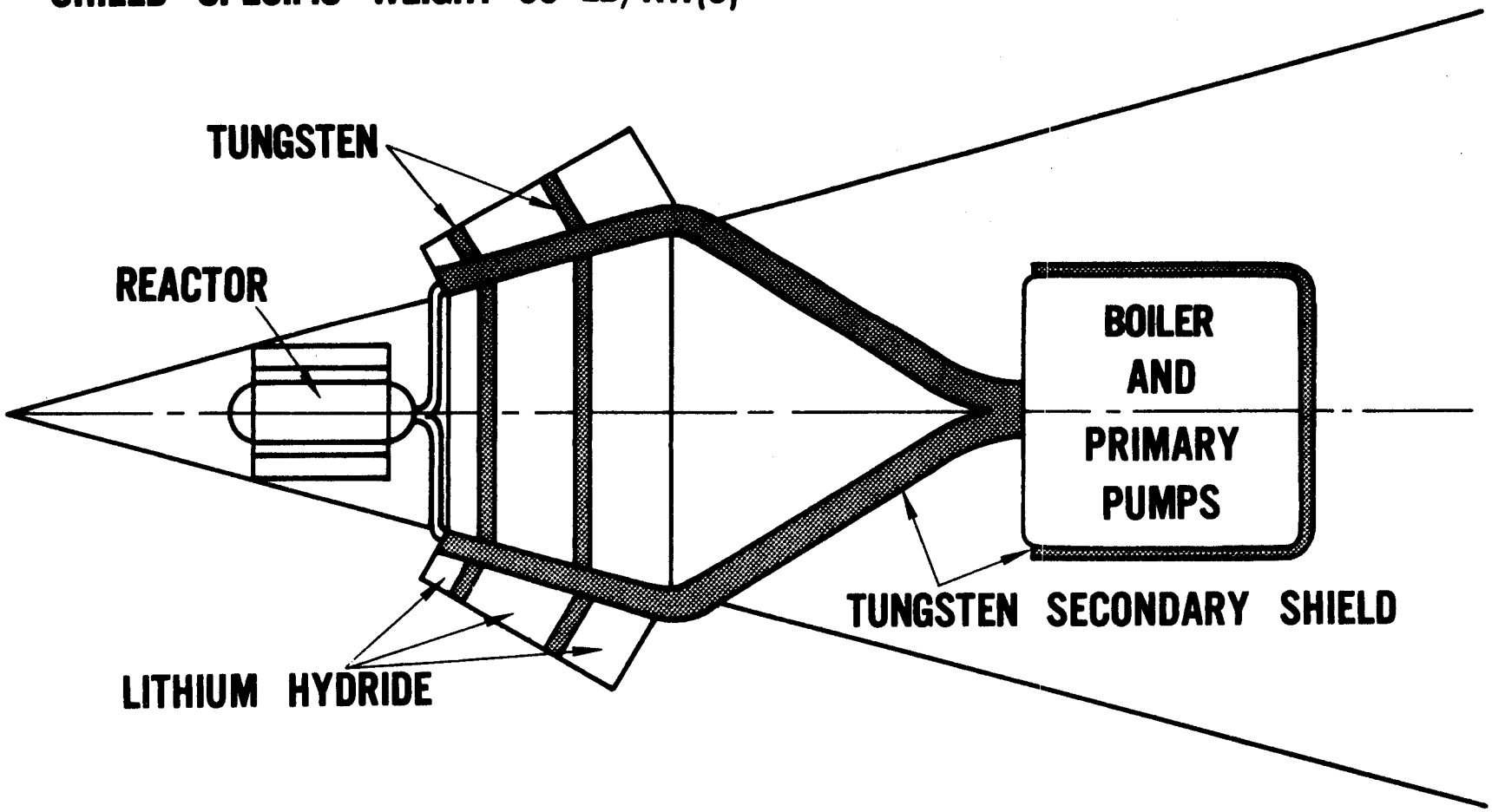

Pratt & Whitney Aircraft
DIVISION OF UNITED AIRCRAFT CORPORATION

M-37477
661003

Figure No. VI-40

LOW ACCELERATION SPACE TRANSPORTATION
SHIELDED PRIMARY SYSTEM

SHIELD SPECIFIC WEIGHT 37 LB/KW(e)

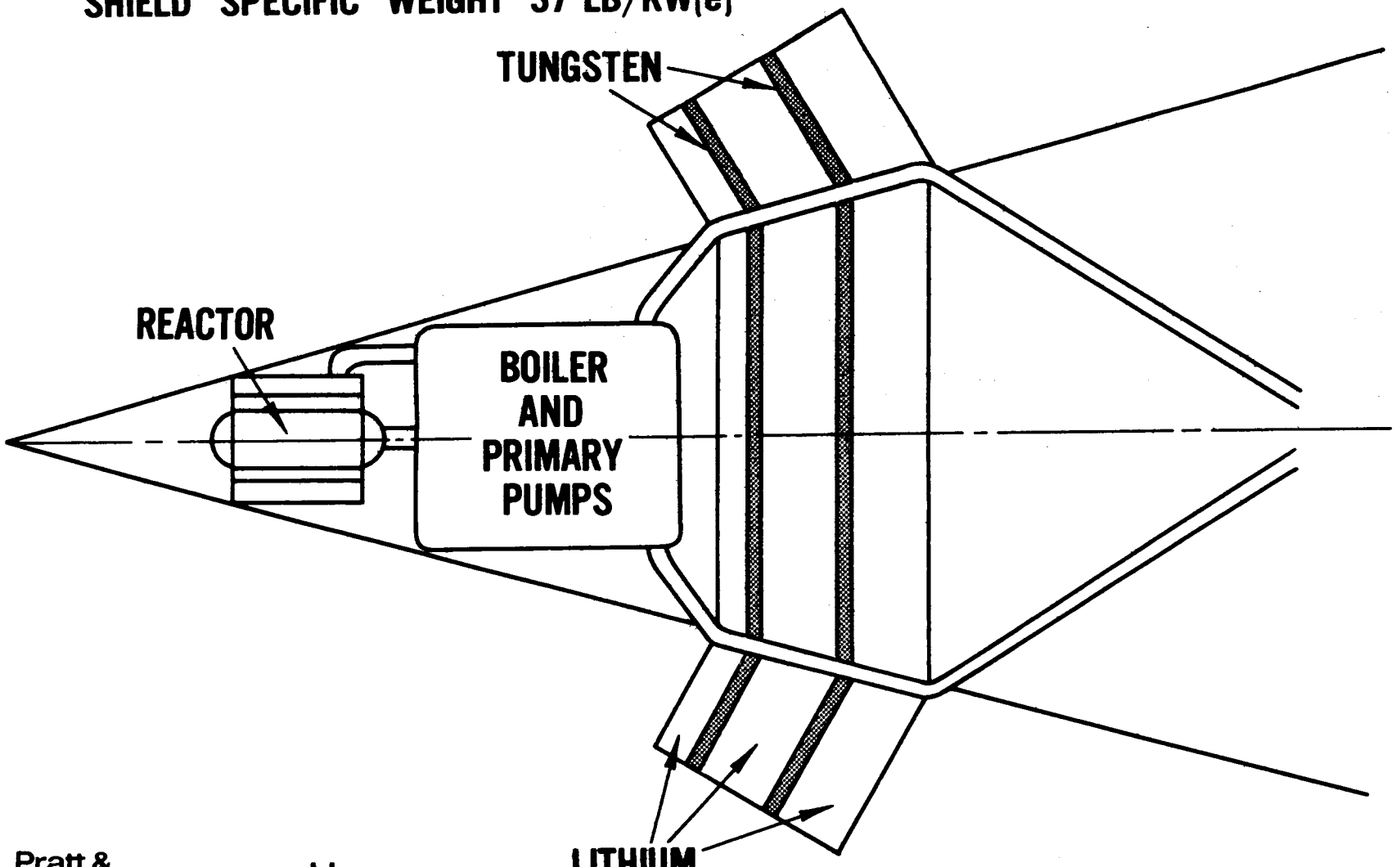

Pratt & Whitney Aircraft
DIVISION OF UNITED AIRCRAFT CORPORATION

M-37476
661003

E-910262-6

Figure No. VI-41

LOW ACCELERATION SPACE TRANSPORTATION
EFFECT OF SHIELDING ENTIRE PRIMARY SYSTEM

∞ SPARES

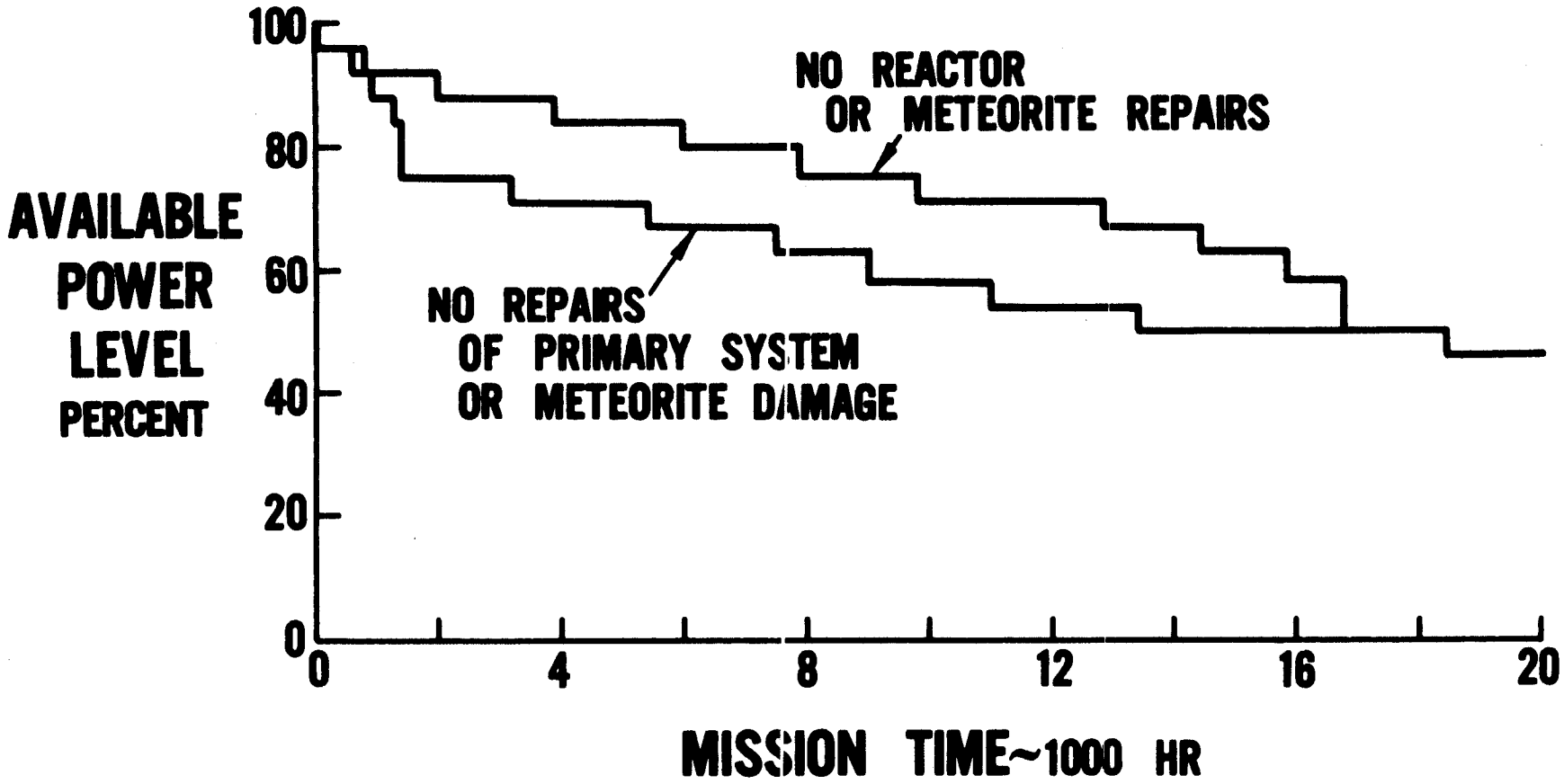

Pratt & Whitney Aircraft
DIVISION OF UNITED AIRCRAFT CORPORATION

M-37442
661003

E-910262-6

Figure No. VI-42

LOW ACCELERATION SPACE TRANSPORTATION

INTERMEDIATE LOOP

SHIELD SPECIFIC WEIGHT 15 LB/KW(e)

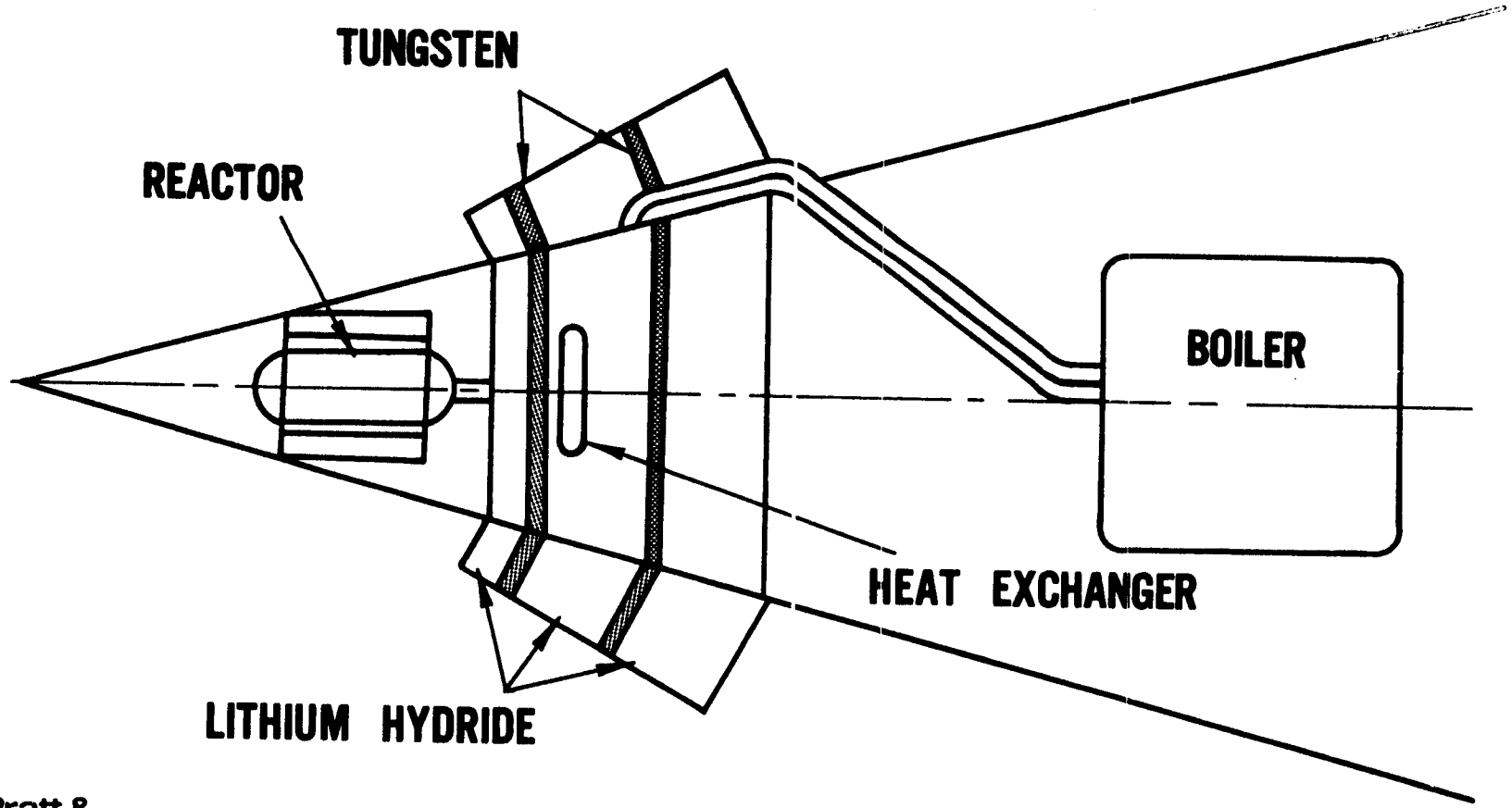

Pratt & Whitney Aircraft

DIVISION OF UNITED AIRCRAFT CORPORATION

M-37475
661003

E-910262-6

Figure No. VI-43

LOW ACCELERATION SPACE TRANSPORTATION

EFFECT OF ADDING INTERMEDIATE LOOP

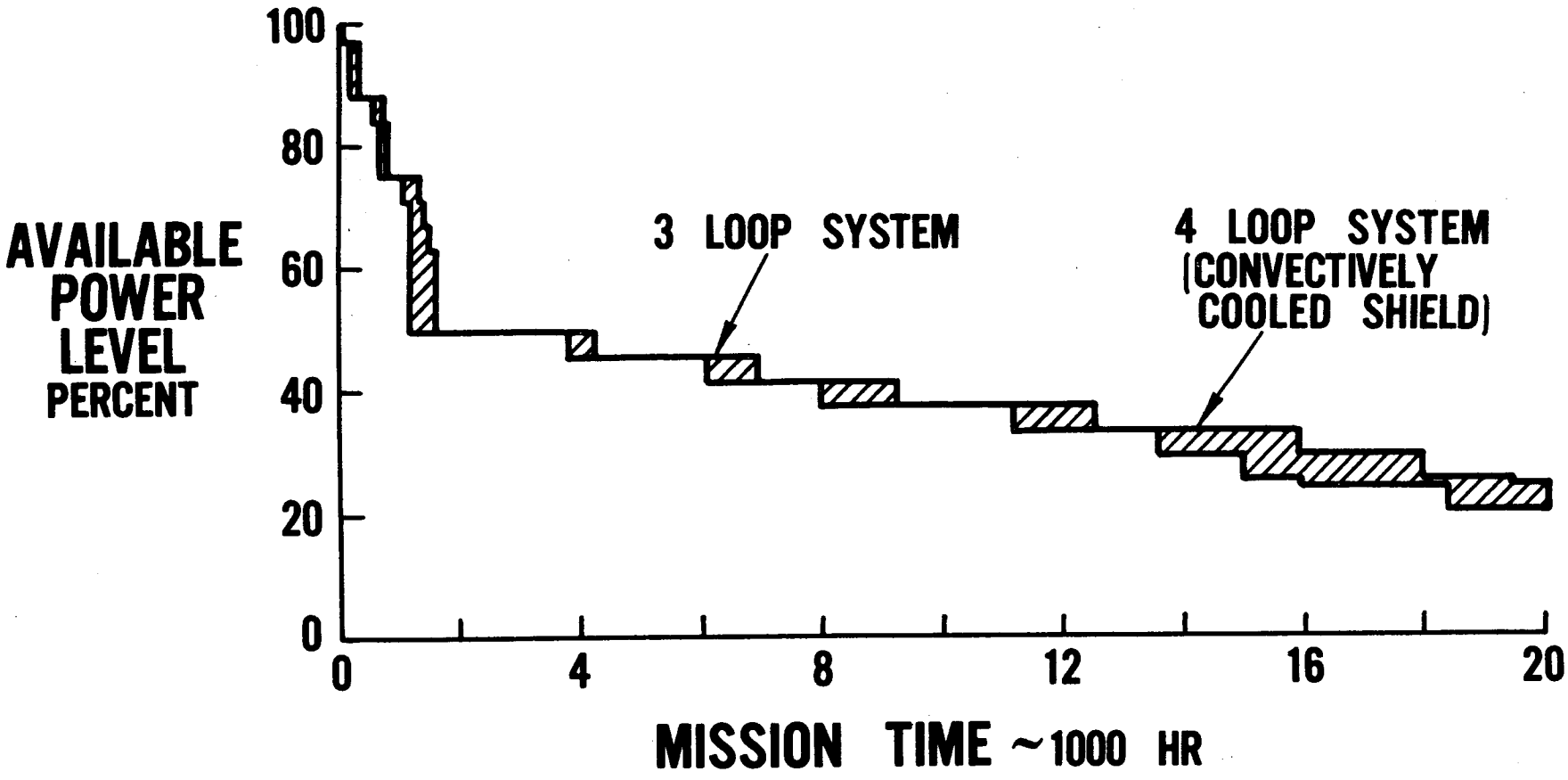

Pratt & Whitney Aircraft

DIVISION OF UNITED AIRCRAFT CORPORATION

M-37472
661003

E-910262-6

Figure No. VI-44

LOW ACCELERATION SPACE TRANSPORTATION

EFFECT OF CREW DOSE ON SHIELD WEIGHT

MAINTENANCE DOSE = 10 M rem/HR

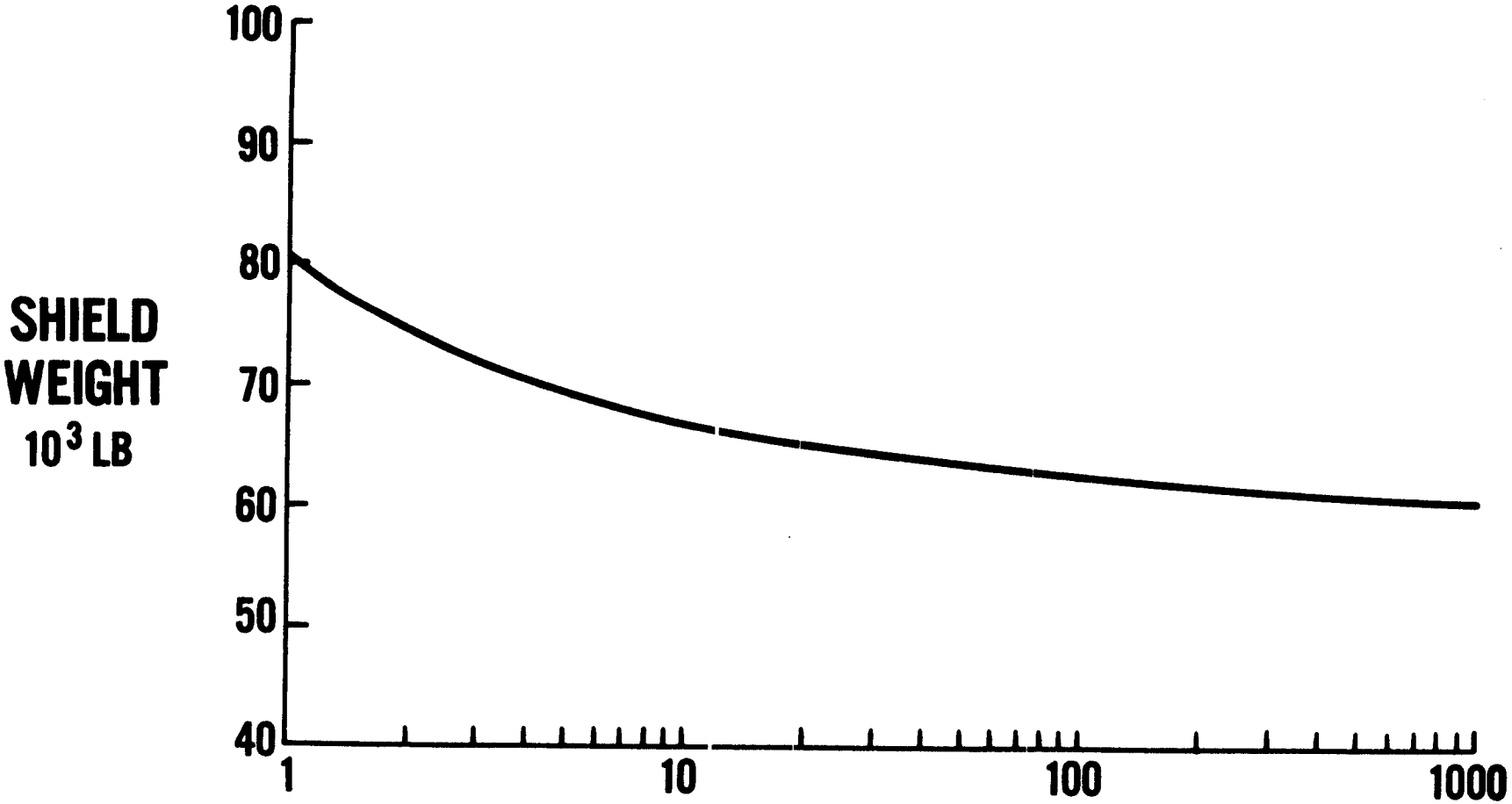

Pratt & Whitney Aircraft
DIVISION OF UNITED AIRCRAFT CORPORATION

M-37512
661503

E-910262-6

Figure No. VI-45

LOW ACCELERATION SPACE TRANSPORTATION
EFFECT OF MAINTENANCE DOSE RATE ON SHIELD WEIGHT

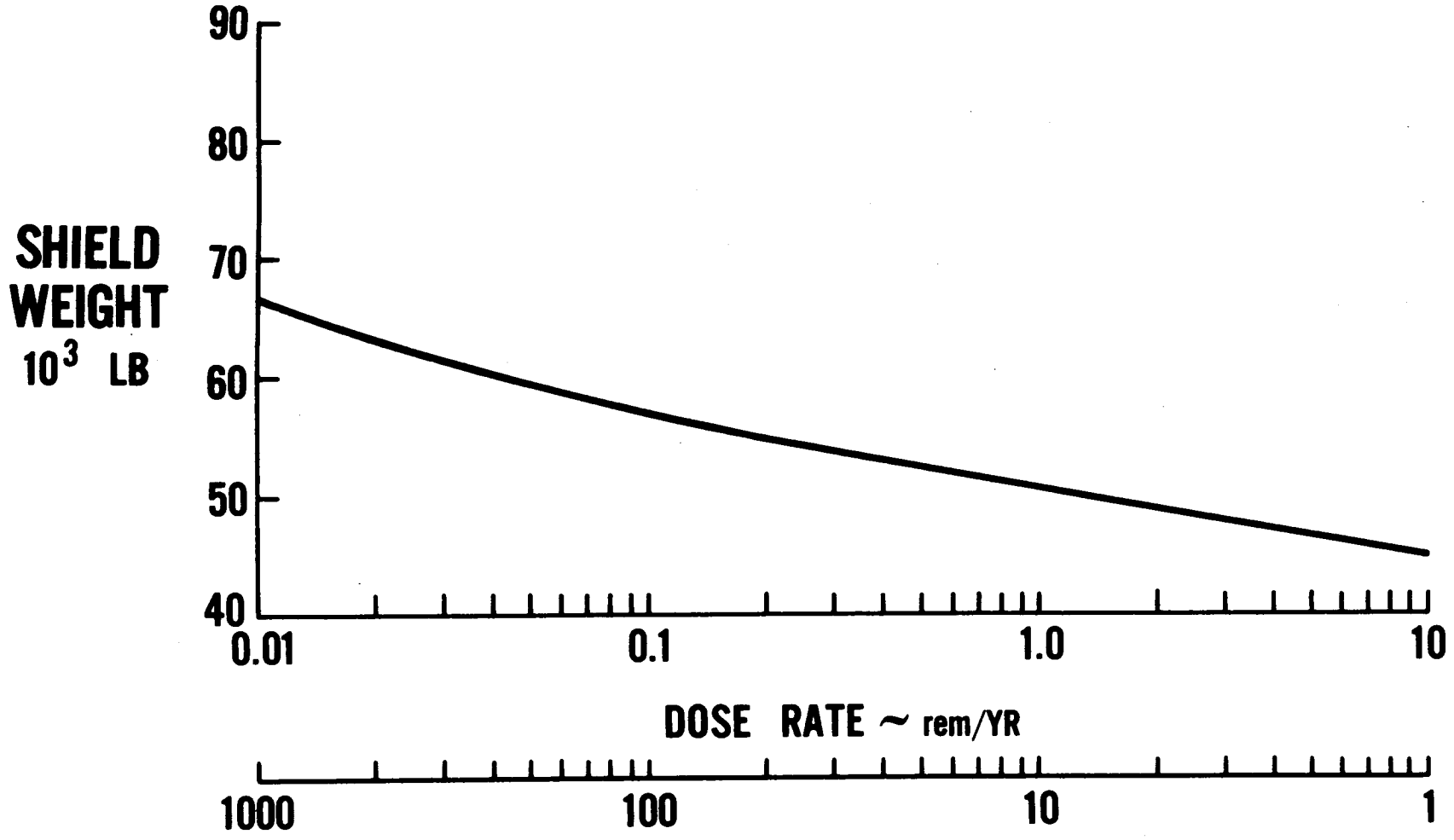

Pratt & Whitney Aircraft
DIVISION OF UNITED AIRCRAFT CORPORATION

M-37511
661503

E-910262-6

Figure No. VI-46

GAS TURBINE DEVELOPMENT PROGRAM CHARACTERISTICS

BASED ON P&WA EXPERIENCE

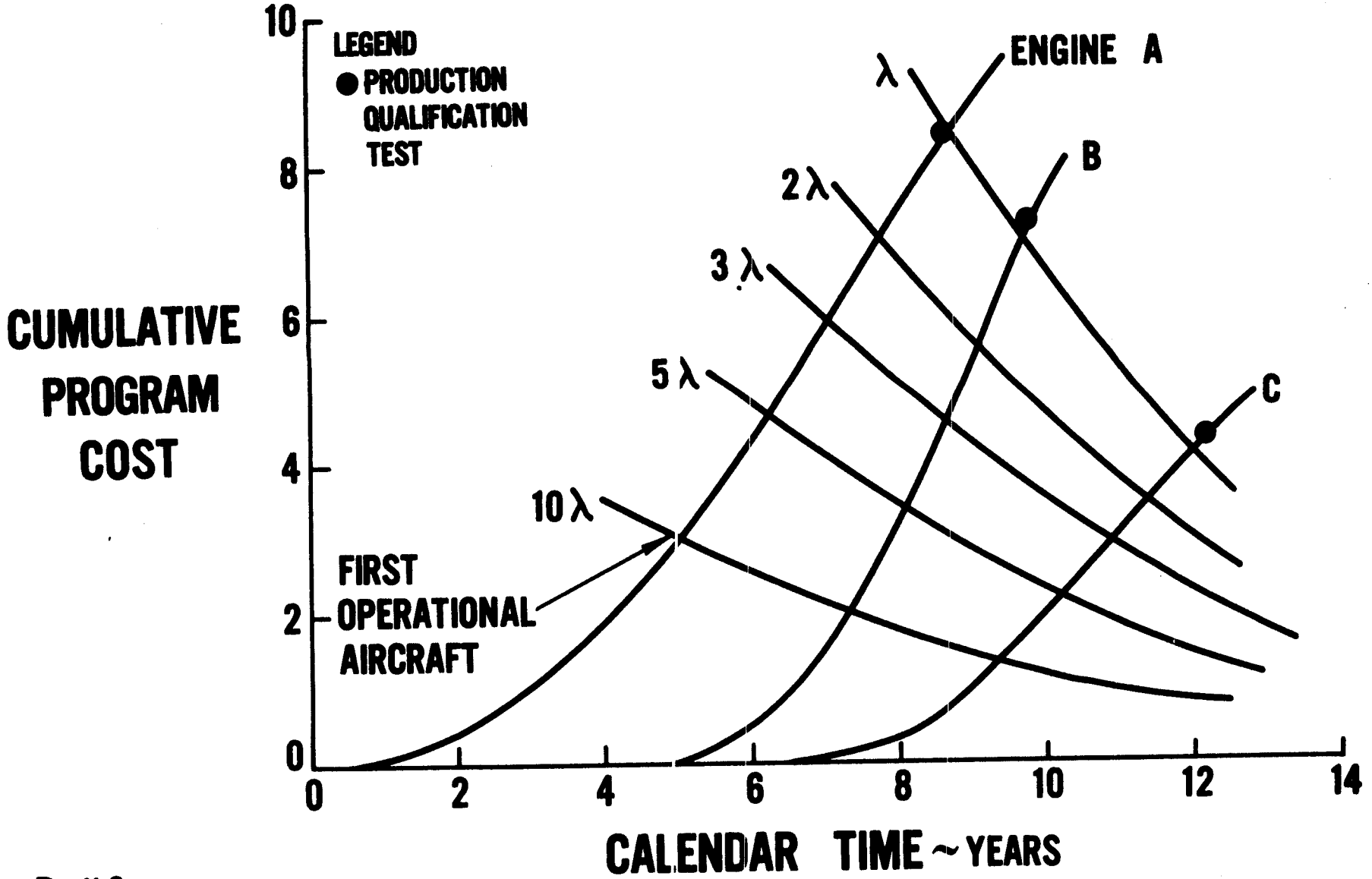

Pratt & Whitney Aircraft

DIVISION OF UNITED AIRCRAFT CORPORATION

M-38902

Figure VI-47

TYPICAL COMPONENT FAILURE RATE HISTORY

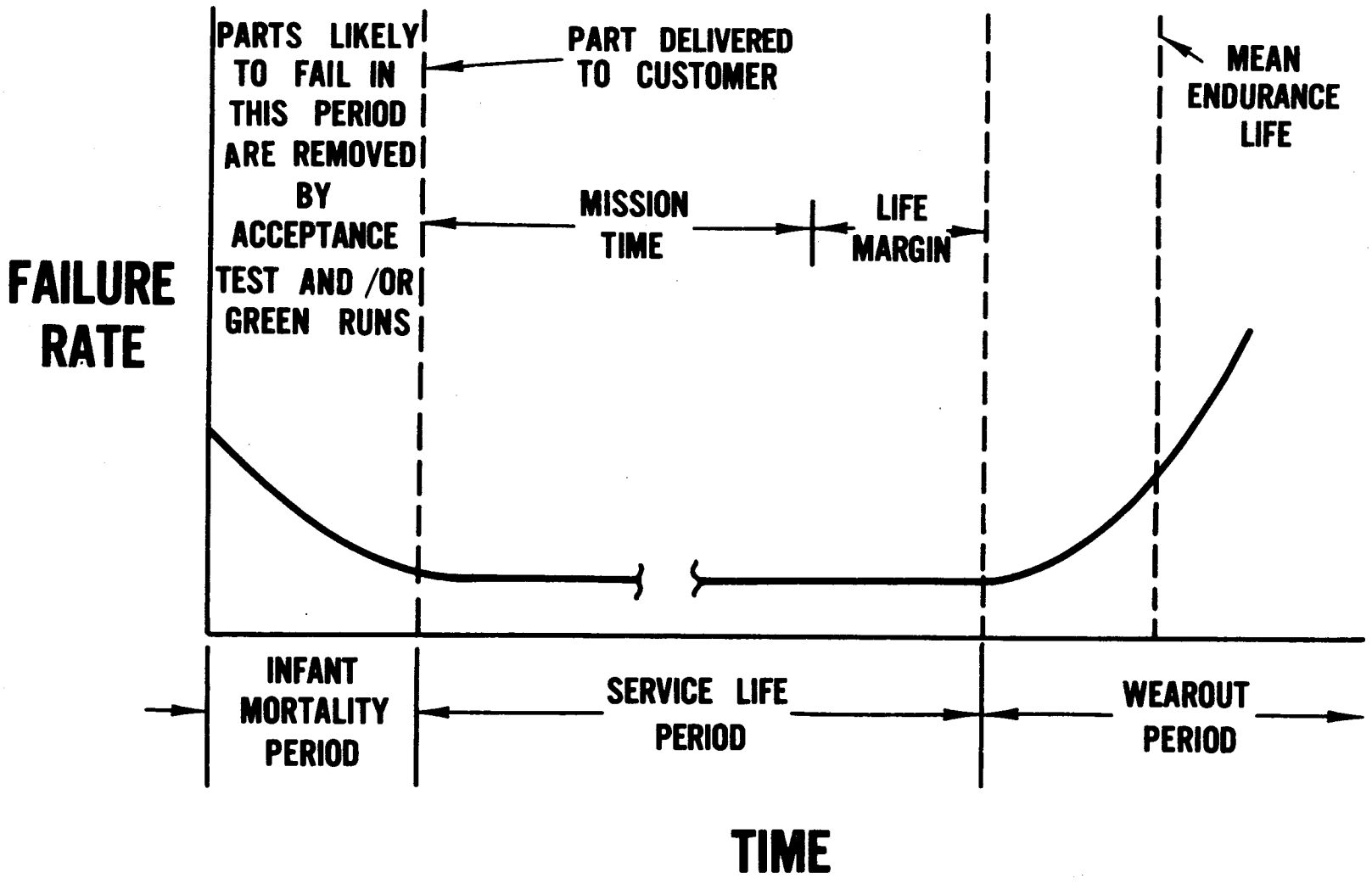

Pratt & Whitney Aircraft
DIVISION OF UNITED AIRCRAFT CORPORATION

M-36321
660801

Figure VI-48

LOW ACCELERATION SPACE TRANSPORTATION

DEVELOPMENT PROGRAM SCHEDULE

1800°F 1 a/o BURNUP SYSTEM

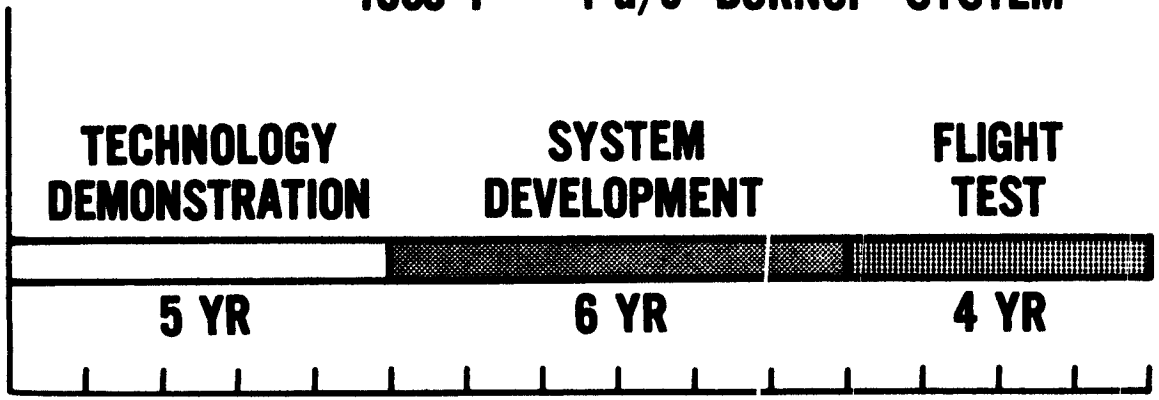

SERIES

TOTAL–15 YEARS

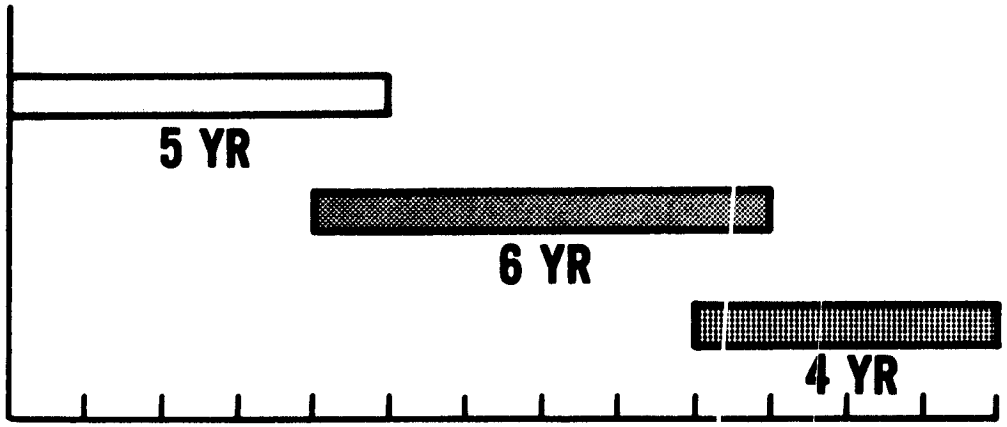

PARALLEL

TOTAL–13 YEARS

Pratt & Whitney Aircraft
DIVISION OF UNITED AIRCRAFT CORPORATION

M-39034
660107

Figure VI-49

SYSTEM DEVELOPMENT TEST SCHEDULE

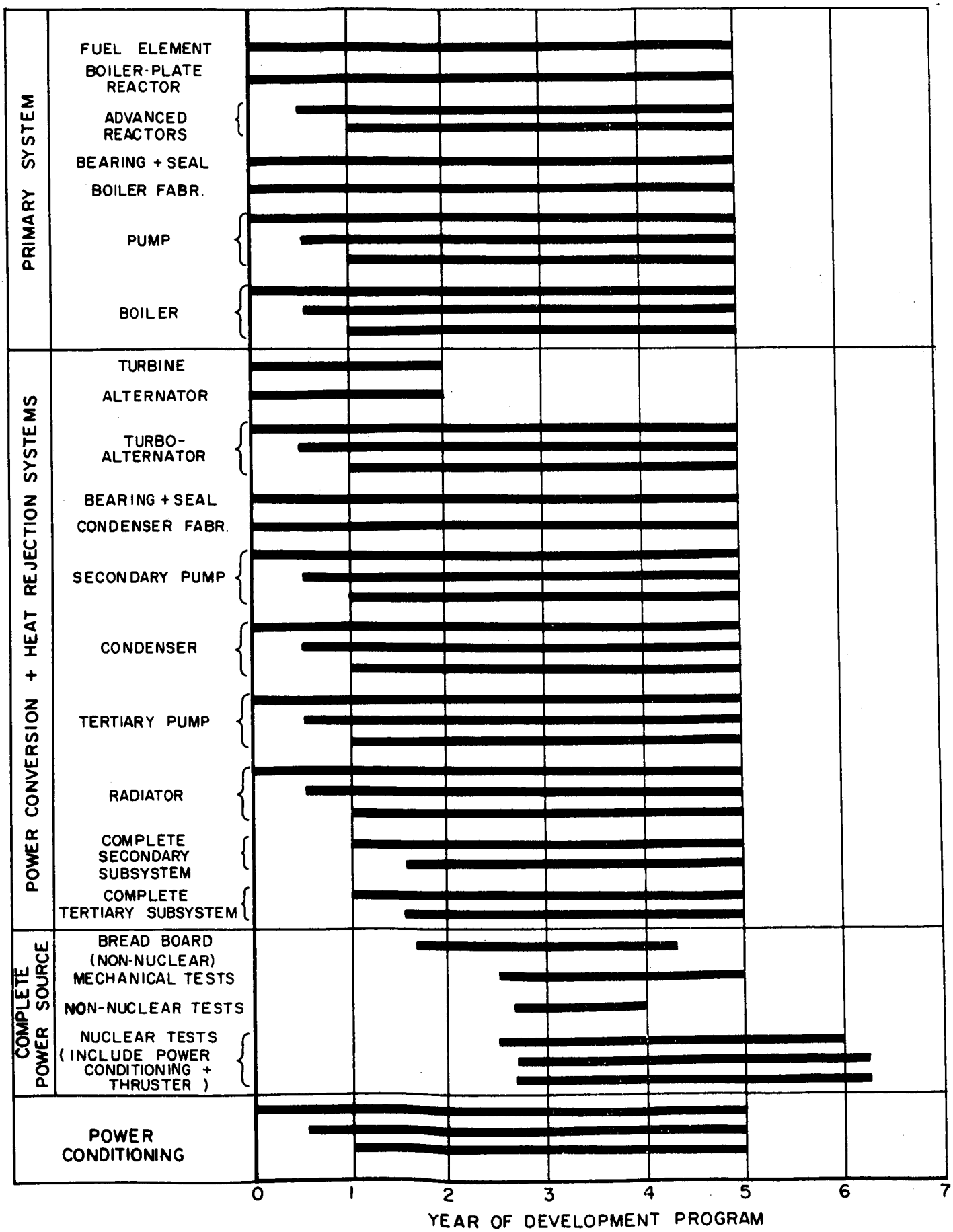

LOW ACCELERATION SPACE TRANSPORTATION

DEVELOPMENT PROGRAM COST

1800°F 1 a/o BURNUP

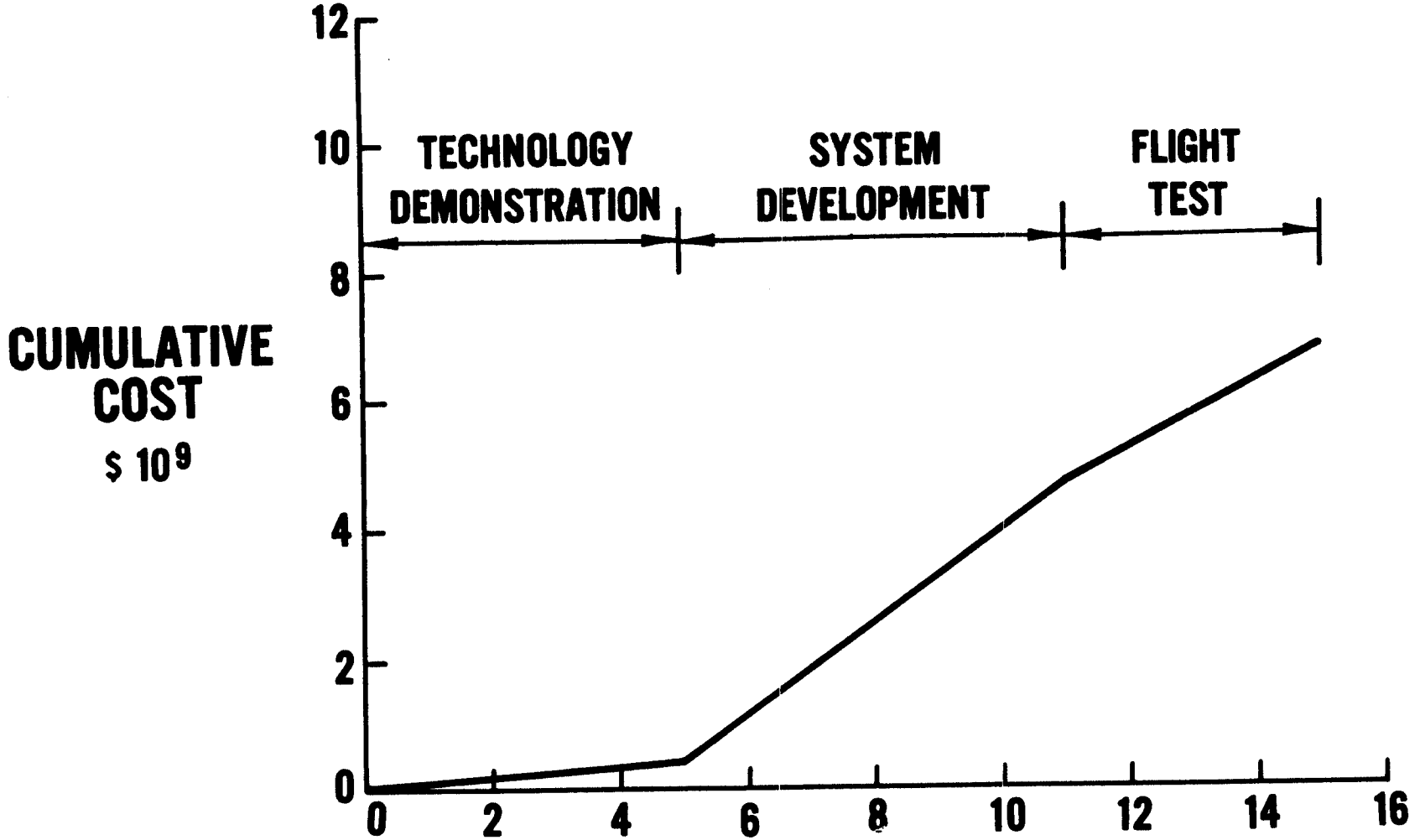

Pratt & Whitney Aircraft

DIVISION OF UNITED AIRCRAFT CORPORATION

M-39037
660107

Figure VI-51

LOW ACCELERATION SPACE TRANSPORTATION

TRIP COSTS AS A FUNCTION OF NUMBER OF MISSIONS

MANNED MARS MISSION

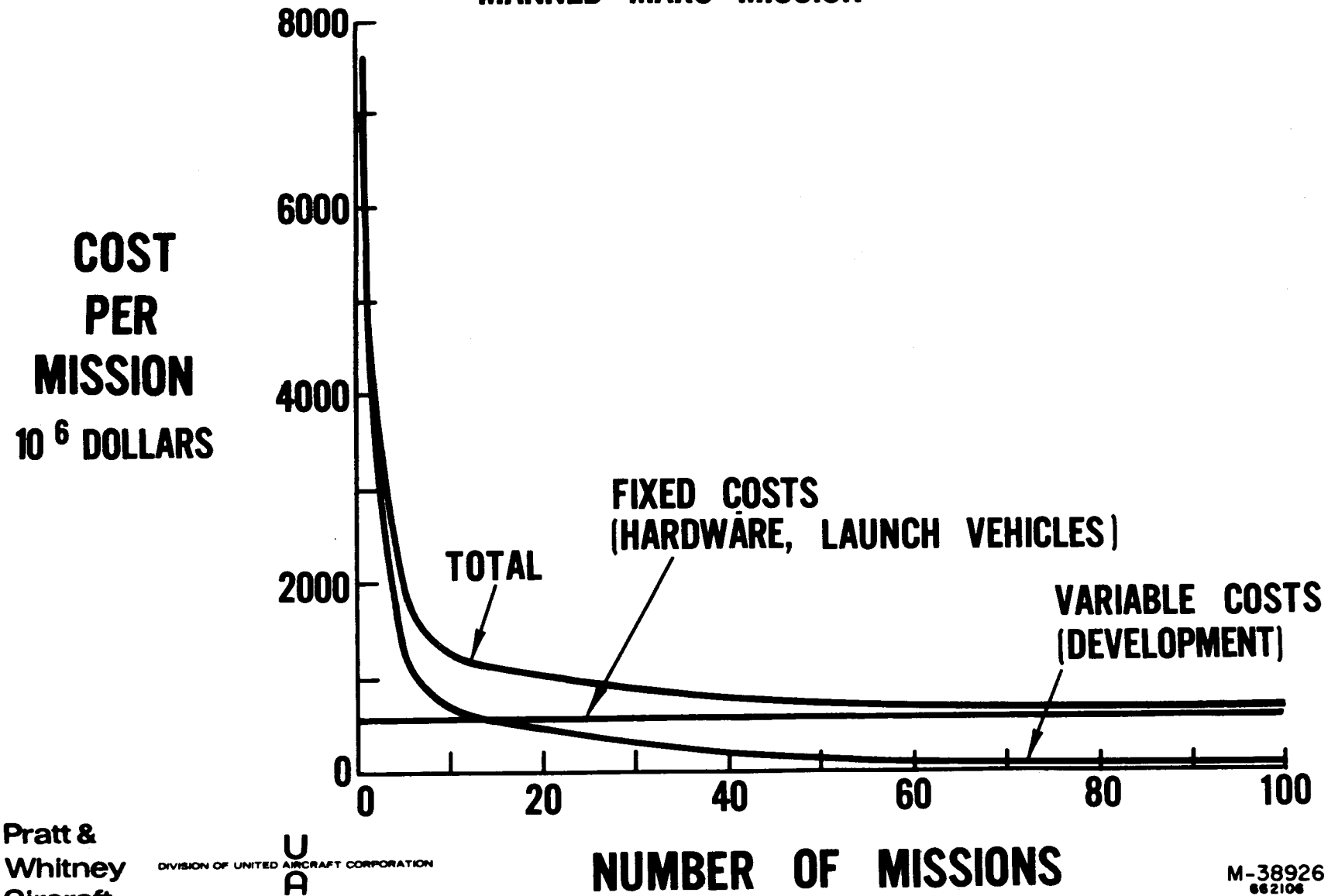

Pratt & Whitney Aircraft
DIVISION OF UNITED AIRCRAFT CORPORATION

M-38926
662106

Figure VI-5

INFLUENCE OF SYSTEM MASS ON R & D COST FOR SYSTEMS OF SIMILAR STATE OF TECHNOLOGY

REFERENCE RM-4056-NASA

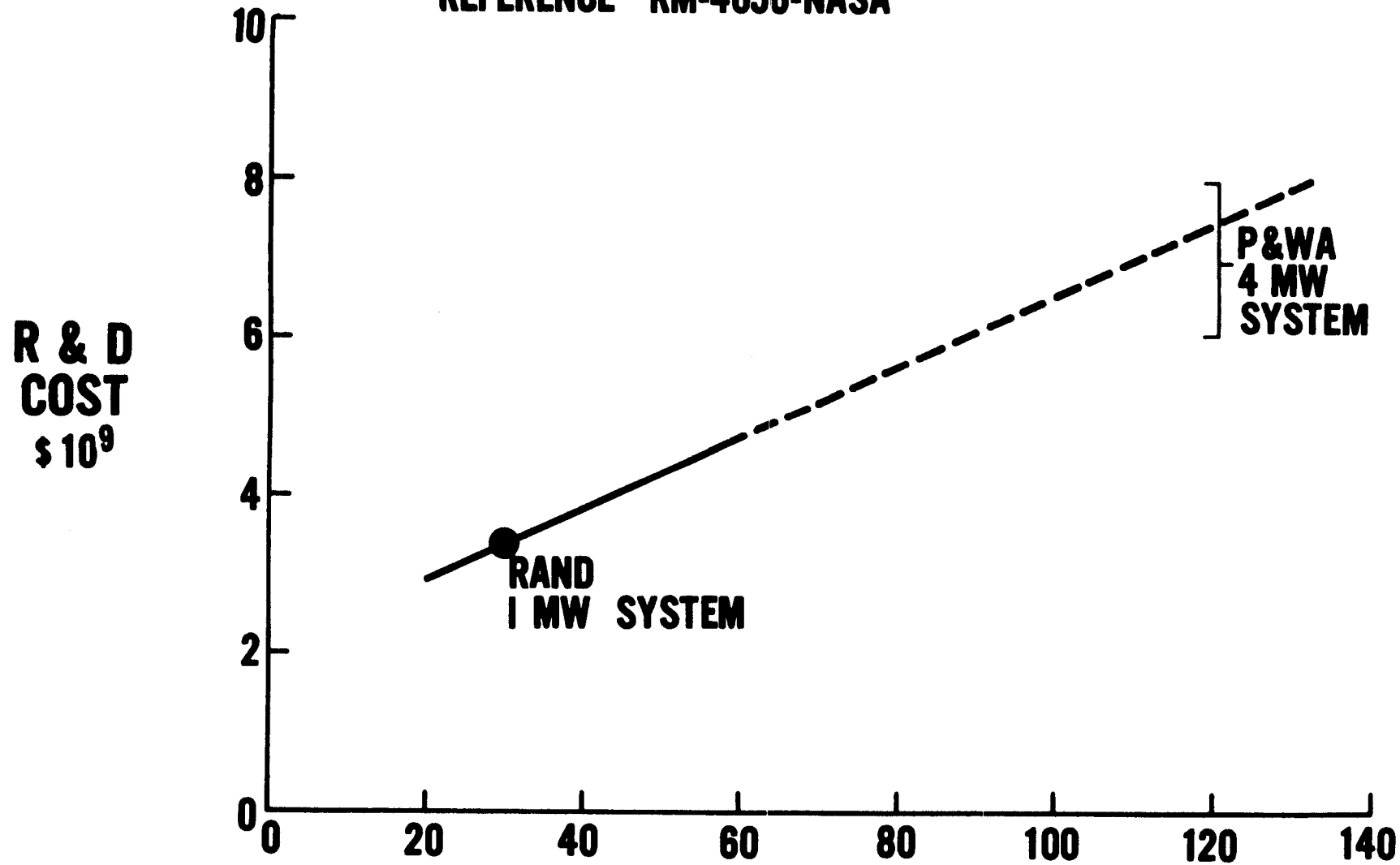

Pratt & Whitney Aircraft
DIVISION OF UNITED AIRCRAFT CORPORATION
UA

M-39063
R660108

FigureVI-53

LOW ACCELERATION SPACE TRANSPORTATION

DEVELOPMENT PROGRAM SCHEDULE

1800°F, 3 a/o BURNUP SYSTEM

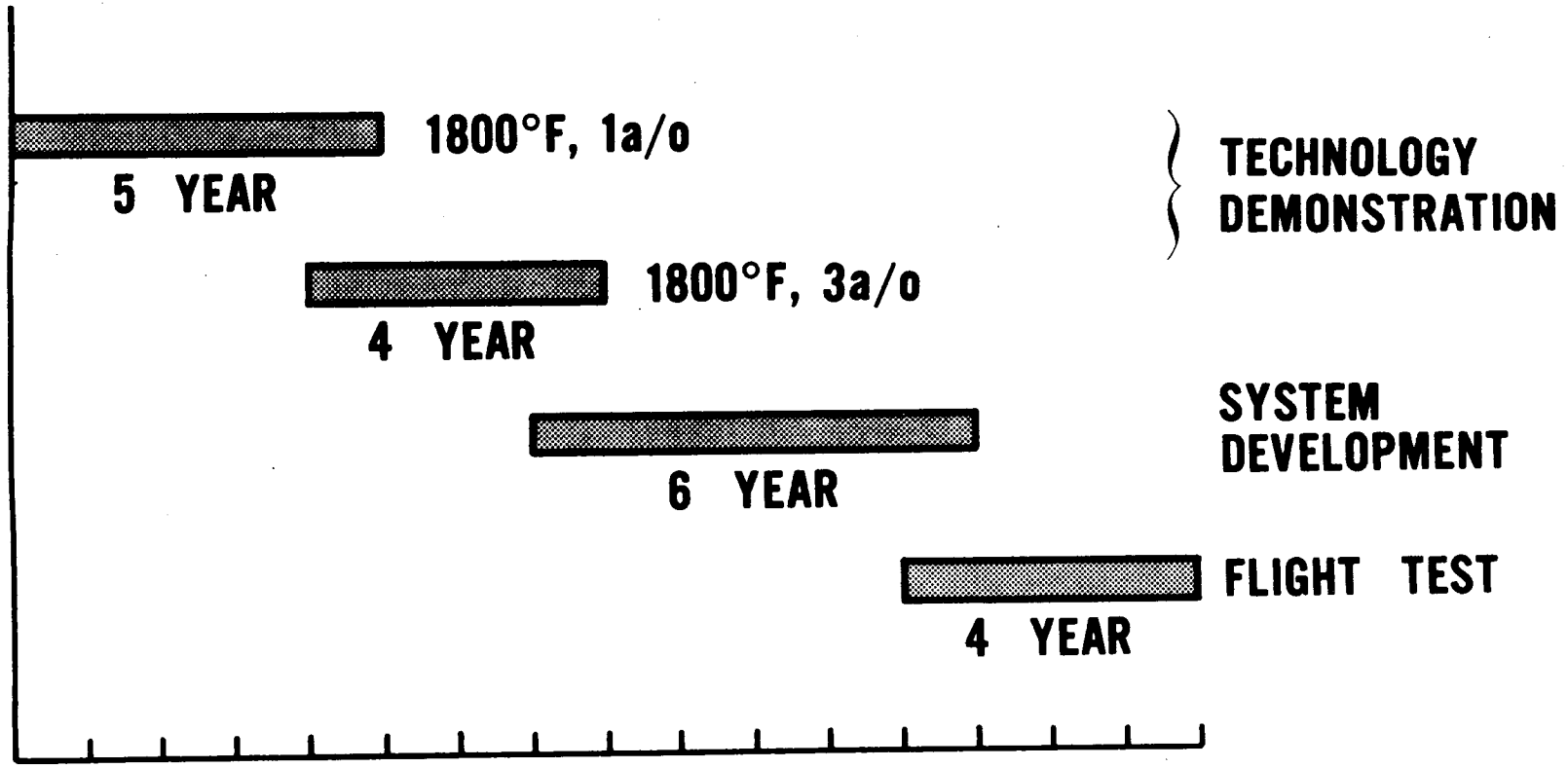

Pratt & Whitney Aircraft
DIVISION OF UNITED AIRCRAFT CORPORATION

M-39062
660107

Figure VI-54

LOW ACCELERATION SPACE TRANSPORTATION

DEVELOPMENT PROGRAM COST

1800°F 3 a/o BURNUP

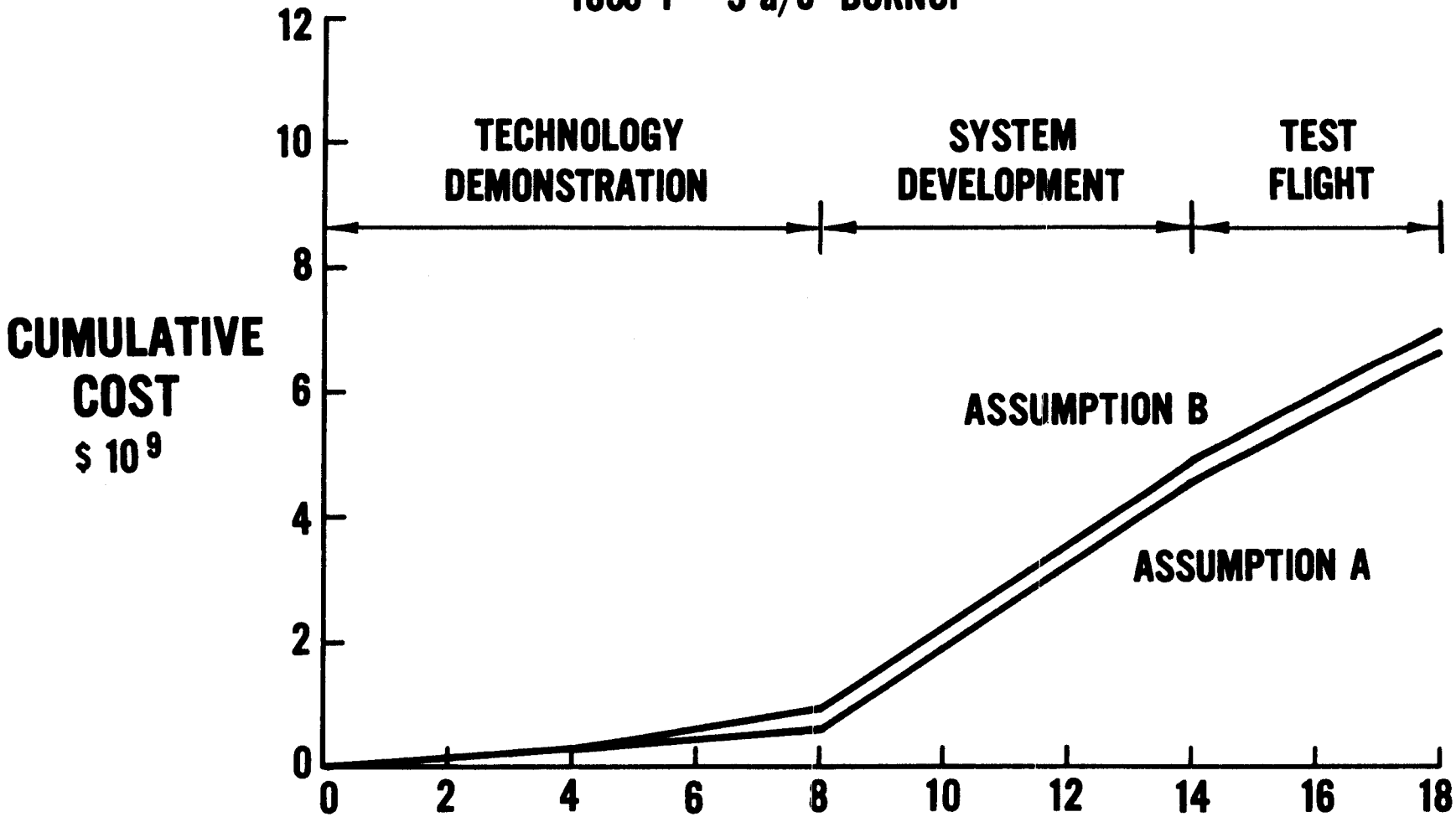

Pratt & Whitney Aircraft

DIVISION OF UNITED AIRCRAFT CORPORATION

M-39036
080107

Figure VI-55

LOW ACCELERATION SPACE TRANSPORTATION

TECHNOLOGY DEMONSTRATION SCHEDULE

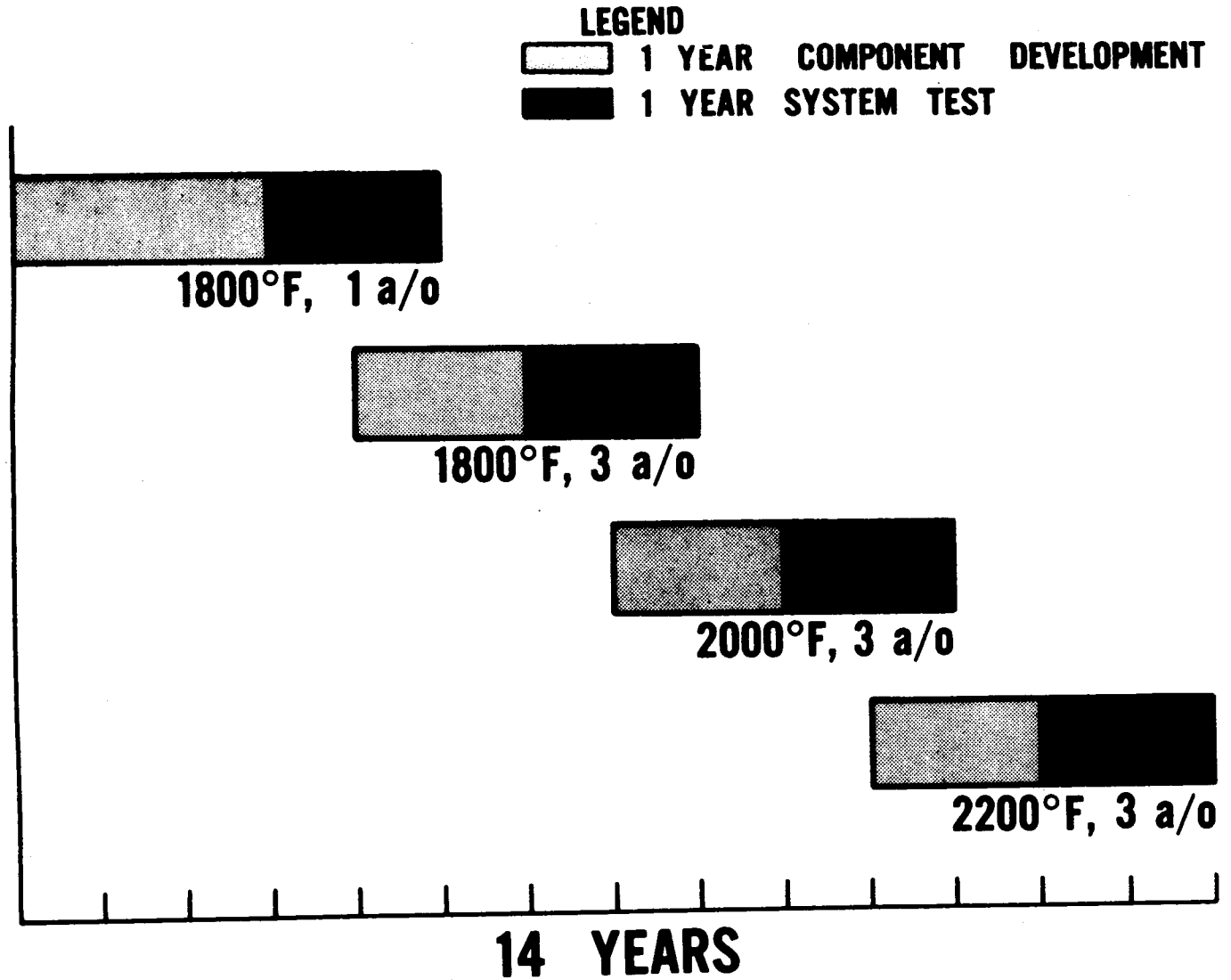

Pratt & Whitney Aircraft
DIVISION OF UNITED AIRCRAFT CORPORATION

M-39013
663006

Figure VI-56

LOW ACCELERATION SPACE TRANSPORTATION
DEVELOPMENT COSTS
AS A FUNCTION OF PEAK CYCLE TEMPERATURE

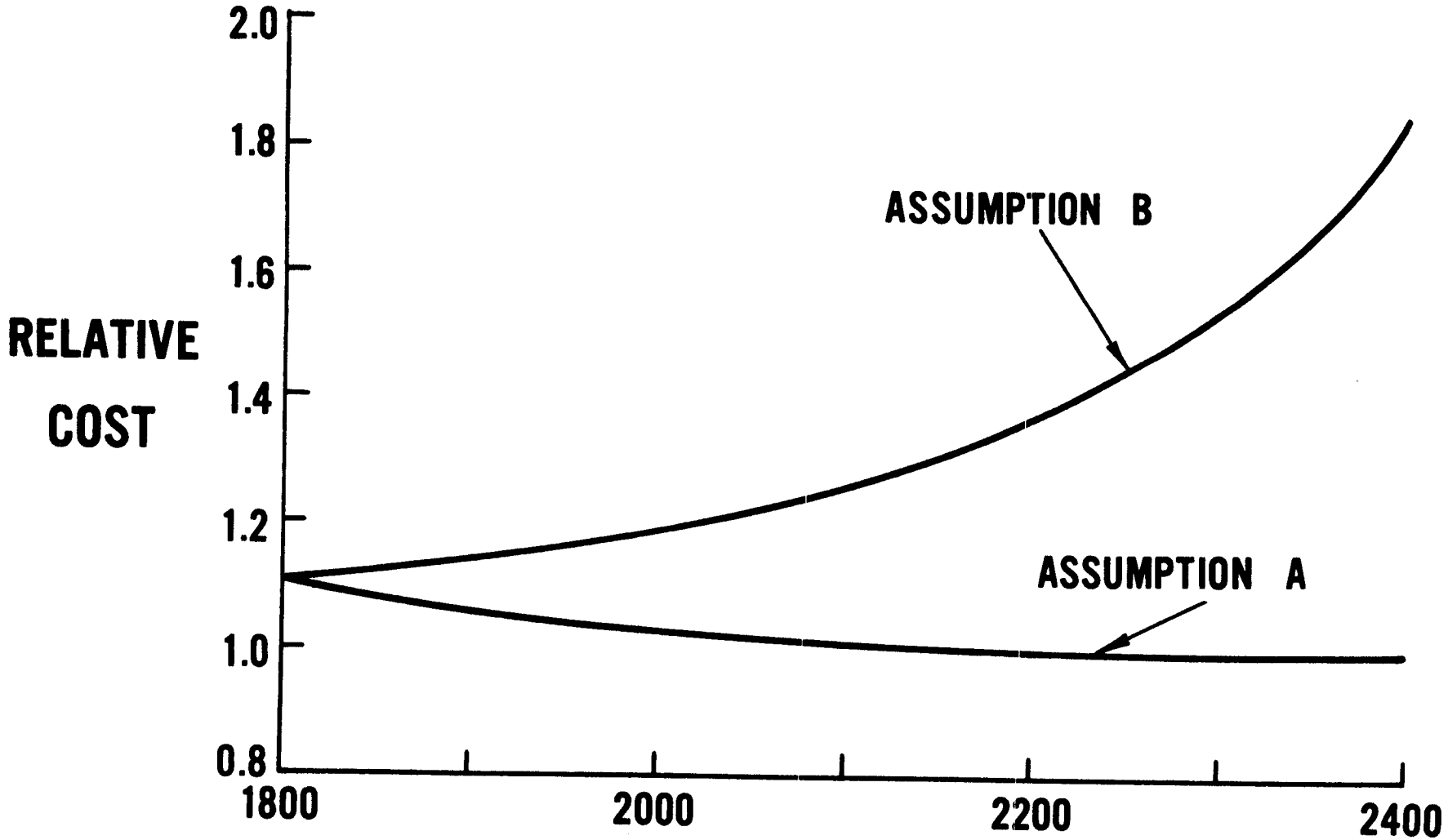

Pratt & Whitney Aircraft
DIVISION OF UNITED AIRCRAFT CORPORATION

M-39011
660107

Figure VI-57

LOW ACCELERATION SPACE TRANSPORTATION

INFLUENCE OF BURNUP ON DEVELOPMENT COSTS

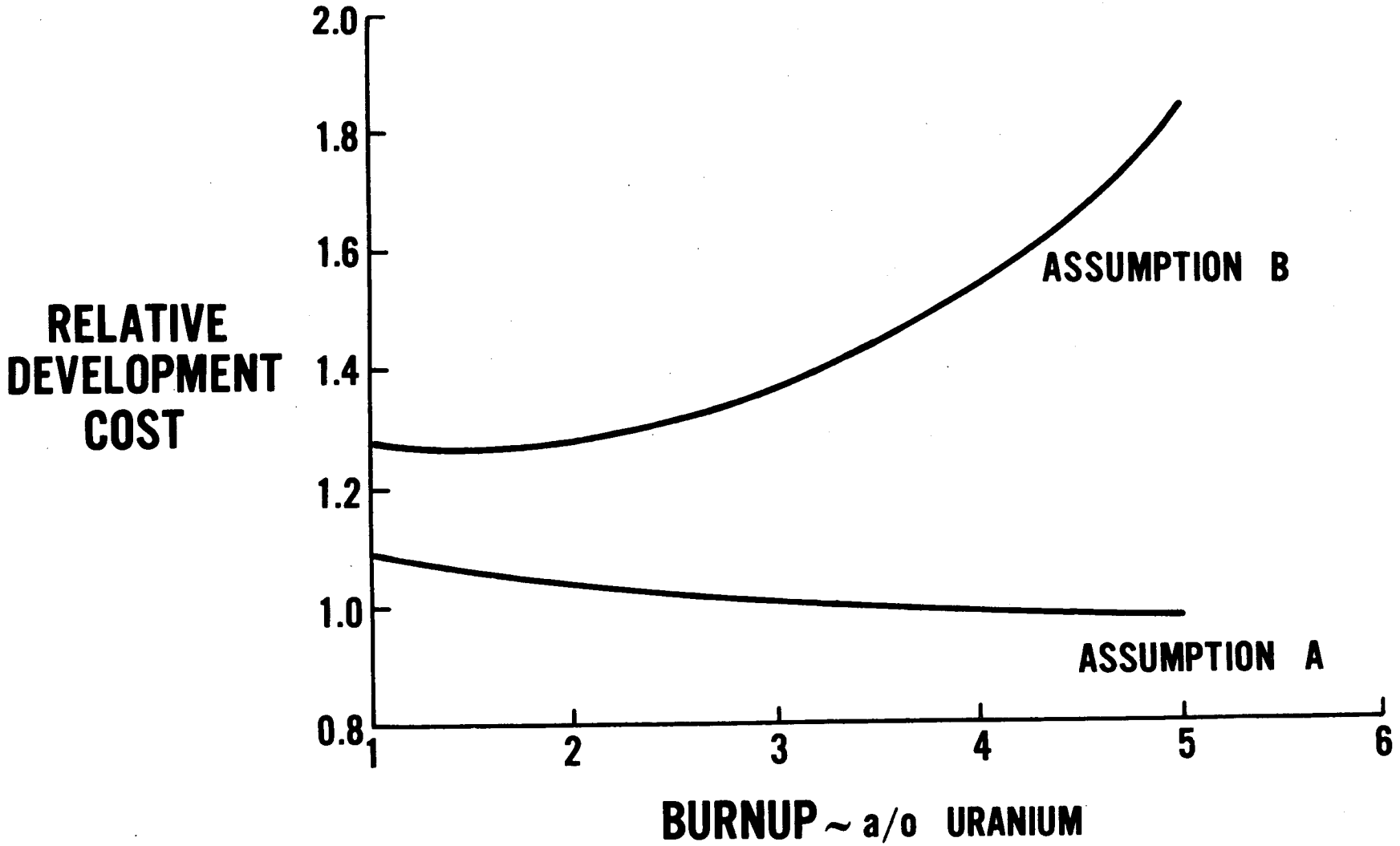

Pratt & Whitney Aircraft
DIVISION OF UNITED AIRCRAFT CORPORATION

M-39008
663006

Figure VI-58

LOW ACCELERATION SPACE TRANSPORTATION

EFFECT OF PEAK CYCLE TEMPERATURE ON MISSION COST

530 DAYS ASSUMPTION a 0.99 PROBABILITY

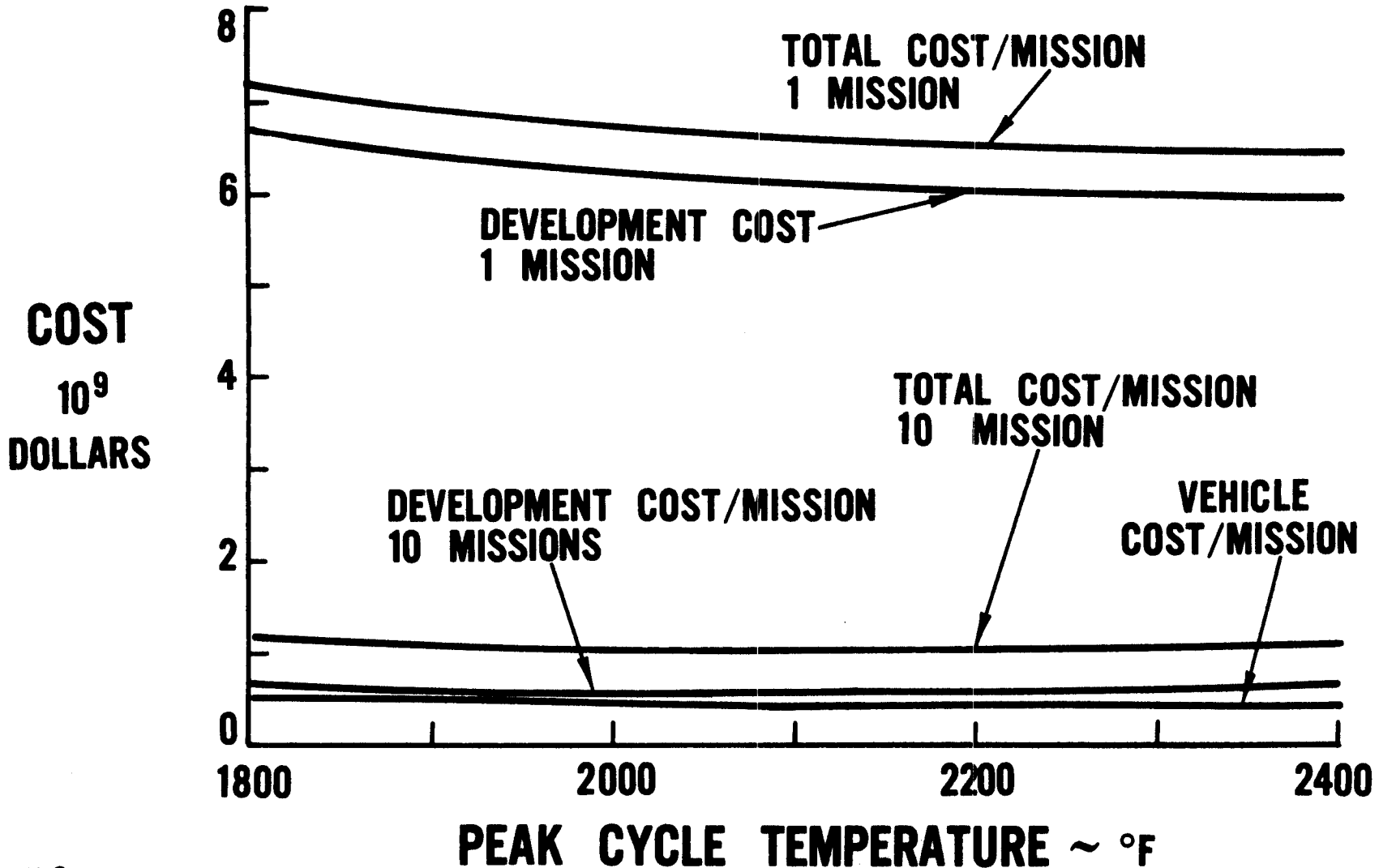

Pratt & Whitney Aircraft

DIVISION OF UNITED AIRCRAFT CORPORATION

M—39010

663006

Figure VI-59

LOW ACCELERATION SPACE TRANSPORTATION

EFFECT OF BURNUP ON MISSION COST

530 DAYS 0.99 PROBABILITY

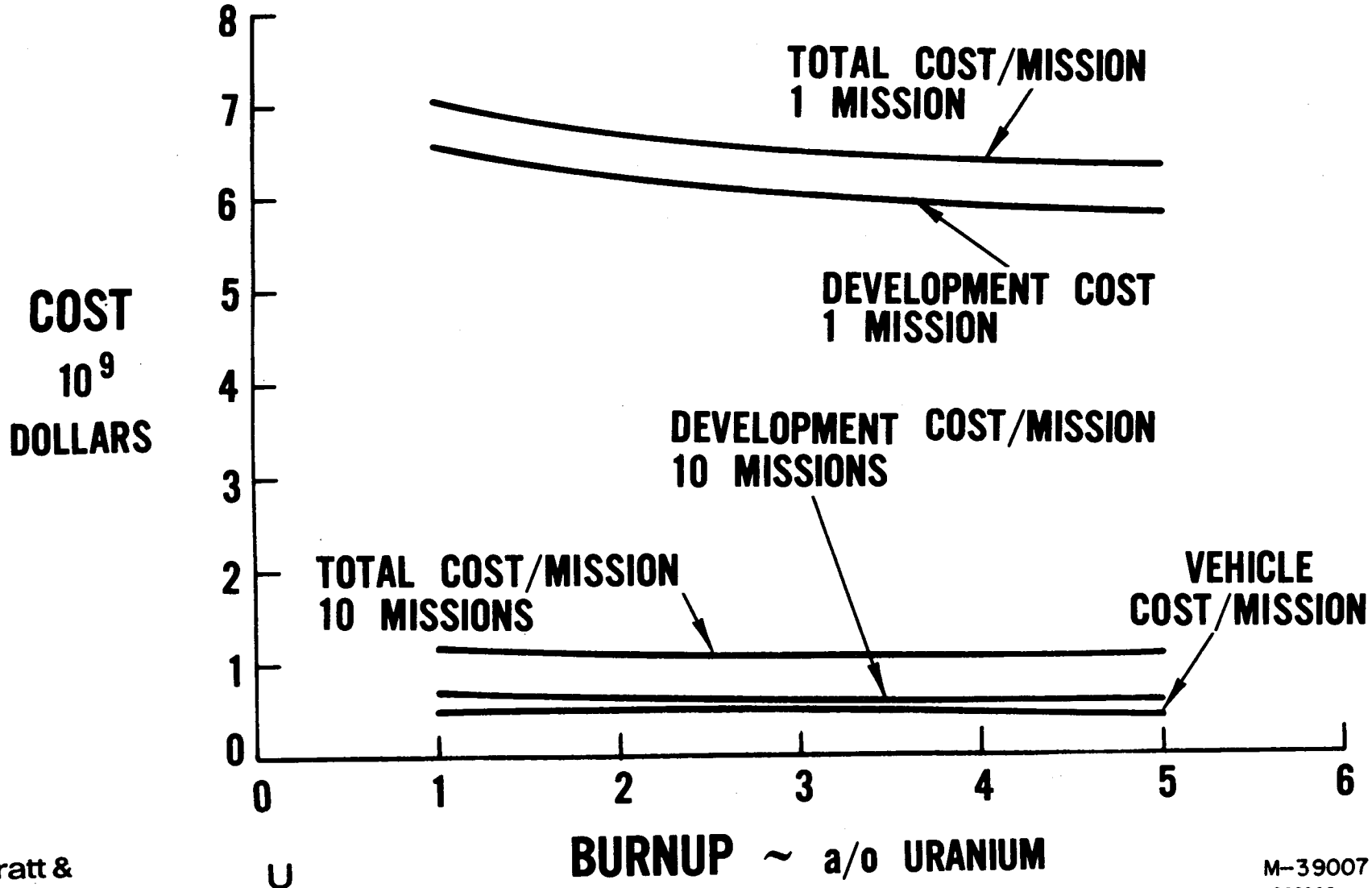

Pratt & Whitney Aircraft

DIVISION OF UNITED AIRCRAFT CORPORATION

M-39007

662906

Figure VI-60

SECTION VII
EARTH ENTRY AND LIFE SUPPORT SYSTEMS

Earth Entry Module

The entry system selected for use in the vehicle model is based largely upon the preliminary design study of an advanced ablative system performed in Ref. VII-1. The double-cone, 4-6 man configuration was designed for entry speeds of up to 20 km/sec, although at the time that study was performed it was determined that approach guidance is marginal at the maximum speed with existing hardware. Nevertheless it was assumed, for purposes of the present study, that the foregoing configuration adequately represents advanced entry system technology for operational requirements in the 1980's.

The basic vehicle used in the present study is the design configuration chosen in Ref. VII-1 for detailed analysis and design integration. The vehicle can accommodate a normal crew of 4 men with provision for two extra men under emergency conditions. The module is occupied during the Earth entry phase only where the entry speed is not to exceed 20 km/sec without retro-propulsion. The gross module weight before entry is about 6.8 metric tons, 454 kg of which is returnable scientific payload. Conventional parachute recovery is assumed for either land or sea touchdown. The total volume of the module is 14 m^3.

This basic design configuration was used to obtain the growth of vehicle mass as a function of the crew size and entry speed, up to a maximum of 12 men and 20 km/sec, respectively. The brief scaling study was performed by assuming a specific volume per man as given in the basic configuration and enlarging the vehicle accordingly to accommodate the crew. The over-all geometric configuration was retained, and the change in surface area due to the different vehicle volume was accounted for to estimate the new structural weight. Under these conditions the ballistic factor changes and, in general, causes the system to operate in a higher heating region. The weight of the ablative heat shield was increased to accommodate the new heating rates. This technique of scaling the entry system is only an approximation, and is not intended to precisely duplicate the results of intensive aerothermodynamic and structural analyses necessary for an optimum point design.

The operational relationship of the entry module to the parent spacecraft is identical to that assumed in Ref. VII-1. Prior to release of the module and after the on-board systems have been checked, the main spacecraft performs a final velocity change of sufficient accuracy to enable the module to enter the Earth's atmosphere within the entry corridor. The nominal entry profile then follows. The actual entry speed utilized in the mission studies is determined by the trade-off between lower electric propulsion requirements and increased entry module mass, both due to the higher hyperbolic excess speed at

Earth. But in no event was the atmospheric entry speed allowed to be more than the maximum of 20 km/sec.

Some consideration was given to the concept of capturing the parent spacecraft in a high parking orbit for purposes of quarantining the crew and possibly inspecting and refurbishing the return vehicle for use in subsequent missions. Return of the crew and scientific payload would be accomplished by an Earth-based shuttle vehicle. Insofar as the mission is concerned, this concept requires no entry module and places the burden of parking-orbit capture on the low-thrust propulsion system. As discussed previously, return of the spacecraft to near-parabolic conditions requires more vehicle mass compared to a direct-entry Earth return. In the mass computation sequence, three possibilities are covered: (1) parking-orbit capture (no entry system), (2) ablative entry module with low-thrust braking, and (3) entry at greater than 20 km/sec with deceleration aided by high-thrust retro-rockets. The second operation was employed in the present studies.

Environmental Control and Life Support System

A comprehensive survey and scaling study was conducted to determine weights, sizes, and electric and thermal power requirements associated with the environmental control (ECS) and life support (LSS) systems for both the Earth entry module and mission module. Extensive use was made of the data presented in Ref. VII-2, which summarizes the results of detailed ECS and LSS optimization studies pertaining to a similar space mission. The scope of the work consisted primarily of an extensive effort to generalize the results presented in Ref. VII-2 so that weights, volumes, and electric and thermal power requirements attributable to the EC and LS systems could be estimated from analytical relationships expressed only in terms of crew size and mission duration. The design specifications for the Earth entry module and mission module are presented in Table VII-1. These specifications are identical to those specified for the studies reported in Ref. VII-2.

Earth Entry ECS and LSS

The environmental control and life support system designs for the Earth entry module provide for the following functions: (1) atmosphere storage; (2) ambient temperature, pressure, and relative humidity control; (3) atmosphere composition control; (4) water management; (5) personal hygiene and waste disposal; and (6) food supply. A schematic drawing of the EC and LS systems is shown in Fig. VII-1.

A mixed-gas atmosphere (oxygen and nitrogen) was selected for the Earth entry module (ERM) atmosphere due to the limited experience gained with a pure oxygen atmosphere and the resulting uncertainty of its after-effect on the crew's well-being. Both the oxygen and nitrogen were considered as being stored

in a pressurized gaseous state in spherical tanks. Two independent atmosphere storage subsystems were selected in order to assure maximum reliability; one was sized for use during the ascent to Earth orbit and main vehicle rendezvous phase, and the other was sized for use during entry to Earth environment.

The heat rejection system would have to provide suitable performance over four different modes of ERM operation. A water boiler was incorporated for the first operational mode (Earth launch to rendezvous with the mission module), since this period would be of relatively short duration. A space radiator was selected for the second operational mode (pre-entry and checkout phase). The water boiler was again used for the third mode (entry) due to the extremely hot environment that would surround the module. An evaporative coolant subsystem (such as a Freon system) would probably be used during the final operational mode (landing and post-landing phase); however, due to the transient conditions that will exist during this phase, sizing of this component was beyond the scope of the study.

A detailed description of the subsystem and space radiator design concepts and the methods used to investigate ambient temperature, pressure, and relative humidity control is presented in Ref. VII-2. In summary, the humidity and temperature control of the ERM was assumed to be performed in two separate loops. The humidity control loop and suit loop were one and the same, and were assumed to be powered by the suit fans even during nonsuit operation. The bulk of the sensible heat load in the cabin was handled by the cabin cooler, which is a high-flow, low-pressure-drop component. The heat-transport fluid loop connects the various components in the system to provide heating or cooling as required and ultimately carries the excess heat to one of the three aforementioned heat sinks for rejection overboard.

The atmosphere composition management subsystem included a debris trap for removal of both solid and liquid particles for the entering air stream; activated charcoal for removal of organic odors; lithium hydroxide for removal of carbon dioxide; a chemisorbent bed for removal of trace contaminants such as nitrogen and sulphur compounds, halogens, metal hydrides, etc.; a particulate filter for removal of aerosols, dust, smoke, etc.; and a catalytic burner for neutralizing toxic gases such as carbon monoxide, hydrogen, and methane. The lithium hydroxide subsystem also included the activated charcoal and fine filters. It was assumed that the chemicals (LiOH and charcoal) would be packaged in a number of separate cartridges which would be replaced as needed.

The water-management subsystem consisted of the required quantity of water, a storage tank for heat rejection purposes, and stored drinking water (and tank) for crew consumption.

It was assumed that elaborate washing facilities would not be required for the ERM, since the crew would be actively engaged in vehicle operations. The weight for personal hygiene equipment was therefore based on the use of impregnated

pads for body cleansing and in-suit devices for urine and feces collection ans storage.

It was assumed that food would be stored in a dry form; hence, an allowance for food spoilage and preparation was not necessary.

Space suit weights were added to the ERM life support system total weight, since the crew would be suited while in the ERM. The Apollo space suit design, with a specific weight of 82 lb/man (including undergarment, pressure suit, and fully charged back pack with an extra charge), was assumed for this purpose.

Mission Module ECS and LSS

Those functions described in the previous section pertaining to the entry module were also essential to the mission module (MM); however, because of the extremely long mission duration associated with the MM, the system design concepts differed considerably between the two modules. The major emphasis was placed on minimizing expendable mass by the use of regenerable subsystem components and by the recovery of essential metabolic constituents from waste products.

A mixed-gas atmosphere consisting of oxygen and nitrogen was also selected for the MM for reasons previously stated. Although the oxygen constituent of metabolic carbon dioxide was recovered, additional oxygen and nitrogen were stored on board to supplement that lost through cabin leakage, to meet the repressurization and portable life support charge requirements, and to provide the additional metabolic oxygen. Subcritical storage was selected to avoid the high pressure requirements of super-critical storage, and to provide a higher allowable heat leak per use rate, thus decreasing insulation requirements. As a result, this method of storage provided minimum weights for the range of mission durations and number of crew considered.

The weight, volume, and thermal and electric power requirements were estimated for the subsystems required to control the temperature, pressure, and relative humidity of the space cabin and the temperature of various electronic equipment on board. The equipment necessary to perform this task consisted of heat exchangers, condensers, fans, water separators, heat-transport fluid, interconnecting ducting and tubing, and a space radiator. Detailed descriptions of the heat transport loop and space radiator configuration are presented in Ref. VII-2. It was assumed, for the purposes of estimating heat-rejection subsystem weights, that the radiator surface would always face a direction perpendicular to a radial from the sun. The space radiator design was based on a maximum influx of 10.5 Btu/ft^2 which would occur in the Mars orbit and would be due to planetary emission and albedo.

The atmosphere composition management subsystem included trace contaminant control, wash water management, carbon dioxide removal, and carbon dioxide reduction. A schematic drawing of the integrated subsystem is shown in Fig. VII-2. Trace contaminant control was performed by components identical to those described for the ERM. Of a total of 40 lb/man-day wash water processed, 14 lb/man-day was processed completely by the use of an air-evaporation subsystem and 26 lb/man-day by ionic filtration. The air-evaporation subsystem utilizes relatively warm cabin air to evaporate the water from a set of wicks, leaving the contaminants behind in the wicks. This moisture-laden air is then cooled, and the water is condensed out and then separated in a water separator. A regenerable solid adsorption subsystem was selected for CO_2 removal, since this method has undergone considerable research and has reached a fairly advanced state of development. This subsystem consists of two sets of silica-gel beds and two sets of artificial zeolite beds for alternately adsorbing water vapor and CO_2, respectively, from the CO_2-laden moist air. The solid-electrolyte CO_2-reduction subsystem was selected for recovering oxygen from the CO_2. Although its state of development does not compare favorably with alternative methods, this sytem has no zero-gravity problems, exhibits the lowest weight of all reduction systems considered, and has been tested sufficiently to prove feasibility. The method selected for transferring the CO_2 from the adsorbent bed to the reduction subsystem consisted of a heat purge utilizing waste heat in coils embedded within the adsorbent beds.

The water management subsystem in the MM was required to process water from urine, wash water, and humidity control for use as potable water for drinking and food preparation, and water for washing. Fecal water was assumed not available. It was further assumed that 95.7% of urine is water and that of this water 4% was unrecoverable; therefore, 0.246 lb/man-day of makeup water was required in addition to that recovered from various sources. Wash water and humidity water were processed by the methods previously described. Urine was processed in a closed-loop air-evaporation system.

Personal hygiene was assumed to cover the areas of bathing, shaving, barbering, and teeth cleaning. Since the expendable mass associated with the use of impregnated pads resulted in a larger weight than that resulting from the use of a shower and water reclamation system, the latter method was selected for bathing. A constant weight of 45 lb was assumed for the shower. Waste management consisted of processing and storing solid waste items such as feces, food wastes, paper wastes, etc. A flat tube and roller scheme (developed by General Dynamics) was selected for urine collection and a conventional toilet seat with a directed air-blast for feces collection. A fixed weight of 20 lb was assumed for the feces collection unit and 0.12 lb/man-day for container weight and chemical treatment for storing feces.

The weight for food requirements was assumed to include the weight of food, 10% for food spoilage, 10% for container weight, and a scaling factor for storage and preparation, based on methods outlined in Ref. VII-3.

The weight of crew support equipment such as medical facilities, fire-fighting equipment, bedding, clothing, and exercise and recreational facilities was assumed to be independent of mission duration and was assessed at 52 lb/man on the basis of studies reported in Ref. VII-3. Spare parts included components for all major subsystems (ventilation, heat-transport loop, CO_2 management, waste management, and atmosphere supply management) that might require replacement. This weight was assessed at 57 lb/man, based on the results of studies reported in Ref. VII-2.

Solar Shelter

The solar shelter was assumed to be located within the mission module. A cylindrical configuration with a specific volume of 55 ft^3/man was assumed for the purpose of estimating the volume and weight penalty. The shielding weights were estimated for a total mission dose of 200 rads with the following breakdown: cosmic ray dose of 30 rads, propulsion reactor dose of 100 rads, power reactor dose of 15 rads, and a solar flare dose of 55 rads. The design techniques proposed in Ref. VII-4 were used to estimate shielding weights. In particular, Fig. 3.3-1 of this reference was used. This figure presents a plot of mean annual sun spot (Wolf) numbers as a function of calendar year. Figure 3.3-2, which presents the variation in storm cellar (solar shelter) shield mass with crew size and number of solar flares, was also used. Borated polyethylene was selected as the primary shielding material; an aluminum structure, having a thickness of 2.0 gm/cm^2 on each side, was used for added strength and durability. It was also assumed that the surrounding structures and assorted equipment would provide an equivalent thickness of 12 gm/cm^2 to partially attenuate space radiation entering through the sides of the shelter.

REFERENCES

VII-1. Lockheed Missiles and Space Company: Preliminary Design of a Mars-Mission Earth Re-entry Module. Summary Report 4-57-64-3, Contract NAS9-1702, March 1964.

VII-2. Hamilton Standard Division: Mars Landing and Reconnaissance Mission Environmental Control and Life Support System Study. SLS 414-2 (Vol. 2), Subsystem Studies, SLS 414-3 (Vol. 3) System Studies. Contract NAS9-1701, March 1964.

VII-3. Lockheed Missiles and Space Company: Manned Interplanetary Mission Study. Summary Report - Vol. I. Report 8-32-63-1, March 1963.

VII-4. General Dynamics/Fort Worth: A Study of Manned Mars Exploration in the Unfavorable Time Period (1975-1985), Vol. II - Summary. Report FZM-4039-2, January 26, 1964.

TABLE VII-1

ENVIRONMENTAL CONTROL AND LIFE SUPPORT SYSTEM DESIGN CONDITIONS

Selected Design Conditions	Re-entry Module	Mission Module
Free air volume, ft^3/man	53.3	583
Cabin pressure, psia	7.0	7.0
Oxygen partial pressure, psia	3.5	3.5
Carbon dioxide allowable partial pressure, psia	0.0965	0.0965
Cabin ambient temperature, F	75	75
Relative humidity, %	60	50
Oxygen input, lb/man-day	2.21	1.84
Carbon dioxide output, lb/man-day	2.50	2.12
Total metabolic heat output, Btu/man-day	14,400	11,200
Water input (food & drink), lb/man-day	7.95	6.2
Urine, lb/man-day	3.34	3.31
Feces, lb/man-day	-	0.5
Respiration, lb/man-day	4.60	2.84
Wash water, lb/man-day	none	40
Food (dry), lb/man-day	1.39	1.39
Portable life support system charges, unit/man	1	2
Number of cabin repressurizations	1	3
Basic Assumptions		
Cabin leakage rate, lb/hr	0.2	0.1
Space radiator orientation	Surface oriented to avoid sun's direct rays and planetary emission from Earth.	Surface faces direction perpendicular to a radial from the sun
Space radiator inlet temperature, F	83	120
Space radiator outlet temperature, F	40	40
Solar influx, Btu/hr ft^2	0	10.5
Water recoverable from urine, lb H_2O/lb urine	-	0.92
Food spoilage, %	-	10

EARTH RE-ENTRY MODULE ENVIRONMENTAL CONTROL AND LIFE SUPPORT SYSTEM SCHEMATIC

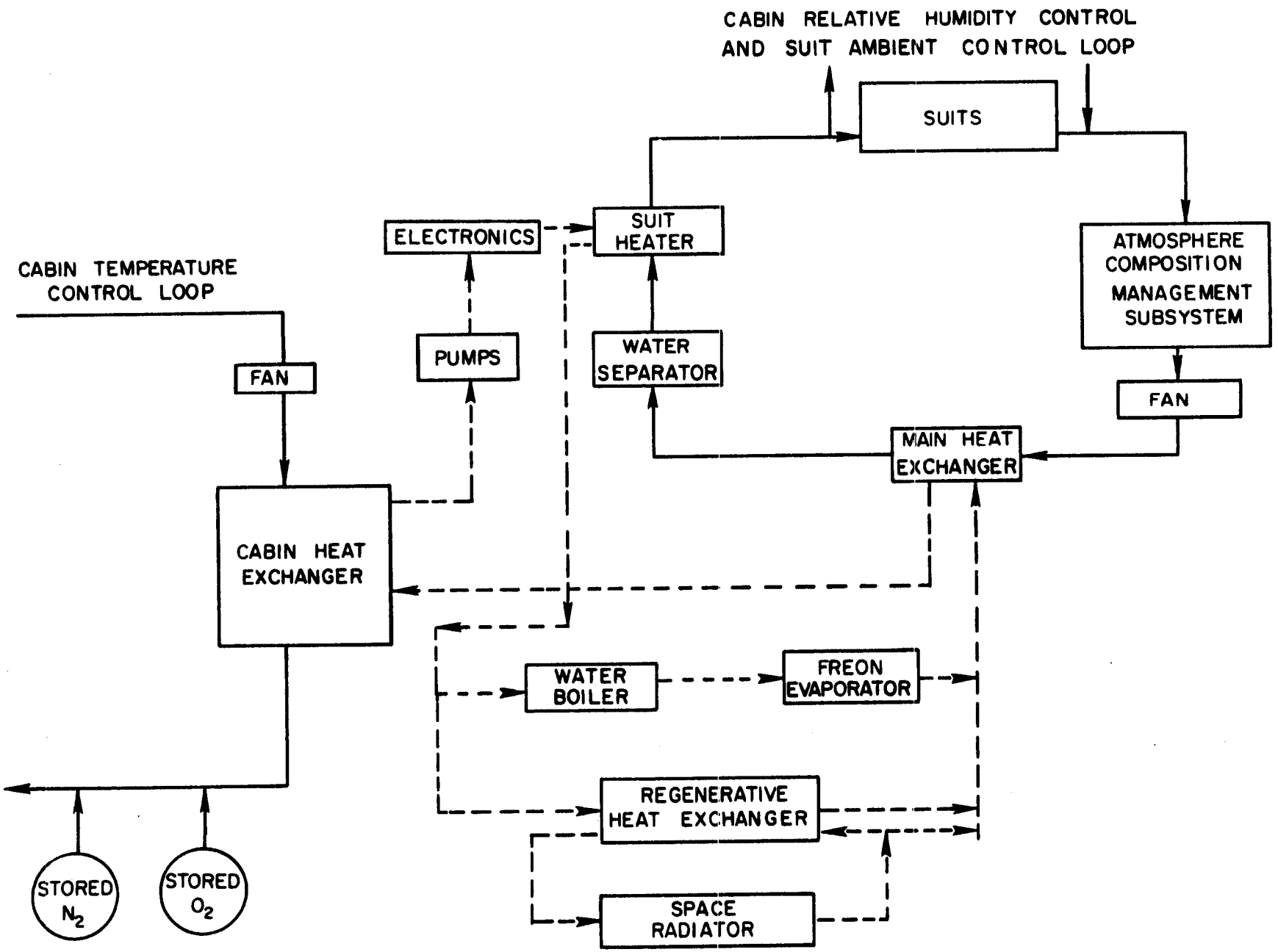

E-910262-6

FIG. VII - 1

E-910262-6

MISSION MODULE ATMOSPHERE COMPOSITION MANAGEMENT SUBSYSTEM SCHEMATIC

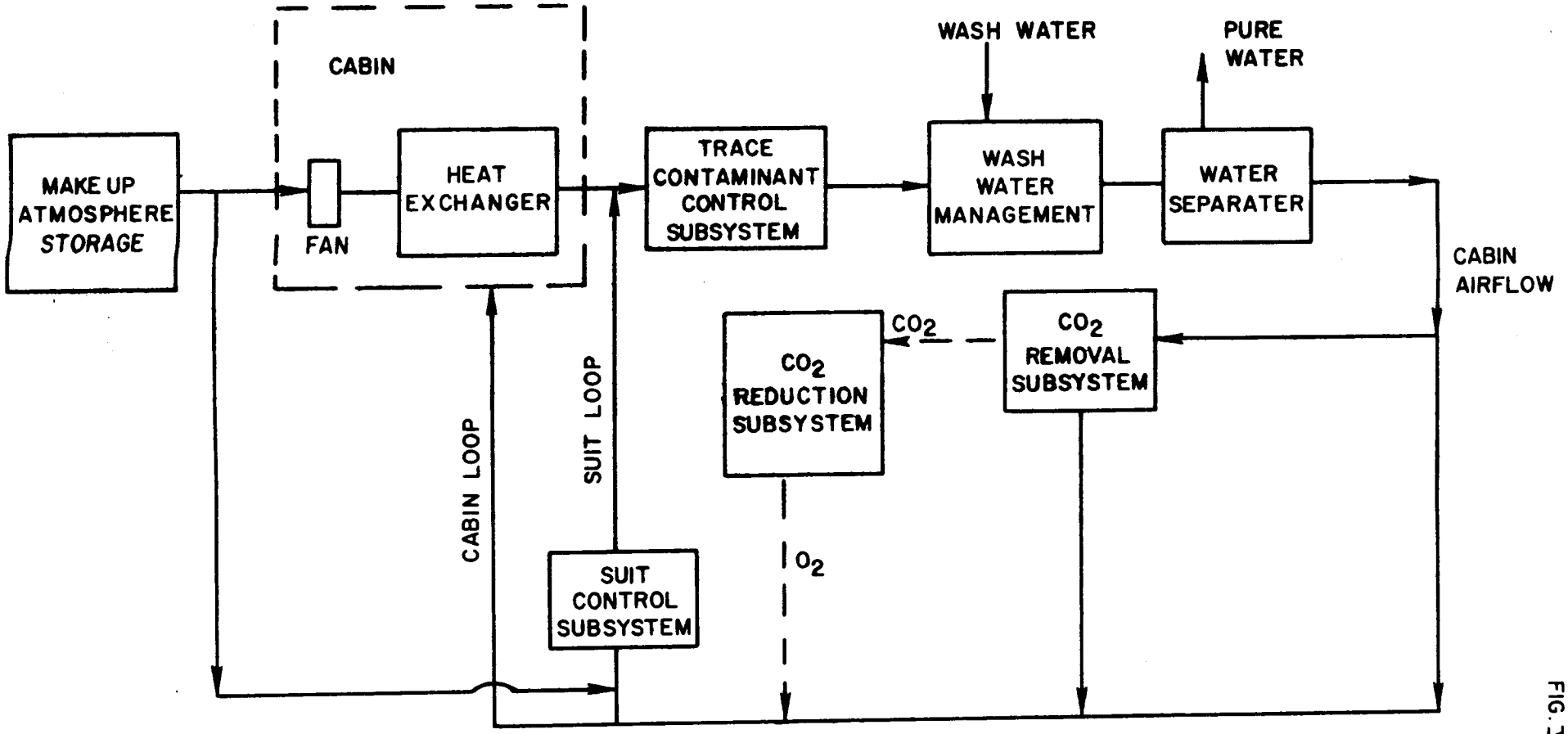

FIG. XII-2

APPENDIX A

THE FINITE-DIFFERENCE NEWTON-RAPHSON ALGORITHM

The finite-difference Newton-Raphson method for solving two-point boundary value problems may be explained by considering the following system of nonlinear second order equations:

$$\ddot{x}_i = f_i\ (x_1, \ldots, x_{2m}, t) \qquad i = 1, \ldots, 2m \qquad \text{(A-1)}$$

with associated boundary conditions

$$\begin{aligned} x_i(a) &= \alpha_{i0} & \dot{x}_i(a) &= \dot{\alpha}_{i0} \\ x_i(b) &= \alpha_{i(N+1)} & \dot{x}_i(b) &= \dot{\alpha}_{i(N+1)} \end{aligned} \qquad i = 1, \ldots, m \qquad \text{(A-2)}$$

on half of the variables and their derivatives at fixed initial and terminal times.

A particular problem of this form arises from a variational trajectory problem where the variables having boundary conditions are the positions in space, and the variables whose boundary values are not specified are the Lagrange multipliers. The method may also be used to solve classical problems in celestial mechanics where boundary conditions would be imposed on all the state variables (orbital elements) but not their derivatives (Ref. A-1).

The second-order form of the equations has been purposely chosen so that a simple, stable finite-difference approximation can be used. Variational problems and celestial mechanics problems are often stated in a first-order Hamiltonian formulation which can generally be transformed into a second-order Lagrangian formulation by the methods of classical mechanics. The resulting equations may contain first derivatives (unlike Eq. (A-1)), but the method can easily handle this case (Ref. A-1).

It is assumed that the Euler-Lagrange equations for the control variables have been explicitly solved in terms of the Lagrange multipliers, so that no control variables appear in Eq. (A-1). For problems where this cannot be done, the generalized Hamiltonian formulation of Ref. A-2 may be used.

The solution of the boundary value system represented in Eqs. (A-1) and (A-2) is approached as follows. If an appropriate space of 2m-tuples of functions

x_i is defined on the interval $a \leq t \leq b$, (A-1) may be considered as defining the operator equation

$$L(X) - F(X) = P(X) = 0. \tag{A-3}$$

L represents the linear operator defined by the second derivatives, and F is the nonlinear operator defined by the right-hand sides. Proceeding formally, the Newton-Raphson iteration,

$$X_{n+1} = X_n - [P'(X_n)]^{-1}P(X_n), \tag{A-4}$$

can be applied to (A-3) when an approximate solution, X_o, is known. Letting $\Delta_n = X_{n+1} - X_n$, multiplying through by the derivative operator $P'(X_n)$, and relating the notation to Eq. (A-3), this iteration becomes

$$[-L + F'(X_n)](\Delta_n) = L(X_n) - F(X_n). \tag{A-5}$$

The quantity $[-L + F'(X_n)]$ is a linear operator which when applied to the iterative change Δ_n yields the value of the operator at the previous iteration. Reference A-3 gives the general conditions under which this approach is applicable and convergent.

The algorithm amounts to putting (A-5) in the form of a large, but easily solved, matrix equation. This end is achieved by imposing a mesh of N points,

$$t_j = a + jh, \; h = \frac{b - a}{N+1}, \text{ and } j = 1,\ldots,N, \tag{A-6}$$

on the interval [a, b]. The value of the n^{th} iterate $x_i^n(t_j)$ is written $x_i^n{}_j$ x_n is thus a $2mN^{th}$ dimensional vector, and its elements $x_i^n{}_j$ are ordered such that i runs through its 2m values for each value of j. Some differences in this arrangement will be encountered on the ends of the vector to accommodate the boundary conditions on $\dot{x}_i$.

By approximating the second derivatives with the central difference quotient,

$$\ddot{x}_{i\,j} \approx \frac{x_{i\,j-1} - 2x_{i\,j} + x_{i\,j+1}}{h^2}, \tag{A-7}$$

2mN linear equations for the unknowns $\delta^n_{i\,j} = x^{n+1}_{i\,j} - x^n_{i\,j}$ are obtained as follows:

$$-\frac{\delta^n_{i\,j-1} - 2\delta^n_{i\,j} + \delta^n_{i\,j+1}}{h^2} + \sum_{v=1}^{2m}\left[\frac{\partial f_i}{\partial x_v}(x^n_{1\,j},\ldots,x^n_{2m\,j},t)\right]\delta^n_{v_j} = p^n_{i\,j}, \qquad \text{(A-8)}$$

where

$$p_{i\,j} = \frac{x^n_{i\,j-1} - 2x^n_{i\,j} + x^n_{i\,j+1}}{h^2} - f_i\,(x^n_{1\,j},\ldots,x^n_{2m\,j},t). \qquad \text{(A-9)}$$

These equations form the major part of the matrix equation, Eq. (A-5). To complete the system, two additional mesh points are added, each being one mesh spacing outside the interval [a, b]. Defining only the state variables at these points, Eq. (A-8) can be written for i = 1,...,m and j = o, N+1 (i.e. for t = a, b). The boundary conditions on $\dot{x}_i$ can now be included in the system with the equations

$$\frac{\delta^n_{i\,j-1} - \delta^n_{i\,j+1}}{2h} = \frac{x^n_{i\,j-1} - x^n_{i\,j+1}}{2h} - \dot{\alpha}_{i\,j} \qquad \text{(A-10)}$$

$$i = 1,\ldots,m \text{ and } j = o,\ N+1.$$

The conditions on x_i are naturally met by using the given $x_{i\,j}$ and noting that the corresponding $\delta_{i\,j} = o$.

These equations form a block tri-diagonal matrix equation of the form:

$$\begin{pmatrix} B_o & C_o & & & & & \\ A_1 & B_1 & -I & & & & \\ & -I & B_2 & -I & & & \\ & & o & & & & \\ & & & \cdot & & & \\ & & & o & & & \\ & & & -I & B_{N-1} & -I & \\ & & & & -I & B_N & C_N \\ & & & & & A_{N+1} & B_{N+1} \end{pmatrix} \begin{pmatrix} D_o \\ D_1 \\ D_2 \\ \cdot \\ \cdot \\ \cdot \\ D_{N-1} \\ D_N \\ D_{N+1} \end{pmatrix} = \begin{pmatrix} P_o \\ P_1 \\ P_2 \\ \cdot \\ \cdot \\ \cdot \\ P_{N-1} \\ P_N \\ P_{N+1} \end{pmatrix} \qquad \text{(A-11)}$$

The matrix elements are each 2mx2m submatrices, and the vector elements represent a corresponding partitioning as follows:

$$P_j = h^2 \begin{pmatrix} p_{1,j} \\ \vdots \\ p_{2m,j} \end{pmatrix}, \text{ and } D_j = \begin{pmatrix} \delta_{1,j} \\ \vdots \\ \delta_{2m,j} \end{pmatrix}, \quad j = 1,\ldots N \tag{A-12}$$

This system must be formed and solved for each iteration, and

$$B_j = 2I + h^2 J_j^n, \quad j=1,\ldots N, \tag{A-13}$$

J_j^n being the 2m x 2m Jacobian matrix with elements $\partial f_i / \partial x_v$ evaluated at the n^{th} iteration. The different blocks at the extremes of the matrix arise from the special boundary condition equations.

For the most part the subdiagonal and superdiagonal blocks are merely negative identity matrices. Denoting these submatrices generally by A_j and C_j ($j = 1,\ldots,N+1$) the solution of Eq. (A-1) is obtained by the following definitions (Ref. A-4, pg. 196):

$$\begin{aligned} &W_0 = B_0^{-1} C_0, \quad G_0 = B^{-1} P_0, \\ &W_j = (B_j - A_j W_{j-1})^{-1} C_j, \quad G_j = (B_j - A_j W_{j-1})^{-1} (P_j - A_j G_{j-1}), j=1,\ldots,N+1. \end{aligned} \tag{A-14}$$

These definitions make possible the recursive computation of the components of the solution

$$D_{N+1} = G_{N+1}, \; D_j = G_j - W_j D_{j+1}, \; j = N,\ldots,1. \tag{A-15}$$

Of course, considerable simplification takes place when -I is substituted for the appropriate A's and C's.

APPENDIX A REFERENCES

A-1. Van Dine, C. P.: An Application of Newton's Method to the Finite Difference Solution of Nonlinear Boundary Value Systems. United Aircraft Research Laboratories Report UAR-D37, March 1965.

A-2. Payne, M.: "Dirais Generalized Hamiltonian Dynamics and the Pontryagin Principle", in NASA TMX-53150, Huntsville, Ala., October 1964.

A-3. Kantorovich, L. V. and G. P. Akilov: Functional Analysis in Normed Spaced Chap. XVIII, Pergamon Press, 1964.

A-4. Varga, R. S.: Matrix Iterative Analysis. Chap. 6, Prentice-Hall, 1962.

APPENDIX B

LOW-THRUST TRAJECTORY ANALYSIS

Variable Thrust

The variable-thrust trajectory analysis and all computations were performed in three dimensions. The analysis was carried out under the following assumptions:

1. The vehicle thrustor is capable of completely variable I_{sp}. The thrustor efficiency, $\eta(I_{sp})$, is taken as unity throughout the powered flight.

2. The departure and destination planets associated with the trajectories are nongravitating points in space; the only gravitation force acting upon the vehicle is that induced by the Sun's mass.

3. The planetocentric and heliocentric trajectories are computed separately and matched such that the asymptotic velocity of the vehicle in the planetocentric frame is added vectorially to the heliocentric velocity of the planet to give the boundary value of velocity for the interplanetary trajectory.

The methods of the calculus of variations are applied to minimizing the integral

$$J = \int_0^\tau \frac{a^2}{2P(X,t)}\, dt$$

subject to the dynamical constraints

$$\begin{aligned}
g_1(\dot{X},X) &= \dot{x} - q = 0 \\
g_2(\dot{X},X) &= \dot{y} - r = 0 \\
g_3(\dot{X},X) &= \dot{z} - s = 0 \\
g_4(\dot{X},X) &= \dot{q} - a_x + \frac{x}{R^3} = 0 \\
g_5(\dot{X},X) &= \dot{r} - a_y + \frac{y}{R^3} = 0 \\
g_6(\dot{X},X) &= \dot{s} - a_z + \frac{z}{R^3} = 0
\end{aligned} \qquad \text{(B-1)}$$

Where a_x, a_y and a_z are the components of the thrust acceleration in the x, y, and z directions respectively, i.e., $a_x^2 + a_y^2 + a_z^2 = a^2$; q, r and s are the components of the vehicle velocity vector and $R^2 = x^2 + y^2 + z^2$. The units of time and length have been chosen such that the value of the Gaussian constant is unity. The optimization problem can now be restated as the minimization of the integral

$$I = \int_0^T F(\dot{X}, X, t)dt \tag{B-2}$$

where

$$F = \frac{a_x^2 + a_y^2 + a_z^2}{2P(X,t)} + \sum_{i=1}^{6} \lambda_i g_i(\dot{X}, X) \tag{B-3}$$

and the λ_i are the Lagrange multipliers associated with the constraints g_i, and are, in general, functions of time, t. Setting the first variation of I equal to zero yields the Euler-Lagrange necessary conditions for the extremization of I:

$$\frac{d}{dt}\frac{\partial F}{\partial \dot{X}_i} - \frac{\partial F}{\partial X_i} = 0 \qquad i = 1,2,.....9 \tag{B-4}$$

where the X_i are now specified as the set $[x,y,z,q,r,s,a_x,a_y,a_z]$.

Before proceeding further it is advantageous to specify the functional form of P(X,t). We have chosen

$$P(X,t) = \frac{P_o e^{-\gamma t}}{R^n} \tag{B-5}$$

where γ and n are time-independent parameters. The proportionality of exhaust power to $1/R^n$ is chosen to allow the solution latitude for taking into account the degrading of solar cell efficiency due to large thermal gradients encountered during close passage of the Sun. The exponential term may represent the time decay of a radioisotope power source or, perhaps more importantly, it may represent the reliability of the power source over the trip duration based upon a postulated powerplant component failure rate. The proper choice of n and γ can represent several different power modes as illustrated below.

Parameter Specification	Power Mode
$\gamma = o;\ n = o$	Constant Power, P_o; [1.0] reliability
γ given; $n = o$	Constant Power, P_o; $[e^{-\gamma t}]$ reliability
$\gamma = \alpha+\beta;\ n = o$	Radioisotope Power, $P_o e^{-\alpha t}$; $[e^{-\beta t}]$ reliability
$\gamma = o$, n given	Solar Power, P_o/R^n; [1.0] reliability
γ, n given	Solar Power, P_o/R^n; $[e^{-\gamma t}]$ reliability

The differential equations governing the optimal trajectory can now be obtained from Eqs. (B-3), (B-4), and (B-5) by the appropriate operations.

$$\ddot{x} = \frac{P_o u}{e^{\gamma t} R^n} - \frac{x}{R^3} \quad , \qquad a_x = \frac{P_o u}{e^{\gamma t} R^n}$$

$$\ddot{y} = \frac{P_o v}{e^{\gamma t} R^n} - \frac{y}{R^3} \quad , \qquad a_y = \frac{P_o v}{e^{\gamma t} R^n}$$

$$\ddot{z} = \frac{P_o w}{e^{\gamma t} R^n} - \frac{z}{R^3} \quad , \qquad a_z = \frac{P_o w}{e^{\gamma t} R^n} \tag{B-6}$$

$$\ddot{u} = -\frac{m P_o \lambda^2 x}{e^{\gamma t} R^{n+2}} + \frac{u(2x^2 - y^2 - z^2) + 3x(vy+wz)}{R^5}$$

$$\ddot{v} = -\frac{m P_o \lambda^2 y}{e^{\gamma t} R^{n+2}} + \frac{v(2y^2 - x^2 - z^2) + (ux+wz)}{R^5}$$

$$\ddot{w} = -\frac{m P_o \lambda^2 z}{e^{\gamma t} R^{n+2}} + \frac{w(2z^2 - x^2 - y^2) + 3z(ux+vy)}{R^5}$$

where $2m = n$, $u \equiv \lambda_4$, $v \equiv \lambda_5$, $w \equiv \lambda_6$ and $\lambda^2 = u^2 + v^2 + w^2$

For the purpose of displaying the explicit form that these equations take on in the numerical solution as set forth in Appendix A, the problem is now considered for the specific trajectory mode of planetary rendezvous with hyperbolic excess velocities assigned to the vehicle at the boundaries. The transversality condition for this problem is

$$\sum_{k=1}^{6} \frac{\partial F}{\partial \dot{x}_k} \delta x_k \Big|_0^T = 0 \qquad \text{(B-7)}$$

where the departure date and trip time have been specified. Making use of Eqs. (B-1) and (B-3) and the fact that the positions at t = 0, T are specified, Eq. (B-7) takes the form

$$u\delta\dot{x} + v\delta\dot{y} + w\delta\dot{z} \Big|_{t=0}^{t=T} = 0 \qquad \text{(B-8)}$$

The case where an excess velocity of prescribed magnitude, V_o, is added vectorially to the given planetary velocity at t = 0 has been treated elsewhere (Ref. B-1) and is briefly repeated here. Only the magnitude of the excess velocity, V_o, has been fixed, hence it can be oriented in any direction and the locus of the tip of the resultant velocity vector is a circle as expressed by Eq. (B-9).

$$(\dot{x}-\dot{\xi}_o)^2 + (\dot{y}-\dot{\eta}_o)^2 + (\dot{z}-\dot{\zeta}_o)^2 - v_o^2 \Big|_{t=o} = 0 \qquad \text{(B-9)}$$

where $\dot{\xi}_o$, $\dot{\eta}_o$ and $\dot{\zeta}_o$ are the velocity components of the departure planet. Taking the variation of (B-9) yields

$$(\dot{x}-\dot{\xi}_o)\,\delta\dot{x} + (\dot{y}-\dot{\eta}_o)\delta\dot{y} + (\dot{z}-\dot{\zeta}_o)\delta\dot{z} \Big|_{t=o} = 0 \qquad \text{(B-10)}$$

Equations (B-8) and (B-10) yield the conditions

$$\frac{u}{v} = \frac{\dot{x}-\dot{\xi}_o}{\dot{y}-\dot{\eta}_o}, \qquad \frac{v}{w} = \frac{\dot{y}-\dot{\eta}_o}{\dot{z}-\dot{\zeta}_o}, \qquad \frac{w}{u} = \frac{\dot{z}-\dot{\zeta}_o}{\dot{x}-\dot{\xi}_o} \qquad \text{(B-11)}$$

evaluated at t = 0. Considerations of Eqs. (B-6) and (B-11) show that V_o is parallel and of the same sense as the low-thrust acceleration vector at t = 0. A similar result can be shown for an excess velocity, V_N, applied to the vehicle at the destination planet at t = T.

Now proceeding with knowledge of the positions and velocities of the departure and destination planets

$$x_i(0) = \alpha_{i0} \qquad \dot{x}_i(0) = \dot{\alpha}_{i0}$$
$$x_i(T) = \alpha_{i(N+1)} \qquad \dot{x}_i(T) = \dot{\alpha}_{i(N+1)} \tag{B-12}$$

the matrices associated with the algorithm of Appendix A can be explicitly set forth. The boundary value blocks take the form

$$B_o = \left(\begin{array}{c|c} I & \beta_o \\ \hline -I & \frac{Poh^2}{A_o^m} \cdot I \end{array}\right)$$

where

$$\beta_o = \frac{2hV_o}{\Lambda_o^{3/2}} \begin{pmatrix} (v_o^n)^2 + (w_o^n)^2 & -u_o^n v_o^n & -u_o^n w_o^n \\ -u_o^n v_o^n & (u_o^n)^2 + (w_o^n)^2 & -v_o^n w_o^n \\ -u_o^n w_o^n & -v_o^n w_o^n & (u_o^n)^2 + (v_o^n)^2 \end{pmatrix}$$

$$C_o = \left(\begin{array}{c|c} -I & 0 \\ \hline -I & 0 \end{array}\right) = A_{N+1} \qquad A_1 = \left(\begin{array}{c|c} 0 & 0 \\ \hline 0 & -I \end{array}\right) = C_N$$

and

$$\left(\begin{array}{c|c} I & \beta_{N+1} \\ \hline -I & \dfrac{Poh^2}{e^{\gamma T} A_{N+1}^{m}} \cdot I \end{array}\right) = B_{N+1}$$

where

$$\beta_{N+1} = \frac{-2hV_N}{\Lambda_N^{3/2}} \begin{pmatrix} (v_N^n)^2 + (w_N^n)^2 & -u_N^n w_N^n & -u_N^n w_N^n \\ -u_N^n v_N^n & (u_N^n)^2 + (w_N^n)^2 & -v_N^n w_N^n \\ -u_N^n w_N^n & -v_N^n w_N^n & (u_N^n)^2 + (v_N^n)^2 \end{pmatrix}$$

The corresponding unknown vectors are

$$D_0 = \begin{pmatrix} x_{-1}^{n+1} - x_{-1}^n \\ y_{-1}^{n+1} - y_{-1}^n \\ z_{-1}^{n+1} - z_{-1}^n \\ u_0^{n+1} - u_0^n \\ v_0^{n+1} - v_0^n \\ w_0^{n+1} - w_0^n \end{pmatrix} \qquad D_{N+1} = \begin{pmatrix} x_{N+1}^{n+1} - x_{N+1}^n \\ y_{N+1}^{n+1} - y_{N+1}^n \\ z_{N+1}^{n+1} - z_{N+1}^n \\ u_N^{n+1} - u_N^n \\ v_N^{n+1} - v_N^n \\ w_N^{n+1} - w_N^n \end{pmatrix}$$

The corresponding right-hand-side vectors are

$$P_0 = \begin{pmatrix} -x_{-1}^n + x_1^n - 2h\left(\dfrac{V_0 u_0^n}{\Lambda_0^{1/2}} + \dot{\alpha}_{x_0}\right) \\ -y_{-1}^n + y_1^n - 2h\left(\dfrac{V_0 v_0^n}{\Lambda_0^{1/2}} + \dot{\alpha}_{y_0}\right) \\ -z_{-1}^n + z_1^n - 2h\left(\dfrac{V_0 w_0^n}{\Lambda_0^{1/2}} + \dot{\alpha}_{z_0}\right) \\ x_{-1}^n - 2\alpha_{x_0} + x_1^n - h^2\left(\dfrac{P_0 u_0^n}{A_0^m} - \dfrac{\alpha_{x_0}}{A_0^{3/2}}\right) \\ y_{-1}^n - 2\alpha_{y_0} + y_1^n - h^2\left(\dfrac{P_0 v_0^n}{A_0^m} - \dfrac{\alpha_{y_0}}{A_0^{3/2}}\right) \\ z_{-1}^n - 2\alpha_{z_0} + z_1^n - h^2\left(\dfrac{P_0 w_0^n}{A_0^m} - \dfrac{\alpha_{z_0}}{A_0^{3/2}}\right) \end{pmatrix}$$

where

$$A_0 = \alpha_{x_0}^2 + \alpha_{y_0}^2 + \alpha_{z_0}^2$$

$$\Lambda_0 = (u_0^n)^2 + (v_0^n)^2 + (w_0^n)^2$$

and

$$P_{N+1} = \begin{pmatrix} x^n_{N-1} - x^n_{N+1} - 2h\left(\dfrac{V_N u^n_N}{\Lambda_N^{1/2}} - \dot{\alpha}_{x(N+1)}\right) \\ y^n_{N-1} - y^n_{N+1} - 2h\left(\dfrac{V_N v^n_N}{\Lambda_N^{1/2}} - \dot{\alpha}_{y(N+1)}\right) \\ z^n_{N-1} - z^n_{N+1} - 2h\left(\dfrac{V_N w^n_N}{\Lambda_N^{1/2}} - \dot{\alpha}_{z(N+1)}\right) \\ x^n_{N-1} - 2\alpha_{x(N+1)} + x^n_{N+1} - h^2\left(\dfrac{P_o u^n_N}{e^{\gamma T} A^m_{N+1}} - \dfrac{\alpha_{x(N+1)}}{A^{3/2}_{N+1}}\right) \\ y^n_{N-1} - 2\alpha_{y(N+1)} + y^n_{N+1} - h^2\left(\dfrac{P_o v^n_N}{e^{\gamma T} A^m_{N+1}} - \dfrac{\alpha_{y(N+1)}}{A^{3/2}_{N+1}}\right) \\ z^n_{N-1} - 2\alpha_{z(N+1)} + z^n_{N+1} - h^2\left(\dfrac{P_o w^n_N}{e^{\gamma T} A^m_{N+1}} - \dfrac{\alpha_{z(N+1)}}{A^{3/2}_{N+1}}\right) \end{pmatrix}$$

where

$$A_{N+1} = \alpha^2_{x(N+1)} + \alpha^2_{y(N+1)} + \alpha^2_{z(N+1)}$$

$$\Lambda_N = (u^n_N)^2 + (v^n_N)^2 + (w^n_N)^2$$

The general unknown vector is

$$D_j = \begin{pmatrix} x^{n+1}_j - x^n_j \\ y^{n+1}_j - y^n_j \\ z^{n+1}_j - z^n_j \\ u^{n+1}_j - u^n_j \\ v^{n+1}_j - v^n_j \\ w^{n+1}_j - w^n_j \end{pmatrix}$$

and the general right-hand-side vector is given by

$$P_j = \begin{pmatrix} x_{j-1} - 2x_j + x_{j+1} - h^2 \left(\frac{P_0 u_j}{e^{\gamma t_j} A_j^m} - \frac{x_j}{A_j^{3/2}} \right) \\ y_{j-1} - 2y_j + y_{j+1} - h^2 \left(\frac{P_0 v_j}{e^{\gamma t_j} A_j^m} - \frac{y_j}{A_j^{3/2}} \right) \\ z_{j-1} - 2z_j + z_{j+1} - h^2 \left(\frac{P_0 w_j}{e^{\gamma t_j} A_j^m} - \frac{z_j}{A_j^{3/2}} \right) \\ u_{j-1} - 2u_j + u_{j+1} - h^2 \left(\frac{P_0 m x_j \Lambda_j}{A_j^{m+1}} + \frac{u_j(2x_j^2 - y_j^2 - z_j^2) + 3x_j(v_j y_j + w_j z_j)}{A_j^{5/2}} \right) \\ v_{j-1} - 2v_j + v_{j+1} - h^2 \left(\frac{P_0 m y_j \Lambda_j}{A_j^{m+1}} + \frac{v_j(2y_j^2 - x_j^2 - z_j^2) + 3y_j(u_j x_j + w_j z_j)}{A_j^{5/2}} \right) \\ w_{j-1} - 2w_j + w_{j+1} - h^2 \left(\frac{P_0 m z_j \Lambda_j}{A_j^{m+1}} + \frac{w_j(2z_j^2 - x_j^2 - y_j^2) + 3z_j(u_j x_j + v_j y_j)}{A_j^{5/2}} \right) \end{pmatrix}$$

Where

$$\Lambda_j = u_j^2 + v_j^2 + w_j^2$$

$$A_j = x_j^2 + y_j^2 + z_j^2$$

and each variable has superscript n. The general coefficient matrix B_j is given on the next page; each variable in the matrix has superscript n and subscript j.

$$B_j = h^2 \begin{bmatrix}
\frac{2}{h^2} - \frac{2\epsilon(t)umx}{(x^2+y^2+z^2)^{m+1}} + \frac{2x^2-y^2-z^2}{(x^2+y^2+z^2)^{5/2}} & \frac{-2\epsilon(t)umy}{(x^2+y^2+z^2)^{m+1}} + \frac{3xy}{(x^2+y^2+z^2)^{5/2}} & \frac{-2\epsilon(t)umz}{(x^2+y^2+z^2)^{m+1}} + \frac{3xz}{(x^2+y^2+z^2)^{5/2}} & \frac{\epsilon(t)}{(x^2+y^2+z^2)^m} & 0 & 0 \\
\frac{-2\epsilon(t)mvx}{(x^2+y^2+z^2)^{m+1}} + \frac{3xy}{(x^2+y^2+z^2)^{5/2}} & \frac{2}{h^2} - \frac{2\epsilon(t)mvy}{(x^2+y^2+z^2)^{m+1}} + \frac{2y^2-x^2-z^2}{(x^2+y^2+z^2)^{5/2}} & \frac{-2\epsilon(t)mvz}{(x^2+y^2+z^2)^{m+1}} + \frac{3yz}{(x^2+y^2+z^2)^{5/2}} & 0 & \frac{\epsilon(t)}{(x^2+y^2+z^2)^m} & 0 \\
\frac{-2\epsilon(t)mwx}{(x^2+y^2+z^2)^{m+1}} + \frac{3xz}{(x^2+y^2+z^2)^{5/2}} & \frac{-2\epsilon(t)mwy}{(x^2+y^2+z^2)^{m+1}} + \frac{3yz}{(x^2+y^2+z^2)^{5/2}} & \frac{2}{h^2} - \frac{2\epsilon(t)mwz}{(x^2+y^2+z^2)^{m+1}} + \frac{2z^2-x^2-y^2}{(x^2+y^2+z^2)^{5/2}} & 0 & 0 & \frac{\epsilon(t)}{(x^2+y^2+z^2)^m} \\
\frac{-\epsilon(t)m\lambda^2[y^2+z^2-(2m+1)x^2]}{(x^2+y^2+z^2)^{m+2}} + \frac{9xu+3yv+3zw}{(x^2+y^2+z^2)^{5/2}} - \frac{15x^2(ux+vy+wz)}{(x^2+y^2+z^2)^{7/2}} & \frac{\epsilon(t)m\lambda^2[2xy(m+1)]}{(x^2+y^2+z^2)^{m+2}} + \frac{3(yu+vx)}{(x^2+y^2+z^2)^{5/2}} - \frac{15xy(ux+vy+wz)}{(x^2+y^2+z^2)^{7/2}} & \frac{\epsilon(t)m\lambda^2[2xz(m+1)]}{(x^2+y^2+z^2)^{m+2}} + \frac{3(uz+wx)}{(x^2+y^2+z^2)^{5/2}} - \frac{15xz(ux+vy+wz)}{(x^2+y^2+z^2)^{7/2}} & \frac{2}{h^2} - \frac{2\epsilon(t)mux}{(x^2+y^2+z^2)^{m+1}} + \frac{2x^2-y^2-z^2}{(x^2+y^2+z^2)^{5/2}} & \frac{-2\epsilon(t)mvx}{(x^2+y^2+z^2)^{m+1}} + \frac{3xy}{(x^2+y^2+z^2)^{5/2}} & \frac{-2\epsilon(t)mwx}{(x^2+y^2+z^2)^{m+1}} + \frac{3xz}{(x^2+y^2+z^2)^{5/2}} \\
\frac{\epsilon(t)m\lambda^2[2yx(m+1)]}{(x^2+y^2+z^2)^{m+2}} + \frac{3(vx+yu)}{(x^2+y^2+z^2)^{5/2}} - \frac{15xy(ux+yv+wz)}{(x^2+y^2+z^2)^{7/2}} & \frac{-\epsilon(t)m\lambda^2[x^2+z^2-(2m+1)y^2]}{(x^2+y^2+z^2)^{m+2}} + \frac{3ux+9vy+3wz}{(x^2+y^2+z^2)^{5/2}} - \frac{15y^2(ux+vy+wz)}{(x^2+y^2+z^2)^{7/2}} & \frac{\epsilon(t)m\lambda^2[2yz(m+1)]}{(x^2+y^2+z^2)^{m+2}} + \frac{3(vz+wy)}{(x^2+y^2+z^2)^{5/2}} - \frac{15yz(ux+vy+wz)}{(x^2+y^2+z^2)^{7/2}} & \frac{-2\epsilon(t)muy}{(x^2+y^2+z^2)^{m+1}} + \frac{3xy}{(x^2+y^2+z^2)^{5/2}} & \frac{2}{h^2} - \frac{2\epsilon(t)mvy}{(x^2+y^2+z^2)^{m+1}} + \frac{2y^2-x^2-z^2}{(x^2+y^2+z^2)^{5/2}} & \frac{-2\epsilon(t)mwy}{(x^2+y^2+z^2)^{m+1}} + \frac{3yz}{(x^2+y^2+z^2)^{5/2}} \\
\frac{\epsilon(t)m\lambda^2[2zx(m+1)]}{(x^2+y^2+z^2)^{m+2}} + \frac{3(wx+uz)}{(x^2+y^2+z^2)^{5/2}} - \frac{15xz(ux+vy+wz)}{(x^2+y^2+z^2)^{7/2}} & \frac{\epsilon(t)m\lambda^2[2zy(m+1)]}{(x^2+y^2+z^2)^{m+2}} + \frac{3(vz+wy)}{(x^2+y^2+z^2)^{5/2}} - \frac{15yz(ux+vy+wz)}{(x^2+y^2+z^2)^{7/2}} & \frac{-\epsilon(t)m\lambda^2[x^2+y^2-(2m+1)z^2]}{(x^2+y^2+z^2)^{m+2}} + \frac{3ux+3vy+9wz}{(x^2+y^2+z^2)^{5/2}} - \frac{15z^2(ux+vy+zw)}{(x^2+y^2+z^2)^{7/2}} & \frac{-2\epsilon(t)muz}{(x^2+y^2+z^2)^{m+1}} + \frac{3xz}{(x^2+y^2+z^2)^{5/2}} & \frac{-2\epsilon(t)mvz}{(x^2+y^2+z^2)^{m+1}} + \frac{3yz}{(x^2+y^2+z^2)^{5/2}} & \frac{2}{h^2} - \frac{2\epsilon(t)mwz}{(x^2+y^2+z^2)^{m+1}} + \frac{2z^2-x^2-y^2}{(x^2+y^2+z^2)^{5/2}}
\end{bmatrix}$$

WHERE $\epsilon(t) = P_0 e^{-\gamma t}$

Transversality Conditions for Variable Low-Thrust Planetary Flyby

The components of the vehicle velocity are unspecified at t = T, hence the transversality condition (B-7) takes the form

$$u\delta\dot{x} + v\delta\dot{y} + w\delta\dot{z}\Big|_{t=T} = 0 \qquad \text{(B-13)}$$

There is no preference regarding the magnitude nor direction of the final velocity, hence $\delta\dot{x}$, $\delta\dot{y}$, and $\delta\dot{z}$ are independent.

$$\therefore\ u(T) = v(T) = w(T) = 0 \qquad \text{(B-14)}$$

The following alterations occur in the matrices associated with the algorithm.

$$P_{N+1} = \begin{pmatrix} \ddot{x}^n_{N-1} - 2\alpha_{x(N+1)} + \ddot{x}^n_{N+1} + h^2 \dfrac{\alpha_{x(N+1)}}{A_{N+1}^{3/2}} \\ \ddot{y}^n_{N-1} - 2\alpha_{y(N+1)} + \ddot{y}^n_{N+1} + h^2 \dfrac{\alpha_{y(N+1)}}{A_{N+1}^{3/2}} \\ \ddot{z}^n_{N-1} - 2\alpha_{z(N+1)} + \ddot{z}^n_{N+1} + h^2 \dfrac{\alpha_{z(N+1)}}{A_{N+1}^{3/2}} \\ U^n_{N+1} + U^n_{N-1} \\ V^n_{N+1} + V^n_{N-1} \\ W^n_{N+1} + W^n_{N-1} \end{pmatrix} \qquad D_{N+1} = \begin{pmatrix} X^{n+1}_{N+1} - X^n_{N+1} \\ Y^{n+1}_{N+1} - Y^n_{N+1} \\ Z^{n+1}_{N+1} - Z^n_{N+1} \\ U^{n+1}_{N+1} - U^n_{N+1} \\ V^{n+1}_{N+1} - V^n_{N+1} \\ W^{n+1}_{N+1} - W^n_{N+1} \end{pmatrix}$$

$$B_{N+1} = \left(\begin{array}{c|c} -I & 0 \\ \hline 0 & -I \end{array}\right) = A_{N+1} \qquad C_N = (0)$$

Transversality Conditions for Variable Low-Thrust Solar Probe

The components of the vehicle position and velocity are unspecified at t = T, hence the transversality condition (B-7) takes the form

$$-\dot{u}\delta x - \dot{v}\delta y - \dot{w}\delta z + u\delta\dot{x} + v\delta\dot{y} + w\delta\dot{z}\Big|_{t=T} = 0 \qquad \text{(B-15)}$$

The magnitude of the radius vector to the vehicle at t = T is constrained to satisfy Eq. (B-16)

$$x^2 + y^2 + z^2 - R_T^2\Big|_{t=T} = 0 \qquad \text{(B-16)}$$

Taking the variation of Eq. (B-16) and solving the resulting expression for δx, Eq. (B-17) is obtained

$$\delta x\Big|_{t=T} = -\,(y/x\,\delta y + z/x\,\delta z)\Big|_{t=T} \qquad \text{(B-17)}$$

Substituting Eq. (B-17) into (B-15)

$$(-\dot{v} + \dot{u}\,y/x)\delta y + (-\dot{w} + \dot{u}\,z/x)\delta z + u\delta\dot{x} + v\delta\dot{y} + w\delta\dot{z}\Big|_{t=T} = 0 \qquad \text{(B-18)}$$

The five variations appearing in Eq. (B-18) are independent; it follows that the conditions to be imposed upon the differential equations at t = T are

$$\begin{aligned} \dot{v} - \dot{u}\, y/x &= 0 \\ \dot{w} - \dot{u}\, z/x &= 0 \\ u = v &= w = 0 \\ x^2 + y^2 + z^2 - R_T^2 &= 0 \end{aligned} \qquad \text{(B-19)}$$

The following alterations occur in the matrices associated with the algorithm.

$$C_N = \left(\begin{array}{c|c} 0 & -I \\ \hline 0 & 0 \end{array}\right)$$

$$B_{N+1} = \left(\begin{array}{ccc|ccc} & I & & & 0 & \\ \hline U_N^n & -X_N^n & 0 & -V_{N+1}^n + V_{N-1}^n & U_{N+1}^n - U_{N-1}^n & 0 \\ Z_N^n & 0 & -X_N^n & -W_{N+1}^n + W_{N-1}^n & 0 & U_{N+1}^n - U_{N-1}^n \\ 0 & 0 & 0 & -2X_N^n & -2Y_N^n & -2Z_N^n \end{array}\right)$$

$$P_{N+1} = \left(\begin{array}{l} (V_{N+1}^n - V_{N-1}^n)\, X_N^n - (U_{N+1}^n - U_{N-1}^n)\, Y_N^n \\ (W_{N+1}^n - W_{N-1}^n)\, X_N^n - (U_{N+1}^n - U_{N-1}^n)\, Z_N^n \\ (X_N^n)^2 + (Y_N^n)^2 + (Z_N^n)^2 - R_T^2 \\ U_{N+1}^n + U_{N-1}^n \\ V_{N+1}^n + V_{N-1}^n \\ W_{N+1}^n + W_{N-1}^n \end{array}\right)$$

$$D_{N+1} = \begin{pmatrix} X_N^{n+1} - X_N^n \\ Y_N^{n+1} - Y_N^n \\ Z_N^{n+1} - Z_N^n \\ U_{N+1}^{n+1} - U_{N+1}^n \\ V_{N+1}^{n+1} - V_{N+1}^n \\ W_{N+1}^{n+1} - W_{N+1}^n \end{pmatrix} \qquad A_{N+1} = \left(\begin{array}{c|ccc} 0 & \multicolumn{3}{c}{-I} \\ \hline & -Y_N^n & X_N^n & 0 \\ 0 & -Z_N^n & 0 & X_N^n \\ & 0 & 0 & 0 \end{array}\right)$$

Constant Thrust with Coast

Optimal Control Analysis

In three dimensions, the classical methods of the calculus of variations are applied to the minimization of the integral

$$J = \int_0^\tau a^2 \, dt \tag{B-20}$$

Subject to the constraints

$$\begin{aligned} z_1 &= \dot{q} - a_x + \frac{x}{R^3} = 0 \\ z_2 &= \dot{r} - a_y + \frac{y}{R^3} = 0 \\ z_3 &= \dot{s} - a_z + \frac{z}{R^3} = 0 \\ z_4 &= \dot{x} - q = 0 \\ z_5 &= \dot{y} - r = 0 \\ z_6 &= \dot{z} - s = 0 \end{aligned} \tag{B-21}$$

where x, y, z are the position coordinates of the vehicle, q, r, s are the components of velocity, a_x, a_y, a_z are the components of the thrust acceleration, i.e., $a_x^2 + a_y^2 + a_z^2 = a^2$, and $R^2 = x^2 + y^2 + z^2$. By virtue of the fact that constant I_{sp} and constant exhaust power characterize the powerplant, the magnitude of the thrust acceleration is given by

$$|\overleftarrow{a(t)}| = \frac{\dot{m}c\alpha_p}{1-\dot{m}t} \tag{B-22}$$

where

$$\alpha_p = \begin{cases} 1, \text{ during thrust} \\ 0, \text{ during coast,} \end{cases}$$

c is the velocity of the exhaust jet relative to the vehicle and $\dot{m}$ is the rate at which the propellant leaves the vehicle, normalized with respect to the vehicle mass at time t = 0. Defining l_i, i = 1, 2, 3 as the direction cosines of the thrust acceleration vector with respect to the x, y, z directions, respectively, the components of the thrust acceleration are given by:

$$a_x = \frac{\dot{m}c\alpha_p}{1-\dot{m}t} \ell_1$$

$$a_y = \frac{\dot{m}c\alpha_p}{1-\dot{m}t} \ell_2$$

$$a_z = \frac{\dot{m}c\alpha_p}{1-\dot{m}t} \ell_3 \tag{B-23}$$

Defining the augmented function

$$F = a^2 + \sum_{i=1}^{6} \lambda_i z_i (\dot{X}, X, t) \tag{B-24}$$

And proceeding as above, we can write the Euler-Lagrange Necessary conditions and the restated equations of motion:

$$\ddot{x} - f_1 = \ddot{x} - \frac{\dot{m}c\alpha_p}{1-\dot{m}t}\frac{u}{p} + \frac{x}{R^3} = 0$$

$$\ddot{y} - f_2 = \ddot{y} - \frac{\dot{m}c\alpha_p}{1-\dot{m}t}\frac{v}{p} + \frac{y}{R^3} = 0$$

$$\ddot{z} - f_3 = \ddot{z} - \frac{\dot{m}c\alpha_p}{1-\dot{m}t}\frac{w}{p} + \frac{z}{R^3} = 0$$

$$\ddot{u} - g_1 = \ddot{u} - \frac{u(2x^2-y^2-z^2) + 3x(vy+wz)}{R^5} = 0$$

$$\ddot{v} - g_2 = \ddot{v} - \frac{v(2y^2-x^2-z^2) + 3y(wz+ux)}{R^5} = 0 \qquad \text{(B-25)}$$

$$\ddot{w} - g_3 = \ddot{w} - \frac{w(2z^2-x^2-y^2) + 3z(ux+vy)}{R^5} = 0$$

where $l_i = \lambda_i/(\lambda_1^2 + \lambda_2^2 + \lambda_3^2)^{1/2}$, $i = 1, 2, 3$ and $\lambda_1 \equiv u$, $\lambda_2 \equiv v$, $\lambda_3 \equiv w$ and $p = (\lambda_1^2 + \lambda_2^2 + \lambda_3^2$

Since Eqs. (B-25) are homogeneous in the adjoint variables, u, v and w, they may be scaled by the expression

$$[p(0)]^2 = 1$$

or

$$[u(0)]^2 + [v(0)]^2 + [w(0)]^2 = 1 \qquad \text{(B-26)}$$

to eliminate arbitrariness in the solution.

As set forth in Ref. B-2, satisfaction of the Weierstrass necessary condition leads to the definition of a switching function, k(t), characterized by

a) $k(t) \geq o$ during thrusting
b) $k(t) \leq o$ during coasting
c) $\dot{k}(t) = \frac{c}{\mu(t)}\dot{p}(t)$ throughout the interval $0 \leq t \leq T$,

where $\mu(t)$ is the vehicle mass at time, t, normalized with respect to vehicle mass at time $t = 0$.

Conditions (a) and (b) indicate that at the thrustor switch-off and switch-on times, t_1 and t_2, respectively, $k(t)$ vanishes, i.e., $k(t_1) = k(t_2) = 0$. Hence, integration of condition (c) between the times t_1 and t_2 leads to the expression

$$[p(t_1)]^2 = [p(t_2)]^2$$

or

$$[u(t_1)]^2 + [v(t_1)]^2 + [w(t_1)]^2 = [u(t_2)]^2 + [v(t_2)]^2 + [w(t_2)]^2 \qquad \text{(B-27)}$$

since $\mu(t)$ = constant between these limits.

Boundary conditions are given by matching the state and its derivative (velocity) to some specified orbit; additionally, a given excess speed may be optimally applied to the orbital velocity.

The formal modification of the algorithm can now be set forth. Setting $x = x_1$, $y = x_2$, $z = x_3$, $u = \lambda_1$, $v = \lambda_2$, $w = \lambda_3$, the problem is now discretized by using a fixed number of equally spaced mesh points in each of the three regions (thrust, coast, thrust). Thus t_1 is always associated with mesh point n_1, t_2 with mesh point n_2, and the total time, $T \equiv t_3$, with the final mesh point n_3. Defining the initial time, t_0, at mesh point $n_0 = 1$, the mesh spacing, h, in each region becomes

$$h_k = \frac{t_k - t_{k-1}}{n_k - n_{k-1}}, \quad k = 1, 2, 3. \qquad \text{(B-28)}$$

At the interior points in each region difference equations for Eqs. (B-25) are derived by using the standard three-point formula.

$$x_i(t-h) - 2x_i(t) + x_i(t+h) = h^2 f_i \qquad \text{(B-29a)}$$

$$\lambda_i(t-h) - 2\lambda_i(t) + \lambda_i(t+h) = h^2 g_i \qquad \text{(B-29b)}$$

At the exterior boundary points, n_0 and n_3, equations for the λ_i must be written. By using (B-29a) and the difference equations for the velocity at the boundary,

$$- x_i(t-h) + x_i(t+h) = 2h\left(x_i \pm \frac{V\lambda_i}{p}\right) = 2hb_i, \qquad \text{(B-30)}$$

where V is the given excess speed, the value of x_i which occurs outside the interval $[t_0, t_3]$ can be eliminated. (The sign of V is + at t_0 and - at t_3.)

$$- x_i(t_0) + x_i(t_0+h_1) = h_1 b_i + \frac{h_1^2}{2} f_i \qquad \text{(B-31a)}$$

$$x_i(t_3-h_3) - x_i(t_3) = - h_3 b_i + \frac{h_3^2}{2} f_i \; . \qquad \text{(-31b)}$$

Similarly, at the switching points, n_1 and n_2, equations for x_i and λ_i are written. The subscripts - and + will be used to denote the variables which occur before and after the switching point. Since $(B\text{-}25_1)$, $(B\text{-}25_2)$ and $(B\text{-}25_3)$ are discontinuous at these points, (B-29a) is written for both f_{i-} and f_{i+} and combined with the equation of continuity for the velocity,

$$\frac{- x_i(t-h_-) + x_i(t+h_-)}{2h_-} = \frac{- x_i(t-h_+) + x_i(t+h_+)}{2h_+} \; . \qquad \text{(B-32)}$$

in order to eliminate the extraneous variables $x_i\ (t+h_-)$ and $x_i\ (t-h_+)$. Since $(B\text{-}25_4)$, $(B\text{-}25_5)$ and $(B\text{-}25_6)$ are continuous, the equation for λ_i may be written using a standard divided difference formula. The resulting equations are

$$h'x_i(t-h_-) - h''x_i(t) + x_i(t+h_+) = \frac{h_+}{2}(h_- f_{i-} + h_+ f_{i+}) \qquad \text{(B-33a)}$$

$$h'\lambda_i(t-h_-) - h''\lambda_i(t) + \lambda_i(t+h_+) = \frac{h_+(h_-+h_+)}{2} g_i \qquad \text{(-33b)}$$

where $h' = h_+/h_-$ and $h'' = (h_- + h_+)/h_-$.

Equations (B-26), (B-27), (B-29), (B-31), and (B-33) now represent $6n_3^3 - 4$ nonlinear algebraic equations in the unknowns

$$x_{ij}\ ,\ 1 \le i \le 3\ ,\ \ 2 \le j \le n_3 - 1\ ;$$

$$\lambda_{ij},\ 1 \le i \le 3\ ,\ \ 1 \le j \le n_3\ ;$$

$$t_1\ ,\ \text{and}\ t_2.$$

After these equations are appropriately ordered, a numerical solution may be determined by successively solving the linear systems defined by the generalized Newton-Raphson iteration. The method essentially follows the details laid down in Ref. B-1.

Optimal Propulsion Parameter Analysis

This analysis is carried out under the assumption that $J = \int_0^T a^2\ dt$ and $\bar{a}$, the arithmetric mean thrust acceleration, are nearly invariant under variations of the powerplant fraction, μ_w, in the neighborhood of its optimal value. The rationale upon which these assumptions are based is discussed in detail in Ref. B-3 and that analysis is summarized and modified here.

The values of J and $\bar{a}$ are obtained from trajectories utilizing constant thrust with coast periods that are optimal in the sense that J is minimized with respect to the control, a slight deviation from the analysis of the above reference. Thus we know the values for

$$\bar{a} = \frac{a_0 + a_T}{2} \quad \text{and} \quad J = \int_0^T a^2\ dt \tag{B-34}$$

from a previous trajectory optimization. The first of Eqs. (B-34) may be written

$$\bar{a} = \frac{a_0}{2}\left(1 + \frac{a_1}{a_0}\right) \tag{B-35}$$

Also we have

$$a(t) = \frac{2\mu_w \eta}{\alpha c \mu} = \frac{a_0}{\mu} \tag{B-36}$$

where μ is the normalized mass of the vehicle as a function of time. The rocket equation gives

$$\frac{1}{\mu_1} = 1 + \frac{\alpha J}{2\mu_w \eta} \tag{B-37}$$

where μ_1 is the final total mass of the vehicle normalized with respect to the initial mass. Combining Eqs. (B-35), (B-36) and (B-37), we obtain Eq. (B-38):

$$\bar{a}\alpha c = 2\mu_w \eta + \frac{\alpha J}{2} \tag{B-38}$$

As done in Ref. B-3, setting the first variation of the payload fraction equal to zero we obtain Eq. (B-39)

$$\mu_w = \frac{\mu_1(1 - \mu_1)}{1-(\frac{2\mu_1}{1+\mu_1})(\frac{\eta' c}{\eta})} \tag{B-39}$$

where $\eta' \equiv d\eta/dc$ and $\eta \equiv \dfrac{1}{1 + d^2/c^2}$, d being a parameter dependent upon the constant value of c.

Thus, Eqs. (B-38) and (B-39) are two equations in the unknowns μ_w and c. They can be numerically solved for the optimal values μ_w^* and c^* when α and η are specified. New values for the thrust magnitude and mass flow rate can then be computed from

$$\dot{m}c = \frac{a^*\mu_w \eta}{ac^*} \quad , \quad \dot{m} = \frac{2\mu_w^* \eta}{\alpha(c^*)^2} \tag{B-40}$$

These values are used in the numerical solution for optimal control (modified Newton-Raphson algorithm) which yields new values for J and $\bar{a}$. This completes one iteration in the propulsion parameter optimization.

APPENDIX B REFERENCES

B-1. Van Dine, C. P.: "Application of a Finite-Difference Newton-Raphson Algorithm to a Problem of Low-Thrust Trajectory Optimization." Vol. 17, Progress in Astronautics and Aeronautics, Methods of Astrodynamics and Celestial Mechanics. Edited by R. L. DunCombe and V. G. Szebehely, Academic Press, May 1966.

B-2. Lawden, D. F.: Optimal Trajectories for Space Navigation, Butterworths, 1963.

B-3. Melbourne, W. G. and C. G. Sauer, Jr.: "Payload Optimization for Power-Limited Vehicles", Vol. 9, Progress in Astronautics and Aeronautics, Academic Press, 1963. Also in JPL Space Programs Summary No. 37-17, Vol. IV, October, 1962; also JPL TR 32-250.

APPENDIX C

MATCHING OF PLANETOCENTRIC AND HELIOCENTRIC TRAJECTORIES

A uniform method of asymptotic matching is used for high-thrust, low-thrust, and dual-thrust vehicles. The planetocentric trajectory far from the planet is asymptotically matched to the heliocentric trajectory close to the planet. For high-thrust trajectories this is the conventional analysis of Ref. C-1.

The analysis for constant-acceleration low-thrust trajectories which depart from a circular orbit was developed in Ref. C-2. In this case the planetocentric trajectory far from the planet and the heliocentric trajectory close to the planet can both be approximated by straight line trajectories under constant acceleration. By simply extending the asymptote of the planetocentric trajectory back to zero velocity, the proper time at which to start a heliocentric calculation with the planet's position and velocity can be determined. The analysis of Ref. C-3 shows that this same approach (and in fact the same formulas) can be used for constant-thrust trajectories if the thrust-to-mass ratio is based on the mass at the juncture with the heliocentric trajectory.

When low acceleration is used in conjunction with high acceleration or atmospheric braking, the terminal conditions on the low-thrust orbit will be a parabolic or hyperbolic trajectory rather than a circular orbit. For these cases it is also important to consider the increased energy input to the vehicle due to the planetary gravitational field. For parabolic or hyperbolic trajectories which terminate close to the planet, the angular momentum will be small, and the trajectory can be approximated by a straight line (Fig. C-1). The constant-acceleration case can then be solved analytically using Perkins' variables (Ref. C-4):

$$X = r\left(\frac{T}{M\mu}\right)^{\frac{1}{2}}$$

$$Y = v\left(\frac{T\mu}{M}\right)^{-\frac{1}{4}}$$

$$T = t\left(\frac{T}{M}\right)^{\frac{3}{4}} \mu^{-\frac{1}{4}}$$

The equation of motion is given by

$$\ddot{X} = \ddot{Y} = 1 - \frac{1}{X^2} \tag{C-1}$$

Multiplying both sides by $\dot{x}$ yields

$$\dot{X}\ddot{X} = \dot{X} - \frac{\dot{X}}{X^2} \tag{C-2}$$

Equation (C-2) can be immediately integrated to yield

$$\frac{\dot{X}^2}{2} = X + \frac{1}{X} - X_0 + \frac{X_0^2}{2} - \frac{1}{X_0} \tag{C-3}$$

Equation (C-3) can now be solved for the time differential

$$\sqrt{2}\, dt = \frac{dx}{\sqrt{X - X_0 + \frac{\dot{X}_0^2}{2} - \frac{1}{X_0} + \frac{1}{X}}} \tag{C-4}$$

The initial energy is

$$U_0 = \frac{X_0^2}{2} - \frac{1}{X} = \frac{Y_{\infty_0}^2}{2}$$

Taking the lower limit of integration at the origin yields

$$T = \frac{1}{\sqrt{2}} \int_0^x \frac{dx}{\sqrt{X + U + \frac{1}{X}}} \tag{C-5}$$

Equation (C-5) is an elliptic integral. There are two cases of interest, depending upon the initial energy.

Case I

$$-2 \le U_0 \le 2$$

(C-6)

$$T = \frac{1}{\sqrt{2}} \int_0^x \left(X + \frac{U_0}{2} + \sqrt{\frac{U_0^2}{4} - 1} \right)\left(X + \frac{U_0}{2} - \sqrt{\frac{U_0^2}{4} - 1} \right)$$

This integral is of the form 239.03 of Ref. C-5, p. 86

$$T = \frac{1}{\sqrt{2}} \int_0^{u_1} \frac{1-cnu}{1+cnu}\, du \tag{C-7}$$

where:

$$cnu = \cos\phi = \frac{1-X}{1+X}$$

$$k^2 = \frac{1}{2} - \frac{U_0}{4}$$

$$\sqrt{2}\, T = F(\phi,k) - 2E(\phi,k) + \frac{2\sqrt{X}}{1+X}\sqrt{1+U_0X+X^2} \tag{C-8}$$

$$\sqrt{2}\, T = F(\phi,k) - 2E(\phi,k) + \frac{2\sin\phi\sqrt{1-k^2\sin^2\phi}}{1+\cos\phi} \tag{C-9}$$

The asymptotic matching of the planetocentric trajectory with the heliocentric trajectory requires the evaluation of this integral as the radius becomes very large.

FOR $X \gg 1$

$$T \approx \sqrt{2}\, K(k) - 2\sqrt{2}\, E(k) + \sqrt{2X} \tag{C-10}$$

$$\sqrt{2X} \approx Y \approx Y_\infty \tag{C-11}$$

$$U_0 \geq 2$$

Case II

Equation (C-6) is now of the form 237.03 on p. 82 of Ref. C-5

$$T = \sqrt{2}\, \frac{\frac{U_0}{2} - \sqrt{\frac{U_0^2}{4}-1}}{\sqrt{\frac{U_0}{2} + \sqrt{\frac{U_0^2}{4}-1}}} \int_0^u tn^2 u\, du \tag{C-12}$$

where

$$\sin^2 u = \sin^2 \phi = \frac{X}{X + \frac{U_0}{2} - \sqrt{\frac{U_0^2}{4} - 1}}$$

If

$$k^2 = \frac{2\sqrt{\frac{U_0^2}{4} - 1}}{\frac{U_0}{2} + \sqrt{\frac{U_0^2}{4} - 1}}$$

then

$$T = \sqrt{2}\sqrt{\frac{U_0}{2} + \sqrt{\frac{U_0^2}{4} - 1}} \left[\sqrt{1 - k^2 \sin^2 u} \sqrt{\frac{X}{\frac{U_0}{2} - \sqrt{\frac{U_0^2}{4} - 1}}} - E(\phi, k) \right] \quad \text{(C-13)}$$

For $x \gg 1$,

$$T \approx \sqrt{2X} - \sqrt{U_0 + \sqrt{U_0^2 - 4}}\ E(k) \quad \text{(C-14)}$$

Equations (C-10), (C-11), and (C-14) may be used to define a new function D which corrects the heliocentric trajectory for the effect of the planetary gravity field.

$$\frac{T}{M} t = V_\infty - V_{\infty_0} - \left(\frac{T}{M} \mu\right)^{\frac{1}{4}} D \quad \text{(C-15)}$$

This function D is plotted in Fig. C-2.

REFERENCES

C-1. NASA SP-35, Planetary Flight Handbook

C-2. Fimple, W. R. and T. N. Edelbaum: Applications of SNAP-50 Class Powerplants to Selected Unmanned Electric Propulsion Missions. AIAA Paper No. 64-494. NASA Contract NASw-737, 1964.

C-3. Edelbaum, T. N.: A Comparison of Nonchemical Propulsion Systems for Round Trip Mars Missions. UAC Research Laboratories Report R-1383-2, October 1960.

C-4. Perkins, F. M.: Flight Mechanics of Low-Thrust Spacecraft. Journal of the Aerospace Sciences 26, 291-297, 1959.

C-5. Byrd, P. F. and M. D. Friedman: Handbook of Elliptic Integrals for Engineers and Physicists. Springer-Verlag, Berlin, 1954.

STRAIGHT LINE TRAJECTORY APPROXIMATION

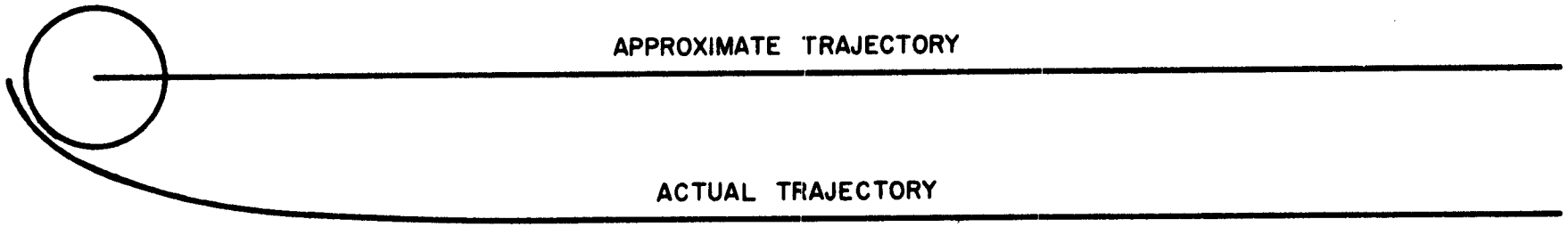

FIG. C-1

CORRECTION TO HYPERBOLIC LOW-THRUST TRAJECTORIES DUE TO PLANETARY ATTRACTION

E-910262-6

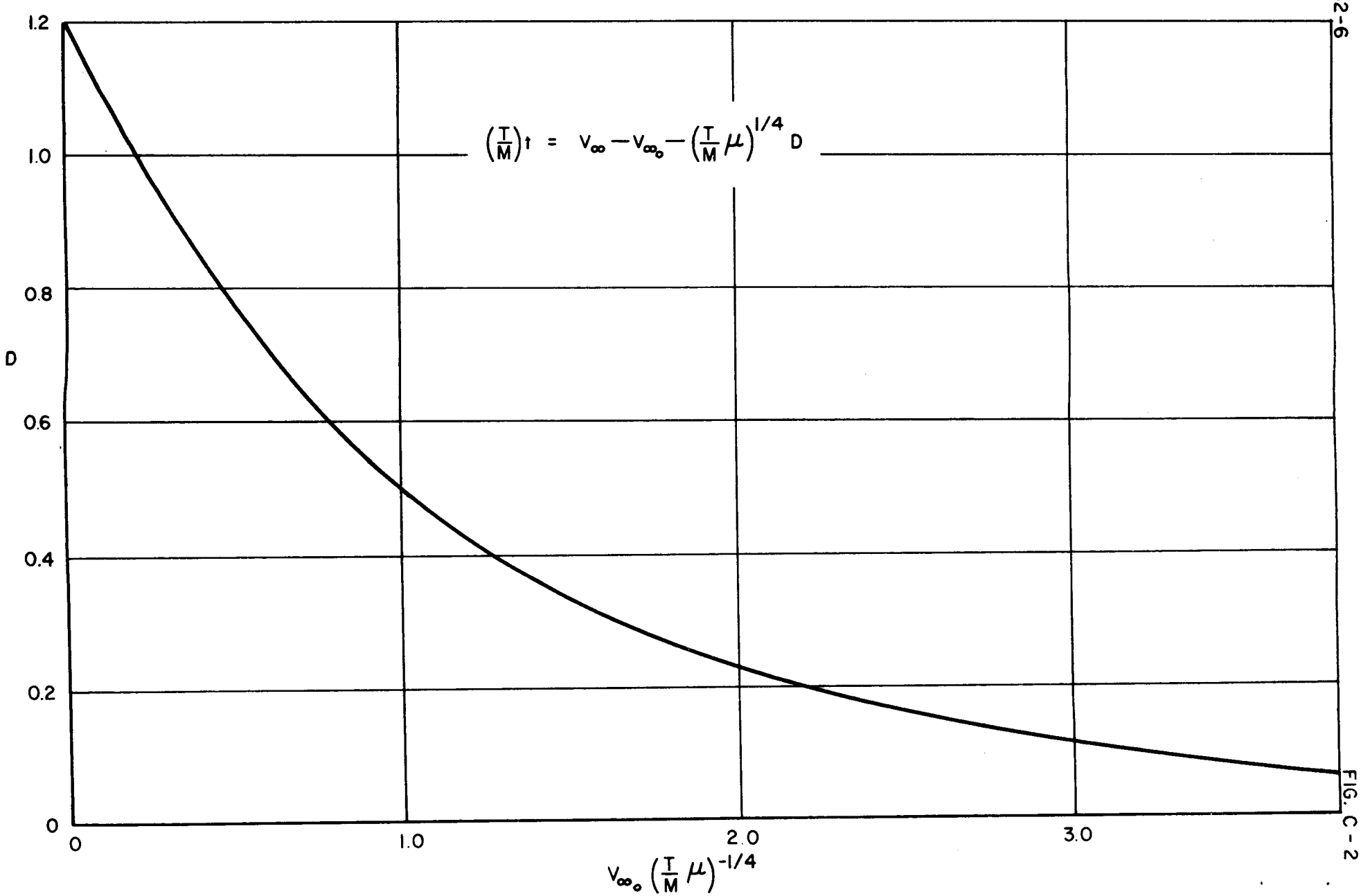

FIG. C-2

APPENDIX D

EXTREMIZATION OF PAYLOAD FRACTION FOR THE CASE OF CONSTANT THRUST, CONSTANT POWER WITH OPTIMUM COAST AND SPECIFIED CONSTANT SPECIFIC IMPULSE

The payload fraction of a power-limited rocket operating at constant power is given by

$$\mu_{pl} = \mu_W \left[\frac{1}{\mu_W + \theta} - 1 \right] \tag{D-1}$$

where μ_{pl} = payload fraction

μ_W = powerplant fraction

$$\theta = \frac{\alpha}{2} \int_0^T a^2 \, dt$$

with α = powerplant specific mass

$\vec{a}(t)$ = thrust acceleration

For the case of constant thrust and constant power, θ is considered to be a function of μ_W. Hence, maximizing u_{pl} with respect to μ_W, $d\mu_{pl}/d\mu_W = 0$, we obtain

$$\frac{d\theta}{d\mu_W} + \theta\left(2 - \frac{1}{\mu_W}\right) + \frac{\theta^2}{\mu_W} = -\mu_W \tag{D-2}$$

This is Riccati's Equation and yields a solution of the form

$$\theta(\mu_W) = \frac{\mu_W \left[b(1-\mu_W)-1\right]}{1 + b\mu_W} \tag{D-3}$$

where b is the integration constant. Substituting Eq. (D-3) into (D-1) we obtain and evaluation of b,

$$(\mu_{pl})_{max} = \frac{1}{b} . \tag{D-4}$$

Proceeding, $\theta(\mu_w)$ is minimized with respect to μ_w yielding

$$b = \frac{(1-2\mu_w) - \sqrt{1-4\mu_w}}{2\mu_w^2} \tag{D-5}$$

μ_w, as it appears in Eqs. (D-1), (D-2), (D-3), and (D-5), has still not attained its optimal value; these expressions hold for any value of μ_w. Consider these additional expressions for the payload and powerplant fractions, respectively:

$$\mu_{p1} = 1 - \dot{m}T_p - \mu_w \tag{D-6}$$

$$\mu_w = \frac{\alpha \dot{m} c^2}{2\eta} = \nu\dot{m} \tag{D-7}$$

where $T_p = T + t_1 - t_2$, the powered time (t_1 is engine cutoff time, t_2 is engine restart time); $\dot{m}$ and c are the mass flow rate and exhuast velocity, respectively, and η is the thruster efficiency.

Substituting Eqs. (D-4), (D-5), and (D-7) into (D-6) we obtain

$$\frac{2\nu^2\dot{m}^2}{1-2\nu\dot{m} - \sqrt{1-4\nu\dot{m}}} + \dot{m}(T_p + \nu) = 1 \tag{D-8}$$

Equation (D-8) provides the essential coupling of the equations of optimal motion and the propulsion parameters in the solution of this problem. As presented in Appendix B, the Euler-Lagrange necessary conditions and the equations of motion for the two-dimensional case are

$$\begin{aligned} \ddot{x} &= \frac{\dot{m}c}{1-\dot{m}t}\frac{u}{p} - \frac{x}{R^3}, & \ddot{u} &= \frac{(2x^2-y^2)u+3vxy}{R^5} \\ \ddot{y} &= \frac{\dot{m}c}{1-\dot{m}t}\frac{v}{p} - \frac{y}{R^3}, & \ddot{v} &= \frac{(2y^2-x^2)v+3uxy}{R^5} \end{aligned} \tag{D-9}$$

where $$p = (u^2 + v^2)^{1/2} .$$

These equations may be obtained also from an extremization of the integral

$$I = \int_0^T \left(\dot{m} + \frac{\mu_w}{T}\right) dt \tag{D-10}$$

where

$$\dot{m} = \begin{cases} A, & 0 \le t \le t_1, \ t_2 \le t \le t \\ 0, & t_1 \le t \le t^2 \end{cases}$$

But, since $\dot{m}$, μ_w and T are constants this integral becomes

$$I = \int_0^{t_1} dt + \int_{t_2}^{T} dt = t_1 + T - t_2 = T_p \qquad \text{(D-11)}$$

Hence, from a consideration of Eq. (D-6) we see that minimizing I maximizes the payload fraction with respect to the thrust control. Now Eqs. (D-9) are four expressions for determining the four functions x(t), y(t), u(t) and v(t); further, we have three unknown parameters $\dot{m}$, t_1 and t_2. These can be determined by the three expressions

$$[u(o)]^2 + [v(o)]^2 = 1$$

$$[u(t_1)]^2 + [v(t_1)]^2 = [u(t_2)]^2 + [v(t_2)]^2$$

$$\frac{2\nu^2 \dot{m}^2}{1-2\nu\dot{m} - \sqrt{1-4\nu\dot{m}}} + \dot{m}(T + t_1 - t_2 + \nu) = 1 \qquad \text{(D-12)}$$

It is noted that c and α/η are specified parameters during the solution.

The Newton-Raphson algorithm can solve the system of differential Eqs. (D-9) (in finite difference form) and the constraint Eqs. (D-12) for the optimal trajectory and mass flow rate.

The trajectory is optimal in this sense:

a. the powered time is minimized

b. the payload fraction is maximized with respect to powerplant fraction

c. the mass of expellant in the exhaust jet is minimized with respect to powerplant fraction

d. a. and c. infer that the mass flow rate, $\dot{m}$, hence the powerplant fraction $\mu_w = \alpha\dot{m}c^2/2\eta$, are simultaneously minimized.

It is noted that Eq. (D-3) may be obtained directly by solving Eq. (D-1) for θ:

$$\theta(\mu_w) = \frac{\mu_w}{\mu_{p1} + \mu_w} - \mu_w \qquad \text{(D-13)}$$

If the analysis was then to proceed from Eq. (D-3) as it did above, the same governing equations [(D-9) and (D-12)] would be obtained. But the trajectory would no longer be formally optimal in the sense that the payload fraction is maximized with respect to the powerplant fraction. The implication is that minimizing the propellant expenditure with respect to the powerplant mass is tantamount to maximizing the payload fraction with respect to powerplant mass. In essence, what has been obtained is a definitive expression for the coupling between optimal control and optimal powerplant characteristics in the constant power, constant thrust with optimum coast trajectory mode.

The analysis must be flavored by those final remarks. The specific mass, α, the thruster efficiency, η, and the specific impulse are chosen at the outset of the analysis, hence the powerplant becomes a linear function of $\dot{m}$. It is felt that this approach to the problem of mission systems design is advantageous since the present state of powerplant technology is characterized by definite limits on these three parameters: α (lower limit), η (upper limit) and I_{sp} (upper limit).

Payload fraction has been maximized by minimizing the integral $I = \int_0^T a^2\, dt$. This is not quite the same as the optimization process that occurred in the variable-thrust case. In the variable-thrust case I is minimized with respect to the thrust control as a function of time (calculus of variations); in the constant-thrust case I is similarly minimized with respect to the thrust control but is further minimized with respect to the powerplant fraction (theory of maxima and minima). This adjoining of the extremization of functions and functionals into a single operation, as the Newton-Raphson algorithm is capable of doing, is the means by which the simultaneous solution of optimal control and optimal powerplant parameters is obtained.

APPENDIX E

VARIABLE-THRUST TRAJECTORY OPTIMIZATION PROGRAM

The basic trajectory optimization program employing the finite-difference Newton-Raphson algorithm (Appendix A) was originally developed to compute the variable-thrust acceleration time-history which minimizes the quantity $J = \int_0^T a^2 dt$, where a is the thrust acceleration over the powered time T. During the latter phases of the study the computer program has been greatly revised to include different options of interest in mission studies and to facilitate use by other organizations.

In its updated form the program computes variable-thrust, variable-power, three-dimensional optimal low-thrust trajectories. Trajectory options include rendezvous and flyby trips both of which may be computed using either constant or variable power sources. The variable power profiles include those arising from solar cells, radioisotope powerplants and probabilistic causes (component failures). In addition to rendezvous and flyby trajectories the program is capable of determining solar probe trajectories to a given heliocentric radius. In any of the above trajectories hyperbolic excess speeds on the boundaries may be included.

It has been found difficult to obtain solutions for some trajectories other than those between Earth and its closest neighbors: Venus, Mars, and Jupiter. Even here, for long trip times and for trips coming close to the Sun, solutions are not readily obtainable. An iterated starting routine has been incorporated into thedeck for just such cases. This routine iterates on circular boundary conditions to the boundary conditions desired in each iteration, computes a trajectory solution, and uses this result as the starting solution for the next iteration. If this method fails to give a solution, since the number of iterations is limited, the input to each case can be controlled in such a way that each case can use an existing, closely related trajectory as its starting solution. This method has been found to work very well, especially for solar probe trajectories to small heliocentric radii.

The general organization of the trajectory optimization program and basic program logic are shown in Fig. E-1.

PROGRAM LOGIC FOR COMPUTING OPTIMUM TRAJECTORIES

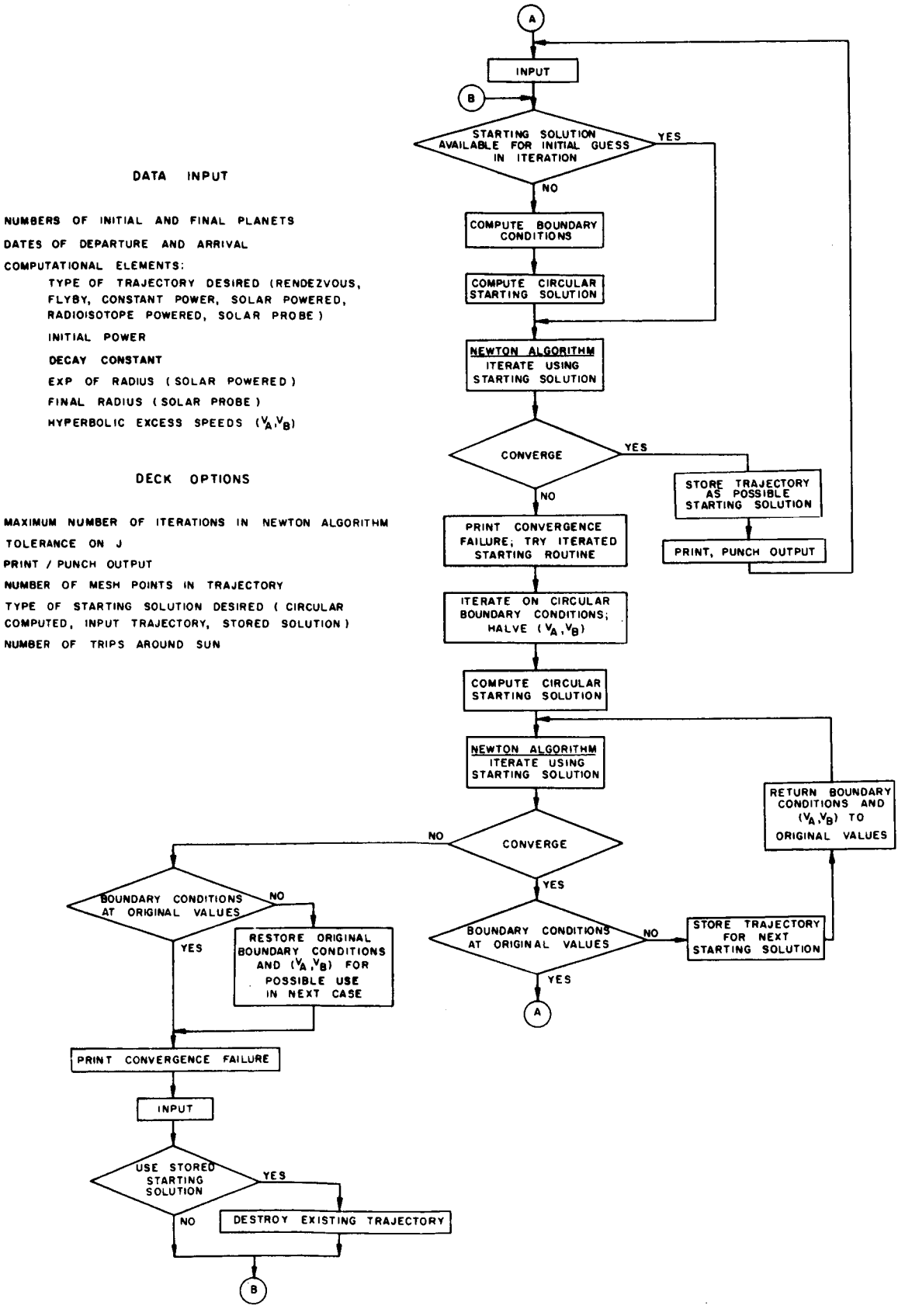

APPENDIX F

MASS COMPUTATION PROGRAM

The mass computation program was designed to calculate the mass of the vehicle system required on Earth parking orbit for various propulsion combinations. Figure F-1 depicts the flow chart for the program. The necessary input for any of the nine available propulsion options (Table F-1) is listed in the INPUT box of the flow diagram. The Earth entry mode may be either all electric, partial electric, or atmospheric. The Julian dates are the departure dates and the arrival dates of the round trip to Mars. The hyperbolic excess speeds (in EMOS) are used in the calculations of the ΔV's for each stage of the vehicle. These options and the others in this box are completely arbitrary for the weight calculation of any trip.

The propulsion-flight profile options, listed in detail in Table F-1, are nine combinations, built into the computer program, of the five possible propulsion stages used in the round trip flight: the nuclear Earth departure stage, the braking stage at Mars, the Mars nuclear departure stage, and the outbound and inbound electric stages. The choice of a propulsion profile is limited only by the choice of a single- or a dual-electric system. But even with this limit all profiles are available. For example, in a dual-electric system option 5 is available to include for one system a nuclear departure stage at Earth, a nuclear braking stage at Mars, a nuclear departure stage from Mars, and an inbound electric stage, but no outbound electric stage. Option 9, also available for a dual-electric system, includes the four stages of option 5 along with the outbound electric stage. Likewise for a dual electric system, option 9 includes a braking stage at Mars which option 7 lacks.

In addition to the masses which vary with crew size and duration, the program sizes the nuclear or electric propulsion stage, gives the appropriate incremental velocity or characteristic power (J), and mass to be accelerated. The major loops programmed in the computation are for the outbound/inbound legs (i.e., a given trip), the crew size and the power system specific weight for either the outbound or inbound legs or both. The scheduling of the mass computation accounts for transporting the 45 metric ton excursion module to Mars and discarding it after rendezvous for the return leg. Allowance is also made for accepting a maximum of 454 kg of scientific data and materials for return to Earth.

Inclusion of a J which exceeds the design limitations results in a negative mass for the electric propulsion system propellant or inert mass. Since these mass values are printed, in addition to the parameter β ($\equiv \sqrt{\alpha J/2\eta}$, which should always be less than unity), the voided mass computations are readily noticed.

Because of uncertainities in the mass values of fixed subsystem hardware, contingencies are provided in the program. This provision is placed appropriately to allow changes in mass values, such as the mission module, solar shelter, and command module (if one is included).

TABLE F-I

PROPULSION OPTIONS FOR MASS COMPUTATION PROGRAM

No.	Options	Lv N[1]	Lv E[2]	Arr N	Arr E	Lv N	Lv E	Arr N	Arr E	Nuclear Lv MIX	Nuclear Lv NUC	Electric SINGLE	Electric DUAL
I	One Electric		x		x		x		x	No	No	Yes	No
II	Dual Electric		x		x		x		x	No	No	No	Yes
III	Nuc/One Elect	x	x		x		x		x	Yes	No	Yes	No
IV	Nuc/Nuc/Elect	x		x			x		x	Yes	No	No	Yes*
V	Nuc/Nuc/Nuc/Elect	x		x		x	x		x	Yes	Yes	No	Yes*
VI	Nuc/Elect/Elect	x	x		x		x		x	Yes	No	No	Yes
VII	Nuc/Elect/Nuc/Elect	x	x		x	x	x		x	Yes	Yes	No	Yes
VIII	Nuc/One Elect/Nuc	x	x		x	x	x		x	Yes	Yes	Yes	No
IX	Hybrid Thrust	x	x	x	x	x	x		x[3]	Yes	Yes	---	Yes*

1 = Nuclear 2 = Electric 3 = Plus Entry System

* Mars retro-brake

I One Electric: Single electric system for all phases

II Dual Electric: Two electric systems, one for Earth-Mars, another for Mars-Earth

III Nuclear/One Elect: Nuclear Earth departure, single electric for remaining phases

IV Nuc/Nuc/Elect: Nuclear Earth departure, nuclear Mars brake, remaining electric

V Nuc/Nuc/Nuc/Elect: Nuclear stages at Earth depart, Mars arrival, Mars depart, each different

VI Nuc/Elect/Elect: Nuclear Earth departure, electric for Mars transfer, another electric for Mars-Earth transfer

VII Nuc/Elect/Nuc/Elect: Different nuclear and electric systems for departure, transfer and capture

VIII Nuc/One Elect/Nuc: Different nuclear systems for Earth and Mars departure, single electric system for transfers to Mars and to Earth

IX Hybrid Thrust: Nuclear stage to depart Earth and Mars, and brake at Mars; Electric systems for trans-Mars and trans-Earth, ablative entry system

PROGRAM LOGIC FOR COMPUTING VEHICLE SYSTEM MASS

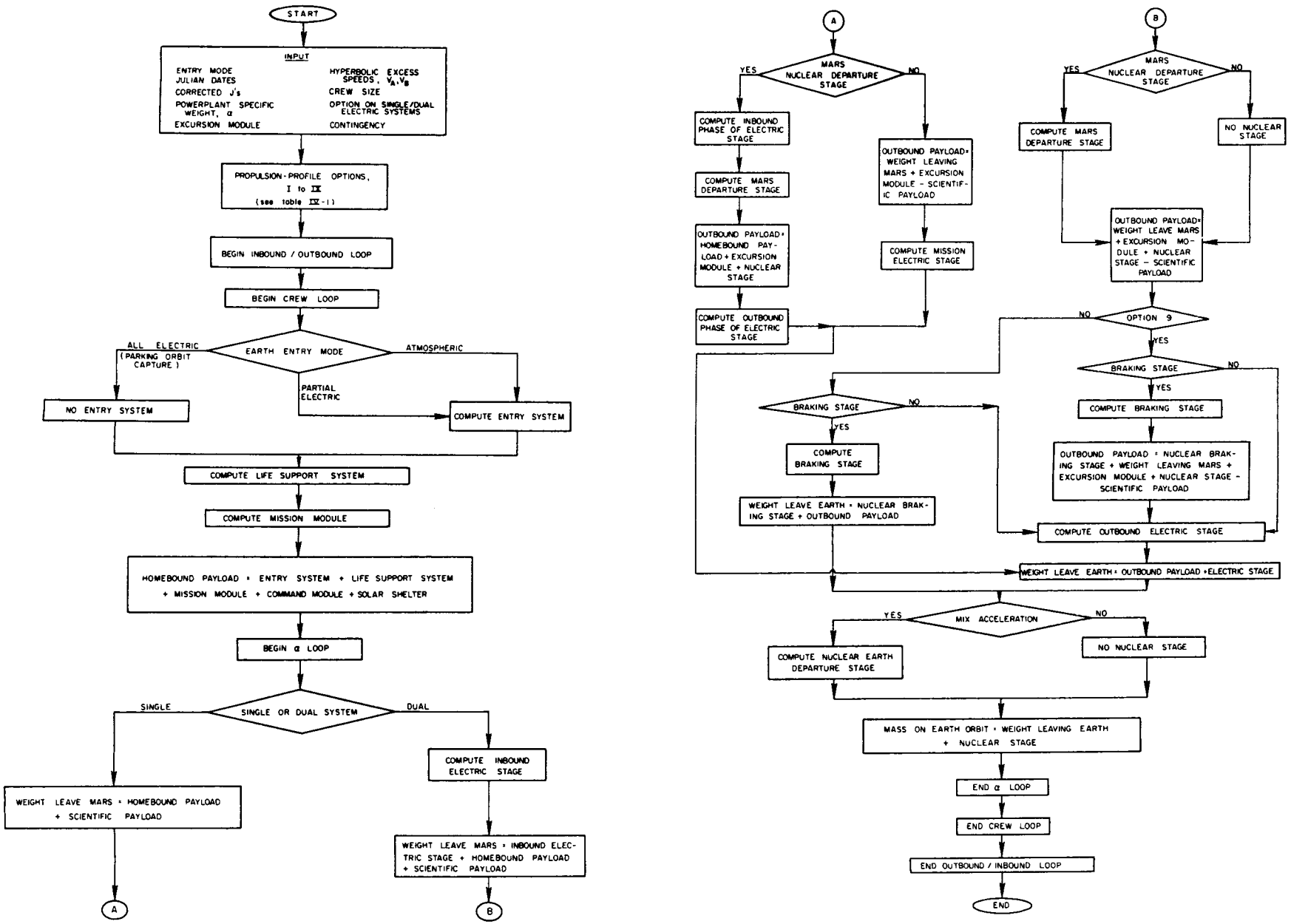

E-910262-6

FIG. F-1

APPENDIX G

NUMERICAL PROCEDURE FOR HYBRID-THRUST OPTIMIZATION

The basic propulsion mixes and resulting payload ratio equations are given in Section IV, Flight Profile Studies. As mentioned in Section IV, the over-all plan of the hybrid-thrust optimization procedure is to determine by analytical means the idealized hyperbolic excess speeds which result in maximum payload ratios for a given propulsion system mix. These hyperbolic speeds and the corresponding value of the intervening low-thrust trajectory requirement (J), are then used in a mass computation procedure which accounts for velocity losses and the variation of high-thrust step inert mass fraction (structural factor).

The purpose of this appendix is to describe in further detail the actual numerical search procedure employed to solve for maximum payload ratio. Actually the method is applicable to other than the solution of maximization (or minimization) problems. The general technique was slightly revised for the purposes of the problem at hand.

Much of the basic theory and the development of the systematic search technique are contained in Ref. IV-2. According to Ref. IV-2, the direct search method has been found to be attractive for the following reasons:

1. No techniques of classical analysis are necessarily involved
2. Repeated arithmetic operations are used with simple logic
3. An approximate solution, improving continuously, is provided at all phases of the computation
4. Other classes of problems are readily attacked

Systematic Search Technique

The basic theory of the method is briefly summarized here for the sake of completeness. For an exhaustive treatment of the subject as well as a formalized definition of direct search the reader is referred to Ref. IV-2.

The problem is to minimize a function $f(x_1, x_2, \ldots, x_n)$. A solution vector or "point" P_i consists of n components $(x_1, x_{2i}, \ldots, x_{ni})$ which when compared to some other solution P_j is better if and only if

$$f(x_{1i}, x_{2i}, \ldots, x_{ni}) < f(x_{1j}, x_{2j}, \ldots, x_{nj})$$

A base point B_0 is determined from initial guesses of the values for the n components or coordinates. Using the strategy discussed below, an adjacent point P_1 is generated and compared to the base point B_0. If P_1 is an improved solution compared to B_0, then P_1 becomes the new base point B_1, and the "move" which resulted in P_1 is termed a success. If P_1 is not better than B_0, then the move was a failure. A success or failure in a move or step is judged solely by the above inequality.

The next trial point P_r is determined relative to B_r by the present state S_r. The states make up part of the logic, since they determine directions for moves in the solution space. They provide new directions if recent moves fail, and they decide when no further progress can be made.

The search procedure employs two types of moves - exploratory and pattern moves. Explorations in the n-coordinates are made to determine how the function $f(x_1, \ldots, x_n)$ behaves in the neighborhood of the base point. The pattern move utilizes the behavioral information to provide a substantial reduction of the function.

The exploratory moves are made one coordinate at a time. Thus x_1 is varied by an increment $+\delta$ while $x_2, \ldots, x_n$ remain fixed. This new vector $(x_1 + \delta, x_2, \ldots, x_n)$ is tested against the base point $(x_1, \ldots, x_n)$. If it is better, the new coordinate value is retained. If it is not, x_1 is varied by $-\delta$ while $x_2, \ldots, x_n$ remains fixed. If this vector yields a smaller f, $x_1 - \delta$ is retained. If both + and - variations do not reduce f, then the original value, x_1, is retained.

The entire procedure is repeated for the remaining coordinates x_2 through x_n. At the completion of the procedure, each coordinate will have associated with it a direction and a slightly reduced value for f if at least one variation succeeded. The set of directions is referred to as a pattern. Hence the pattern move consists of changing all the coordinates simultaneously in the indicated directions or patterns as obtained from the exploratory moves.

The new values of the coordinates after the pattern move form the new base point from which exploratory moves may be made as discussed above. Alternatively, the same pattern may be used repeatedly with a test for improvement in the value of the function made after each move. Each success updates the base point. In this approach, if a pattern move fails, exploratory moves are then made from the current base point. The present version of the computer program uses this approach. The justification for this approach is based on the fact that, for problems so far encountered, shorter machine times are realized.

If a combination pattern and exploratory move fails and if exploratory moves from the last base point fail, a decrease in the variation, or step size, δ, is required. The criterion for a final solution is when δ is reduced below some input tolerance, ϵ. Ideally, this final solution occurs

when the function is at a minimum or near-minimum solution. However, the fact that no further progress can be made beyond the tolerance ϵ does not always indicate that a solution has been found. As is characteristic of direct search methods, no sufficiency conditions are available for the success of the method. Thus, Hooke and Jeeves recommend the search technique for the following types of problems:

1. problems for which the answers may be tested,

2. problems consisting of many separate cases, a few of which can be checked by alternative means.

If (1) and (2) are not feasible, partial checks may be obtained by using the method several times, with different starting solutions.

An over-all view of the systematic search technique may be obtained from Figs. G-1, -2, and -3 which present the basic logic in flow chart form.

Application to Hybrid-Thrust Optimization

As noted above the procedure is based primarily on the minimization of a function. Since a maximization of the payload ratio function is required, the problem is reformulated whereby a minimum to the inverse function (i.e., $1/\mu_L$) is sought. The important function for the numerical procedure is $\Gamma(\nu_A, \nu_B)$ which in general is known only through the trajectory optimization program. Because certain fixed dates of departure and arrival were used which infer minimum vehicle mass from a leg-time distribution viewpoint, it was expedient to utilize a two-dimensional table whose entries are the Γ's which correspond to the pair of normalized speeds (ν_A, ν_B). Such a table was generated for each given set of dates and was used repeatedly for different propulsion parameters.

The method requires a starting guess for the variables (ν_A, ν_B) which can be easily given since these normalized variables range from 0 to 1. In practically all cases convergence is quite rapid and starting guesses far from the solution pose no problem. The major exception is the case of atmospheric Earth entry for the return leg. In those instances where the entry system mass changes slowly with entry speed the optimization procedure attempts to assign a value of 1.0 or greater to ν_B. An automatic stop is written into the program such that if this does occur ν_B is set equal to unity. The maximum allowable entry speed (20 km/sec) could be used as the normalizing parameter in ν_B thereby indirectly imposing this restriction on the solution.

The main computer program which implements the basic logic given by the general flow charts is quite simple to write. The information presented in the flow charts is sufficient to code a program for a given problem or general use. Thus it was not deemed necessary to include a description of the computer program.

FIG. G-1

DECK F365 SEARCH PROCEDURE

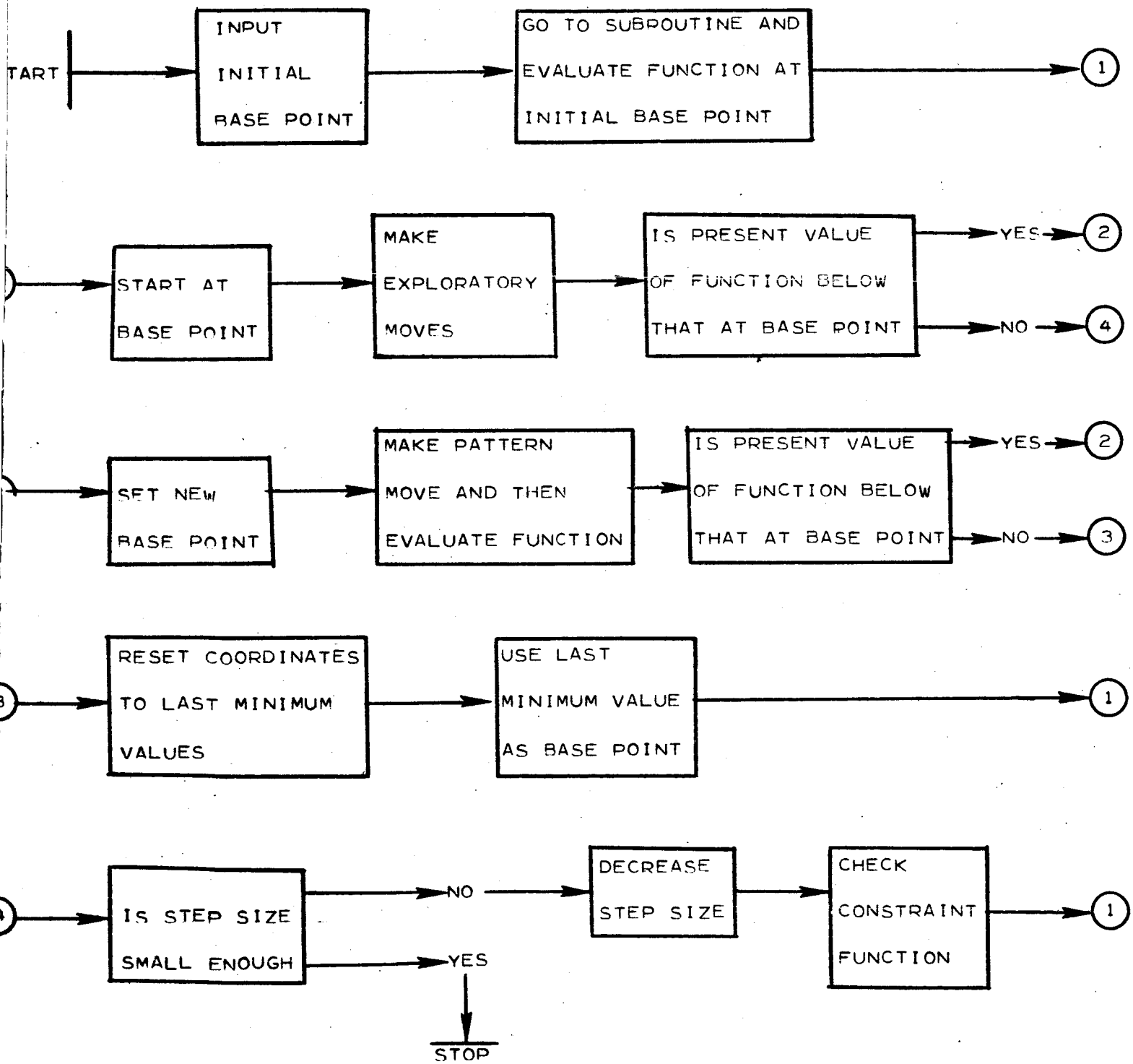

FLOW CHARTS DESCRIBING EXPLORATORY AND PATTERN MOVES ARE DESCRIBED ON THE FOLLOWING PAGES

FIG. G-2

EXPLORATORY MOVES

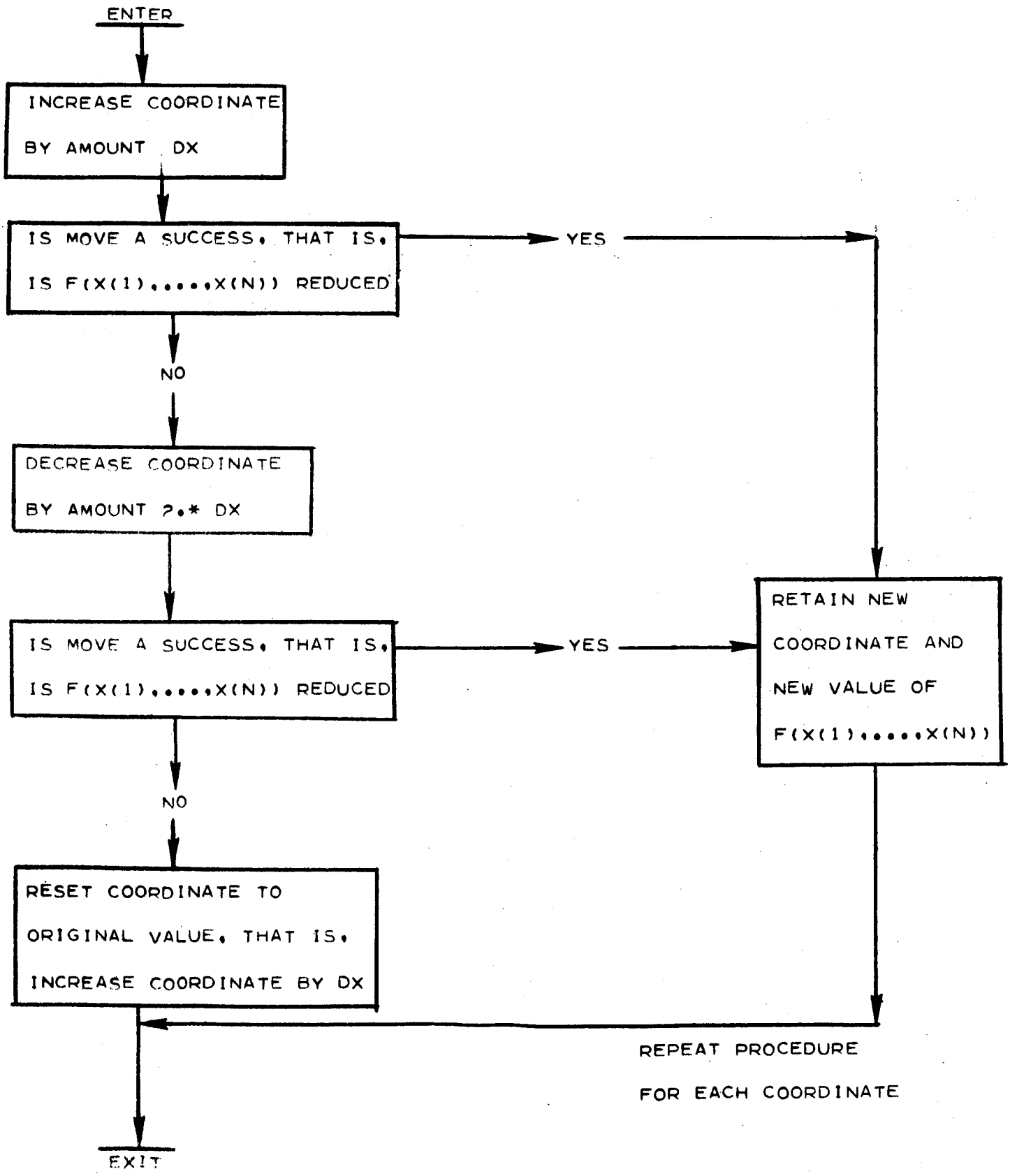

FIG. G-3

PATTERN MOVE

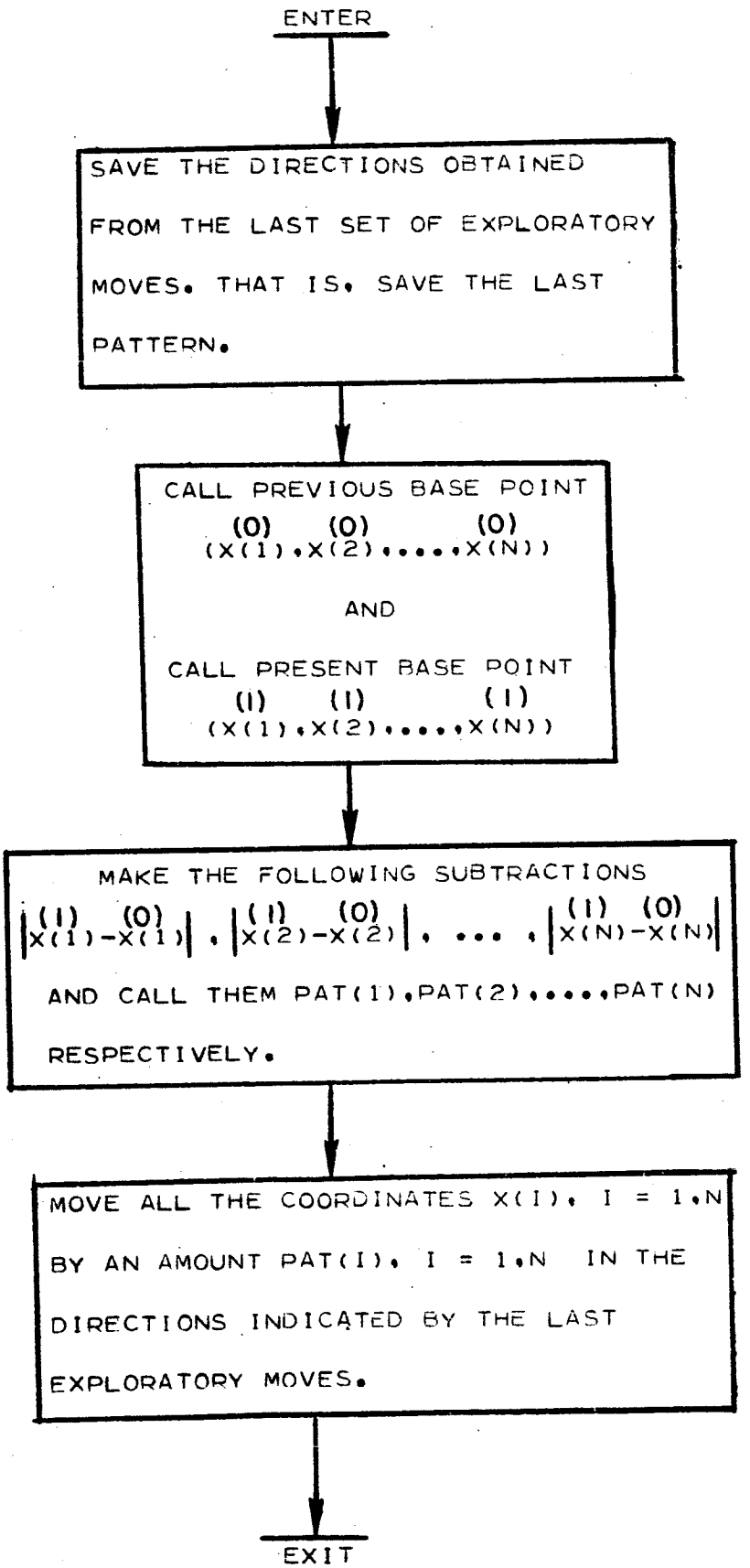

APPENDIX H

PROCEDURE USED TO GENERATE THE POWER LEVEL CURVES

Configuration 2 was selected to explain the procedure. The reliability block diagram for this configuration is shown in Fig. H-1. The table below lists the effect of main radiator (R_4) failures on system power output as follows:

No. of R_4 Failures on a given R_3	% Power Loss
1	11.3
2	22.1
3	25.0

Any other combination of R_4 failures can be computed from the above data. For example:

3 R_4's failed on one R_3
2 R_4's failed on another R_3
0 R_4's failed on the remaining 2 R_3's

Total power loss = 25.0 + 22.1 = 47.1%

Step 1

All possible combinations of the 12 R_4's failing in the system were ranked in the descending order of the remaining power down to 15%. These combinations with the corresponding power levels and ranks are listed in Table H-1.

Step 2

Using the logic depicted in the reliability block diagram, the probability of each event (combination) occurring was expressed as a function of R_1, R_2, R_3 and R_4, where R_i's are the block reliabilities. For example:

$$P(E_o) = R_1 R_2^2 R_3^4 R_4^{12}$$

$$P(E_1) = R_1 R_2^2 R_3^4 12 R_4^{11} Q_4$$

$$P(E3B) = R_1 R_2^2 R_3^4 108 R_4^9 Q_4^3$$

$$P(E7B) = R_1 R_2^2 R_3^4 108 R_4^5 Q_4^7 + 4 R_3^3 Q_3 27 R_4^5 Q_4^4$$

where $Q_i = 1 - R_i$

The coefficients represent the number of ways certain combinations may occur. For example, from the last equation; if no R_3's fail, there are 108 ways in which 7 of the 12 R_4's can fail; that is,

3 fail on any one of the 4 R_3's,
2 fail on any one of the remaining 3 R_3's,
2 fail on any one of the remaining 2 R_3's, and
0 fail on the remaining 1 R_3.

Thus, $\frac{4!}{2!}\binom{3}{3}\binom{3}{2}\binom{3}{2}\binom{3}{0} = 108$

There are 4 ways one R_3 can fail (any one of the 4). If an R_3 fails, 3 R_4's are lost with it, and there are 27 ways 4 of the remaining 9 R_4's can fail. Hence the pattern is (2, 2, 0).

$$\frac{3!}{2!}\binom{3}{2}\binom{3}{2}\binom{3}{0} = 27$$

Step 3

With P (c%) = probability of maintaining at least c% power, then,

P (100%) = P(E0)

P (88.7%) = P(100%) + P(E1)

P (77.9%) = P(88.7%) + P(E2A)

.
.
.

P (30.8%) = P(33.2%) + P(E7B)

.
.
.

P (16.6%) = P(19.5%) + P(E9B)

To compute the power level as a fun tion of time for a desired probability, say 90%, the lefthand sides of the above equations are set equal to 0.90 and each one of them is solved to t. Analytically, however, this is not easy. Each P(c%) is a summation of P(E)'s, each P(E) is a function of R_i's and each R_i is a function of t and not necessarily as a simple exponential, e.g., in the form of $R_i = \exp(-\lambda_i t)$.

Each major block could have internal redundancy and/or components which do not follow the exponential failure law.

Step 4

Because of the foregoing difficulties, the desired step function was generated graphically. It is belived that the graphical solution is adequate within the accuracy warranted at this time.

A computer program was written to generate P (ϵ%) versus time curves for all the ϵ's. Figure H-2 plots the results of the computer program for configuration 2 using state-of-the-art failure rates and no internal block redundancies.

Step 5

The desired step function (power profile), presented in Fig. H-3 is a cross plot of Fig. H-2 at given levels of probability.

TABLE H-1

POWER LEVEL RANKS FOR CONFIGURATION 2

Event	Total	R_3-	No. of R_4's Lost W	X	Y	Z	% Power Lost	% Power Left	Rank
E0	0		0	0	0	0	0.0	100.0	1
E1	1		1	0	0	0	11.3	88.7	2
E2A	2		2	0	0	0	22.1	77.9	3
B			1	1	0	0	22.6	77.4	4
E3A	3		3	0	0	0	25.0	75.0	5
B			2	1	0	0	33.4	66.6	6
C			1	1	1	0	33.9	66.1	7
E4A	4		3	1	0	0	36.3	63.7	8
B			2	2	0	0	44.2	55.8	9
C			2	1	1	0	44.7	55.3	10
D			1	1	1	1	45.2	54.8	11
E5A	5		3	2	0	0	47.1	52.9	12
B			3	1	1	0	47.6	52.4	13
C			2	2	1	0	55.5	44.5	15
D			2	1	1	1	56.0	44.0	16
E6A	6		3	3	0	0	50.0	50.0	14
B			3	2	1	0	58.4	41.6	17
C			3	1	1	1	58.9	41.1	18
D			2	2	2	0	66.3	33.7	20
E			2	2	1	1	66.8	33.2	21
E7A	7		3	3	1	0	61.3	38.7	19
B			3	2	2	0	69.2	30.8	22
C			3	2	1	1	69.7	30.3	23
D			2	2	2	1	77.6	22.4	27
E8A	8		3	3	2	0	72.1	27.9	24
B			3	3	1	1	72.6	27.4	25
C			3	2	2	1	80.5	19.5	28
D			2	2	2	2	>85.0	----	--
E9A	9		3	3	3	0	75.0	25.0	26
B			3	3	2	1	83.4	16.6	29
C			3	2	2	2	>85.0	----	--
	10, 11 & 12						>85.0	----	--

FIG. H-1

RELIABILITY BLOCK DIAGRAMS

REPRESENTATIVE POWERPLANT CONFIGURATIONS

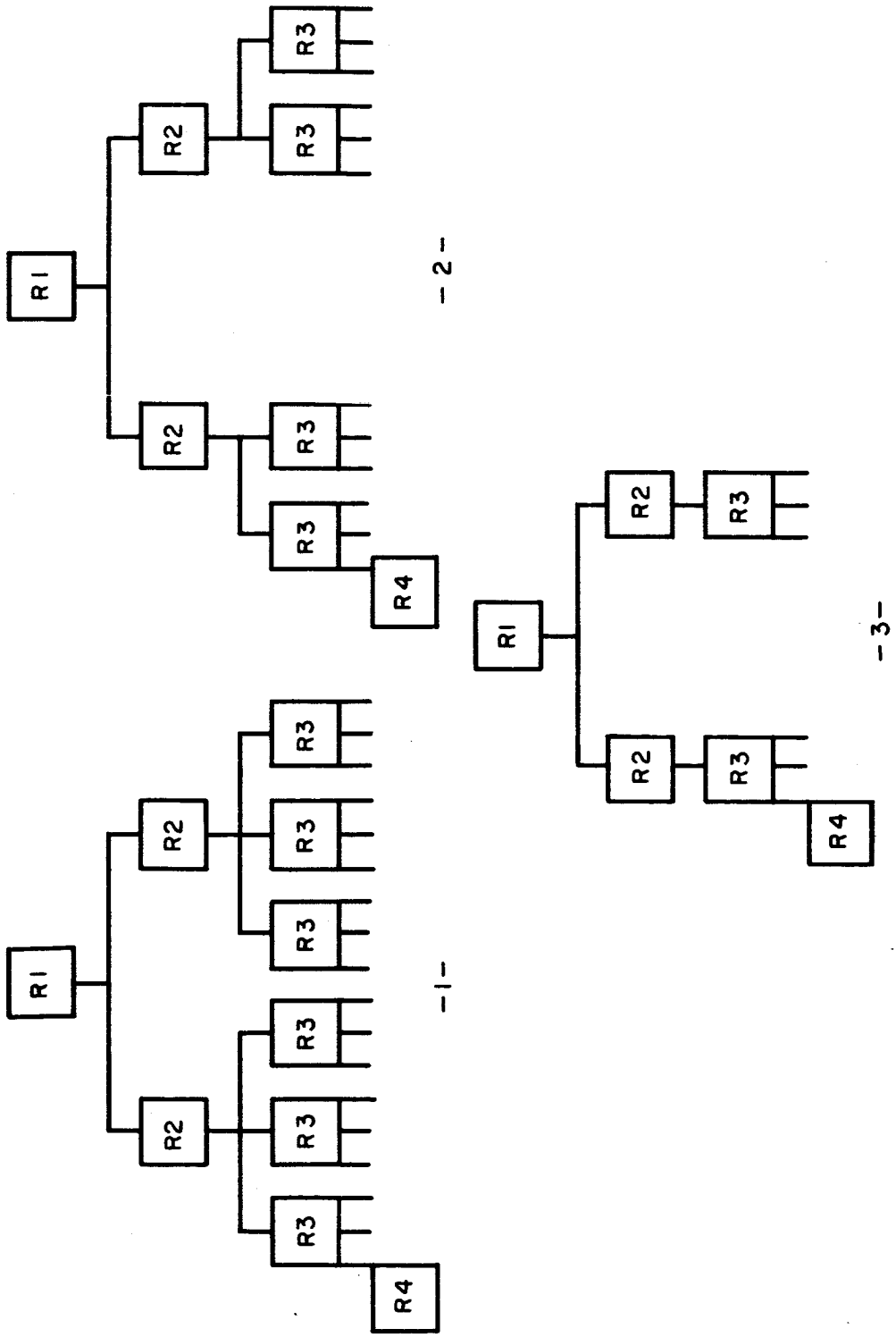

FIG. H-2

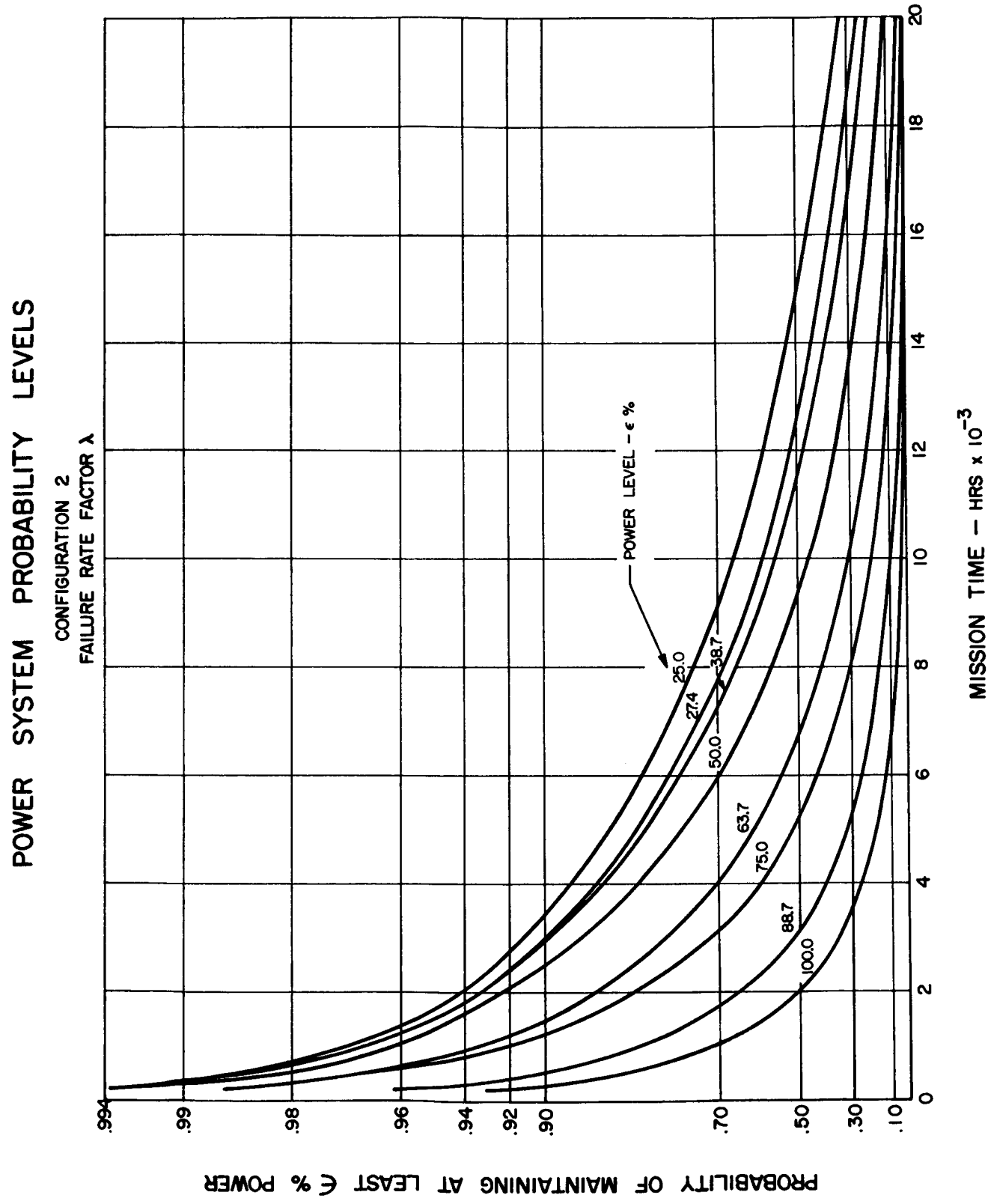
POWER SYSTEM PROBABILITY LEVELS
CONFIGURATION 2
FAILURE RATE FACTOR λ
POWER LEVEL - ε %
25.0
27.4
38.7
50.0
63.7
75.0
88.7
100.0
PROBABILITY OF MAINTAINING AT LEAST ε % POWER
.994
.99
.98
.96
.94
.92
.90
.70
.50
.30
.10
0
2
4
6
8
10
12
14
16
18
20
MISSION TIME - HRS x 10^-3

FIG. H-3

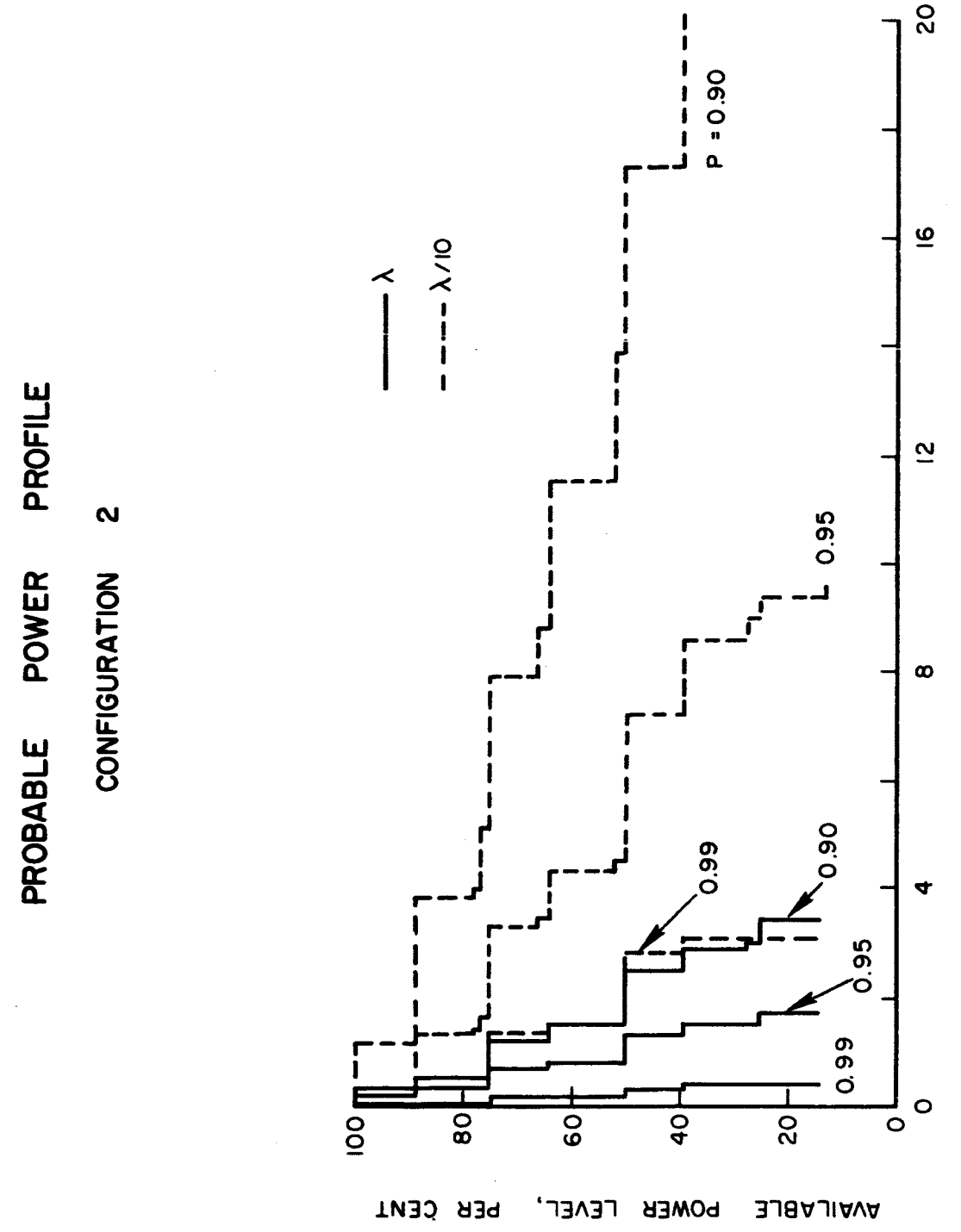
PROBABLE POWER PROFILE
CONFIGURATION 2
λ
λ/10
P = 0.90
0.95
0.99
0.90
0.95
0.99
AVAILABLE POWER LEVEL, PER CENT
MISSION TIME, 1000 HR
0
20
40
60
80
100
4
8
12
16
20

APPENDIX J

RESEARCH AND TECHNOLOGY IMPLICATIONS

This section summarizes some of the important technical problems which must be solved in the development of a nuclear electric powerplant. Advanced research and technology programs are recommended which will contribute to the solution of these key problems.

Major Technical Problems

Powerplant Startup

An important problem affecting the complete system is startup in a space environment. Included in the startup considerations are shutdown time prior to starting or restarting, and the associated possibility of freezing various liquid metals, the initiation of stable boiling without significant liquid carryover, control of condensation and flooding in the turbine, adequate bearing fluid supply, stable condensing at low flow rates and startup thermal stresses.

One startup approach involves a long routine with turbine bypass. The reactor would be started and the boiler brought up to temperature with the radiators still covered by a fairing. Boiling would be established with the vapor bypassing the turbine and being condensed. The bearing flow would be established by a startup pump. Some potassium vapor would be admitted to the turbine and the turbine would be warmed up slowly and gradually brought up to speed. This approach is modeled after stationary or marine powerplant practice and requires valves capable of reliable operation in high temperature potassium vapor. Also this approach requires a significant amount of energy storage to generate the electric power to operate the auxiliary equipment during the extended startup period.

An alternate startup concept would involve a relatively fast automatic programmed procedure. This approach minimizes the number of startup valves and energy storage required but it demands a detailed knowledge of the interaction of system components during a fast startup transient. Model testing and eventually flight testing would be required to develop such a system.

The need for reliable valves in liquid-metal systems is generally recognized. However, this is an area in which relatively little technical effort has been expended. Control valves, shutoff valves, and check valves capable of extended operation in contact with high-temperature alkali metals will be required.

Another component important to the startup and operation of the Rankine-cycle space powerplant is an accumulator for service with high-temperature liquid metals in a space environment. The accumulator stores liquid metal for system makeup during starting and transient operation. It also must supply this liquid metal at nearly constant pressure to maintain the condensing temperature. An additional requirement for a maintainable liquid-metal system is a drain-and-fill system for the storage of liquid metals during some of the maintenance operations. One possibility is to combine the drain-and-fill and the accumulator functions into a single system.

Reactor

The development of a lithium-cooled reactor capable of operation at high temperature is required. The magnitude of temperature and power reactivity coefficients remains to be demonstrated before a complete understanding of the reactor control requirements is established. Obviously, the operation and test of a power reactor of this type is required.

The development of a long-life high-temperature fuel presents an important development problem to be solved. The desirable properties for the fuel are low fission-gas release, high allowable burnup and resistance to cracking and swelling.

DMIC Report 189[1] gives some metallurgical and fabrication data for the tantalum alloys T-111 and T-222. From the data given for T-111, it appears that tubing can be drawn for fuel pins. The data also indicates that the fabrication of a pressure vessel and piping is promising.

Progress has been made in the development of the BeO reflector material. The most promising form to be developed for the material is rectangular blocks. They will probably be arranged around the reactor with the long axis aligned parallel to the reactor radius, and held in place by a wire grid.

Control drum alignment will pose a problem since the drum will bow due to the thermal gradient across the reflector material. The surface of the drum facing the reactor will be hotter than the outer surface. Therefore, the drum will tend to bow in towards the reactor and impose high stresses on the control drum bearings and bearing supports. Adequate clearance must be provided between the drums and the reactor vessel. Because the amount of reactivity associated with the drums is a function of the radial gap between the drums and the vessel, the reduction of reactivity caused by an increase in clearance may result in a heavier reactor configuration in order to compensate for the reactivity reduction.

1. F. F. Schmidt and H. R. Ogden, The Engineering Properties of Tantalum and Tantalum Alloys

Control drum rotation will be accomplished by motors located behind the shield. The long shaft required between the motors and the drums will cause alignment and distortion problems that must be investigated.

Shield

When LiH is incorporated into a shield design, its containment produces a major problem. If the LiH in the shield is allowed to reach temperatures around 800 F, it will dissociate to form gaseous hydrogen and liquid lithium. An overpressure of hydrogen can slow this dissociation, but hydrogen gas diffuses through most materials such as stainless steel, and will be lost during operation for extended periods at high temperatures. Also, the ability of the shield to stop neutrons will be decreased and liquid lithium will be liberated with its attendant corrosion problem. If the LiH containment problem dictates the canning of LiH in small sections, the heat removal capability of the shield could be decreased, causing temperature problems. Heat generation rates in the shield are significant and a detailed examination of the shield design problem is warranted.

Boiler

Boiling instabilities in a space environment represents a major problem to be solved. Based on the available data, a serpentine boiler tube configuration was chosen for design.

Fabrication of the boiler from T-222 will require the shaping of the serpentine tubes and the welding of the tubes to the tubesheets. The forging of the boiler shell and headers will also be required. The previous reference indicates that forging is possible and that the forged slabs can be cold-rolled. No information is given regarding welding.

Turbine

Materials

The peak temperature in the power-conversion system is determined by the capability of the turbine. Data is required which defines the long-term strength and corrosion resistance of high strength-to-weight ratio materials capable of operating for a long period in a potassium vapor environment at temperatures close to 2000 F. Experience must be gained with casting, forging, machining and welding of such materials in the forms required for the construction of a turbine. Materials must be developed which can guarantee the structural integrity of the turbine rotor. The effects of liquid potassium on blade life and turbine performance must be determined and methods of interstage moisture removal developed.

Bearings

The hydrostatic bearings employed in the turbine require extensive development. Particular problems will be the startup of the turbine in a dry condition and the evaluation of liquid-metal flow rates required during startup and operation. The stability of radial bearings and the stiffness of these bearings needs to be investigated for the high rotational speeds anticipated in this application. The possibility of bearing damage due to solid impurities in the liquid metal is relatively unknown and needs to be investigated in order to provide proper clearances and flow rates. The possibility of requiring filters to remove these particles should be investigated.

Seals

The use of dynamic seals in the turbine appears to be feasible approach to provide for prevention of leakage of potassium liquid into the vapor section of the turbine. Extensive experience with this type of seal in liquid-metal pumps has been obtained at the CANEL facility. However, development work is required to produce a reliable seal with adequate cooling and startup characteristics. The problem of interface instabilities caused by changes in turbine rpm must also be investigated. This problem will be particularly important when the turbine is shut down for maintenance.

Condenser

The major problems for the condenser are the heat transfer and two-phase pressure drop correlations and condensing stability in a space environment. Further data on condensing heat transfer of liquid metal vapors is required.

Radiators

The extent and nature of meteoroid damage to be expected on the Mars trip is still uncertain. The criterion used for the design of this powerplant was taken from a NASA report[1].

The main and high-temperature auxiliary radiator are constructed of stainless steel tubes which contain the liquid metal. The tubes are covered with a beryllium barrier and have beryllium fins. A good metallurgical bond is required between the tube and barrier in order to assure good thermal contact. The bond between these materials must be strong enough to withstand the large thermal stresses imposed during fabrication and system operation. Materials are required with similar thermal expansion coefficients, which are chemically compatible and which are functionally suitable as tube and barrier.

1. Recent Developments in Space Power System Meteoroid Protection, by Irwin J. Loeffler, Nestor Clough and Seymour Lieblein.

The radiator surfaces is designed with a high-emissivity coating and such coatings have demonstrated high performance and extensive life in a high vacuum environment[2]. However, an examination of high emissivity coatings on beryllium is required to demonstrate the compatibility of the coating with beryllium.

Electrical

Electromagnetic materials which would permit operation at higher temperatures and higher stress levels could improve efficiency and reduce auxiliary cooling system weight. Switch gear which can be developed to operate in a high-temperature vacuum environment without welding or extensive contact resistance would be attractive in this application. Also, efficient electrical power-conditioning equipment which can operate above the present limiting temperature for semiconductors would allow system weight reductions. A major development item is the nonmagnetic and nonconducting bore seal required to separate the alternator rotor and stator. The seal will probably be made of a ceramic material. Fabrication of a ceramic component of this size and shape is a complete unknown at this time.

System Maintenance

The results of this study indicate that an inflight liquid-metal system repair capability is required. Feasible methods must be developed for providing such a capability without excessive shield and equipment weight or powerplant shutdown penalties. Tools and equipment are required for cutting and welding of liquid-metal systems. Systems are required for detecting component failures, isolating components, and draining and filling liquid-metal systems.

Recommended Advanced Research and Technology Programs

Startup

The feasibility of space startup of the powerplant in various flight modes must be demonstrated. Turbine startup, including bearing supply, flooding and draining, and thermal transients are particularly important.

Reactor

Development of a high-temperature liquid-metal-cooled reactor is a requisite for this system. The key item in the reactor development is that of a reactor fuel which will tolerate the high-temperature long-lifetime

2. Determination of the Emissivity of Materials, Pratt & Whitney Aircraft Report PWA-2206, Contract NASw-104.

environment, and which can tolerate the effects of radiation damage without failure. An additional item of importance is the development of a reliable reactor control concept with a sufficient reactivity effect for all mission modes. Control system development includes the development of a reactor vessel material capable of operating at high temperature with nuclear properties which do not adversely affect reactor control.

Radiation Shielding

The radiation shielding requirements are the single most significant consideration in determining powerplant weight. Extensive study is required in the determination of shield criteria. Development programs should cover the areas of shield materials and fabrication. This requirement is common to all types of nuclear power systems.

Boiler and Condenser

The question of boiling and condensing stability is not yet well understood and further investigation of these phenomena is warranted.

Turbine

Key items in turbine development include a high-temperature material with a high strength-to-weight ratio and good resistance to erosion by moisture in the vapor stream, the development of reliable turbine bearings and seals, and a method of extracting moisture between stages.

Radiator

The fabrication procedure for the beryllium and stainless steel radiator requires development. The key element is a stainless steel tube with a finned beryllium barrier. A metallurgical bond is required between the stainless steel tube and the beryllium barrier in order to provide good heat transfer from the radiator.

Valves

All power systems share a requirement for reliable valves. Development of valves for high-temperature liquid-metal systems will require an extensive program of materials development, design and fabrication techniques, and reliability demonstration.

Electrical

The development of alternators and motors in the size required and suitable for operation in the required environment needs to be continued.

Reliability and Maintenance

The requirements for powerplant reliability and maintenance are prime considerations for manned missions. Study programs are required to understand the interaction between reliability and maintenance. Development programs are required to demonstrate feasible and reliable maintenance techniques and equipment. A related development item is a reliable liquid-metal fill-and-drail system.

Recommendations for General Future Studies

The following list presents the recommendations for further analysis based on the results and conclusions of this study.

1. Manned missions to planets other than Mars should be analyzed to clarify the mission spectrum which favors the use of combined high- and low-thrust space transportation systems.

2. Unmanned, automatic, planetary orbital and surface probe missions employing hybrid-thrust vehicles should be studied and compared against the system requirements of all high-thrust vehicles in order to establish further the role of mixed-thrust systems in planetary exploration.

3. Different mission modes employing constant- rather than variable-thrust trajectories should be analyzed to further check the validity of the conclusions derived herein.

4. Hybrid-thrust planetary missions employing swingby profiles should be investigated to determine possible mass savings and to uncover other types of propulsion-profile mixes which may prove advantageous mass-wise.

5. Solar cell and radioisotope power sources employing constant-thrust operating modes should be studied and compared with reactor power sources to establish the favored powerplant for various interplanetary missions and flight profiles.

6. Further analysis should be applied to identifying the influence of probable decreasing powerplant output with time (regardless of power source) on the vehicle mass requirements and to establishing the tradeoff of power system reliability with specific weight.

7. Investigations should be initiated into the effect that planetary parking orbit operations have on the over-all hybrid-thrust optimization.

8. An in-depth design study should be made of mixed-thrust vehicle systems in order to uncover operational and integration problems and to establish engineering feasibility of such spacecraft designs (especially

in regard to the use of nuclear propulsion for planetary capture and departure and to the packaging requirements for orbital assembly).

9. Additional effort should be expended in analyzing the constant-thrust operating mode to determine the classes of trajectories which possess two rather than one coasting arc.

10. The basic Newton-Raphson algorithm should be applied to the constant-thrust with coast trajectory problem which has the payload optimization aspect as an integral part of the computational procedure.